MASS TRANSFER AND HYDRODYNAMICS IN STIRRED GAS-LIQUID-LIQUID CONTACTORS

Samenstelling promotiecommissie:

Prof. dr. ir. J.W.M Noordermeer, voorzitter	Universiteit Twente
Prof. dr. ir. G.F. Versteeg, promotor	Universiteit Twente
Dr. ir. D.W.F. Brilman, assistent-promotor	Universiteit Twente
Prof. dr. ir. J.A.M. Kuipers	Universiteit Twente
Prof. dr. ir. M.M.C.G. Warmoeskerken	Universiteit Twente
Prof. dr. ir. P.P.L. Regtien	Universiteit Twente
Prof. dr. ir. J.C. Schouten	Technische Universiteit Eindhoven
Dr. ir. A.B. Pandit	University of Mumbai, India

The research reported in this thesis was funded by the Dutch Organization for Scientific Research (NWO).

Cents, A.H.G.
Mass Transfer and Hydrodynamics in Stirred Gas-Liquid-Liquid Contactors
Thesis, University of Twente, The Netherlands
ISBN: 9036519942

MASS TRANSFER AND HYDRODYNAMICS IN STIRRED GAS-LIQUID-LIQUID CONTACTORS

PROEFSCHRIFT

ter verkrijging van
de graad van doctor aan de Universiteit Twente,
op gezag van de rector magnificus,
prof. dr. F.A. van Vught,
volgens besluit van het College van Promoties
in het openbaar te verdedigen
op donderdag 4 december 2003 om 15.00 uur

door

Antonius Harold Gerrit Cents

geboren op 13 augustus 1976

te Deventer

Dit proefschrift is goedgekeurd door de promotor

Prof. dr. ir. G.F. Versteeg

en de assistent-promotor

Dr. ir. D.W.F. Brilman

Aan Leonie

Summary

Multi-phase systems, e.g. gas-liquid-liquid systems, have gained interest in the past decade, due to the introduction of homogeneous biphasic catalysis in various reaction systems, e.g. hydroformylation, carbonylation, hydrogenation and oligomerization (Cornils, 1999). The main advantage of these systems over catalysis in one phase is the easy separation of the catalyst from the reactants and products. In this way, advantages of homogeneous catalysis (no internal mass transfer limitations and often higher selectivities) and of heterogeneous catalysis (easy catalyst separation) can be combined. Important industrial applications are e.g. the SHOP-process and hydroformylation of propene to butyraldehyde.

The rate of gas-liquid mass transfer is very important in several industrial chemical engineering applications. In many types of reaction systems, however, the mechanism of mass transfer is not well understood. This is for instance the case in Gas-Liquid-Solid (G-L-S) and Gas-Liquid-Liquid (G-L-L) systems. In literature, most research studies on mass transfer in gas-liquid-liquid systems are confined to the measurement of the volumetric mass transfer coefficient, $k_L a$. However, to obtain more knowledge of the mechanism of mass transfer, it was decided to study the mass transfer coefficient, k_L, and the interfacial area, a, separately.

A well known method to determine these mass transfer parameters is use of the the Danckwerts-plot technique. By operating a chemical reaction in a moderately fast reaction regime with a first order reaction, it is possible to obtain both k_L and a by measurement of the absorption rate at different values for the reaction rate. This technique was used in this work to study the effect of different volume fractions of four selected dispersed organic phases, 1-octanol, toluene, n-heptane and

n-dodecane, on the gas-liquid mass transfer parameters in systems with an aqueous continuous liquid phase. It was shown in the present study that two types of gas-liquid-liquid systems exist; systems with dispersed phases that enhance gas-liquid mass transfer and systems that do not enhance mass transfer. Mass transfer enhancement was observed in case of toluene and 1-octanol as a dispersed phase and this enhancement could be well described using a homogeneous model of the shuttle mechanism (see e.g. Bruining et al. (1986)). In this mechanism, the enhancement of mass transfer is based on the presence of dispersed phase droplets, with a higher capacity for the component to be transferred, in the mass transfer zone. In this way, a higher local driving force for mass transfer can be obtained, which leads to an increased flux.

However, with n-heptane and n-dodecane, both also having a higher capacity for the component to be transferred, no enhancement of mass transfer was found. Apparently, two different mechanisms must exist, accounting for the difference in this behaviour. When the correct mechanism was accounted for in the mass transfer calculations (shuttle mechanism for octanol and toluene and no enhancement for heptane and dodecane), the value of k_L, represented as the surface renewal frequency in the Danckwerts model, remained constant up to 40% dispersed phase.

For the Danckwerts-plot technique a pseudo-first order system was used to perform mass transfer measurements, as no convenient first order reaction system is available. In the present study the absorption of CO_2 in a carbonate/bicarbonate buffer was used, in which the reaction rate rate is varied by the addition of different amounts of sodium hypochlorite as a catalyst. Although this system has been frequently applied by several researchers, it was never verified that the addition of larger amounts (up to 0.2 M) of catalyst did not cause changes in the hydrodynamics and physical properties of the system. For this reason, the absorption of CO_2 in the buffer solution was carried out simultaneously with the desorption of oxygen from the solution. The desorption rate of oxygen was not affected by the addition of the catalyst, which is a strong indication that the hydrodynamics and physical properties of the system did not change. Therefore, the variation of reactivity in the construction of the Danckwerts-plot by changing the catalyst concentration is

justified over a large catalyst concentration range.

The measured absorption rate for CO_2 was, however, much lower compared to the desorption rate of O_2. This phenomenon was probably caused by the high amount of gas depletion from bubbles with a long residence time in the solution. This has a larger effect on the determination of the mass transfer parameters with carbon dioxide compared to oxygen, due the the higher CO_2 solubility in water.

A disadvantage of the Danckwerts-plot technique is that it is confined to some specific chemical systems. To study the gas-liquid interfacial area in non-chemical systems a physical measurement technique was developed, making use of the attenuation and sound velocity of ultrasonic waves. The method was preferred over other methods (i.e. digital camera, laser light transmission and capillary suction probes), as it is applicable in opaque systems (which G-L-L systems are) and it can be used in-situ in the reactor without sampling. Furthermore, the droplet size, which can be an important parameter in the mechanism of gas absorption in gas-liquid-liquid systems, could be determined simultaneously.

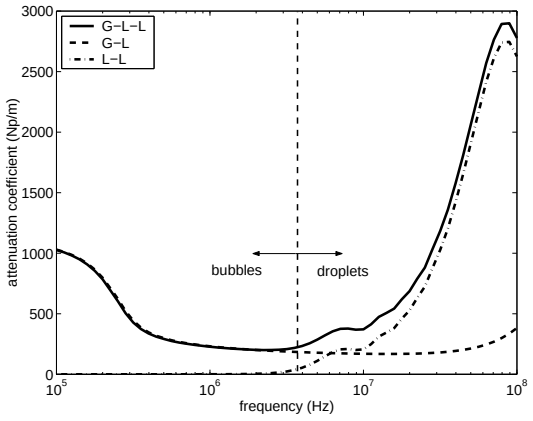

Figure 1: Attenuation coefficient of a G-L-L system with 10% air bubbles of 1 mm and 10% hexadecane droplets of 100 μm.

To obtain this information, both the ultrasonic velocity and the attenuation coefficient of tone-burst signals are determined for a large frequency range (typically 100 kHz - 100 MHz). The attenuation due to the gas bubbles (having a diameter in the order of a few millimeters) is most strong in the lower frequency domain ($<$ 1 MHz). The droplets, which are typically in the range of a few hundred micron or smaller, attenuate in the higher frequency domain (see Figure 1). From the determination of these parameters in a large frequency range, the size distributions and the volume fraction of the different dispersed phases (gas bubbles, liquid drops and/or solid particles) can determined

using a scattering model. It was shown that the gas-liquid interfacial area could be determined very accurately. For the exact size distribution of the gas bubbles in the used size range (1-3 mm) an independent gas hold-up determination is, however, required. Accurate results were obtained for the size distributions in gas-liquid, solid-liquid and gas-liquid-solid systems. The determined size distribution of the solids, both with and without gas bubbles present, showed good agreement with the distribution obtained with a commercial laser-scattering analyzer.

The ultrasonic technique was further used to study the gas-liquid interfacial area in a vessel of standard geometry agitated by a Rushton type turbine. To obtain values for the mass transfer coefficient, k_L, the measurements were combined with experimental determination of the volumetric mass transfer coefficient, k_La, using the dynamic oxygen method. Additionally, the gas hold-up was determined, using an electrical conductivity method, to obtain values for the Sauter mean bubble diameter at different positions in the vessel. In case of a coalescing water system, the interfacial area and bubble size in the vessel were highly non-uniform. A map of 13 points in the vessel was selected and used in an integration procedure, in order to obtain integral values for the mass transfer parameters. The results for the integral values of the interfacial area and the Sauter mean diameter in a coalescing air-water system were in good agreement with the established work of Calderbank (1958). In non-coalescing systems the gas distribution was much more homogeneous and the bubble size could be obtained using measurements at only one or two positions inside the vessel.

The addition of small volume-fractions of toluene to an air-water system caused a strong decrease in both the volumetric mass transfer coefficient and in the gas hold-up. The interfacial area, however, increased. It was shown that this was due to the presence of microbubbles in the solution, which do not take part in the mass transfer process. The enhancing effect on gas-liquid mass transfer due to the addition of larger volume-fractions of toluene could be described reasonably well by a homogeneous model of the shuttle mechanism.

The addition of toluene to a non-coalescing ionic buffer system caused a strong decrease in the gas-liquid interfacial area, as measured using the Danckwerts-

plot technique. These results were confirmed qualitatively by making use of the ultrasonic method in a stirred vessel and in a bubble column. It was shown that the interaction of the gas bubbles with the toluene droplets most likely supports the formation of a small toluene layer around the gas bubble (through bubble-droplet coalescence or via spontaneous formation of this layer). In case of the presence of such a layer, the coalescence properties are no longer determined by the ionic solution around the bubble, but by the toluene layers and then coalescence inhibition probably does not take place. In other words, the non-coalescing ionic buffer solution is transferred into a coalescing system due to the added toluene. Furthermore, a remarkable effect was observed around the point of maximum toluene solubility in an air-water-toluene system. Around this point the system was changed from coalescing to non-coalescing with an increase of interfacial area by a factor of 4. The main cause of this effect lies in the large difference (8 mN/m) of the surface tension (σ) of water with a small toluene layer and water, which is saturated with toluene. Around the point of maximum solubility a large value the surface tension gradient with the concentration ($d\sigma/dc$) exists, which increases the coalescence time of two touching bubbles.

Mass transfer effects in the presence of chemical reaction were studied for the industrially important biphasic hydroformylation of propylene. In this process propylene reacts with carbon monoxide and hydrogen to form mainly n-butyraldehyde, a versatile chemical intermediate. It was shown from model experiments that accurate knowledge of the mass transfer parameters is required to optimize the production rate in this process, as the plot of the production rate versus the power input of the impeller contains a maximum, which is caused by the negative reaction orders of both carbon monoxide as well as propylene. It was determined from separate experimental studies, that the plot of k_La versus the fraction of n-butyraldehyde contained a general trend: the addition of a small fraction of butyraldehyde causes a relatively small increase in k_La, which was most likely caused by the partially compensating effects of a large increase in a accompanied by a decrease in k_L. Beyond the point of maximum butyraldehyde solubility a strong increase (factor 2.5-3) was observed. Experiments showed that this increase was due to an increase in

the mass transfer coefficient, k_L, and was probably caused by the formation of a small butyraldehyde layer around the bubble, thereby removing the rigid layer of butyraldehyde molecules, which was originally responsible for the decrease in the mass transfer coefficient.

It can be concluded from the research study described in this thesis that the mechanism of mass transfer in gas-liquid-liquid systems is still not completely clear. In this work mass transfer experiments were carried out with five different organic dispersed liquids, toluene, 1-octanol, n-heptane, n-dodecane and n-butyraldehyde. Toluene and octanol increased the gas-liquid mass transfer rate, after an initial decrease in k_L (octanol) or a (toluene). The increase in mass transfer could be well described using a homogeneous model of the shuttle mechanism. No strong effects on the mass transfer were observed on the addition of n-heptane and n-dodecane. The addition of butyraldehyde to water initially caused an increase in the gas-liquid interfacial area and a simultaneous decrease in the mass transfer coefficient, but this decrease disappears beyond the point of maximum solubility. Ultrasonic spectroscopy was shown to be a valuable tool in the determination of size distributions of different phases in multi-phase systems, and can therefore be used to perform additional research on this topic.

Samenvatting

De interesse in meer-fasen systemen (gas-vloeistof-vloeistof) is de laatste jaren sterk gegroeid, met name door de introductie van homogene twee-fase katalyse in verschillende reactiesystemen. Voorbeelden hiervan zijn: hydroformylering, carbonylering, hydrogenering en oligomerizatie (Cornils, 1999). Het grote voordeel van deze systemen in vergelijking tot katalyse in één fase sytemen is de eenvoudige scheiding van de reactanten en de producten. Op deze manier worden de voordelen van homogene katalyse (geen interne stofoverdrachtslimiteringen en vaak hogere selectiviteiten) en van heterogene katalyse (simpele scheiding van de katalysator) gecombineerd. Belangrijke industriële applicaties zijn het SHOP-proces en de hydroformylering van propeen tot butyraldehyde.

De snelheid van stofoverdracht is veelal een bepalende factor in industriële toepassingen, maar vaak is het mechanisme van stofoverdracht nog niet goed bekend. Dit is bijvoorbeeld het geval voor gas-vloeistof-vast (G-L-S) en gas-vloeistof-vloeistof (G-L-L) systemen. De wetenschappelijke publicaties over stofoverdracht in G-L-L systemen beperken zich tot de experimentele bepaling van de volumetrische stofoverdrachtscoëfficiënt, $k_L a$. Echter, om meer inzicht in het mechanisme van stofoverdracht te vergaren, is besloten om in dit onderzoek de stofoverdrachtscoëfficiënt, k_L en het specifiek uitwisselend oppervlak, a, afzonderlijk te bepalen.

Een bekende methode voor de bepaling van beide stofoverdrachtsparameters is het gebruik van de Danckwerts-plot techniek. Door een gasfase component te laten reageren via een matig snelle reactie, is het mogelijk om zowel k_L als a te bepalen door het meten van de absorptiesnelheid bij verschillende reactiesnelheden. Deze techniek is gebruikt om het effect van de toevoeging van verschillende volume

fracties van vier disperse organische fasen ,te weten 1-octanol, tolueen, heptaan en dodecaan, aan een waterige fase op de stofoverdrachtsparameters te bestuderen. De resultaten van dit werk laten zien dat er twee soorten G-L-L systemen bestaan; systemen met een disperse fase die de stofoverdracht versnelt en systemen waarin de stofoverdracht niet versneld wordt. Versnelling is waargenomen in geval van octanol en tolueen en deze kon goed beschreven worden met een homogeen model op basis van het shuttle-mechanisme (Bruining et al., 1986). In dit mechanisme ontstaat er versnelling van de stofoverdracht door de aanwezigheid van disperse druppels in de stofoverdrachtszone, met een grotere capaciteit voor het over te dragen gas. Zo onstaat er lokaal een grotere drijvende kracht voor stofoverdracht, wat weer leidt tot een verhoogde flux.

Echter, in het geval van heptaan en dodecaan, die ook een grotere capaciteit voor het over te dragen gas hebben, is geen versnelling van de stofoverdracht geconstateerd. Schijnbaar zijn er dus twee mechanismen voor dit verschil verantwoordelijk. Wanneer het correcte mechanisme wordt gebruikt in de stofoverdrachtsberekeningen (shuttle-mechanisme voor octanol en tolueen en geen versnelling voor heptaan en dodecaan), blijft de waarde voor k_L (in feite de oppervlakte verversingssnelheid in het Danckwerts model) constant tot 40 volume-% disperse fase.

In de stofoverdrachtsexperimenten ter bepaling van k_L en a is een pseudo-eerste orde reactie systeem is gebruikt, omdat er geen bruikbaar eerste orde reactie systeem beschikbaar was. Er is gebruik gemaakt van absorptie van CO_2 in een carbonaat/bicarbonaat buffer oplossing met verschillende hoeveelheden natriumhypochloriet als katalysator. In de literatuur is geen bewijs gevonden voor de aanname dat de additie van grotere hoeveelheden katalysator (tot 0.2 M) geen invloed heeft op de hydrodynamica van het systeem, terwijl dit systeem al door meerdere onderzoekers gebruikt is. Om deze aanname te staven zijn experimenten uitgevoerd waarin simultaan de absorptiesnelheid van CO_2 en de desorptiesnelheid van zuurstof werden gemeten. De desorptiesnelheid van zuurstof werd niet beïnvloed door de toevoeging van de katalysator, hetgeen een sterke indicatie is dat de hydrodynamica en de fysische eigenschappen van het systeem onveranderd zijn gebleven. In de constructie van het Danckwerts-plot is de variatie van de reactiesnelheid door het veranderen

van de katalysator concentratie over een groot bereik dus gerechtvaardigd.

De gemeten absorptiesnelheid van CO_2 was echter veel lager in verhouding tot de desorptiesnelheid van zuurstof. Dit is waarschijnlijk het gevolg van de hoge uitputtingsgraad van de gasbellen met een lange verblijftijd in de oplossing. Dit heeft een groter effect op de bepaalde stofoverdrachtsparameters voor CO_2 dan op die voor zuurstof door de hogere fysische oplosbaarheid van CO_2 in waterige oplossingen.

Een nadeel van de Danckwerts-plot techniek is het feit dat deze beperkt is tot een aantal specifieke chemische systemen. Om het gas-vloeistof specifiek oppervlak te bestuderen in niet-chemische systemen is er een fysische meettechniek ontwikkeld die gebruik maakt van de demping en de snelheid van ultrasone geluidsgolven. Deze methode is geselecteerd ten faveure van andere technieken (zoals digitale camera, laser licht transmissie en iso-kinetisch afzuigen) vanwege de toepasbaarheid in ondoorzichtige systemen (wat G-L-L systemen zijn) en vanwege het feit dat de methode in-situ (zonder bemonstering) gebruikt kan worden. Een bijkomend voordeel is dat de druppelgrootte, die een belangrijke parameter kan zijn in het mechanisme van gas absorptie, simultaan bepaald kan worden.

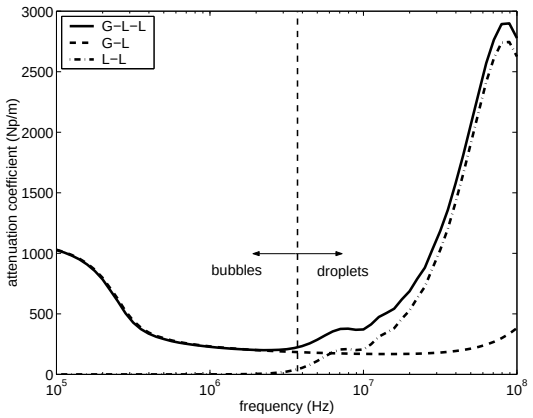

Figuur 1: Dempingscoëfficiënt van een G-L-L systeem met 10% luchtbellen van 1 mm en 10% hexadecaan druppels van 100 μm.

Om deze informatie te verkrijgen zijn de ultrasone geluidssnelheid en de demping bepaald over een groot frequentiebereik (100 kHz - 100 MHz). De demping door de aanwezigheid van de gasbellen is erg sterk in het lage-frequentie gebied ($<$ 1 MHz). De druppels, meestal 100 micrometer of kleiner, veroorzaken een hoge demping in het hoge-frequentie gebied (zie Figuur 1). Door het bepalen van de demping en de geluidssnelheid over een groot frequentiebereik is het mogelijk om de grootteverdelingen en de volume fractie van verschillende disperse fasen (bellen, druppels en deeltjes) te bepalen met behulp van

een diffractie model. Het bleek tevens mogelijk om zeer nauwkeurig het specifiek oppervlak van de bellen te bepalen. Voor de exacte distributie van de belgrootte in het bereik van 1 tot 3 mm is echter een onafankelijke meting van de gas fractie noodzakelijk. In gas-vloeistof, vloeistof-vast en gas-vloeistof-vast systemen zijn goede resultaten behaald in de bepaling van de grootteverdelingen. De bepaalde deeltjesgrootteverdeling kwam goed overeen met de distributie die bepaald was met een commerciële laser-diffractie methode, zowel met als zonder gasbellen in de dispersie.

De ultrasoon-techniek is verder gebruikt om het specifiek gas-vloeistof oppervlak te bepalen in een vat van standaard afmetingen, met daarin een Rushton turbine roerder. Om waarden voor de stofoverdrachtscoëfficiënt, k_L, te bepalen werden deze metingen gecombineerd met de experimentele waarden van de volumetriche stofoverdrachtscoëfficiënt, k_La, die werden verkregen via de dynamische zuurstof methode. Uit de gemeten electrische geleidbaarheid van de dispersie werd de lokale gas fractie bepaald, waarmee de oppervlakte gemiddelde diameter berekend kon worden. In het geval van een coalescerend lucht-water systeem waren het specifiek oppervlak en de beldiameter sterk niet-uniform verdeeld over het vat. De integrale waarden voor de stofoverdrachtsparameters werden verkregen door een integratie over 13 geselecteerde posities in het vat. Deze waarden voor het oppervlak en de beldiameter in coalescerende lucht-water systemen kwamen goed overeen met het gevestigde werk van Calderbank (1958). In niet-coalescerende systemen was de distributie van het gas veel meer homogeen en de beldiameter kon bepaald worden door het meten op één of twee goed gekozen posities in het vat.

De toevoeging van kleine fracties tolueen aan een water-lucht systeem veroorzaakte een sterke daling van de volumetrische stofoverdrachtscoëfficiënt en van de gas fractie. Het bepaalde specifiek oppervlak was daarentegen hoger. Dit wordt veroorzaakt door de aanwezigheid van micro-bellen die niet deelnemen aan het stofoverdrachtsproces. Het stofoverdrachtsversnellende effect van grotere fracties tolueen kon redelijk goed beschreven worden met een homogeen model van het shuttlemechanisme.

Uit metingen met de Danckwerts-plot techniek bleek dat het toevoegen van

tolueen aan een niet-coalescerend carbonaat/bicarbonaat buffer-systeem een sterke daling van het specifiek oppervlak tot gevolg had. Deze resultaten werden kwalitatief bevestigd door metingen met de ultrasoon-techniek in een bellenkolom en in een geroerd vat. De interactie van gasbellen met tolueendruppels bleek de vorming van van een kleine tolueen film rond de gasbel mogelijk te maken (door druppel-bel coalescentie of door de spontane vorming van die laag). Wanneer er zo'n laag om de bel aanwezig is worden de coalescentie eigenschappen niet langer bepaald door het electroliet, maar door de tolueen laag, wat tot gevolg heeft dat coalescentie waarschijnlijk niet meer onderdrukt wordt. Met andere woorden: door het toevoegen van tolueen wordt de niet-coalescerende buffer oplossing veranderd in een coalescerend systeem. Verder werd een een opzienbarend effect waargenomen rond het oplosbaarheidspunt van tolueen in een lucht-water-tolueen systeem. Rond dit punt veranderde de toestand van het systeem van coalescerend naar niet-coalescerend, hetgeen gepaard ging met een stijging van het specifiek oppervlak met een factor 4. Dit lijkt het gevolg van het grote verschil in oppervlaktespanning (σ) van 8 mN/m tussen water met een dunne laag tolueen erop en water verzadigd met tolueen. Hierdoor ontstaat er rond het oplosbaarheidspunt een sterke gradiënt in de oppervlaktespanning ($d\sigma/dc$), die de coalescentietijd tussen twee bellen die elkaar raken doet toenemen.

Stofoverdracht in combinatie met een chemische reactie is bestudeerd voor de industrieel relevante hydroformylering van propeen naar butyraldehyde. In dit proces reageert propeen met koolmonoxide en waterstof tot voornamelijk n-butyraldehyde, wat een veelgebruikt tussenproduct is. Uit modelberekeningen is gebleken dat nauwkeurige kennis van de stofoverdrachtsparameters noodzakelijk is om de productiesnelheid te optimalizeren. Dit komt voornamelijk doordat de grafiek van de productiesnelheid tegen de energie invoer via de roerder een maximum heeft, wat veroorzaakt wordt door de negatieve reactie ordes voor zowel koolmonoxide als propeen. Door het uitvoeren van een experimentele stofoverdrachtsstudie bleek dat de grafiek van k_La tegen de butyraldehydefractie een trend vertoonde: de additie van een kleine hoeveelheid butyraldehyde leidde tot een kleine stijging van k_La, die op zijn beurt werd veroorzaakt door de deels compenserende effecten van een

sterke stijging van a en een daling van k_L. Deze laatste daling is waarschijnlijk het gevolg van de vorming van een rigide laag butyraldehyde moleculen aan het grensvlak. Bij butyraldehyde concentraties hoger dan de oplosbaarheid werd een sterke stijging van de waarde van $k_L a$ (factor 2.5-3) geconstateerd. Uit afzonderlijke experimenten bleek dat deze stijging veroorzaakt werd door een toename van de stofoverdrachtscoëfficiënt, k_L. Dit lijkt het gevolg van de vorming van een butyraldehyde film rond de bellen, die de rigide laag van butyraldehyde moleculen kan opheffen.

Dit onderzoek heeft duidelijk gemaakt dat het mechanisme van stofoverdracht in G-L-L systemen nog steeds niet volledig duidelijk is. In dit werk zijn experimenten uitgevoerd met vijf verschillende oranische disperse fasen: tolueen, 1-octanol, heptaan, dodecaan en butyraldehyde. Tolueen en octanol veroorzaakten een stijging van de stofoverdrachtssnelheid, na een initiële afname van k_L (octanol) of van a (tolueen). De stijging van de stofoverdrachtssnelheid kon goed worden beschreven met een homogeen model van het shuttle-mechanisme. Geen sterke effecten op de stofoverdracht werden geconstateerd na toevoeging van dodecaan en heptaan. De additie van butyraldehyde aan water leidde aanvankelijk tot een toename van het specifiek stofuitwisselend oppervlak en tegelijkertijd een daling in de stofoverdrachtscoëfficiënt. De daling verdween na het bereiken van de maximale butyraldehyde oplosbaarheid.

Ultrasone spectrometrie is een zeer waardevolle techniek gebleken voor de bepaling van grootteverdelingen van verschillende fasen in meerfase-systemen en kan daarom gebruikt worden bij verder onderzoek op dit gebied.

Contents

Chapter 1

Gas absorption in agitated Gas-Liquid-Liquid systems using the Danckwerts-plot technique

Abstract

Gas-liquid-liquid systems have gained interest during the past decade and are encountered in several important industrial applications. In these systems the presence of an immiscible liquid phase may affect the gas absorption rate significantly. This phenomenon, however, is not completely understood and the underlying mechanisms need further clarification. In the present study the well known Danckwerts-plot technique is used to determine simultaneously the liquid side mass transfer coefficient k_L and the gas-liquid interfacial area a in this type of system. As absorption/reaction system CO_2 absorption in a 0.5 M K_2CO_3 / 0.5 M $KHCO_3$ buffer solution catalysed by sodium hypochlorite was chosen. Toluene, n-dodecane, n-heptane and 1-octanol were applied as dispersed liquid phases. The Danckwerts-plot could be well used in gas-liquid-liquid systems and from the results it appeared that two types of systems exist; systems in which mass transfer is enhanced by dispersed phase droplets and systems that do not show enhanced mass transfer. Effects at low dispersed phase hold-up were observed to be very strong and are thus important, but were not taken

into account in further analysis of the effect of the dispersed phase hold-up on mass transfer. In systems where dodecane and heptane were added to the buffer solutions no enhancement of mass transfer was observed. However, the addition of toluene and 1-octanol caused an enhancement of mass transfer that could be well described using a homogeneous model of the shuttle mechanism.

1.1 Introduction

Gas-liquid-liquid systems have gained interest in the past decade due to the introduction of homogeneous biphasic catalysis in various reaction systems, e.g. hydroformylation, carbonylation, hydrogenation and oligomerization (Cornils, 1999). The main advantage of these systems over catalysis in one phase is the easy separation of the catalyst and the reactants or products. In this way advantages of homogeneous catalysis (no internal mass transfer limitations and often higher selectivities) and of heterogeneous catalysis (easy catalyst separation) can be combined. Important industrial applications are e.g. the SHOP-process and hydroformylation of propene to butyraldehyde.

Gas-liquid-liquid systems are further encountered in reaction systems that inherently consist of three phases due to two (or more) immiscible reactants, reaction products or catalyst. For example, in the Koch reaction system all three reactants originate from different phases (Falbe, 1980). Gas-liquid-liquid systems are also encountered in areas in which an additional inert liquid phase is added on purpose to a gas-liquid system to increase the mass transfer rate. This latter concept is e.g. applied in a few biochemical applications (Rols et al., 1990). However, the addition of a second liquid phase can also retard the gas-liquid mass transfer (Yoshida et al., 1970).

In this latter perspective, especially when considering that the gas absorption rate is frequently the capacity determining factor, it is very important to understand the phenomena occurring in these systems for design and operation of these systems. The gas absorption rate in stirred multiphase reactors is usually characterized by the volumetric mass transfer coefficient $k_L a$. In this coefficient the liquid

side mass transfer coefficient k_L as well as the interfacial area a are discounted.

To study the underlying phenomena of the effect of adding an immiscible liquid phase on the gas absorption rate for a gas-liquid system, it is considered necessary to separate the effects on the interfacial area a from those on the liquid side mass transfer coefficient k_L. In this work the Danckwerts-plot technique, to measure k_L and a simultaneously by chemical absorption, is used to study the effects of the addition of different immiscible organic phases. In this work four different gas-liquid-liquid systems will be studied.

1.2 Previous work

One of the first encounters in literature on gas-liquid-liquid systems is the work of Yoshida et al. (1970). In their work the oxygen absorption rate was measured in aqueous dispersions of kerosene and toluene. The observed effects on the addition of these dispersed phases were very different. The addition of kerosene resulted in a decrease of the volumetric mass transfer coefficient k_La. On the other hand, toluene caused, after a sharp initial decrease, a strong increase in k_La at higher hold-ups.

Linek and Beneš (1976) studied gas absorption in liquid-liquid systems with a known value for the gas-liquid interfacial area to determine the influence on the liquid side mass transfer coefficient k_L. They studied oxygen absorption in aqueous emulsions with a mixture of n-alkanes and with oleic acid. The value of k_L remained practically constant in the presence of n-alkanes before phase inversion, while the addition of oleic acid caused an initial decrease of k_L. When more oleic acid was added, k_L increased again.

A few studies have been presented in literature on the influence of a second immiscible liquid on the gas-liquid interfacial area. Mehta and Sharma (1971) used a fast reaction, CO_2 - NaOH system, to study the influence of 2-ethyl-hexanol on the specific gas-liquid interfacial area. According to the authors the area increased due to a prevention of bubble coalescence. Das et al. (1985) studied the interfacial area in gas-liquid-liquid systems with both a physical and a chemical method. As dispersed phases 2-ethyl-hexanol, toluene and methyl-isobutyl-ketone were used.

All systems showed initially an increase in the interfacial area with higher dispersed phase fraction, but above approximately 10% hold-up the area started decreasing. The increase was explained by prevention of bubble coalescence, while a diminished level of turbulence in the reactor caused the decrease at higher hold-ups, according to the authors.

Two types of mechanisms have been proposed in literature to explain the experimental results, thereby focussing on the gas absorption enhancement effect. The first one is the so-called shuttle- or grazing mechanism, analogous to the one in gas-liquid-solid three phase systems. The mechanism is based on dispersed phase drops entering the mass transfer film at the gas-liquid interface to enhance mass transfer due to their higher solubility for the gas phase component to be transferred and is explained in Figure 1.1A. A homogeneous model describing this mechanism was proposed by Bruining et al. (1986). They tested the model using oxygen absorption in aqueous solutions using n-hexadecane as a dispersed phase. Brilman et al. (2000) recently developed 3-D heterogeneous mass transfer models to study this grazing effect in more detail. From their overview of all models describing these effects, it can be concluded that, although these heterogeneous models are to be preferred from a physical point of view, the homogeneous models describe the experimental data equally well for simple cases and require less detailed input parameters. The second mechanism proposed to describe the mass transfer enhancement is the so-called coalescence-redispersion mechanism, which is based on direct contact between gas and the dispersed phase by formation of gas-liquid complexes (Rols et al., 1990). This mechanism is outlined in Figure 1.1B. The gas absorption rate is then enhanced due to the introduction of this second transfer path.

Concluding from experiments and models reported in the literature, it appears that there is a lot of confusion about the gas absorption mechanism and effects in gas-liquid-liquid systems. By studying experimentally the effects on k_L and a separately, more insight on the mechanisms that occur may be obtained.

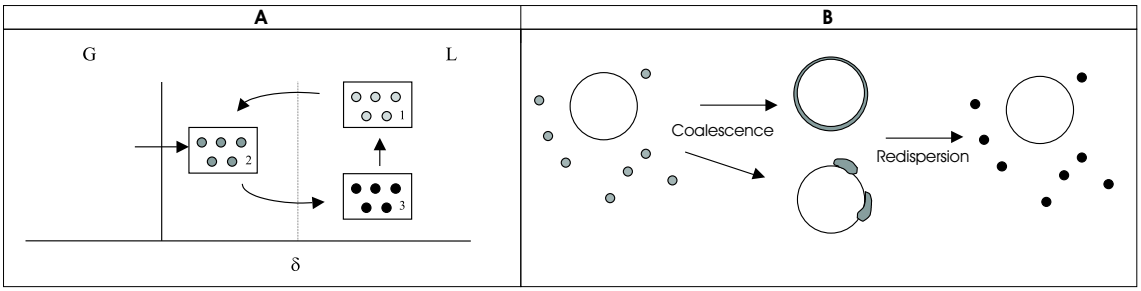

Figure 1.1: A: shuttle-mechanism; B: coalescence-redispersion mechanism.

1.3 Experimental technique

1.3.1 Danckwerts-plot

For a better analysis of the observed effects on the mass transfer rate, the simultaneous determination of the liquid side mass transfer coefficient k_L and the interfacial area a has been selected, using the well-known Danckwerts-plot technique (Danckwerts, 1970). The major advantage of this chemical absorption method over a physical absorption technique is that, when the reaction is fast enough, the bulk concentration of the dissolved gas is negligible, which implies that the driving force for mass transfer is well known. This allows for accurate determination of the mass transfer parameters k_L and a during stationary conditions. The determination of the interfacial area by physical measurement techniques in gas-liquid-liquid systems is also difficult to perform. The dispersions are often completely opaque, which implies that laser- and photographic techniques are difficult to use in these systems. Also the use of intrusive methods like a capillary technique to determine bubble sizes is not without severe complications in these systems. Non-representative sampling, coalescence and break-up during sampling and the disturbance of the flow-pattern can be disadvantageous in these methods. By using the Danckwerts-plot technique a representative tank-averaged absorption rate is determined, circumventing the above mentioned difficulties.

According to the Danckwerts surface renewal model for mass transfer, the rate of absorption for a irreversible, first order reaction with negligible bulk concentration can be described as:

$$R_A = k_L \sqrt{1 + Ha^2}\, c_{AiL}\, a\, V_L \tag{1.1}$$

This equation holds when the gas side mass transfer resistance can be neglected. Ha is the Hatta-number that is defined for a first order or pseudo-first order reaction by:

$$Ha = \sqrt{\frac{k_{1,app} D_A}{k_L^2}} \tag{1.2}$$

From these equations it can be seen that by changing the value of the apparent rate constant $k_{1,app}$ a straight line can be obtained by plotting $(R_A/c_{AiL}V_L)^2$ versus $k_{1,app}D_A$. In this plot the slope is equal to a^2 and the intercept with the vertical axis equals $(k_L a)^2$. In this way k_L and a can be determined simultaneously.

1.3.2 System

As an absorption/reaction system carbon dioxide absorption in a 0.5 M potassium carbonate / 0.5 M potassium bicarbonate buffer solution was used. This carbonate / bicarbonate buffer solution is the continuous liquid in the experiments done. As dispersed liquid phase several different organic liquids have been applied; toluene, n-dodecane, n-heptane and 1-octanol. In the continuous liquid phase the following reactions occur:

$$CO_2 + H_2O \underset{k_{-H_2O}}{\overset{k_{H_2O}}{\rightleftharpoons}} HCO_3^- + H^+ \tag{1.3}$$

instantaneously followed by the equilibrium reaction:

$$CO_3^{2-} + H^+ \longleftrightarrow HCO_3^-$$

As a catalyst for reaction of CO_2 with water, sodium hypochlorite is used. This allows for a wide variation of the reaction rate on addition of only small amounts

of catalyst, so that the psycho-chemical parameters of the catalyst/buffer system do not change significantly. As catalytic species hypochlorite was chosen over arsenite because of its lower toxicity.

Due to the pH (≈ 10) also hydroxyl ions will be present in the buffer solution. Carbon dioxide reacts with OH^- according to the following reaction:

$$CO_2 + OH^- \underset{k_{-OH^-}}{\overset{k_{OH^-}}{\rightleftharpoons}} HCO_3^- \tag{1.4}$$

The reaction rates for the reactions with water and hydroxyl ions are both first order with respect to CO_2. Danckwerts (1970) has shown that under certain conditions, which are all fulfilled in this work, the reaction is pseudo-first order with respect to CO_2 and the rate equation is given:

$$r_{CO_2} = \left(k_{H_2O} + k_c c_{cat} + k_{OH^-} c_{OH^-}\right)\left(c_{CO_2} - c_{CO_2,e}\right) \tag{1.5}$$

In this equation $c_{CO_2,e}$ represents the equilibrium concentration of carbon dioxide, which depends among other things on the carbonate and bicarbonate concentrations (Danckwerts, 1970). Under the experimental conditions the equilibrium concentration $c_{CO_2,e}$ is quite small and Equation 1.5 can now be simplified to:

$$r_{CO_2} = k_{1,app} c_{CO_2} \tag{1.6}$$

Already at very low catalyst concentrations the catalyzed reaction is dominant: $k_c c_{cat} >> k_{H_2O}$ and $k_c c_{cat} >> k_{OH-} c_{OH-}$. This means that the rate of reaction can be easily varied by changing the catalyst concentration.

The kinetics of the uncatalyzed reaction ($k_{H_2O} \approx 0.02 s^{-1}$) were determined by Danckwerts and Sharma (1966). The value of k_{OH-} is strongly dependent on ionic strength and the nature of the cations. k_{OH-} was estimated to be 11.6 $m^3\ mol^{-1}\ s^{-1}$ using the work of Pohorecki and Moniuk (1988). Sharma and Danckwerts (1963) and Benadda et al. (1994) measured kinetic constants of the sodium hypochlorite catalyzed reaction in a 0.5 M Na_2CO_3 / 0.5 M $NaHCO_3$ buffer and in a 0.4 M

K_2CO_3 / 0.4 M $KHCO_3$ buffer respectively. Although the value of k_c depends on ionic strength and on the counter ion of the buffer, the values were not very different at 293 K. A value for k_c of 1.8 m^3 mol^{-1} s^{-1} (at 294 K) was used in the mass transfer calculations. For studying the effect of an immiscible liquid phase on the mass transfer coefficient k_L and a their absolute values are of minor importance. Therefore, in this work especially the relative changes in k_L and a will be studied. The solubility of carbon dioxide in the buffer solution is estimated using the work of Weisenberger and Schumpe (1996).

$$\log\left(\frac{c_{G,0}}{c_G}\right) = \sum (h_i + h_G) \cdot c_i \tag{1.7}$$

The constant for the influence of the gas was found to be linearly dependent on temperature:

$$h_G = h_{G,0} + h_T(T - 298.15) \tag{1.8}$$

in which c_i are the concentrations of all the ions present in the solution. The value of $(c_{G,0}/c_G)$ was determined to be 1.66. The solubility of carbon dioxide and the diffusion coefficient in water were determined using correlations proposed by Versteeg and Van Swaaij (1988):

$$He_{CO_2/H_2O} = 3.59 \cdot 10^{-7} \exp\left(\frac{2044}{T}\right) \tag{1.9}$$

$$D_{CO_2/H_2O} = 2.35 \cdot 10^{-6} \exp\left(\frac{-2119}{T}\right) \tag{1.10}$$

The diffusion coefficient of CO_2 in the (K_2CO_3 / $KHCO_3$) buffer solution can be estimated by a correlation of Joosten and Danckwerts (1972) and was estimated to be $1.5 \cdot 10^{-9}$ m^2 s^{-1}.

$$\left(\frac{D_{CO_2/buffer}}{D_{CO_2/water}}\right) = \left(\frac{\mu_{water}}{\mu_{buffer}}\right)^{0.818} \tag{1.11}$$

Table 1.1: Physical and chemical parameters at 21 °C.

parameter	value	unit	parameter	value	unit
k_{H_2O}	0.02	s^{-1}	$h_{CO_2,T}$	-0.338	10^3 m^3/(kmol K)
k_{OH^-}	11.6	m^3/(mol s)	m_{CO_2}	0.554	-
k_c	1.8	m^3/(mol s)	D_{CO_2}	1.49	10^9 m^2/s
h_{K^+}	0.0922	m^3/kmol	ρ_{buffer}	1084	kg/m^3
$h_{HCO_3^-}$	0.0967	m^3/kmol	μ_{buffer}	1.21	10^3 Pa s
$h_{CO_3^{2-}}$	0.1423	m^3/kmol	V_L	2.50	10^3 m^3
$h_{CO_2,0}$	-0.0172	m^3/kmol	Φ_G	1.69	10^4 m^3/s

The viscosity of the buffer solution was estimated from the Handbook of Chemistry and Physics (Lide, 1994). All physical and chemical parameters used in the calculations are summarized in Table 1.1.

1.3.3 Set-up

The set-up consists of a gas premix section, a reactor and an analysis section, which is schematically shown in Figure 1.2. In the premix section the feed gas is composed using two mass flow controllers (one for CO_2 and one for N_2). The feed gas is introduced at the bottom of the stirred tank using a single orifice (1 mm). The unabsorbed carbon dioxide and nitrogen leave the reactor at the top. Condensable liquid components from the reactor are condensed in a cold trap. This cold trap consists of an ice bath at 273 K and a cryostat at 258 K. The CO_2-concentration is then analyzed by an infrared analyzer and recorded versus time by a personal computer.

The reactor is jacketed and has a working volume of 2.5 liters and an inner diameter of 149 mm. The dispersions inside the reactor are agitated by a 6-bladed Rushton-turbine. The diameter of the turbine is 1/3 of the inner diameter of the tank and is placed 50 mm above the bottom of the reactor. Four baffles with a width of 15 mm ensure adequate mixing within the reactor. The pressure control in the reactor consists of a 1.5 meter water column, which also serves as a sparge for the gas that is not led through the CO_2-analyzer. Experiments were carried

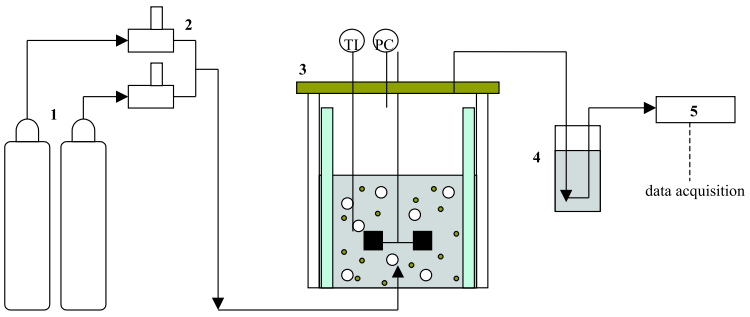

Figure 1.2: Experimental set-up 1:gas cylinders, 2:mass flow controllers, 3:reactor, 4:cold trap, 5:CO_2-analyzer.

out at a constant temperature of 294 K and a pressure of approximately 1.15 bars. Power input and total liquid volume were kept constant during all the experiments. The stirrer rate was approximately 1100 rpm in all the experiments. The different amounts of buffer solution and organic liquid phase were used batchwise in the reactor.

The inlet flow consisted of 1.70 % carbon dioxide, which could be accurately determined (within 0.3 %) by leading the gas directly to the CO_2-analyzer. Gas absorption rate could be calculated by measuring the steady state value of the CO_2 concentration in the outgoing flow. Depletion of CO_2 in the gas phase was always less then 70%, implying that the assumption of an ideally mixed gas phase does not influence the results as indicated by Oyevaar and Westerterp (1989). The depletion of carbonate ions in the liquid phase could be neglected. The gas hold-up was determined using the liquid height before the gassing and the height of the dispersions during the experiments.

The Danckwerts-plot technique was initially applied for the CO_2-buffer two-phase system to check the validity of the method and operating conditions. Subsequently, the same technique was used in the presence of toluene, n-heptane, n-dodecane and 1-octanol as dispersed liquid phase. All chemicals used in this research were of high purity (>99%). Because sodium hypochlorite solutions may decompose spontaneously, the hypochlorite concentration was determined before every experiment by standard iodometric titration.

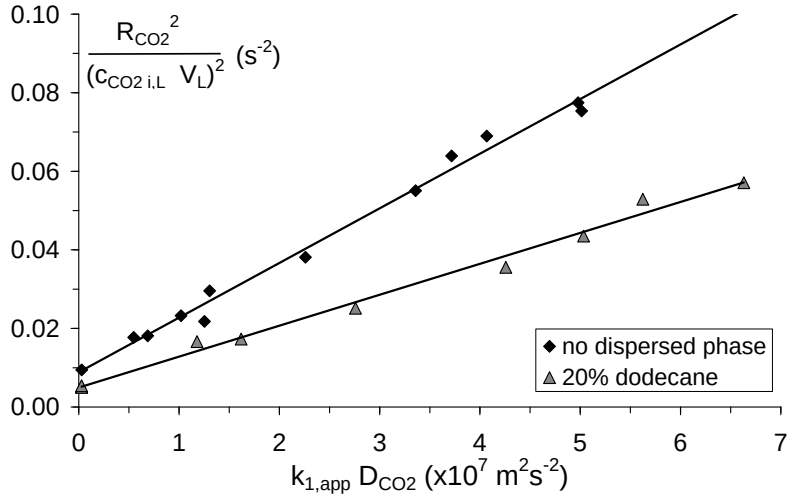

Figure 1.3: Danckwerts-plot without a dispersed phase and in the presence of 20% n-dodecane.

1.4 Results and Discussion

1.4.1 Danckwerts-plots

Both for the CO_2-K_2CO_3/$KHCO_3$ two-phase system as well as for the systems in the presence of a dispersed organic liquid phase the Danckwerts-plots showed excellent linearity, implying that this method can be used for determining the mass transfer coefficient and the interfacial area simultaneously. In Figure 1.3 the Danckwerts-plot for the CO_2-K_2CO_3/$KHCO_3$ two-phase system and an example of a plot for a system with a dispersed organic phase (20 vol-% dodecane) are presented.

1.4.2 Mass transfer parameters

The Danckwerts-plots have been constructed for each dispersed phase at different hold-ups of the organic liquids. In Figure 1.4 the results are presented for the volumetric mass transfer coefficient, k_La, for every dispersed phase used, as determined by the Danckwerts-plot technique.

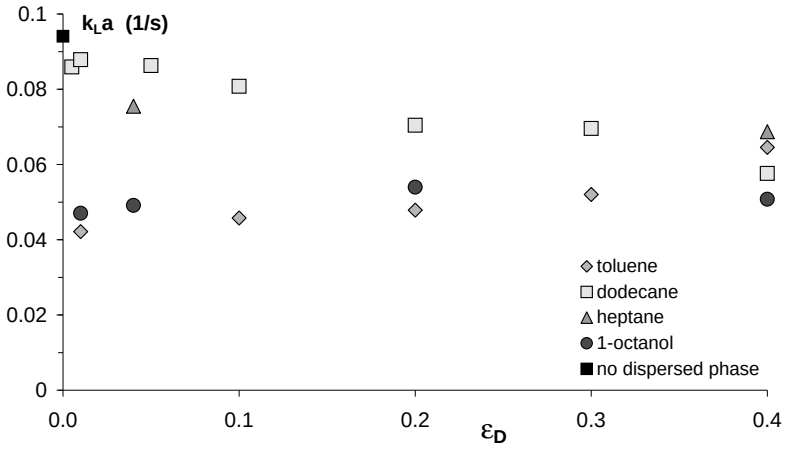

Figure 1.4: Absolute k_La values for the four dispersed phases used.

The initial decrease in k_La at low dispersed organic phase hold-ups is striking, as can be seen in Figure 1.4. These initial effects are very strong in the case of toluene and 1-octanol and less pronounced with dodecane and heptane. From the results of the Danckwerts-plots it was possible to determine both k_L and a. It was found that the initial decrease in k_La on the addition of toluene was completely due to a decrease in the interfacial area (a part of this decrease could be contributed to a decrease in the gas hold-up). The initial decrease in k_La with toluene as a dispersed phase was also observed by Yoshida et al. (1970) in their work on oxygen absorption in aqueous dispersions.

On the other hand, the initial decrease in k_La with the addition of 1-octanol was completely due to a decrease in the value of the mass transfer coefficient k_L, and are probably due to changes in the surface chemistry of the system (surface tension and the formation of semi-rigid boundary layers). Analogous results were also observed by Eckenfelder and Barnhart (1961) in their work on the influence of surfactants (to which 1-octanol can also be accounted for) on mass transfer. As the scope of this work is to study the influence of adding a dispersed phase on the mass transfer rate, the initial effects are important and are studied in more detail in Chapter 5 and in Appendix B. However, to be able to compare the results for the

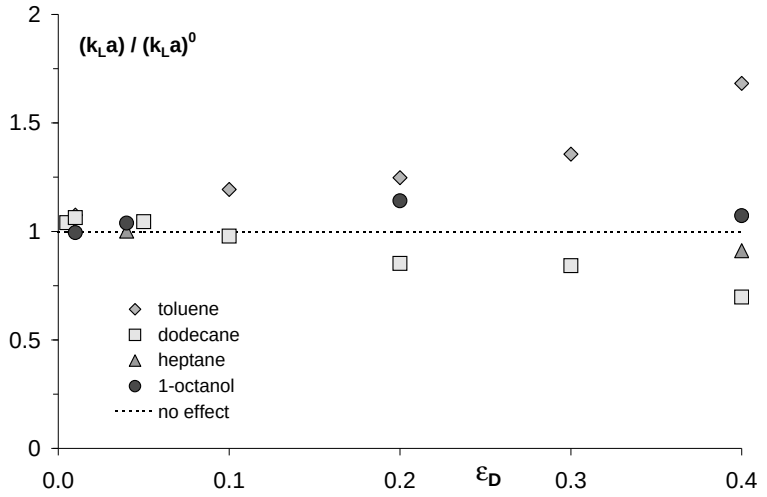

Figure 1.5: Relative k_La values for the four dispersed phases used.

four dispersed phases used at higher organic phase hold-ups the initial effects should not be taken into account. In Figure 1.5 the relative values for k_La are presented for the organic phases used. The relative value of k_La is defined by the ratio of the absolute value of k_La at higher hold-ups to the value obtained from extrapolation to zero hold-up.

From Figure 1.5 it can be seen that the relative values of k_La increase significantly on addition of toluene. The addition of 1-octanol caused a slight increase up to 20% organic phase and at 40% 1-octanol the increment was somewhat lower. The addition of dodecane (and heptane) caused a decrease in the mass transfer rate, despite the fact that all organic dispersed phases used have a higher physical solubility for carbon dioxide when compared to the aqueous buffer solution. Two types of systems appear to exist; one that enhances mass transfer and one that retards mass transfer. This effect was also observed by Yoshida et al. (1970) (see Section 1.2). In their work the addition of kerosene, which is in fact comparable to dodecane, retarded mass transfer and the addition of toluene enhanced mass transfer (after a sharp initial decrease). The effects on the relative values of the mass transfer coefficient k_L as determined from the Danckwerts-plots are presented in Figure 1.6, showing that the relative value of k_L increased on the addition of toluene and

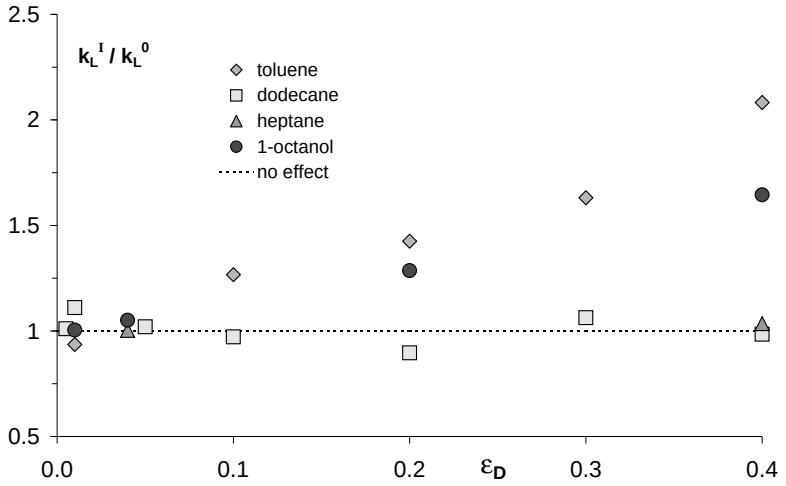

Figure 1.6: Relative k_L values for the four dispersed phases used.

1-octanol. When dodecane and heptane were added to the buffer solutions the liquid side mass transfer coefficient remained practically constant.

In Figure 1.7 the relative values of the interfacial area are plotted versus the fraction dispersed organic phase in the reactor. The absolute value of the interfacial area decreased already at low dispersed phase fractions with the addition of toluene. The relative value of the gas-liquid interfacial area remained approximately constant up to 20% dodecane. Beyond this value, the area started also decreasing.

1.4.3 Interpretation

When a dispersed phase is present in the reactor it is very important that the values for the mass transfer parameters which are obtained from the Danckwerts-plots are analysed correctly. In absence of a second liquid phase the rate of absorption is described by equation 1.1, as is confirmed by the linearity of the Danckwerts-plot (Figure 1.3). Droplets with a higher solubility for the gas phase component to be transferred, however, may change the concentration profile within the mass transfer zone at the gas-liquid interface (if the droplets actually are present in that zone). To describe the rate of absorption in this latter situation a homogenous model of the

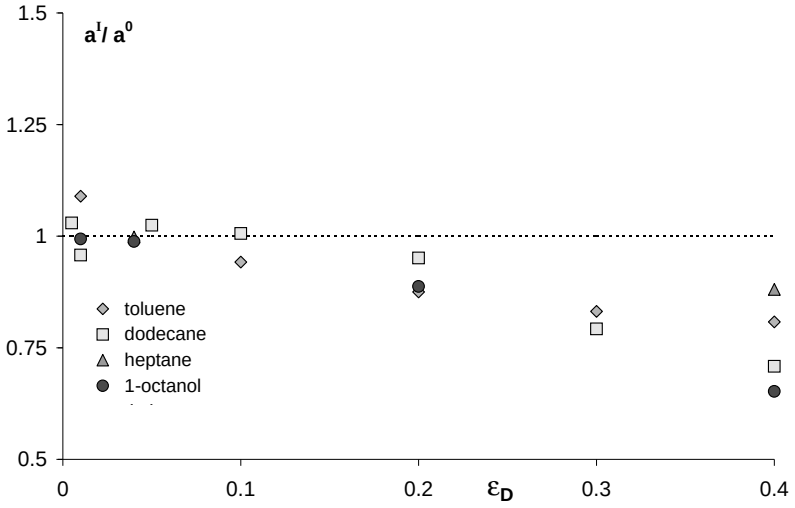

Figure 1.7: Relative values of the interfacial area for the four dispersed phases used.

shuttle-mechanism (Section 1.2) was used. This model was chosen to determine if the presence of immiscible dispersed phase droplets within the mass transfer zone could explain the observed effects on the gas-liquid absorption rates measured and on the corresponding mass transfer parameters k_L and a as determined by the Danckwerts-plot technique. When using a homogeneous model of the shuttle-mechanism for the description of the absorption process, implicitly a few assumptions are made:

1. The dispersed phase is equally divided throughout the gas-liquid mass transfer zone.

2. The concentration of carbon dioxide in the dispersed phase is at any time and place within the mass transfer zone at equilibrium with its concentration in the surrounding continuous phase.

3. The presence of the microphase droplets does not influence the surface renewal frequency of the continuous liquid phase.

The second assumption implies that liquid-liquid mass transfer resistance is neglected, which may not necessarily be true. The liquid-liquid mass transfer

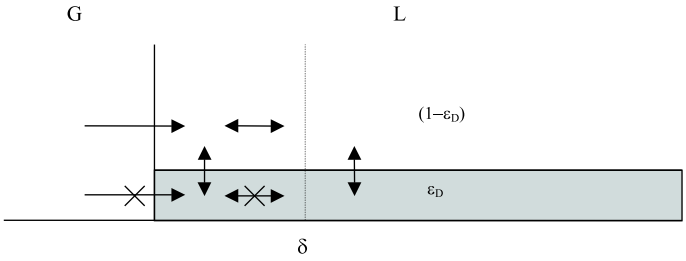

Figure 1.8: Homogeneous model of the shuttle-mechanism.

coefficient depends among other things upon the diffusion coefficients and the diameter of the droplets. Detailed information on these parameters was not available for the systems under consideration. The liquid-liquid interfacial area is, however, in most cases much larger compared to the gas-liquid interfacial area, because the droplets are in general one order of magnitude smaller compared to the gas bubbles. A schematic overview of the homogeneous model of the shuttle mechanism is given in Figure 1.8.

According to the Danckwerts surface renewal model the concentration profile of a gas phase component A, that is being absorbed in a liquid containing microphase droplets within the mass transfer zone, can be described by equation 1.12, assuming a first order reaction in the continuous phase:

$$D_A \frac{\partial c_A^2(x,t)}{\partial x^2} = k_1(1-\varepsilon_D)c_A(x,t) + (1+\varepsilon_D\,(m_R-1))\,\frac{\partial c_A(x,t)}{\partial t} \tag{1.12}$$

with boundary conditions:

$$\begin{aligned} &t = 0, x > 0 : c_A(x,t) = c_{A,bulk} \\ &t > 0, x = 0 : c_A(x,t) = c_{AiL} \\ &t > 0, x = \infty : c_A(x,t) = c_{A,bulk} \end{aligned} \tag{1.13}$$

When the capacity of the liquid bulk is sufficient, the concentration of the gas in the bulk can be assumed zero; $c_{A,bulk} = 0$. Equation 1.12 can now be solved

Table 1.2: Interpretation of the Danckwerts-plot.

	Case I	Case II
Slope	a^2	$a^2 \cdot (1 - \varepsilon_D)$
Intercept	$(k_L a)^2$	$(k_L a)^2 \cdot (1 + \varepsilon_D(m_R - 1))$

analytically and the flux through the gas-liquid interface, according to the Danckwerts surface renewal model, is given in equation 1.14:

$$R_A = k_L \sqrt{1 + \varepsilon_D(m_R - 1) + (1 - \varepsilon_D)Ha^2} c_{aiL} a V_L \tag{1.14}$$

The Hatta-number is defined in equation 1.2. Now it is possible to define an enhancement factor for the presence of a dispersed phase and a first order reaction in the continuous phase according to a homogeneous model of the shuttle-mechanism. The enhancement factor E_D in equation 1.15 is the ratio of the flux in equation 1.14 and the flux in case there is no dispersed phase present ($\varepsilon_D = 0$):

$$E_D = \frac{R_A(\varepsilon_D \neq 0)}{R_A(\varepsilon_D = 0)} = \sqrt{\frac{1 + \varepsilon_D(m_R - 1) + (1 - \varepsilon_D)Ha^2}{1 + Ha^2}} \tag{1.15}$$

As is shown in equation 1.14 there is a difference in the interpretation of the Danckwerts-plot when there are no dispersed phase drops present in the mass transfer region (case I) and when there are (case II). When the results of the gas absorption measurements are plotted as explained in paragraph 1.3.1, $(R_A/c_{AiL}V_L)^2$ versus $k_{1,app}D_A$, the intercept with the vertical axis and the slope of the Danckwerts-plot can be interpreted as shown in Table 1.2.

Analysis of the mass transfer parameters for the different organic liquid phase fractions in the reactor showed two different effects for the dispersions used in this research. The addition of toluene and 1-octanol caused an increase in the value of the mass transfer coefficient when case I is applied for analysis of the Danckwerts-plot, like is done in Fig. 1.6. However, this k_L value remained practically constant in case II, when assuming organic drops to be present within the mass transfer zone enhancing absorption rate. The value of k_L was expected to remain practically

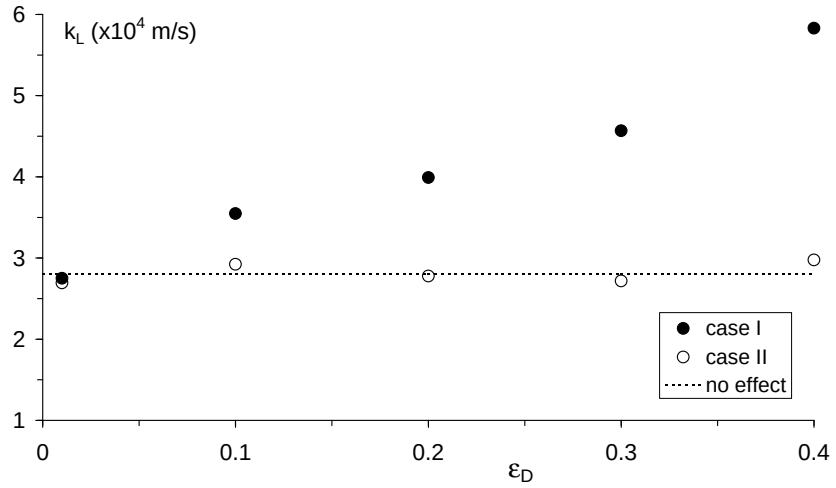

Figure 1.9: k_L versus toluene hold-up when both case I and case II are assumed.

constant, because this value mainly depends on power dissipation and hydrodynamic conditions, which could be assumed constant in all experiments. In Figure 1.9 the dependence of k_L on the toluene fraction is presented when cases I and II are assumed.

From Figure 1.9 it appears that the Danckwerts-plot in the presence of toluene and 1-octanol is probably best interpreted using case II. Mass transfer in these systems is then enhanced by the addition of a dispersed phase and the surface renewal frequency is constant and thus not influenced by the dispersed phase droplets. However, with dodecane and heptane as dispersed phases a completely different effect was observed. When case I was chosen for the interpretation of the Danckwerts-plot the value of k_L remained at a constant level, while under case II the value decreased with increasing fraction of dispersed phase. In Figure 1.10 an example of this effect is shown with dodecane as the dispersed phase.

From Figure 1.10, and the fact that mass transfer is not enhanced by dodecane or heptane (see Section 1.4.2), it can be concluded that for these systems no dispersed phase is likely to be present in the mass transfer region and case I is favored to interpret the mass transfer parameters. The mass transfer parameters k_L and a as determined from the Danckwerts-plots when case II is applied are presented

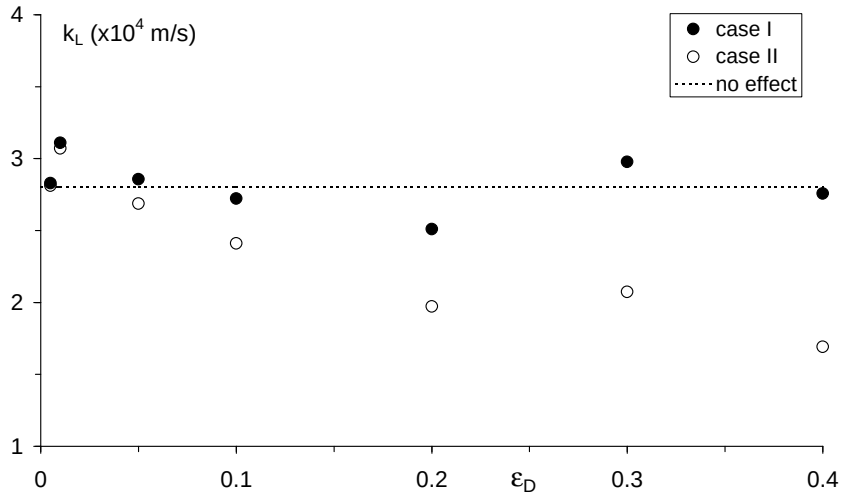

Figure 1.10: k_L versus dodecane hold-up when both case I and case II are assumed.

in Figures 1.11 and 1.12.

The results indicate that probably two types exist within the four of gas-liquid-liquid systems studied. In this work an enhancement of mass transfer was observed (when initial effects are discarded) with increasing amounts of toluene and 1-octanol added to the buffer solutions. The addition of dodecane and heptane, however, caused a decrease of mass transfer.

For the addition of toluene and 1-octanol the effects on k_L can be explained best when assuming dispersed droplets to be present in the mass transfer zone (case II, see Fig. 1.11). The value of k_L^{II}/k_L^0 now remains practically constant as was expected for constant power dissipation.

In Fig. 1.13 the data of Fig. 1.6 are re-plotted together with the model predictions for the shuttle mechanism. When using a Case I Danckwerts'plot interpretation for a situation in which droplets are present within the mass transfer zone, the apparent k_L^I coefficient is described by Eq. (1.16) (see Table 1.2):

$$\frac{k_L^I}{k_L^0} = \sqrt{\frac{1+\varepsilon_D(m_R-1)}{1-\varepsilon_D}} \tag{1.16}$$

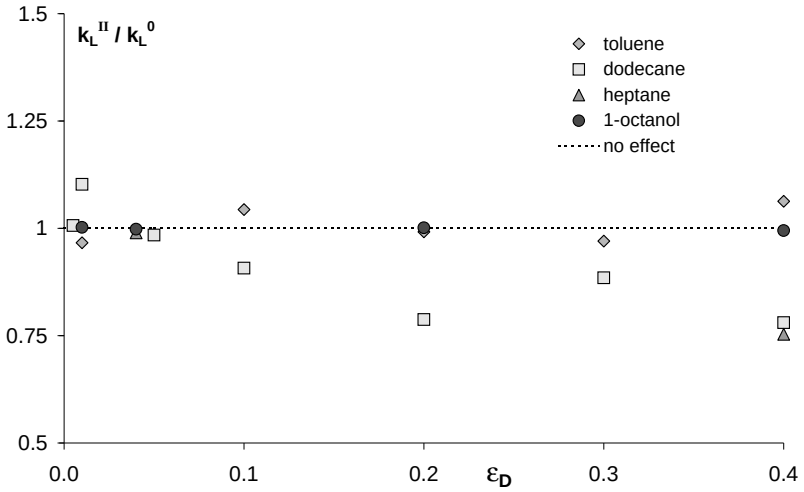

Figure 1.11: k_L/k_L^0 versus dispersed phase hold-up when case II is assumed.

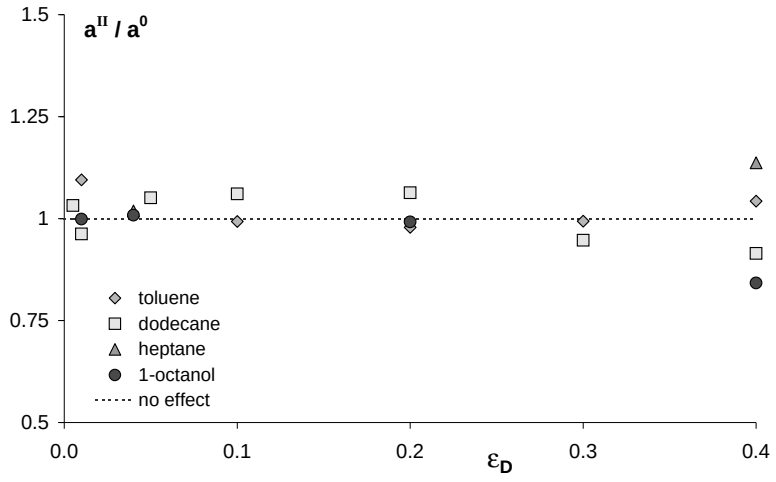

Figure 1.12: a/a^0 versus dispersed phase hold-up when case II is assumed.

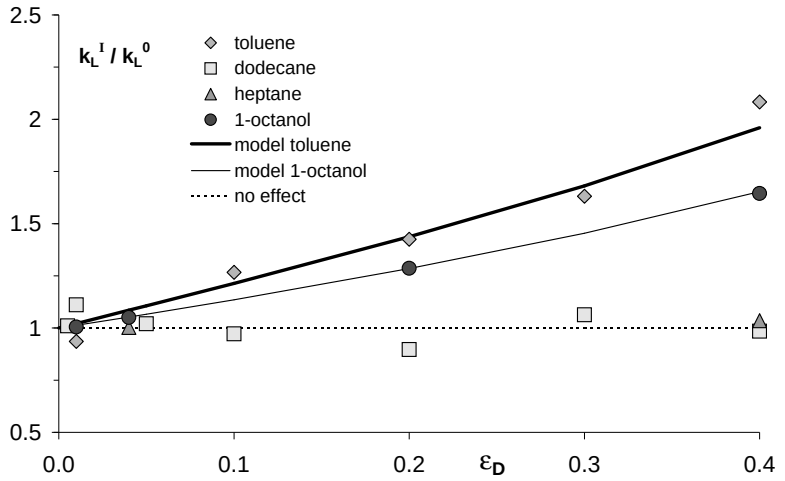

Figure 1.13: Relative values for k_L when case I is applied. The model lines represent the enhancement factor as determined from the model.

The value for the interfacial area, after accounting for initial effects, remains constant up to at least 20% organic phase hold-up (Fig. 1.12).

The experimental results of dodecane and heptane dispersions, however, are best described assuming no dispersed phase in the mass transfer zone (case I). The value of the mass transfer coefficient then remained practically constant (as expected) and in dodecane dispersions the interfacial area was constant up to 20% dispersed phase fraction and then started decreasing (Fig. 1.7). In Figure 1.13 the absence of mass transfer enhancement is clearly shown.

When applying the most probable situations for each of the gas-liquid-liquid systems studied (thus: Case I for dodecane and heptane and Case II for toluene and 1-octanol) the resulting k_L values are plotted in Fig. 1.14. For a/a^0 the value remained constant in all cases up to 20%.

If this interpretation is valid (which needs further validation), these results show that the surface renewal frequency in these multiphase systems is not influenced by the presence of dispersed phase droplets.

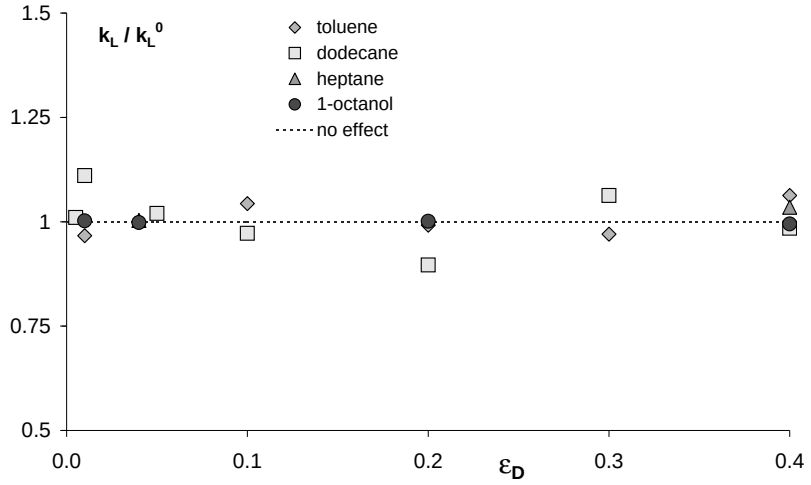

Figure 1.14: Interpreted k_L values.

1.5 Conclusions

The Danckwerts-plot technique was used for analysis of mass transfer parameters in gas-liquid-liquid systems. From the experimental results and by interpretation of the Danckwerts plots the existence of two types of gas-liquid-liquid systems is indicated. Mass transfer is enhanced due to the addition of toluene and 1-octanol to aqueous buffer solutions, which could be well described by a homogeneous model of the shuttle mechanism. Addition of n-dodecane and n-heptane, however, causes no enhancement of mass transfer. Initial effects (at low dispersed phase fraction) can be very strong and further study on these effects is required. To validate the conclusions drawn from the experimental results in this work for the effect on the mass transfer parameters k_L and a, independent physical measuring techniques will be developed.

Acknowledgement

B. Knaken is acknowledged for the construction of the set-up.

Chapter 2

Measurement of bubble, drop and particle size distribution in multi-phase systems using ultrasonic spectroscopy

Abstract

A technique is developed for measurement of bubble, droplet and particle size distributions in multi-phase systems, based on the propagation speed and attenuation of ultrasound. The measurement of the size distribution of the dispersed phase in multi-phase systems was desired to analyze the mass-transfer mechanism in gas-liquid-liquid and gas-liquid-solid systems. To obtain this information both the ultrasonic velocity and the attenuation coefficient of tone-burst signals are determined for a large frequency range (typically 100 kHz - 100 MHz). From these parameters the size distributions and the volume fraction of the different dispersed phases can be determined using a scattering model. It was shown that the interfacial area can be determined very accurately, however, for the exact size distribution of the gas bubbles in the used size range (1-3 mm) an independent gas hold-up determination is required. Experiments were performed in gas-liquid, solid-liquid and gas-liquid-

solid systems. The results showed good agreement of the particle size distribution compared to a commercial laser-scattering analyzer both with and without gas bubbles present. In systems that contained gas bubbles, good agreement between the scattering model and the experiments was obtained. Furthermore, measurements of the Sauter mean diameter in a flat bubble column were found to be in good agreement with the values that were obtained by using a digital camera technique.

2.1 Introduction

In chemical engineering the rate of mass transfer between two different phases often directly determines the production rate of the process (e.g. the gas absorption rate in gas-liquid systems). This mass transfer rate is proportional to both a mass transfer coefficient as well as the specific interfacial area between the different phases. Both parameters depend mainly on the (local) hydrodynamic situation inside the system. Both for design purposes and for improvement of existing production facilities it is very important to be able to analyze and to predict these parameters. Especially for three phase systems the prediction of the gas-liquid mass transfer rate is rather difficult as the interaction between dispersed phase particles, which can be either solid particles or liquid phase droplets of an immiscible phase, is not yet understood. In literature (Yoshida et al., 1970) both enhancements as well as retardations of mass transfer (gas absorption) rates on the addition of a dispersed phase are reported. Recent investigations (Cents et al., 2001) have shown that for some specific systems the enhancement of mass transfer in stirred vessels could be well described by the so-called shuttle-mechanism, which assumes dispersed phase droplets to be present in the mass transfer zone, thereby facilitating mass transfer due to their higher solubility for the gaseous component to be transferred. On the other hand, some other dispersed phases, also having a higher solubility for the gas, did not enhance the mass transfer rate. Therefore a conclusive understanding of this phenomenon does not yet exist. A possible correlation may exist with the size of the dispersed droplets, which can influence the liquid-liquid mass transfer and can also play a role in the attraction of the droplets to the gas-liquid interface. For

this reason it is important to develop a technique, which can measure the bubble size distribution (from which the Sauter mean diameter can be calculated) and the gas volume fraction, as well as the size distribution of the dispersed droplets simultaneously. The bubble size distribution and gas hold-up are very important in gas-liquid mass transfer, because they determine the specific interfacial area. The determination of the droplet size distribution is necessary to improve on the insight in the mechanisms of mass transfer in gas-liquid-liquid (G-L-L) and gas-liquid-solid (G-L-S) systems.

Characterization of size distributions and phase volume fractions is a recognized problem in chemical engineering. The specific gas-liquid interfacial area can be determined using a light scattering technique (Calderbank, 1958; Calderbank et al., 1960) or by simultaneous determination of the gas hold-up and the bubble size distribution. Methods to determine the bubble diameter include photography (with digital image analysis) (Machon et al., 1997; Pacek et al., 1994), capillary techniques, with light transmission analysis (Barigou and Greaves, 1991; Bae and Tavlarides, 1989) or using by contact probes (Burgess and Calderbank, 1975; Calderbank and Pereira, 1977). However, all these techniques have limited applicability, because they only allow for small volume fractions and require transparent solutions. Capillary techniques can also be inaccurate, because of possible coalescence and break-up of bubbles inside the sampling probe and the difficulties related to isokinetic sampling. Also the presence of small droplets or particles in G-L-L or G-L-S systems often interferes with the traditional measurement techniques and it is definitely not possible to measure the size distribution of the additional liquid or solid phase in this way.

In this work a novel technique has been developed, which can simultaneously determine the size distributions of both dispersed phases in G-L-L or G-L-S systems using ultrasonic spectroscopy. The measurement principle of this technique is the dependency of ultrasonic velocity and attenuation on particle size and dispersed phase hold-up and this varies with frequency.

In the past, some work was done on the determination of particle sizes in two-phase systems with ultrasonic spectroscopy. Bubble size distribution determina-

tion with ultrasound has been used in oceanographic applications for measurement of small bubble sizes near their resonance frequency (Medwin, 1977). Stravs and von Stockar (1985) and Stravs et al. (1986) used high frequency (1-10 MHz) ultrasound for on-line monitoring of the interfacial area in fermentation bubble columns. These authors were able to measure interfacial areas up to 350 m^{-1} in their set-up, but did not determine bubble size distributions. An ultrasonic pulse technique was used by McClements and Fairley (1991) and McClements (1996) for determination of droplet size distributions in stabilized liquid-liquid emulsions. In this work velocity and attenuation measurements of the ultrasonic waves were performed in order to measure small (< 1 mm) droplets. For the characterization of solid particle size distributions both the attenuation coefficient as well as the velocity of ultrasonic waves were used by Khatchikian et al. (1999). These authors, who used glass beads of 24-485 mm, obtained a good agreement with the theory for scattering of ultrasound by particles.

In this work an ultrasonic measurement system is developed, which can measure bubble, droplet and particle size distributions in multi-phase systems. Due to the broad range of frequencies used (100 kHz - 100 MHz), particle sizes from 1 μm to approximately 1 cm can be determined. The technique is able to measure the volume fractions and the size distributions, because it makes use of both the velocity of sound as well as the attenuation coefficient at the used frequency band. Both these profiles contain useful information for in-situ determination of the important characteristics of three phase systems.

2.2 Theory

2.2.1 General theory

The theory of ultrasonic propagation in multi-phase systems is based on mathematical treatment of the behaviour of an incoming ultrasonic wave in a fluid containing an ensemble of particles. The ultrasonic velocity and attenuation coefficient of a multi-phase system are directly related to the physical properties of the individual phases and also depend on the size and volume fraction of the particles as well as on the frequency of the transmitted wave. As the wave travels through the liquid

the velocity and the amplitude of the wave are changed due to the interaction with the particles that are present in the fluid. Several mechanisms can account for the alteration of the incoming wave (McClements, 1996):

1. scattering of the wave into directions that are different from that of the incoming wave
2. conversion of ultrasonic energy into heat due to various absorption mechanisms
3. interference of the waves, which travel through a particle with waves that travel only in the continuous phase and with scattered waves

The full ultrasonic theory to describe these phenomena was first derived by Epstein and Carhart (1953). They investigated the attenuation of sound in fogs, so their analysis was based on liquid drops in air. Allegra and Hawley (1972) modified the stress tensor of a viscous fluid into that of an elastic solid to obtain the wave equations for a system of solid particles in a liquid. Together these two theories are commonly referred to as the ECAH-theory. The basis of this theory is the linearization of the equations for conservation of mass, momentum and energy. Together with a thermal and a caloric equation of state, relating the density and internal energy to pressure and temperature, the equations can be rewritten to obtain the following set of acoustic wave equations:

$$(\nabla^2 + k_c^2)\phi_c = 0 \tag{2.1}$$

$$(\nabla^2 + k_T^2)\phi_T = 0 \tag{2.2}$$

$$(\nabla^2 + k_s^2)\mathbf{A} = 0 \tag{2.3}$$

with the propagation constants:

$$k_c = \omega/c + i\alpha \qquad \text{(compressional wave)} \tag{2.4}$$

$$k_T = (1+i)\sqrt{\omega/2\sigma} \qquad \text{(thermal wave)} \tag{2.5}$$

$$k_s = (1+i)\sqrt{\omega/2\nu} \qquad \text{(shear wave)} \tag{2.6}$$

Using these equations the problem of a plane wave encountering a sphere suspended in a liquid can be solved using spherical co-ordinates. The sphere gives rise to a reflected compressional wave, a compressional wave inside the sphere and

thermal and shear waves in- and outside the sphere. The solution of the wave equations consists of series expansions of spherical Bessel functions and spherical harmonics with 6 unknown scattering coefficients (A_n, B_n, C_n, A'_n, B'_n, and C'_n). In order to solve the complete acoustic field, these coefficients need to be determined using 6 boundary conditions: continuity of temperature, heat flux, radial and tangential stress and radial and tangential velocity at the surface of the particle. When these boundary conditions are applied the following set of 6 linear equations result, from which the 6 unknown scattering coefficients can be determined.

continuity of radial velocity:

$$\begin{aligned} &a_c j_n'(a_c) + A_n a_c h_n'(a_c) + B_n a_T h_n'(a_T) - C_n n(n+1) h_n(a_s) = \\ &A'_n a'_c j_n'(a'_c) + B'_n a'_T j_n'(a'_T) - C'_n n(n+1) j_n(a'_s) \end{aligned} \tag{2.7-a}$$

continuity of tangential velocity:

$$\begin{aligned} &j_n(a_c) + A_n h_n(a_c) + B_n h_n(a_T) - C_n \left(h_n(a_s) + a_s h_n'(a_s)\right) = \\ &A'_n j_n(a'_c) + B'_n j_n(a'_T) - C'_n \left(j_n(a'_s) + a'_s j_n'(a'_s)\right) \end{aligned} \tag{2.7-b}$$

continuity of temperature:

$$\begin{aligned} &b_c \left(j_n(a_c) + A_n h_n(a_c)\right) + B_n b_T h_n(a_T) = \\ &A'_n b'_c j_n(a'_c) + B'_n b'_T j_n(a'_T) \end{aligned} \tag{2.7-c}$$

continuity of heat flux:

$$\begin{aligned} &\tau \left(a_c b_c \left(j_n'(a_c) + A_n h_n'(a_c)\right) + B_n b_T a_T h_n'(a_T)\right) = \\ &\tau' \left(A'_n b'_c a'_c j_n'(a'_c) + B'_n b'_T a'_T j_n'(a'_T)\right) \end{aligned} \tag{2.7-d}$$

continuity of radial stress:

$$\eta \begin{Bmatrix} [(a_s^2 - 2a_c^2) j_n(a_c) - 2a_c^2 j_n''(a_c)] + A_n \left[(a_s^2 - 2a_c^2) h_n(a_c) - 2a_c^2 h_n''(a_c)\right] + \\ B_n \left[(a_s^2 - 2a_T^2) h_n(a_T) - 2a_T^2 h_n''(a_T)\right] + 2n(n+1) C_n \left[a_s h_n'(a_s) - h_n(a_s)\right] \end{Bmatrix} =$$

$$\eta' \begin{Bmatrix} A'_n \left[\left(a_s'^2 - 2a_c'^2\right) j_n(a'_c) - 2a_c'^2 j_n''(a'_c)\right] + \\ B'_n \left[\left(a_s'^2 - 2a_T'^2\right) j_n(a'_T) - 2a_T'^2 j_n''(a'_T)\right] + 2n(n+1) C'_n \left[a'_s j_n'(a'_s) - j_n(a'_s)\right] \end{Bmatrix}$$

(2.7-e)

continuity of tangential stress:

$$\eta \begin{Bmatrix} a_c j_n'(a_c) - j_n(a_c) + A_n \left[a_c h_n'(a_c) - h_n(a_c)\right] + \\ B_n \left[a_T h_n'(a_T) - h_n(a_T)\right] - \tfrac{1}{2} C_n \left[a_s^2 h_n''(a_s) + (n^2+n-2) h_n(a_s)\right] \end{Bmatrix} =$$

$$\eta' \begin{Bmatrix} A_n' \left[a_c' j_n'(a_c') - j_n(a_c')\right] + B_n' \left[a_T' j_n'(a_T') - j_n(a_T')\right] \\ -\tfrac{1}{2} C_n' \left[a_s'^2 j_n''(a_s') + (n^2+n-2) j_n(a_s')\right] \end{Bmatrix} \tag{2.7-f}$$

In the equations the following notation is used: j_n and h_n are spherical Bessel functions of order n and spherical Hankel functions of the first kind and order n respectively. Primed functions are first or second derivatives of these functions. $a_c = k_c r$, $a_T = k_T r$ and $a_s = k_s r$. For primed and unprimed quantities the following abbreviations are used:

$$b_c = \frac{(1-\gamma)\omega^2}{\beta c^2} \tag{2.8}$$

$$b_T = \frac{i\omega}{\beta\sigma} = i\omega \frac{\rho C_p}{\beta\tau} \tag{2.9}$$

$$\gamma = 1 + \frac{T\beta^2 c^2}{C_p} \tag{2.10}$$

When $n = 0$ equation 2.7-b and 2.7-f are not valid and all terms containing C_n and C_n' vanish from the remaining equations. Now a system with four equations (2.7-a, 2.7-c, 2.7-d and 2.7-e) and four unknowns (A_n, A_n', B_n and B_n') has to be solved. In case of a solid as the dispersed phase the viscosity (η') in equations 6, 2.7-e and 2.7-f has to be replaced with $\mu'/(-i\omega)$, where μ' is the shear rigidity of the solid. For b_T' the following relation then has to be applied:

$$b_T' = \frac{\gamma}{c_1^2 \beta} \left[\omega^2 - \left(\frac{c_1^2}{\gamma} - \frac{4i\omega\mu}{3\rho}\right) \frac{i\omega}{\sigma}\right] \tag{2.11}$$

In this equation c_1 is the speed of sound for spherical compressional waves in an elastic isotropic solid.

2.2.2 Relationship between the scattering coefficient and velocity and attenuation

In the previous section the complete ultrasonic field around a single particle was described with the ultrasonic theory. It is important to relate the calculated scattering coefficient of the compressional wave in the continuous phase (A_n) into measurable quantities: the ultrasonic velocity (c) and the attenuation coefficient (α). These quantities are contained in the complex propagation constant K, which is defined as:

$$K = \omega/c + i\alpha \tag{2.12}$$

In dilute systems the scattering and absorption of a wave encountering a particle is not influenced by the neighbouring particles. The complex propagation constant is then calculated as (Foldy, 1945):

$$\left(\frac{K}{k_{c1}}\right)^2 = 1 + \frac{4\pi N f(0)}{k_{c1}^2} \tag{2.13}$$

In more concentrated systems interaction between the particles becomes significant. In these systems multiple scattering has to be taken into account. A comprehensive and widely used relation is the one proposed by Waterman and Truell (1961):

$$\left(\frac{K}{k_{c1}}\right)^2 = 1 + \frac{4\pi N f(0)}{k_{c1}^2} + \frac{4\pi^2 N^2}{k_{c1}^4}\left(f(0)^2 - f(\pi)^2\right) \tag{2.14}$$

In equations 2.13 and 2.14 N is the number density of the particles ($N = 3\varepsilon/4\pi r^3$) and $f(0)$ and $f(\pi)$ are the so-called far-field scattering amplitudes, that are defined as:

$$f(0) = \frac{1}{ik_{c1}} \sum_{n=0}^{\infty} (2n+1) A_n \tag{2.15}$$

$$f(\pi) = \frac{1}{ik_{c1}} \sum_{n=0}^{\infty} (-1)^n (2n+1) A_n \tag{2.16}$$

2.2.3 Size distributions

Bubbles, drops and particles in multi-phase systems are usually not mono-size, but have a certain size distribution. The most practical way to determine the velocity and the attenuation coefficient in such a system is to make use of superposition of discrete particle size classes. The Waterman Truell equation (2.14) applied to distributions then becomes:

$$\left(\frac{K}{k_{c1}}\right)^2 = 1 + \frac{4\pi}{k_{c1}^2} \sum_j N_j f_j(0) + \frac{4\pi^2}{k_{c1}^4} \sum_j N_j^2 \left(f_j(0)^2 - f_j(\pi)^2\right) \tag{2.17}$$

in which index j corresponds to the discrete size class j.

2.2.4 Simplified interaction regimes

To get a better understanding of the mechanisms that can account for the change of the incoming wave it is convenient to divide the interaction between the ultrasonic wave and the particle into three regimes (Figure 2.1).

I) The long wavelength regime (LWR): $r << l$

II) The intermediate wavelength regime (IWR): $r \approx l$

III) The short wavelength regime (SWR): $r >> l$

In this work measurements in the LWR as well as the IWR are performed. The SWR is not reached and will therefore not be discussed. In the LWR three types of interactions are of importance: intrinsic absorption, particle pulsation and particle oscillation. The intrinsic absorption is equal to the sum of the absorption of acoustic energy in the continuous and dispersed phases and depends on their volume fractions and not on the size of the particles. The pulsation of particles occurs due to the difference in compressibility and/or difference in thermal properties between the particle and the surrounding continuous phase. The pulsation of the particle leads to scattering of the ultrasonic wave in all directions (monopole scattering) and the conversion of ultrasonic energy into heat (thermal absorption). Particle oscillations

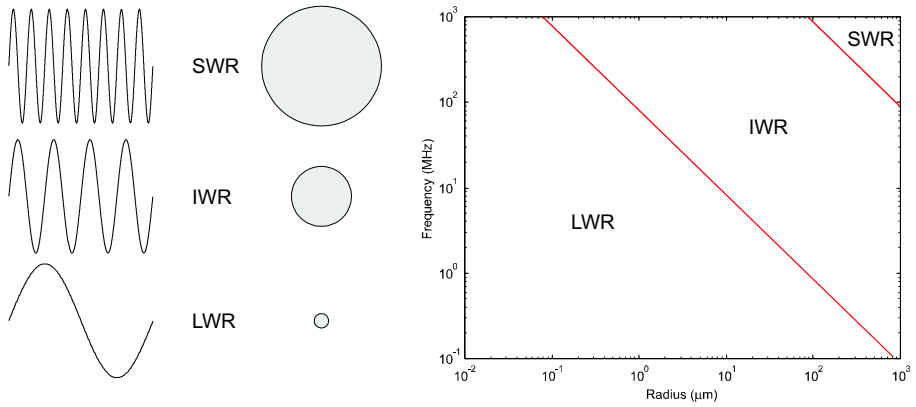

Figure 2.1: Different regimes for interaction of ultrasonic waves with particles (following McClements (1996))

occur due to a density difference between the particle and the surrounding fluid. The particle moves forward and backward because its inertia differs from the continuous phase. A part of the incoming wave is scattered away (dipole scattering) and part of the ultrasonic energy is converted into heat (visco-inertial absorption), due to the damping of the particle movement, because of viscous drag. In the IWR the interactions between the particle and the ultrasonic wave are much more complex. For gas-liquid (G-L) and liquid-liquid systems (L-L) the scattering of the waves is dominant over other types of interaction. Because of the complicated interactions much higher orders of scattering have to be taken into account. The scattering coefficients can be calculated from the following equation, which can be derived from equations 2.7-b and 2.7-e, neglecting thermal and shear waves and terms that do no contribute significantly in equation 2.7-e:

$$A_n = \frac{\rho_1 a_c' j_n(a_c) j_n'(a_c') - \rho_2 a_c \, j_n(a_c') j_n'(a_c)}{\rho_2 a_c \, j_n(a_c') h_n'(a_c) - \rho_1 a_c' j_n'(a_c') h_n(a_c)} \tag{2.18}$$

where $a_c = k_c r$ and where j_n are spherical Bessel functions and h_n are spherical Hankel functions of the first kind. Primed quantities are derivatives of the spherical harmonics. This result was also obtained by Gaunaurd and Überall (1981). The results for the ultrasonic velocity and the attenuation coefficient in G-L systems were also compared to the theory of Nishi (1975). The results of both theories are

in complete agreement for bubbles in the range of 0.5 - 20 millimeters in diameter, which are discussed in this work. In solid-liquid (S-L) systems viscous forces are important and always have to be taken into account. Thermal waves are relatively unimportant in these systems and can therefore be neglected. For measurements that are completely in either the LWR or the IWR simplified solutions can be used. Otherwise the complete ultrasonic theory has to be applied.

2.2.5 Three-phase systems

In the case of three phase systems (G-L-S or G-L-L) two different types of dispersed phase particles (gas bubbles and solid particles or gas bubbles and liquid droplets), each having its own size distribution, will influence the propagation of sound through the medium. In dilute systems these size distributions can be determined by superposition of the two phases. In non-dilute systems interactions between the particles are important. The complex propagation constant, K, can be calculated using equation 2.17 including both phases in the summation. In Figures 2.2 and 2.3 the attenuation and velocity coefficient in a G-L-L system are presented.

From these figures it can be concluded that characteristic profiles from both phases are retained in both the velocity as well as in the attenuation coefficient profile. From Figure 2.2 it can be seen that the attenuation due to the gas bubbles of the order of millimeters is most strong in the lower frequency domain ($<$ 1MHz). The droplets, which are typically in the range of a few hundred micron or smaller, attenuate in the higher frequency domain. This type of behaviour is also present in the velocity profile, but on a different scale. From Figure 2.3 it seems that the velocity is only changed by the presence of the gas bubbles. However, in Figure 2.4 the effect of the droplets on velocity is very clear. The attenuation coefficient and to a lesser extent the velocity are very useful in the determination of the broadness of the size distributions. Strong effects, due to the resonance of particles with a certain size, are damped due to the presence of particles with a different diameter, which have a different resonance frequency. From the smoothness of both profiles the variance of the distribution can be determined. When both the attenuation coefficient as well as the velocity are measured sufficiently accurate it is possible to

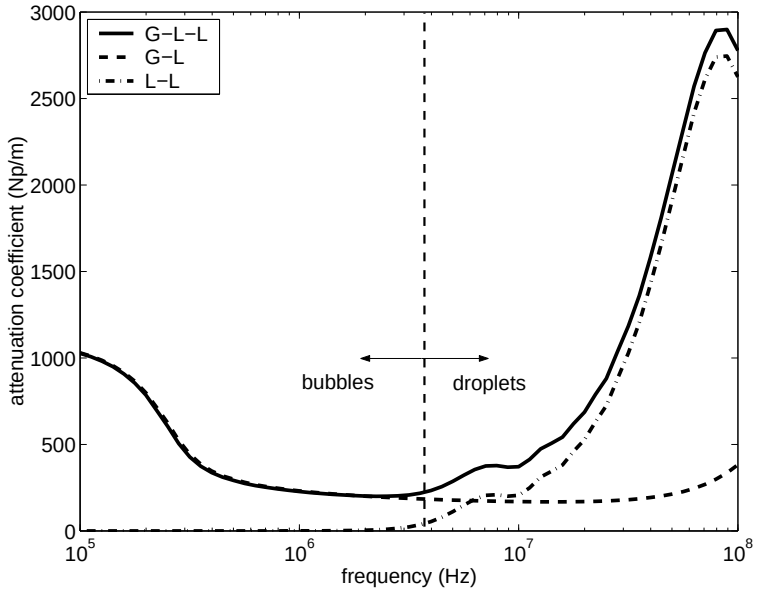

Figure 2.2: Attenuation coefficient of a G-L-L system with 10% air bubbles of 1 mm and 10% hexadecane droplets of 100 μm.

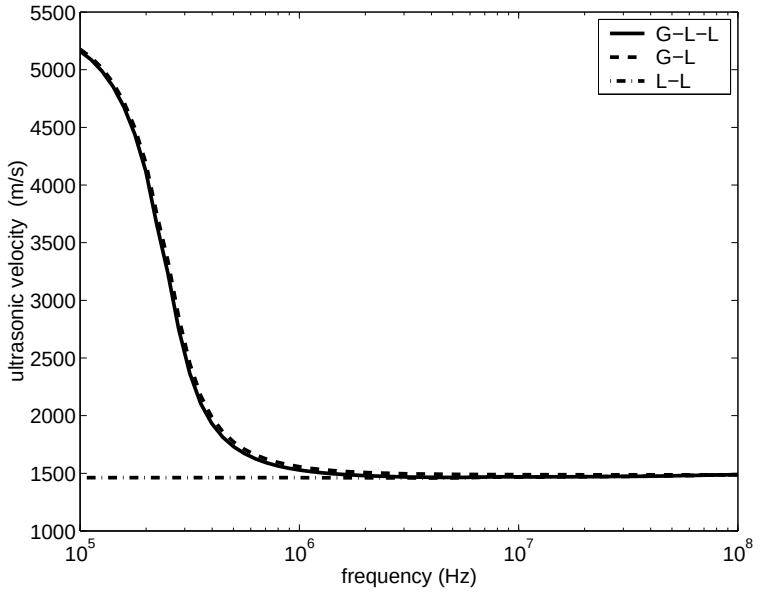

Figure 2.3: Ultrasonic velocity of a G-L-L system with 10% air bubbles of 1 mm and 10% hexadecane droplets of 100 μm

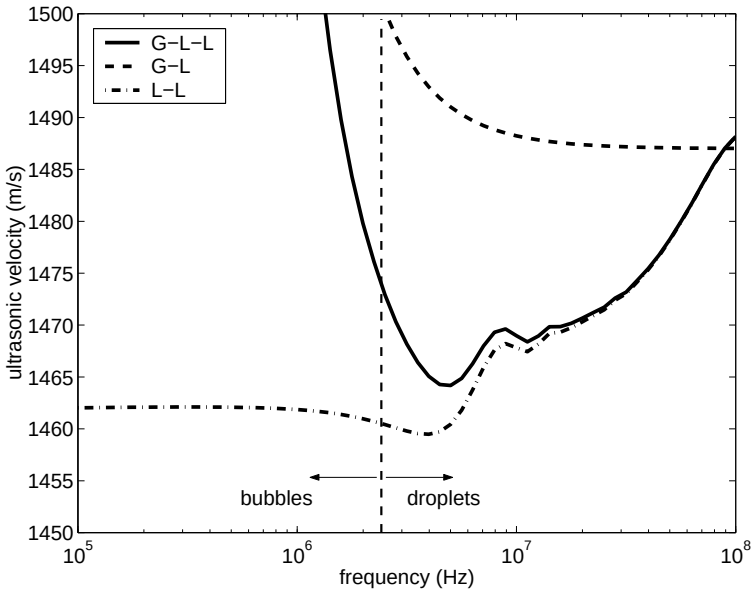

Figure 2.4: Zoom of the ultrasonic velocity of a G-L-L system with 10% air bubbles of 1 mm and 10% hexadecane droplets of 100 μm (Note the scale).

extract the size distributions for both phases from the experiments.

2.2.6 The inverse problem

In the previous section it was explained how to determine the velocity and the attenuation coefficient using the ECAH-theory when the size distributions and the dispersed phase hold-up are known. The actual problem is opposite: the derivation of the size distributions and the volume fractions of the different dispersed phases from the experimental values of the velocity and the attenuation coefficient respectively. Ideally, it would be desirable to solve this problem without making any assumption on the size distribution (Spelt et al., 1999; Duraiswami et al., 1998). However, this is more laborious and increases the sensitivity to experimental errors significantly. Therefore, in this work the size distribution type (normal, log-normal, etc.) is pre-selected. An advantage of using a model distribution is that only two or three parameters (depending on the distribution) have to be optimized. In chemical engineering applications the dispersed phase size distribution can often be described

satisfactorily accurate using a log-normal distribution in case of gas bubbles and liquid droplets. Of course, it is important to verify whether the assumption of a distribution influences the results significantly using different distributions. The log-normal distribution is described by:

$$P(x) = \frac{1}{Sx\sqrt{2\pi}} \exp\left(-\frac{(\ln(x) - M)^2}{2S^2}\right) \tag{2.19}$$

The mean diameter and variance can be calculated from this distribution:

$$\mu = \exp\left(M + \tfrac{1}{2}S^2\right) \tag{2.20}$$

$$\sigma = \exp\left(S^2 + 2M\right) \cdot \left(\exp(S^2) - 1\right) \tag{2.21}$$

The Sauter mean diameter for an arbitrary distribution is defined as:

$$d_{32} = \frac{\sum\limits_i N_i d_i^3}{\sum\limits_i N_i d_i^2} \tag{2.22}$$

The best fit between the experiments and the model is determined by minimizing the sum of the squares of both the velocity and the attenuation measurements. As an objective function for this minimization the following equation is proposed:

$$f = y \sum_i \left(c_E(i) - c_M(i)\right)^2 + (1 - y) \sum_i \left(\alpha_E(i) - \alpha_M(i)\right)^2 \tag{2.23}$$

Depending on the absolute values of the velocity and the attenuation coefficient a suitable coefficient y can be chosen.

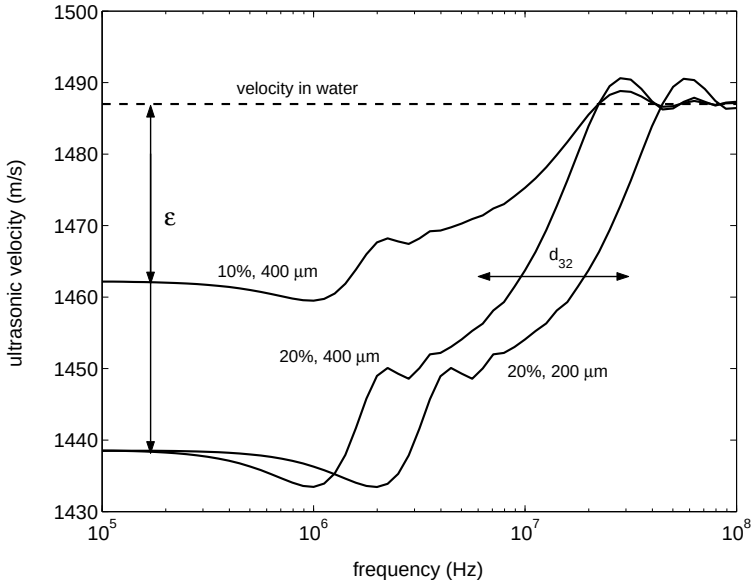

Figure 2.5: Ultrasonic velocity of a L-L system with different size and volume fractions of hexadecane droplets

2.2.7 Alternative determination of volume fraction

In order to determine the specific interfacial area (a) between different phases, not only the size distribution of the particles, but also their volume fraction, ε, must be known. This area can be determined from:

$$a = \frac{6 \cdot \varepsilon}{d_{32}} \tag{2.24}$$

For solid-liquid (S-L) and liquid-liquid (L-L) systems determination of the volume fraction from the ultrasonic velocity and attenuation coefficient measurements is relatively simple, because the frequency dependent profiles are very characteristic to both particle diameter as well as volume fraction. The effect of volume fraction and particle diameter on ultrasonic velocity in L-L systems is shown in Figure 2.5.

From Figure 2.5 it can be seen that it is possible to extract the volume fraction of the dispersed phase from the velocity measurements at the lower frequencies. The mean diameter, d_{32}, can be determined from the position of the positive slope

in this measurement. In gas-liquid (G-L) systems, however, the profiles are much less characteristic and problems can arise with simultaneous determination of d_{32} and ε. In Figure 2.6a this problem is visualized. When bubbles are in the range of millimeters the velocity vs. frequency profile has an exponentially decreasing shape. The shift of the profile due to a change in volume fraction is vertical and the shift due to a change in bubble diameter is horizontal. This results in an overlap, where it is possible to have multiple solutions (i.e. different combinations of bubble size and gas hold-up leading to the same profiles) for a single set of experiments. The attenuation coefficient cannot be used to discriminate between a broad size distribution and a mono-size bubble distribution. This phenomenon is also depicted in Figure 2.6. An advantage of the method is that the interfacial area, calculated using equation 2.24, can be determined very accurately from the profiles, which is, in fact, the most important parameter in many applications.

In case both the size distribution as well as the volume fraction have to be determined independently, an alternative measurement of the gas hold-up is necessary. A relatively simple and accurate method is to make use of electrical conductivity, which was applied among others by Yianatos et al. (1985). The electrical conductivity of an aqueous medium is changed by the presence of non-conducting particles, droplets or bubbles. The conductivity of the medium is proportional to the effective cross-sectional area of the bubbles and inversely proportional to the effective path length between the electrodes.

$$G = 1/R \sim A/L \tag{2.25}$$

The dimensionless conductivity of the medium is defined as the ratio of the conductivity of the dispersion to the continuous phase and is given by:

$$\gamma = \frac{G_\varepsilon}{G} = \frac{A_\varepsilon/A}{L_\varepsilon/L} \tag{2.26}$$

where:

$$A_\varepsilon = A\,(1-\varepsilon) \tag{2.27}$$

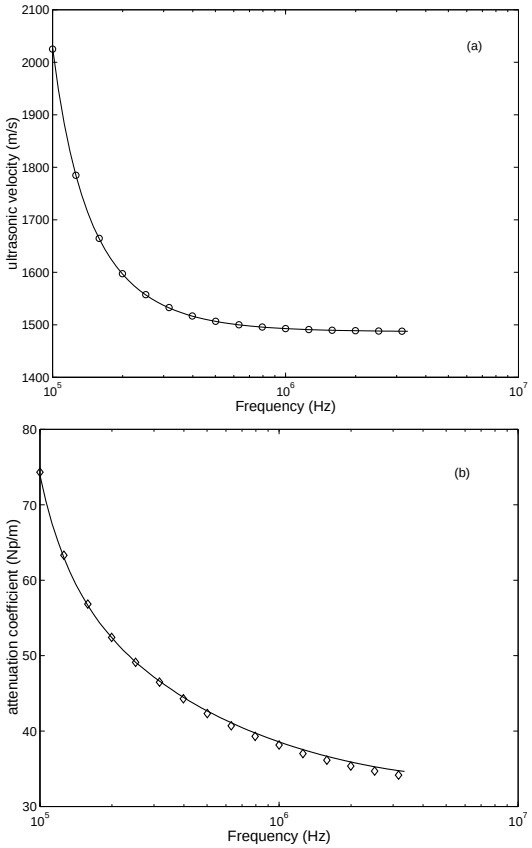

Figure 2.6: Multiple solutions for gas-liquid systems with different gas fraction and Sauter diameter. open symbols: $\varepsilon = 6.0\%$, $\mu = 3.00$ mm, $\sigma = 0$ mm (monosize), $d_{32} = 3.00$ mm and $a = 120.2$ m^2/m^3. closed lines: $\varepsilon = 6.5\%$, $\mu = 2.78$ mm, $\sigma = 0.75$ mm , $d_{32} = 3.23$ mm and $a = 120.9$ m^2/m^3.

$$L_\varepsilon = \xi\, L \tag{2.28}$$

In Equation 2.28 ξ is the tortuosity for which different models are developed. The model of Weissberg (1963) holds in bubbly zones (0-30% gas hold-up) and froth zones (65-90% gas hold-up):

$$\xi = 1 - 0.5 \ln(1 - \varepsilon) \tag{2.29}$$

In the experiments in this work the gas hold-up never exceeds 20%. In

this range the different models for the tortuosity do not differ significantly. From measurements of the ratio of the conductivity in the dispersion and the continuous fluid it is possible to determine the gas hold-up using Eq. 2.25-2.29.

When a non-polar solvent is used as the continuous phase, this technique cannot be applied due to the absence of electrical conductivity in the continuous phase. The local gas hold-up should then be determined using an alternative technique (for instance with a fiber optic probe).

2.3 Measurement method

2.3.1 Set-up

The experimental set-up consists of an arbitrary waveform generator (AWG), which sends any desired electric signal to a piezo-electric transducer (T). The signal is amplified with a maximum of 44 dB with a variable power amplifier. The transmitting transducer converts the electric signal to a pressure wave that is received in another transducer (R) and converted into an electric signal. This signal is acquired with a sampling rate of 2 Gs/s and with 8 bit resolution in a digital oscilloscope. The amount of noise is suppressed by averaging a large number of signals (100-1000) and by making use of low pass filters of 20 and 250 MHz. In this way also the resolution of the measurement is increased. A pre-amplifier with 31 dB gain in front of the oscilloscope amplifies the signal to a few millivolts, creating a maximum attenuation of approximately 110 dB for the complete measurement system. When the AWG sends the electric signal, at the same time a trigger signal is transmitted to the oscilloscope. In this way in every measurement the starting point, $t = 0$, is determined. The measurement system is fully automated by a GPIB interface bus for transmission of the signals and signal acquisition in the oscilloscope. A schematic representation of the set-up is shown in Figure 2.7

To cover the complete frequency range from 100 kHz-100 MHz 8 pairs of broadband immersion transducers are used with center-frequencies of 200 kHz, 300 kHz, 800 kHz, 2.2 MHz, 5 MHz, 15 MHz, 50 MHz and 80 MHz. These frequencies were selected in such a way that for measurements away from the centre-frequency

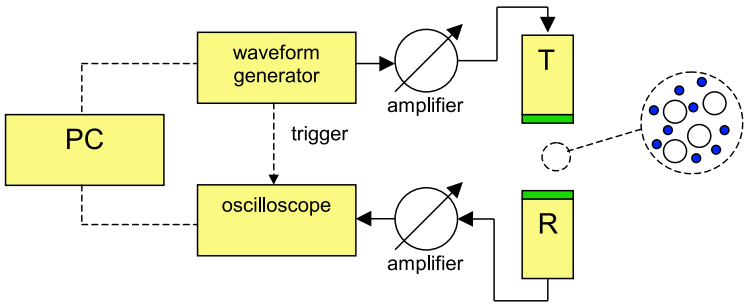

Figure 2.7: Schematic representation of the set-up.

of the transducers a maximum of 6 dB additional attenuation is allowed.

2.3.2 Signal transmission

The combination of the AWG and the broad-band transducers allows for different types of output signals. A method of extracting the phase velocity and the attenuation is calculation of the fast fourier transform (FFT) of a broad-band input signal, which was used in the work of Alig and Lellinger (1992). However, in this work for each frequency a narrow-band tone-burst was used, which was also applied with good results by Khatchikian et al. (1999). This method was applied, because the transmission of tone-bursts with different frequencies is very simple in the fully automated set-up and this technique is probably somewhat more accurate than determination of the phase velocity with FFT with a broad-band input. The amplitude of the individual transmitted signals was adjusted to the efficiency of the transducers for a certain frequency, by transmitting the signal with an amplitude proportional to the inverse of the transducer characteristic. In this way better results were obtained at frequencies that are not close to the center frequency of the transducer.

2.3.3 Data-analysis

To determine the velocity (c) and the attenuation coefficient (α), the received signal is compared in reference of a wave in a known fluid (e.g. the continuous phase), which in the present study will always be distilled water. Distilled water is used

because all ultrasonic properties are well known. In this way, the transfer function of the complete measurement system is not important and only the excess properties of the dispersion compared to water are determined. The ultrasonic velocity and the attenuation coefficient in the dispersion are calculated using:

$$c = \frac{d}{t} = \frac{d}{d/c_w(T) + \Delta t} \tag{2.30}$$

$$\alpha = \frac{-\ln\left(I_2/I_1\right)}{d} + \alpha_w(T) \tag{2.31}$$

In these equations d is the path-length between the transducers. The ultrasonic velocity (c_w) and the attenuation coefficient (α_w) in water are temperature dependent and are determined by making use of well-established experimental values from Del Grosso and Mader (1972) and Lide (1994) respectively. The time difference (Δt) between the signal that has travelled through the dispersion and the reference signal is determined by a cross-correlation of the two signals. This function is of the form:

$$R_{xy}(\Delta t) = \sum_t x(t)y(t + \Delta t) \tag{2.32}$$

When two tone-bursts are compared this function has a triangular shape and the time at which this function has its maximum, represents the time difference between the two signals. An example is presented in Figure 2.8.

A tone-burst signal consists of a limited number of cycles, which implies that the signal is not completely narrow-banded, but has a certain frequency spectrum. Only in the limit of an infinite number of cycles (a continuous wave) the signal consists of one single frequency. The frequency spectrum broadens when the number of cycles decreases. The presence of other frequencies in the transmitted signal can give rise to problems, because these frequency components can travel with a different velocity and can undergo less or more attenuation than the actual burst frequency. This can result in a received signal with heavily disturbed sides (Figure 2.9).

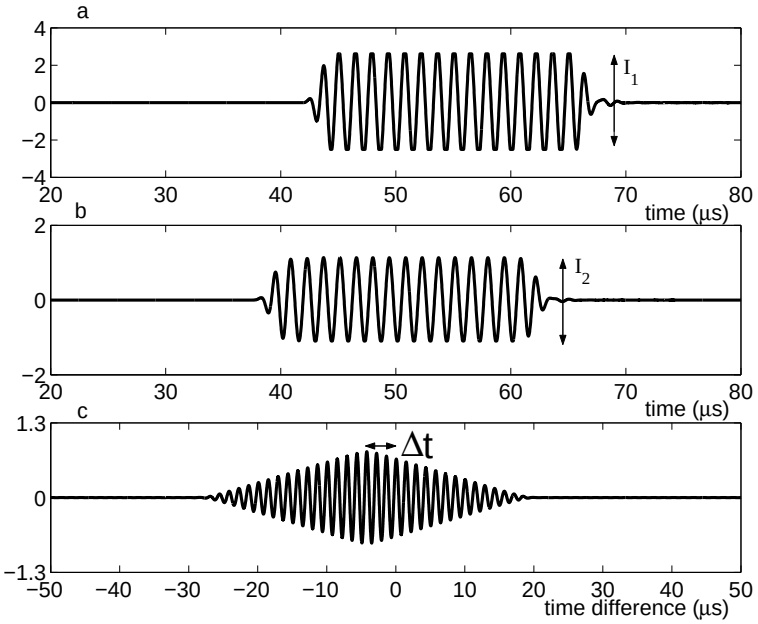

Figure 2.8: a) signal in water. b) signal in dispersion. c) cross-correlation of signals a and b

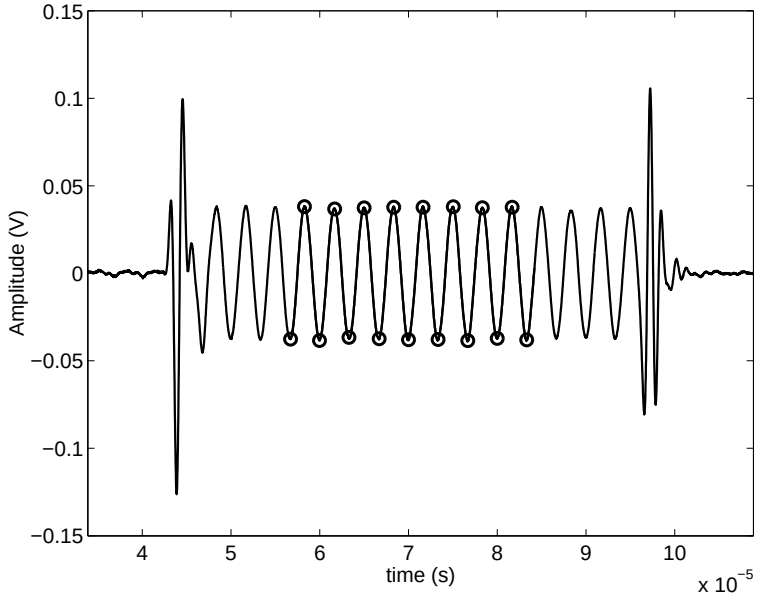

Figure 2.9: Distorted signal with large side maximums.

A drawback of these side effects is that they can lead to more than one maximum in the cross-correlation function, leading to uncertainty that the absolute maximum corresponds to the correct time delay. This can result in discontinuous velocity vs. frequency profiles, which is not possible from a physical point of view. To solve this problem the method explained by Khatchikian et al. (1999) was adopted. These authors have shown that the presence of the distortions did not affect the position in time of the maximums, but only their height, which reduces the problem to finding the correct maximum from the different possibilities. From that point it is possible to calculate the complete velocity profile starting from an undistorted measurement with low attenuation, assuming small differences in time delay with a small change in frequency. The attenuation coefficient is easily calculated from an undistorted signal taking the peak-peak (maximum minus the minimum of the burst) value of the signals as shown by I_1 and I_2 in Figure 2.8. However, when the signals have large side maximums (as in Figure 2.9) this method gives erroneous values for the attenuation coefficient. To solve this problem the average amplitude is determined from the middle 50% of the signal, as is shown by the open circles in Figure 2.9.

2.3.4 Gas hold-up

For the independent measurement of the gas hold-up using electrical conductivity a probe containing two round stainless steel electrodes was used. A 1 kHz signal of 4-Volt was send by the Arbitrary Waveform Generator to the measurement probe and a reference resistance (6.75 kΩ) in series. From the measurement of the voltage over the reference resistance using the oscilloscope it is possible to determine the resistance (and consequently the conductivity) of the medium in between the stainless steel plates. The frequency of the used signal (1 kHz) was high enough to avoid polarization of the electrodes.

2.4 Experimental

Measurements of the ultrasonic velocity and the attenuation coefficient as a function of frequency in three phase systems are new and to our knowledge have never been published in literature. In order to develop the measuring technique, before applying it to a G-L-S system, first two-phase systems (S-L and G-L) were studied. The tank in which the G-L and the G-L-S measurements were performed is shown in Figure 2.10. Air was used as the dispersed gas phase and deionized water as the continuous liquid. The stirred vessel has an inner diameter of 15 cm and a height of 25 cm above the glass sintered porous plate. A six-bladed Rushton turbine with a diameter of 7.5 cm and four baffles assure equal dispersion of the particles. The temperature is controlled within 0.1 $^{\circ}$C by a thermostatic bath and measured with a PT-100 temperature sensor. The transducers are aligned in a probe with a variable distance with a maximum of 6 cm. To minimize the hydrodynamic influence of the size differences between the different transducer pairs, all the transducers are covered with a stainless steel jacket with equal outer dimensions. When a highly attenuating medium is used this distance between the transducers can be as small as 1 mm. This distance should, of course, be much (say minimally 20x) larger than the size of the particles to ensure a representative sample between the transducers. Solid-liquid measurements were performed in a similar tank without the porous plate. A Plexiglas disc on top of the stirrer just below the surface prevented unwanted air induction into the liquid. Glass beads of 100-350 μm were used as the solid in S-L and G-L-S applications with the ultrasound method and their size distribution was measured for comparison with a commercially available particle sizer (Microtrac X-100) using a laser scattering technique.

2.5 Results and Discussion

2.5.1 S-L two-phase system

The results of measurements of the ultrasonic velocity and the attenuation coefficient in a system with glass beads of a known size distribution in water are presented in

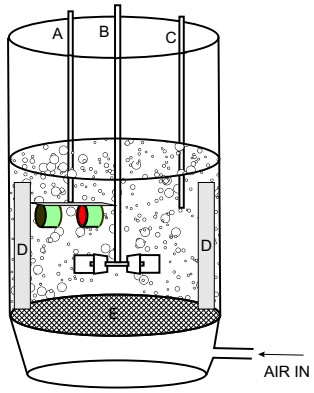

Figure 2.10: Schematic drawing of the stirred vessel A: Transducer probe B: Six-bladed Rushton turbine C: Temperature sensor (PT-100) D: Baffles E: Porous plate

Figures 2.11 and 2.12.

The properties of the different compounds used in for the model lines are listed in Table 2.1. The model line in Fig. 2.11-2.12 was determined by using the mean, the variance and the solid fraction as fit parameters in an optimization routine using the Nelder-Mead Simplex method (Nelder and Mead, 1965). The coefficient y in Eq. 2.23 was put 0.8 to normalize the two profiles on the basis of absolute values of the total velocity difference and the total attenuation coefficient difference. The value of y ($0 < y < 0.9$) influenced the results only marginally as long as the attenuation coefficient profile was correctly taken into account. When only the velocity profile was taken into account (i.e. $y = 1$) in the optimization the results were substantially different and the general trend of the results obtained with both profiles was not followed. Perhaps this could be overcome by taking into account a larger frequency region. The results are listed in Table 2.2. A comparison of the obtained particle size distribution with the results obtained with the laser scattering technique is also listed in Table 2.2 and is visually represented in Fig. 2.13.

The assumption of a log-normal distribution was reasonably good as is shown in Fig. 2.13. It should be mentioned that this assumption did not affect the mean, variance and Sauter diameter when compared to a normal distribution. The results obtained with ultrasonic spectroscopy are in good agreement with the results obtained with the laser scattering technique as can be seen from Table 2.2.

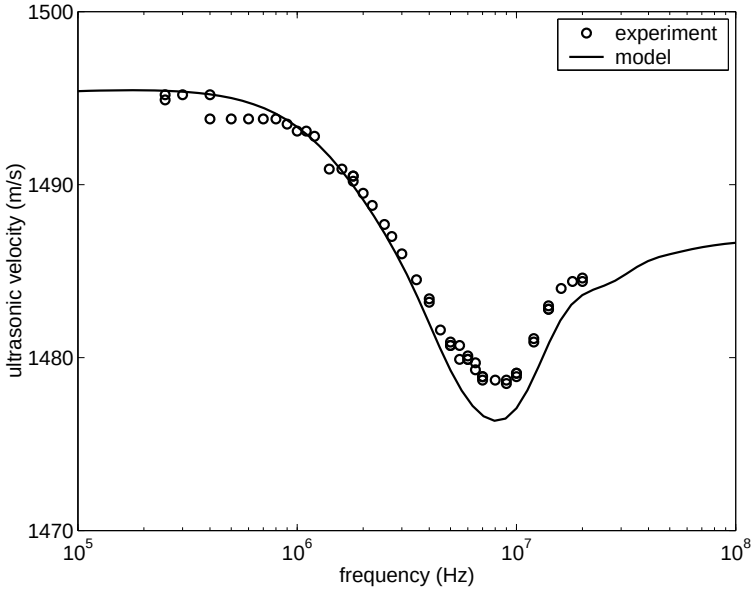

Figure 2.11: Ultrasonic velocity profile of 5% glass beads in water (S-L system). The model line is the best fit through the experiments using a log-normal distribution.

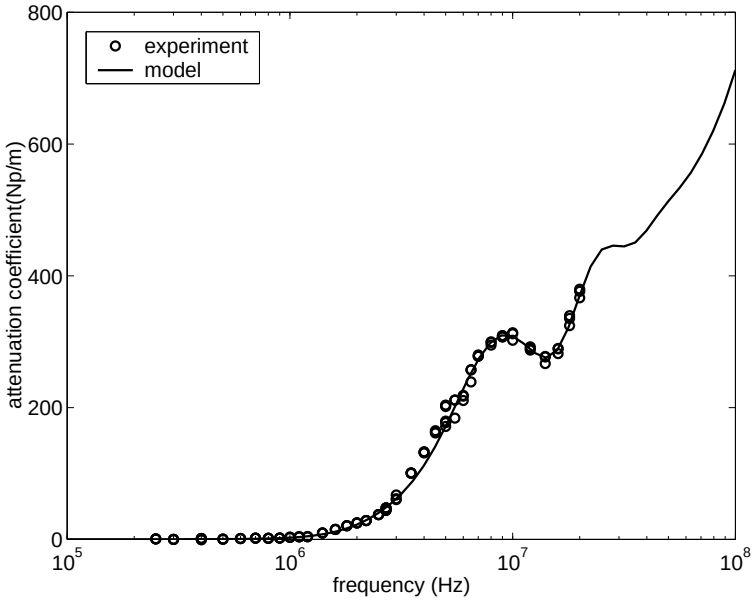

Figure 2.12: Attenuation coefficient profile of 5% glass beads in water (S-L system). The model line is the best fit through the experiments using a log-normal distribution.

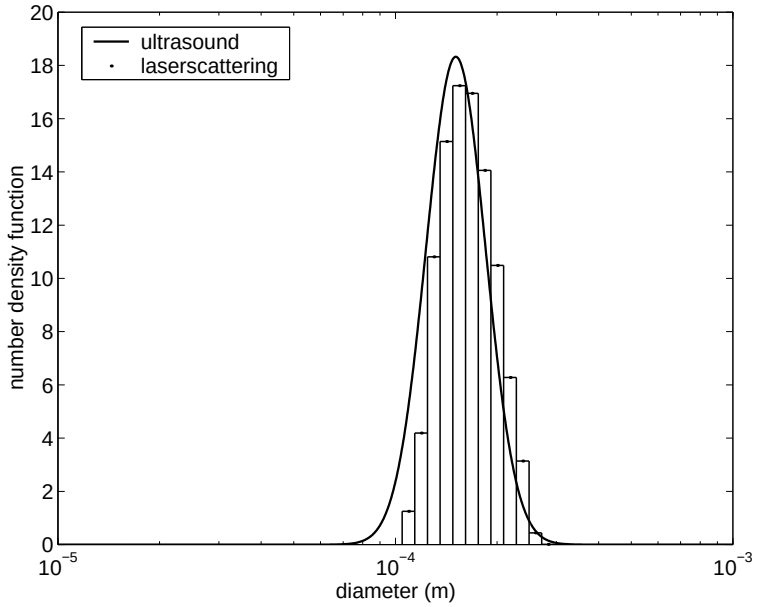

Figure 2.13: Comparison of ultrasound and laser scattering results for the glass beads particle size distribution.

The deviation in both Sauter and mean diameter is within 4%, which seems satisfactorily accurate. Also the width of the distribution matches very well. The deviation between the measured solid hold-up and the hold-up based on the volume of glass added to the liquid in the reactor is small. It seems that this can be attributed to local differences of solids hold-up within the tank, however, this has to be validated at a later stage.

From Fig. 2.11 and 2.12 it can be seen that both for the attenuation coefficient as well as for the ultrasonic velocity the experiments and the fitted model line are in good agreement. Measurements of the velocity profile in the region below 1 MHz were somewhat more laborious, because it was difficult to prevent air entrainment at the stirring speed used and therefore not a completely pure S-L system could be realized. The largest deviation between the model and the experiments is found in the frequency region 6-24 MHz, where the velocity deviates approximately 2 m/s from the experiments. A possible explanation for this could be that the actual profile of the volume fraction in the tank is changed owing to a different distance between the transducers. The distance between transducers that transmit frequencies

Table 2.1: Physical properties at 21 °C of the compounds used in the experimental and theoretical work.

	Glass [a]	Air [b]	Hexadecane [c]	Water [b]
density (kg m^{-3})	2500	1.2	769.3	998.0
thermal conductivity (J^{-1} s^{-1} K^{-1})	0.96	0.026	0.143	0.598
specific heat (J kg^{-1} K^{-1})	$0.836 \cdot 10^3$	$1.007 \cdot 10^3$	$2.217 \cdot 10^3$	$4.18 \cdot 10^3$
thermal expansion coefficient (K^{-1})	$3.2 \cdot 10^{-6}$	$3.4 \cdot 10^{-3}$	$8.15 \cdot 10^{-4}$	$2.04 \cdot 10^{-4}$
attenuation coefficient per $freq^2$ (Np s^2 m^{-1})	$1 \cdot 10^{-13}$	$1.15 \cdot 10^{-11}$	$1.01 \cdot 10^{-13}$	$2.3 \cdot 10^{-14}$
speed of sound (m s^{-1})	5200	344	1340	1485
shear viscosity (kg m^{-1} s^{-2})	-	$1.8 \cdot 10^{-5}$	$3.34 \cdot 10^{-3}$	$0.98 \cdot 10^{-3}$
shear rigidity (kg m^{-1} s^{-2})	$2.8 \cdot 10^{10}$	-	-	-
speed of sound for spherical compressional waves in an elastic isotropic solid (m s^{-1})	3200	-	-	-

[a] Properties are taken from the manufacturer or Spelt et al. (1999)
[b] Properties are taken from the Handbook of Chemistry and Physics (Lide, 1994)
[c] Properties (at 25 °C) are taken from Herrmann and McClements (1999)

between 2.7 and 20 MHz was approximately 2 cm and between the other transducers was app. 6 cm, because of the higher attenuation in the high frequency region. This hypothesis, however, is not supported by the profile of the attenuation coefficient, which seems quite continuous. Also the actual shape of the size distribution can influence the profile of the velocity, and could account for some deviation.

2.5.2 G-L two-phase system

The results of measurements of the ultrasonic velocity and the attenuation coefficient in a system with air bubbles in water are presented in Figures 2.14 and 2.15.

The reactor was operated as a bubble column, so no stirring was applied during the experiments. The model lines in these figures were obtained from the optimization of the mean and variance of a log-normal distribution. The gas hold-up was determined to be 5.8 vol-% by the conductivity measurement technique. The gas hold-up was determined from 7 readings (100 times averaged) with a standard deviation of 0.2 vol-% using a probe which had exactly the same dimensions as the transducer probe in order to minimize differences in the tank hydrodynamics. The

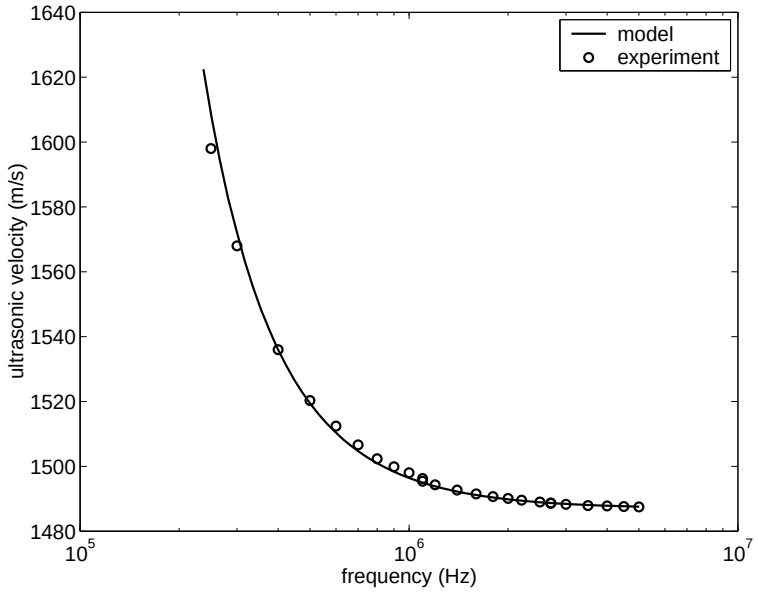

Figure 2.14: Ultrasonic velocity profile of 5.8% air bubbles in water (G-L system). The model line is the best fit through the experiments using a log-normal distribution.

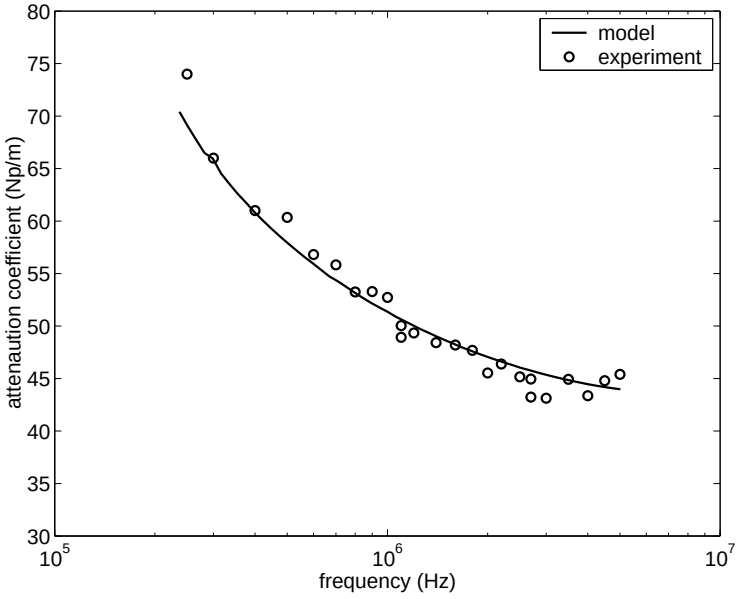

Figure 2.15: Attenuation coefficient profile of 5.8% air bubbles in water (G-L system). The model line is the best fit through the experiments using a log-normal distribution.

mean and the variance of the bubble size distribution were 2.24 mm and 0.03 mm respectively. The coefficient y in equation 2.23 was put to 0.5, because Δc and $\Delta\alpha$ are of the same order of magnitude. The absolute value of y did not influence the results to a large extent, which was expected from the very good agreement between the model and the experiments. The agreement between model and experiments is excellent in the velocity profile (Figure 2.14), but some irregularities can be observed in the attenuation coefficient profile (Figure 2.15) and also in the gas hold-up from the conductivity measurements. The irregularities can be attributed to local differences in hold-up and distribution in time, which can also be observed from the large time variation of the amplitude of the received signals through the dispersion. For this reason time averaging of the signals during at least 5 minutes turned out to be necessary.

The obtained variance of the distribution was small and the narrow shape of the size distribution was confirmed by visual observation of the dispersion in the vessel. However, the actual value of the variance of the distribution also depends on the value obtained for the gas hold-up that is used in the model calculation. When, for instance, a gas hold-up of 6.0% (mean (5.8%) + standard deviation (0.2%)) was used in the calculation the mean and variance were 2.29 and 0.10 mm, respectively. This causes a difference of 3% in the Sauter diameter. An advantage of the technique is that the values of the calculated interfacial areas lie within 0.5% and can thus be determined very accurately, which was also shown by Stravs and von Stockar (1985). These authors compared the interfacial area obtained using ultrasound with the interfacial area obtained with laser scattering with good results. This good agreement between the experiments and the ultrasonic scattering theory in G-L systems originates partly from the relatively high frequencies used. In this frequency regime thermal waves do not contribute significantly to the total absorption/scattering, which implies that scattering of the incoming wave is the dominant mechanism over others. A minimization of the sum of squares between the model and the experiments without fixing the gas hold-up resulted in a gas hold-up of 5.85%, which supports the result obtained with the conductivity measurements.

In order to test the technique for the measurement of bubble size more ex-

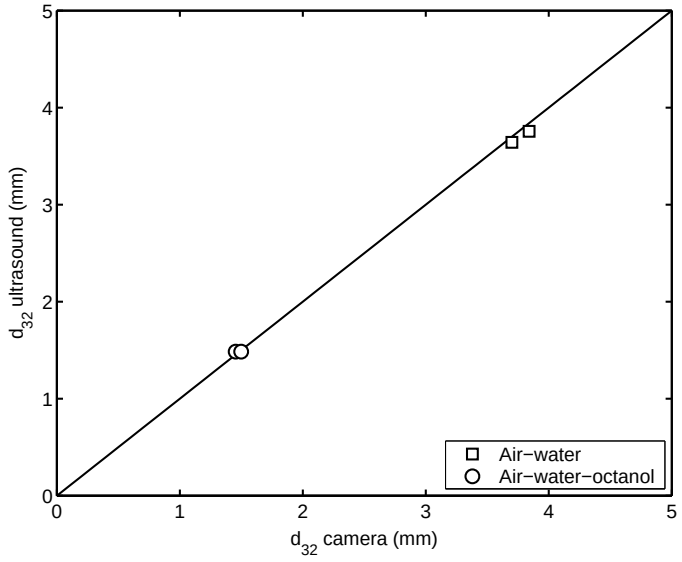

Figure 2.16: Parity-plot of the Sauter mean diameter obtained with the ultrasonic technique and with a digital camera technique.

tensively a comparison of ultrasonic spectroscopy with a digital camera technique was performed. The bubble size was measured in a flat (20x3x150 cm) bubble column using the ultrasonic technique in combination with the electrical conductivity method and using a digital camera technique with digital image analysis, simultaneously. The camera was placed 10 cm in front of the column and the ultrasonic transducers were mounted into the wall of the column (the measurement path length was 20 cm). Measurement of the exact size distribution using the ultrasonic technique was difficult, mainly due to the small attenuation and ultrasonic velocity differences. These differences were small due to low gas hold-ups that were applied ($\approx$ 1%), which was necessary for the digital camera technique to work optimally. The interfacial area could, however, be determined accurately and together with the measurement of the gas hold-up using the electrical conductivity technique, the Sauter mean bubble diameters were calculated. As can be seen in Figure 2.16 a good agreement between the two methods was obtained for coalescing (air-water) and non-coalescing (air-water-0.5 g/l octanol) systems, respectively.

Table 2.2: Results of ultrasonic measurement of a 5% dispersion of glass beads in water in comparison with results obtained by a laser scattering technique.

Glassbeads:	ultrasound (S-L)	ultrasound (G-L-S)	laserscattering
mean (μ), μm	161	160	167
variance (σ),μm	33	32	31
d_{32}, μm	175	173	179
volume fraction, %	5.5 (in: 5.0)	6.1 (in: 6.7)	-

2.5.3 G-L-S three-phase system

The results of measurements of the ultrasonic velocity and the attenuation coefficient in a system with glass beads of a known size distribution in water in the presence of air bubbles are presented in Figures 2.17 and 2.18. The results show that a good agreement between the model and the experiments can be obtained using the properties of air, water and glass from Table 2.1. In Table 2.2 the mean diameter and variance of the solid phase fraction are presented. The values are in good agreement with the values when there are no bubbles present, which means that the technique can be used with a high accuracy in bubbly systems. The gas bubbles in this system are smaller ($d_{32} = 1.67$ mm) compared to the gas-liquid two-phase system discussed above, probably due to the high stirring intensity (550 rpm). The gas hold-up was determined by the conductivity method and was 3.25%. The value of the coefficient y was set to 0.5 and variation thereof did not influence the results.

2.5.4 Miscellaneous

- An advantage of the developed technique is that it can be operated completely non-invasively, for instance in bubble columns, where the attenuation is not too high. This means that the transducers can be inserted in the walls of the column and therefore the flow pattern is not disturbed. In systems with small droplets or solid particles the attenuation is higher in the frequency region that is needed for the determination of particle size and smaller path lengths

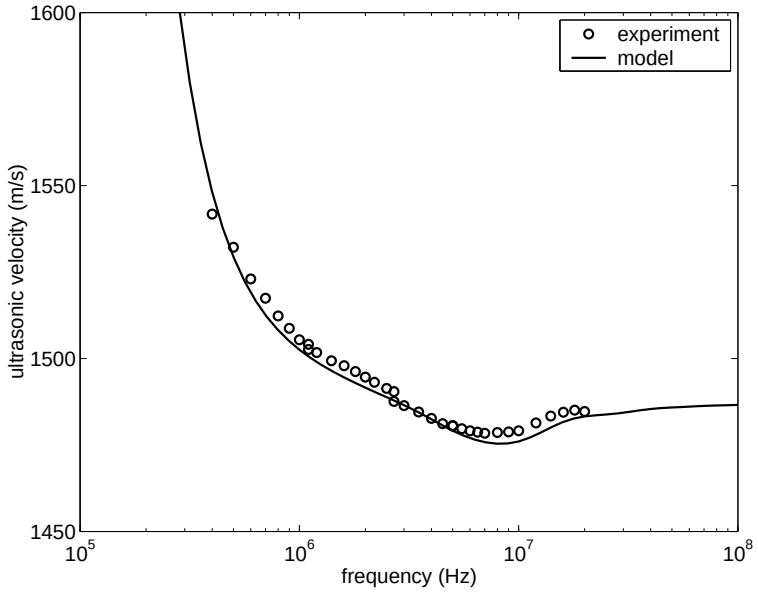

Figure 2.17: Ultrasonic velocity profile of a G-L-S system of 3.25% air bubbles and 6.1% glass beads in water. The model line is the best fit through the experiments using log-normal distributions.

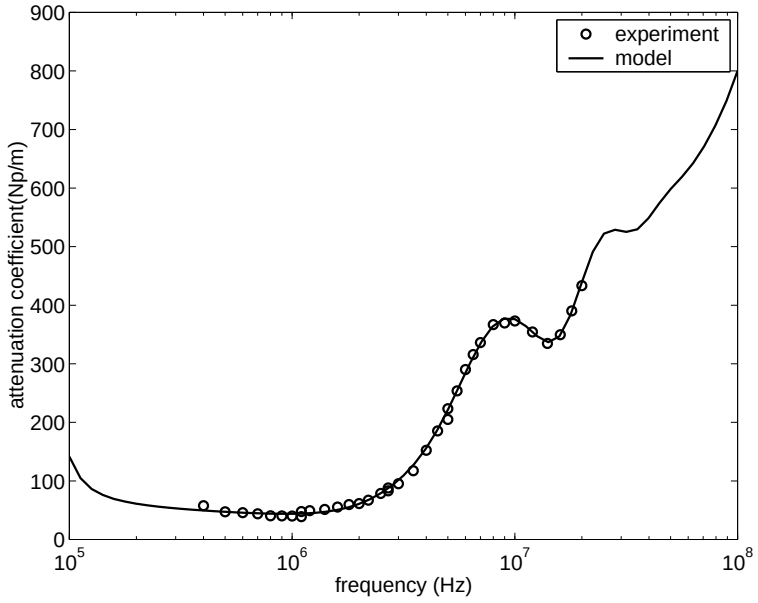

Figure 2.18: Attenuation coefficient profile of a G-L-S system of 3.25% air bubbles and 6.1% glass beads in water. The model line is the best fit through the experiments using log-normal distributions.

(for instance in a probe) are required.

- By making use of the tone-burst operating mode the power input due to the ultrasonic waves can be set to any desired level. In this work the average power input due to ultrasound was below 0.25 W (a transmitted signal frequency of 20 Hz was used), which avoids temperature differences between the transducers and the system and does not cause changes in the bubble distribution.

- The model that is used in this work assumes spherical particles, droplets and bubbles. In literature (Schaafsma and Hay, 1997) modifications of the theory are suggested to take different particle shapes into account.

- The influence of performing the measurements in the near-field of the transducers was studied using the tone-burst transmission method around an upward bubbly gas-flow with a certain, fixed diameter. The attenuation of the signal was not dependent on the path length between the transducers (with or without bubbly free zones in the near field of the transducers), which suggests that the influence is not significant. This is supported by the fact that the measurements in the solid-liquid system were performed at different measurement path lengths of the different transducer pairs that lead to continuous profiles of the attenuation coefficient and ultrasonic velocity.

2.6 Conclusions

In this work a novel technique is developed for the in situ measurement of size distributions and phase hold-up of particles, droplets and bubbles in two-phase as well as in three-phase systems respectively. It is shown that it is possible to resolve the size distribution of solid particles in the presence of gas bubbles and without. The results were compared with a commercial laser-scattering technique and were in good agreement.

For systems of gas bubbles in water it was possible to describe the obtained experimental sound velocity and attenuation coefficient profiles accurately. The interfacial area could be determined very accurately from these measurements. The

Sauter mean bubble diameters were in good agreement with results obtained by a digital camera technique, but the determination of the bubble size distribution from the ultrasonic velocity and attenuation coefficient profile still needs experimental validation. From an overall perspective, it can be stated that this method is readily applicable in industrial applications for in situ determination of dispersed phase properties, which can be very important for design and control of chemical and physical processes.

Acknowledgement

The author wishes to gratefully acknowledge B. Knaken for the construction of the measurement system and the technical advice and support. Prof. A. Prosperetti is acknowledged for his contribution in the preparation of this manuscript. P.J. Wijnstra and E. van der Woude are acknowledged for their help in the experimental work.

Chapter 3

Validation of the Danckwerts-plot technique by simultaneous chemical absorption of CO_2 and physical desorption of O_2

Abstract

The Danckwerts-plot technique (Danckwerts et al., 1963) is used in chemical engineering to simultaneously obtain the mass transfer parameters, k_L and a, from mass transfer experiments. This method requires variation of the reaction kinetics by adding different amounts of catalyst. Although the method is known for several decades, it was never verified that the variation of the amount of catalyst does not affect the hydrodynamics of the system under investigation. To study this, absorption of CO_2 in a carbonate/bicarbonate buffer solution was performed simultaneously with desorption of oxygen from this solution, after verification that absorption and desorption are processes, taken place at identical rates, but in a different direction. It was shown that the addition of catalyst did not affect the desorption rate of oxygen, which validates above assumptions used in the Danckwerts-plot technique, for the system presently used. The obtained k_La for oxygen was, however, 64% higher

compared to the k_La of carbon dioxide. This was probably due to a lower effective interfacial area, caused by the complete depletion of small bubbles containing CO_2. Mass transfer experiments with oxygen, with a low gas phase conversion, are therefore to be preferred, as the measured mass transfer parameters are less affected by the gas phase RTD and the shape of the bubble size distribution.

3.1 Introduction

The Danckwerts-plot technique was originally proposed by Danckwerts et al. (1963) and is a recognized method in chemical engineering research and development for simultaneous determination of the gas-liquid mass transfer coefficient (k_L) and the specific interfacial area (a). From the measurements of the gas absorption rate, R_A (mole s^{-1}), at different apparent first order reaction rate constants the values of k_L and a can be determined simultaneously using the Danckwerts surface renewal model (Danckwerts, 1950) with a (pseudo) first order reaction.

$$\left(\frac{R_A}{m_A \cdot c_A \cdot V_L}\right)^2 = (k_L \cdot a)^2 + k_{1,app} \cdot D_A \cdot a^2 \tag{3.1}$$

When the left hand side of Equation 3.1 is plotted versus the apparent first order rate constant times the diffusion coefficient of the gas into the liquid ($k_{1,app}D_A$), the slope equals the squared specific gas liquid interfacial area (a^2) and the intercept matches the square of the volumetric mass transfer coefficient $(k_La)^2$. The reactivity of the solution (the apparent first order rate constant) is, therefore, changed by variation of the catalyst concentration in a catalyzed pseudo first order reaction or by changing the bulk concentration of the reactant that is used in excess in a pseudo-first order reaction. A reaction system that is very suitable for this technique is the absorption of CO_2 in carbonate/bicarbonate buffer solutions. The dissolved CO_2 can react with water as well as with hydroxyl ions, which are formed from the equilibrium between carbonate and bicarbonate ions. The overall reaction that occurs is:

$$CO_2 + CO_3^{2-} + H_2O \rightarrow 2HCO_3^- \tag{3.2}$$

The reaction of CO_2 and water can be catalyzed by a number of compounds, e.g. hypochlorite, arsenite, carbonic anhydrase and different sugars. The apparent first order rate constant for this system is given by:

$$k_{1,app} = k_{H_2O} + k_{OH}[OH^-] + k_c[cat] \tag{3.3}$$

From this equation it must be concluded that that the apparent first order reaction system is in fact a much more complex system. For a more detailed description of this reaction system the reader is referred to Appendix A. For a convenient and accurate description of the absorption process it is important that the reaction can be assumed to be pseudo-first order in the hydroxyl and/or catalyst concentration. To consider the reaction to be pseudo first order, it is important that the concentrations of all the ionic species (CO_3^{2-}, HCO_3^-, H^+ and OH^-) up to the interface are uniform and identical to the bulk concentrations, i.e no depletion of ionic species within the mass transfer zone. The criterion that determines whether the concentrations of all ions are uniform, throughout the mass transfer zone, was derived by Danckwerts and Sharma (1966):

$$m \cdot [CO_2] \cdot \left(\frac{1}{[CO_3^{2-}]} + \frac{2}{[HCO_3^-]} \right) \cdot \left(\sqrt{\left(1 + \frac{D_{CO_2} \cdot k_{1,app}}{k_L^2} \right)} - 1 \right) << 1 \tag{3.4}$$

In this equation full dissociation of the catalyst ion is assumed, which is generally the case when sodium hypochlorite is used as a catalyst (Danckwerts et al., 1963). The validity of this criterion is discussed more thoroughly in Appendix A.

The Danckwerts-plot technique has been applied for a long time in literature (Richards et al., 1964; Mehta and Sharma, 1971; Kon and Sandall, 1978; Alper et al., 1980; Benadda et al., 1994) and usually a straight line is obtained, when plotting Equation 3.1, which suggests that the method is valid for the systems used. In order to validate the Danckwerts method, Kon and Sandall (1978) and

Alper et al. (1980) used gas absorption in a liquid with a flat interface to test the technique by comparison of the known geometric gas-liquid interfacial area with the area as determined by the Danckwerts-plot. The first authors found the interfacial area determined with the Danckwerts plot to be considerably less than the actual geometric interfacial area, although they obtained straight lines using Equation 3.1. Alper et al. (1980), however, performed similar experiments and found straight lines, but only upto $k_{1,app} = 6$ s^{-1}. Beyond this value the slope of the line decreased, due to non-uniform ion concentrations (the criterion in Eq. 3.4 was no longer satisfied), at least according to the authors. The slope of the plot up to $k_{1,app} = 6$ s^{-1} was indeed equal to the square of the geometric gas-liquid interfacial area. Alper et al. (1980) also discussed in detail the results of Kon and Sandall (1978) critically and concluded that the results of the latter authors were not reliable because the criterion in equation 3.4 was not fulfilled.

This example shows that obtaining a straight line from the Danckwerts plot does not automatically imply that all requirements for successful application of the technique are fulfilled. Alper et al. (1980) have tested the method only up to catalyst concentrations of 0.02 M. That means that no experimental evidence is provided that the addition of larger amounts of catalyst (which is necessary in systems with a higher mass transfer coefficient), does not influence the physical properties that may affect the hydrodynamics of the system, which could lead to erroneous determinations of the mass transfer parameters. It is not possible to test this at concentration above 0.02 M using gas absorption in a stirred cell with a flat interface, because then the criterion in equation 3.4 can never be fulfilled due to the relatively low value of the mass transfer coefficient.

To study the influence of the catalyst on hydrodynamics, the mass transfer rate of a non-reactive gas can be determined simultaneously with the chemical absorption of a reactive gas. When the gas-liquid mass transfer rate of the non-reactive gas is not influenced by the addition of the catalyst, the assumption that the catalyst does not change the hydrodynamics of the system is very likely to hold. The main objective of the present study is therefore to validate the results obtained by Cents et al. (2001) by showing that the hydrodynamics of the reaction system used were

not affected, by adding different amounts of catalyst, when the Danckwerts-plot technique is applied.

3.2 Experimental

To study the influence of the catalyst on hydrodynamics, the mass transfer rate of a non-reactive gas can be determined simultaneously with the chemical absorption of the reactive gas. The reactive system used in this work is the chemical absorption of CO_2 in potassium carbonate/bicarbonate solutions in which the reactivity was varied using different concentrations of sodium hypochlorite as a catalyst.

$$CO_2 + CO_3^{2-} + H_2O \xrightarrow{\text{NaOCl}} 2HCO_3^- \tag{3.5}$$

The simultaneously occurring physical mass transfer experiment for a non-reacting gas phase component should now be selected and designed. In order to arrive at an optimum system for this purpose, a more detailed analysis is presented here.

3.2.1 Design criteria for physical mass transfer experiments

In order to obtain an accurate determination of k_La for the non-reactive gas, design criteria for physical mass transfer experiments are derived. In case of a chemical system the liquid can often be operated batchwise. This method of operation can also be used in case of physical mass transfer measurements (dynamic methods, e.g. Linek et al. (1987)), but a continuous operation of the liquid phase is more accurate, and will therefore be used in this work. Two choices must be made to arrive at the most accurate method to determine the mass transfer rate: firstly, the outlet concentration can be measured in the gas phase or in the liquid phase and, secondly, the direction of mass transfer of the gas phase component (absorption or desorption) is a degree of freedom, under the assumption that these are mirror image processes. For the first selection a criterion is derived based upon the relative change in outlet concentration with a variation in k_La. If it is assumed that the

accuracy of the measurement in the liquid phase is equal to the measurement in the gas phase, the variation of the outlet concentration with k_La determines the overall accuracy of the measurement. In a system with a continuous and well-mixed liquid phase and a continuous well-mixed gas phase the steady-state mass balances for the component to be transferred in the gas and the liquid phase respectively are:

$$0 = \frac{\Phi_G}{V_L}(c_{G,0} - c_G) - k_La(mc_G - c_L) \tag{3.6}$$

$$0 = \frac{\Phi_L}{V_L}(c_{L,0} - c_L) + k_La(mc_G - c_L) \tag{3.7}$$

From these two balances the volumetric mass transfer coefficient can be determined by making use of the steady state concentration in the gas- or in the liquid phase outlet stream, which will be measured experimentally.
Making use of $\tau_G = V_L/\Phi_G$, the k_La based on gas phase analysis is then given by:

$$k_La_{GAS} = \frac{c_{G,0} - c_G}{\tau_G(mc_G - c_{L,0}) + \tau_L(c_G - c_{G,0})} \tag{3.8}$$

and with $\tau_L = V_L/\Phi_L$ the k_La based on liquid phase analysis equals:

$$k_La_{LIQ} = \frac{c_L - c_{L,0}}{m\,\tau_G(c_{L,0} - c_L) + \tau_L(mc_{G,0} - c_L)} \tag{3.9}$$

For both these cases it is possible to calculate the change of the outlet concentration in the steady state with a small variation in k_La (thus $dc/d(k_La)$). This ratio is shown in Figures 3.1A and 3.1B in case of desorption for two different values of the distribution coefficient, m ($m = 0.9$ resembles carbon dioxide and $m = 0.032$ resembles oxygen).

A large value for $dc/d(k_La)$ means that a small variation in k_La causes a relatively large change in the experimentally measured outlet concentration, which improves the accuracy of the measurement. It is made clear from Figure 3.1 that in case of oxygen desorption, measurement of the concentration in the liquid phase

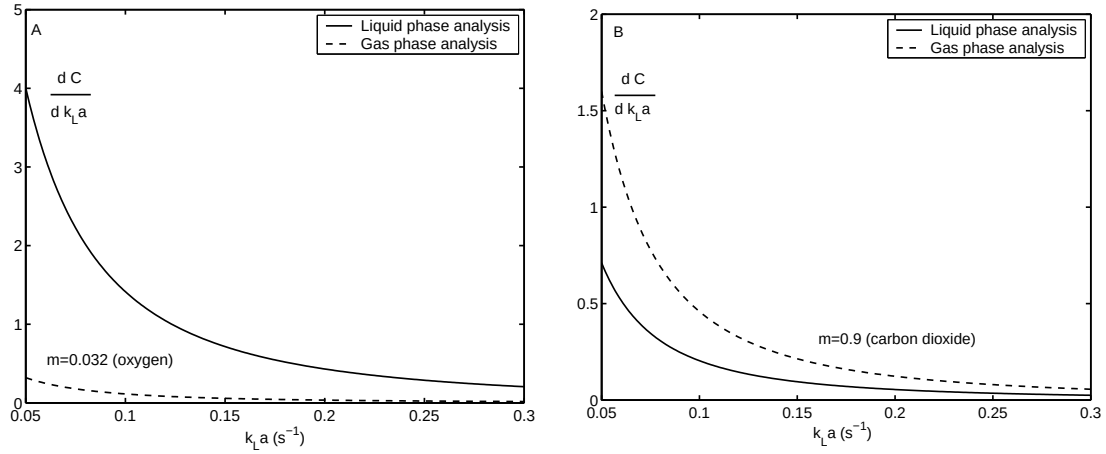

Figure 3.1: The variation of the normalized concentration ($C = c/c_0$) with k_La as a function of k_La. A: $m = 0.032$, B: $m = 0.9$. τ_G =100 s and $\tau_L = 40$ s in both cases.

is more accurate and in case of desorption of CO_2 the concentration is preferably determined in the gas phase.

In general, a relation can be derived from the ratio of this parameter using gas phase analysis and when using liquid phase analysis. This ratio can be determined, and is identical, for both absorption ($c_{L,i} = 0$) and desorption ($c_{G,i} = 0$) experiments and equals:

$$\frac{dc_G/d(k_La_{GAS})}{dc_L/d(k_La_{LIQ})} = \frac{m\tau_G}{\tau_L} \tag{3.10}$$

Using this relation it can be determined whether gas- or liquid phase analysis is favourable. For $m\tau_G > \tau_L$ concentration measurement in the gas phase is favourable and otherwise measurement in the liquid phase is more accurate.

The second selection (absorption or desorption) depends upon the first one, because desorption is favoured in case of liquid concentration measurement and absorption in case of gas phase measurement. This is shown from a sensitivity analysis for the effects of small disturbances in temperature and pressure on determination of the volumetric mass transfer coefficient. As an example measurement of a component in the liquid phase during absorption or desorption will be studied. The k_La for desorption equals:

$$k_L a_{LIQ\_DES} = \frac{(1-C)}{C \cdot \tau_L - m \cdot \tau_G \cdot (1-C)} \tag{3.11}$$

with:

$$C = \frac{c_L}{c_{L,0}} \tag{3.12}$$

There is no effect of pressure on the measured $k_L a$, due to the fact that the inlet and the outlet concentration can be measured at similar conditions. There is an effect of temperature as the m-value is dependent on temperature, but at conditions where $\tau_L \approx \tau_G$ and with a small m-value (oxygen) this effect is not significant.

In case of absorption with liquid phase analysis the $k_L a$ is given by:

$$k_L a_{LIQ\_ABS} = \frac{C}{\tau_L - C \cdot (\tau_L + m \cdot \tau_G)} \tag{3.13}$$

with:

$$C = \frac{c_L}{m \cdot c_{G,0}} = \frac{c_L}{m \cdot \frac{f \cdot p}{R \cdot T}} \tag{3.14}$$

In this case the inlet concentration in the gas phase should be known very accurately, while the measurement takes place in the liquid phase. Deviations from the reactor conditions in temperature and pressure in the inlet gas directly cause errors in the determined value for $k_L a$. In general, it is thus favourable when the dimensionless concentration in the reactor (c/c_0) can be used, which means that absorption should be used for gas phase analysis and desorption for liquid phase experiments. The design criteria for physical mass transfer experiments are summarized in Table 3.1. Note that for all considerations above equal accuracy for the liquid and gas phase analysis has been assumed.

In the present study oxygen was selected as the non-reactive gas and by using the above criteria it was calculated that the influence of the addition of catalyst

Table 3.1: Design criteria for physical mass transfer experiments.

favourable	gas phase measurement	liquid phase measurement
absorption	$m\tau_G > \tau_L$	never
desorption	never	$m\tau_G < \tau_L$

in the chemical absorption of CO_2 can best be studied with the desorption of O_2 using liquid phase analysis. An important condition to allow for the use of the desorption of a non-reactive gas, to study the possible effect of changing catalyst concentration in the Danckwerts-plot technique, is that absorption and desorption are mirror-image processes. This aspect will be studied (and the validity of this assumption will be demonstrated) in this research by comparing absorption and desorption rates of oxygen in water.

3.2.2 Physical parameters

The estimation of the physical parameters that are required for simultaneous determination of k_L and a using the Danckwerts-plot at 21 $^\circ$C are given in Section 1.3.2. The mole fraction of oxygen in water at 1 atmosphere partial pressure of oxygen is taken from IUPAC Solubility Data Series (Lorimer, 1979). The distribution coefficient of oxygen m_{O_2} in water was derived from the mole fraction and was calculated to be 0.0326 at 21 $^\circ$C. The salting out effect that decreases the oxygen solubility was estimated using the Sechenov equation and the parameters were taken from Weisenberger and Schumpe (1996). The oxygen distribution coefficient in the 0.6 M/0.6 M potassium carbonate/potassium bicarbonate buffer was determined to be 0.0160 at 21 $^\circ$C.

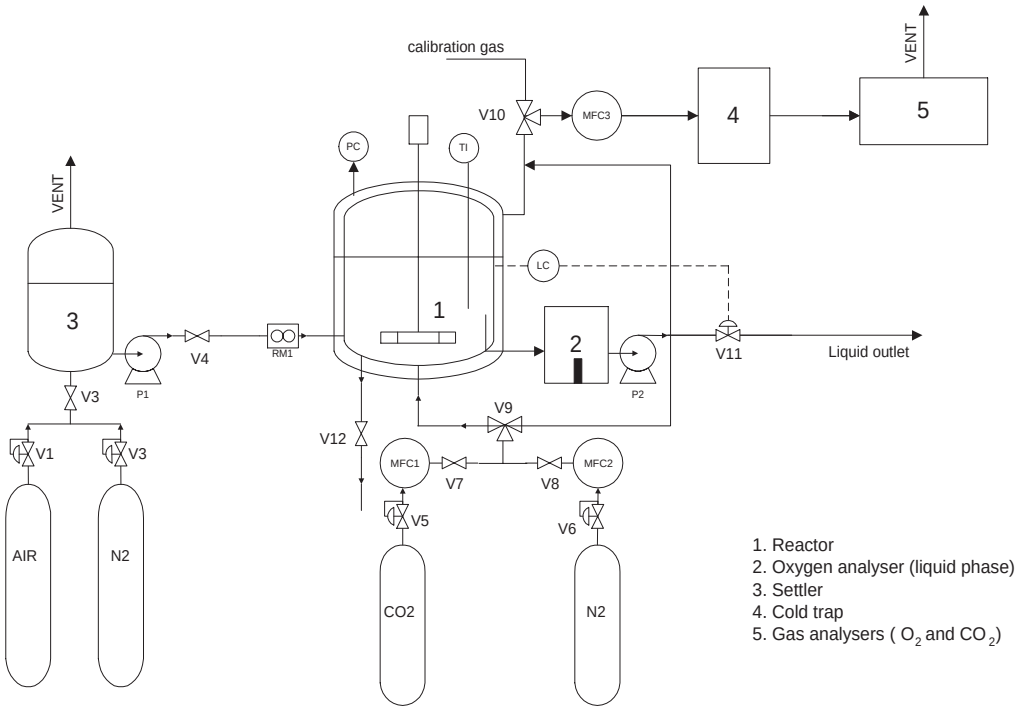

Figure 3.2: Experimental set-up.

3.2.3 Experimental set-up

The absorption and desorption experiments were performed in a set-up which consisted of a liquid storage vessel, in which the aqueous solution was saturated with the gas, a stirred reactor with a maximum working volume of 3.5 liters and an analytical section. A schematical representation of the set-up is presented in Figure 3.2. The liquid is pumped into the reactor from the storage vessel and the oxygen content of the liquid leaving the reactor can be measured. Gas entering the reactor is brought to the desired composition using mass flow controllers and the outlet oxygen and carbon dioxide gas concentrations can be determined using gas-analyzers. In the reactor a six-bladed Rushton turbine and four baffles ensure adequate mixing and the power input can be set to any desired level. The set-up is described more in detail in Section 1.3.3 and the dimensions are given in Table 3.2. In all experiments a volume fraction of 1.7% CO_2 was used and oxygen was introduced as air (20.9%).

Table 3.2: Standard reactor dimensions.

parameter	symbol	value	dimension	remarks
tank diameter	T	0.149	m	
impeller diameter	D	0.049	m	
liquid volume	V	2.53	dm^3	
impeller blade width	W	9.3	mm	
impeller blade length	L_B	12.3	mm	
baffle width	B	15.0	mm	
impeller height above bottom	H_I	0.049	m	
impeller power number	N_P	5.8	-	
diameter of the sparger	d_s	3	mm	1 hole below the impeller
height of the sparger	h_s	20	mm	above the bottom

3.3 Results and discussion

3.3.1 Physical mass transfer experiments

To test the experimental technique a mass balance check was performed using gas- and liquid phase oxygen analysis in both absorption and desorption experiments. An example of an experiment is presented in Figure 3.3. The maximum error in the mass balance experiments was 2% of the total moles of oxygen, which is sufficiently accurate.

In order to make a good comparison between the chemical absorption of a gas and the physical desorption of a non-reactive gas it is very important to prove that absorption and desorption are exactly identical processes, but in a different direction. For this reason absorption and desorption of oxygen in water were compared at different liquid hold-up volumes (1.5-3.5 liters), different gas flow rates (0.27-11.8 l/min) and different gassed power inputs (1-7 $\cdot$ 10^3 W/m^3). The results of these experiments are presented in Table 3.3.

From Table 3.3 it can be seen that absorption and desorption are mirror image processes for all the conditions used in this research. As expected from the design criteria for physical mass transfer experiments desorption experiments are

Table 3.3: Comparison of absorption and desorption rates of oxygen in water.

exp.	volume liquid V_L	gas flow rate $\Phi_{G,0}$	liquid flow rate Φ_L	N	# of des.	# of abs.	k_La desorption	k_La absorption	relative deviation
	dm^3	$dm^3\ min^{-1}$	$dm^3\ min^{-1}$	rpm	-	-	s^{-1}	s^{-1}	-
1	3.49	0.628	3.1	1000	2	3	0.017 ± 2%	0.018 ± 4%	− 6%
2	2.53	0.628	3.1	1000	5	8	0.028 ± 3%	0.029 ± 10%	− 2%
3	3.38	3.73	1.26	1060	1	1	0.036	0.038	− 5%
4	3.49	0.27	1.26	1830	3	2	0.037 ± 13%	0.039 ± 1%	− 4%
5	1.69	0.635	3.1	1010	5	12	0.046 ± 5%	0.047 ± 8%	− 2%
6	2.53	0.628	3.1	1300	5	4	0.056 ± 4%	0.059 ± 3%	− 5%
7	2.53	11.7	1.25	1090	7	5	0.071 ± 6%	0.078 ± 2%	− 8%
8	1.69	0.635	3.1	1330	6	10	0.119 ± 3%	0.124 ± 9%	− 4%
9	2.53	11.7	1.23	1620	2	2	0.166 ± 5%	0.158 ± 12%	+ 6%

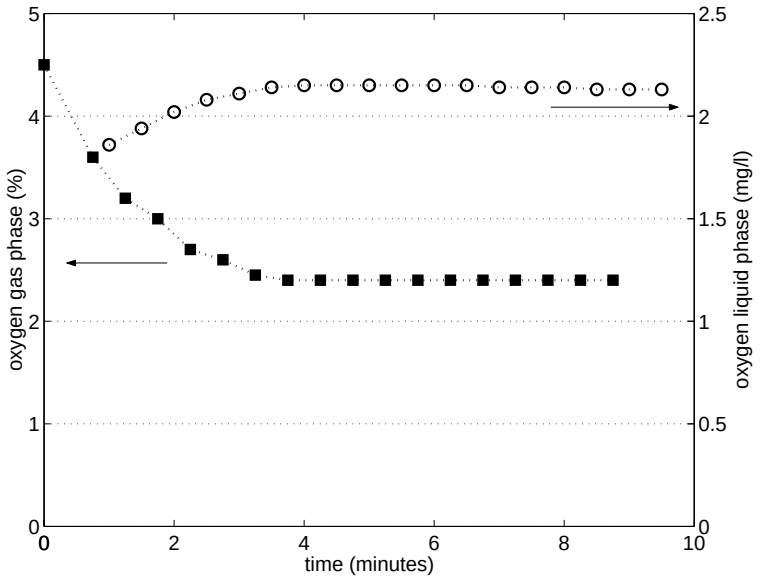

Figure 3.3: Mass balance experiment (V_L =3.49 $\cdot$ 10^{-3} m^3, Φ_L =2.15 $\cdot$ 10^{-5} m^3/s, Φ_G=4.48 $\cdot$ 10^{-6} m^3/s, T=21 $^\circ$C, p=1.05 bar.)

somewhat more accurate compared to absorption experiments.

The determined k_La values for both absorption and desorption, respectively, can be compared with the results from the work of Linek et al. (1987), who measured oxygen mass transfer coefficients using different methods and combined these data with experimental results from literature to obtain:

$$k_La = 4.95 \cdot 10^{-3} \left(\frac{P_g}{V_L}\right)^{0.593} u_G^{0.4} \tag{3.15}$$

In this correlation, u_G is the superficial gas velocity and P_g/V_L is the gassed power input per unit of volume. The ungassed power input (P) is given by:

$$P = N_P\, \rho N^3 D^5 \tag{3.16}$$

Hughmark (1980) correlated an extensive amount of data on the influence of the sparged gas on the power input and found the following relation:

$$\frac{P_g}{P} = 0.10 \left(\frac{\Phi_G}{N V_L} \right)^{-1/4} \left(\frac{N^2 D^4}{W g V_L^{2/3}} \right)^{-1/5} \tag{3.17}$$

A comparison between the data obtained in this work and the correlation of Linek et al. (1987) is shown in Figure 3.4 in a parity plot. From this figure it can be concluded that the range of the obtained mass transfer coefficients is in agreement with Equation 3.15, but the deviation from the correlation is rather large (an average relative deviation of 32%). The root cause of this deviation can probably be found in the non-standard tank dimensions and the wide range of conditions used in the experiments. The standard dimensions of the experimental set-up included that V_L = 2.53 dm^3, which means that the clear liquid height is equal to the tank diameter ($H_L = T$) and the distance from the bottom to the impeller is one third of the clear liquid height ($H_I = 1/3 H_L$). In the experiments with standard dimensions (2,6,7 and 9) the trend of Equation 3.15 is well followed, but a somewhat higher $k_L a$ is obtained in this work. The main deviation from the correlation is observed for the experiments with non-standard tank dimensions: V_L = 3.49 dm^3 (H_L/T = 1.38, exp:1,4), and when V_L = 1.69 dm^3 (H_L/T = 0.67, exp:5,8).

These results suggest that the effect of the liquid volume is not taken into account correctly. This phenomenon was was also observed by Schlüter and Deckwer (1992) who suggested that instead of the superficial gas velocity (u_G) the space velocity of the gas ($\varphi_G = \Phi_G / V_L$) should be used in the data correlation. When this is done in case of the experimental data for $k_L a$ in this work the average relative deviation decreased by more than 50%. The best values for the coefficients were obtained by a least squares regression analysis of the experimental values, which resulted in: $k_L a = 1.5 \cdot 10^{-3} \cdot (P_g/V)^{0.67} \cdot \varphi_G^{0.4}$. The exponent for the power input per unit volume (0.67) obtained in this correlation is in reasonable agreement with the work of Linek et al. (1987), 0.593 and with the work of Schlüter and Deckwer (1992), 0.62. The influence of the space velocity on the volumetric mass transfer coefficient is larger in this work (exponent of 0.4) compared to the correlation of Schlüter and Deckwer (1992) (0.23). The effect of the gas flow rate, which is present in u_G as well as in φ_G, is, however, exactly equal to the effect in the work of Linek

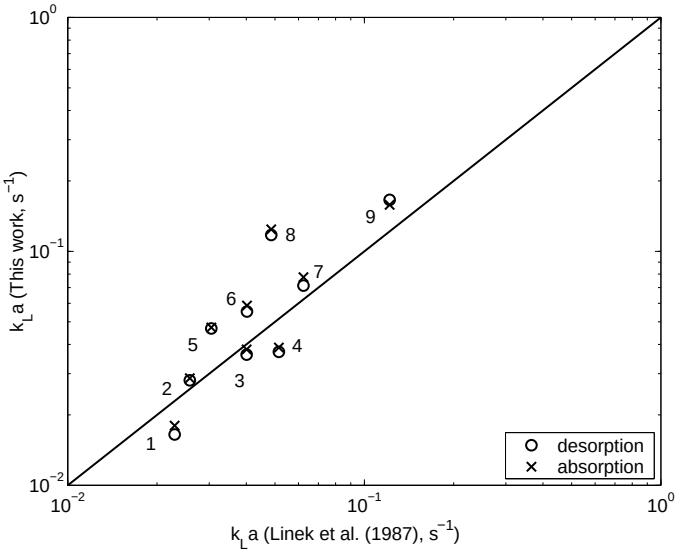

Figure 3.4: Comparison of absorption and desorption experiments with the correlation of Linek et al. (1987).

et al. (1987).

3.3.2 Chemical absorption of CO_2 compared to physical desorption of O_2

In the first set of experiments The Danckwerts-plot was applied with the liquid phase operated batchwise. As a buffer solution 0.5 M/0.5 M potassium carbonate/potassium bicarbonate was chosen. Using different molarities of sodium hypochlorite the Danckwerts-plot as given in Figure 3.5 was determined. The experimental conditions are given in Table 3.4.

From the slope and the intercept of this graph the following results are obtained, when both phases are assumed to be ideally mixed: $k_L = 2.0 \cdot 10^{-4}$ m/s, $a = 403$ m^2/m^3, $k_L a = 0.079$ s^{-1}. In Appendix E it is shown that the absolute values of the mass transfer parameters depend quite strongly on the assumed gas phase mixing pattern. Therefore the obtained experimental values are dependent on the assumed gas-phase mixing. The Danckwerts-plot technique can, however, safely be used to measure relative differences in the mass transfer parameters. In addition,

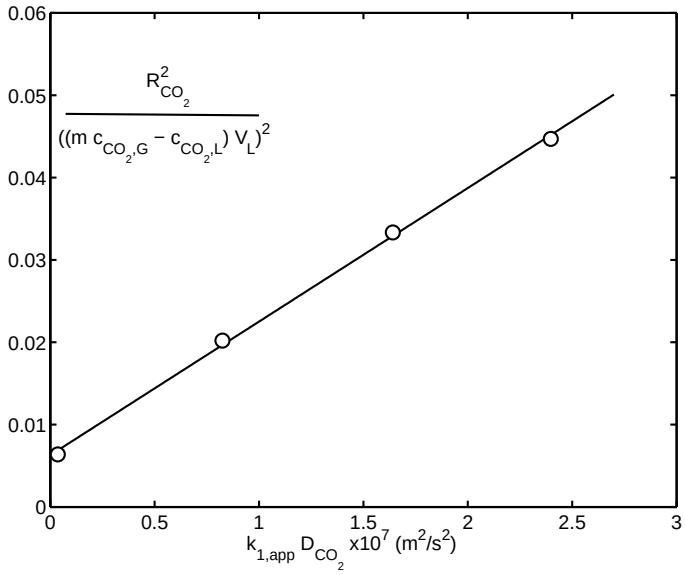

Figure 3.5: Danckwerts plot with batchwise operation of the liquid phase.

the absolute value for $k_L a$ is always obtained accurately.

The measurements for the validation of the Danckwerts-plot technique are represented in Figure 3.6. The absorption rate of carbon dioxide and the desorption rate of oxygen are plotted versus the product of the pseudo first order reaction rate constant, which was varied by changing the catalyst concentration for each experiment, and the diffusion coefficient. The experimental conditions are given in Table 3.4.

As is shown in Figure 3.6, the rate of desorption of oxygen from the liquid phase is not influenced by the addition of catalyst up to 178 mol m^{-3}. Deviations from the average are most likely due to experimental errors. This is supported by the fact that the deviations occur simultaneously for carbon dioxide and for oxygen and in the same direction. The chemical absorption measurements of carbon dioxide are somewhat more inaccurate when the reactor is operated continuously than when the liquid phase is operated batchwise (compare Figure 3.5 and 3.6), probably due to a more difficult operation of the set-up. Also the obtained mass transfer parameters deviate (max. 20%) from the batchwise operation. The results for carbon dioxide are (under the assumption of an ideally mixed gas and liquid phase):

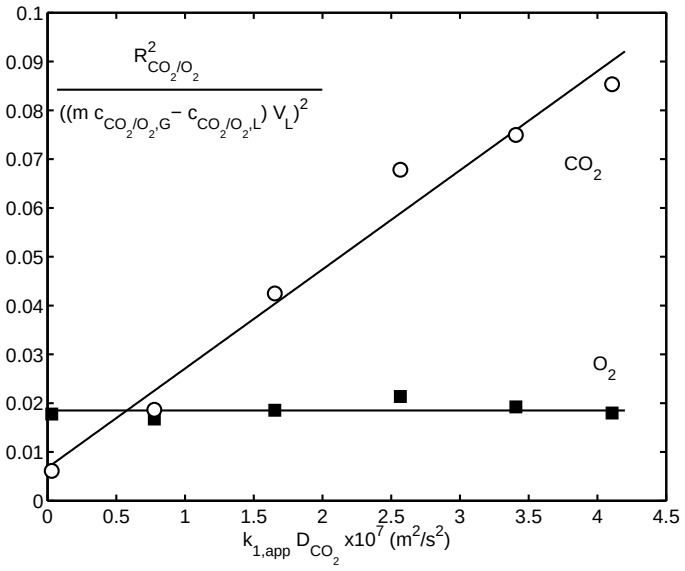

Figure 3.6: Validation of the Danckwerts-plot technique by comparison of the absorption rate of carbon dioxide and the desorption rate of oxygen at different catalyst (NaOCl) concentrations.

$k_L = 1.8 \cdot 10^{-4}$ m/s, $a = 451$ m^2/m^3, $k_La = 0.083$ s^{-1}.

The results of the present study show very clearly that the addition of catalyst does not influence the physical desorption of oxygen and that the application of the Danckwerts-plot is allowed over a large concentration range. The absolute value of the volumetric mass transfer coefficient of oxygen is, however, not completely in line with the k_La of carbon dioxide. The average k_La for oxygen is found to be 0.136 s^{-1} +/- 5%, which is 64% higher than the k_La for carbon dioxide under similar conditions. This cannot be explained with the existing theories for mass transfer, from which a relationship of the following form would be expected:

$$(k_La)_{O_2} = (k_La)_{CO_2} \left(\frac{D_{O_2}}{D_{CO_2}} \right)^n \tag{3.18}$$

where n is typically between 0.5-1. The observed large difference in volumetric mass transfer cannot be explained by the difference in the diffusion coefficients, because the diffusion coefficient of oxygen is approximately only 16% higher than the diffusion coefficient of carbon dioxide (assuming that the ratio in the buffer so-

Table 3.4: Experimental conditions used in the chemical absorption/physical desorption experiments in a 0.6 M/ 0.6 M potassiumcarbonate/bicarbonate buffer solution.

	continuous	batch
gas flow rate, Φ_G, $m^3\ s^{-1}$	$1.98 \cdot 10^{-4}$	$1.95 \cdot 10^{-4}$
liquid flow rate, Φ_L, $m^3\ s^{-1}$	$5.17 \cdot 10^{-5}$	-
liquid volume reactor, V_L, m^3	$2.53 \cdot 10^{-3}$	$2.53 \cdot 10^{-3}$
impeller speed, N, rps	18.3	18.3
temperature, T, $^\circ$C	21.0	21.0
reactor pressure, p, bar	1.18	1.18
catalyst concentration, c_{cat}, mol m^{-3}	0-178	0-92

lution is equal to the ratio in water, which was taken from the work of Díaz et al. (1987)). Furthermore, the observed difference in k_La cannot be explained by the assumed gas-phase residence time distribution (CISTR), as this difference increases with decreasing gas phase mixing.

A possible explanation for the observed discrepancy may be attributed to the difference in solubility in water of oxygen and carbon dioxide. The solubility of carbon dioxide is approximately 25-30 times higher when compared to the oxygen solubility. This can cause differences in the effective gas-liquid interfacial area when the bubble size is non-uniform and consists of a certain size distribution. Small bubbles containing carbon dioxide deplete much faster from the gas to be absorbed and therefore stop taking part in the mass transfer process at an earlier stage compared to bubbles containing oxygen. These effects were also recognized and analyzed by Schumpe and Deckwer (1980), who compared interfacial area data in bubble columns of different authors that either made use of CO_2 absorption in alkali or used O_2 absorption in sulfite solutions. Under (approximately) identical conditions oxygen absorption in sulfite solutions yields interfacial areas that are 50-500% higher compared to absorption of carbon dioxide in alkali solutions. An attempt was made to model these effects by taking the size distributions and the corresponding bubble rise velocities into account. To be able to explain the observed large differences in the interfacial area very broad size distributions should be assumed, containing a

relatively large fraction of small bubbles, with a long residence time in solution.

Another explanation for this phenomenon can be a smaller mass transfer coefficient, k_L, in case of carbon dioxide. Hallensleben (1980) measured lower values for the k_L of carbon dioxide compared to oxygen in water and showed that the values were both dependent on the inlet concentrations and on the direction of mass transfer. The authors stated that the lower k_L might be due to a resistance in the gas phase, although this was not expected at these low k_L values (2-3·10^{-4} m/s). To be able to explain the observed phenomenon a k_G value of 1·10^{-3} m/s should be assumed which is an order of magnitude lower than expected (by taking for instance the correlations from Carberry and Varma (1987)). Furthermore, the k_L was determined by indirect measurement of the k_La and the interfacial area that was determined by photography, which means that these results only indicate that there might be a difference between absorption of oxygen and carbon dioxide, but it is not clear whether this effect is due to a different effective interfacial area or due to a different mass transfer coefficient. Measurement of the k_L for a single rising bubble did not show a difference between O_2 and CO_2 that could not be explained by differences in the diffusion coefficients as was shown by Hallensleben (1980).

To gain understanding about the nature of the measured differences, three additional types of experiments were conducted.

- Absorption of pure CO_2 (no gas phase resistance) in non-coalescing water-butyraldehyde solutions was performed in the set-up described in Chapter 6 in order to determine the effect of the gas phase resistance. The k_La obtained with pure H_2, CO and propylene was on average 75% higher compared to CO_2 (after correction for the diffusion coefficients, see Figure 3.7), which indicates that (at least in this case) the gas phase resistance is not likely to be responsible for the obtained lower volumetric mass transfer coefficients. The difference is in these experiments most likely caused by the higher shrinking rate of gas bubbles containing CO_2 compared to the other gasses, which causes a lower interfacial area.

- The interfacial area was determined using the ultrasonic technique, which is described in Chapter 2 and was compared with the interfacial area determined

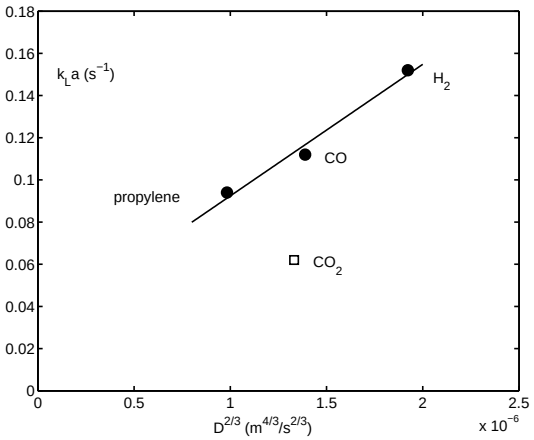

Figure 3.7: Volumetric mass transfer coefficients of pure gasses.

using the Danckwerts-plot technique. As it is shown in Appendix E the absolute value of the interfacial area as determined by the Danckwerts-plot is quite strongly dependent on the assumed residence time distribution (RTD) of the gas phase. Measurements were performed in a larger stirred vessel, which is described in more detail in Section 4.3, and the results are presented in Table 3.5. Even at the RTD assumption which yields the largest interfacial area (CISTR), the value of the interfacial area measured by the ultrasonic technique is on average 70% higher. The obtained difference is probably higher, as the measured RTD curves show increasing plug flow behaviour with increasing stirrer speed as shown in Appendix D. These results indicate that the (effective) interfacial area as measured by the CO_2 absorption using the Danckwerts-plot technique is smaller than the actual interfacial area (as can be measured by physical measurement techniques).

- An indication of the width and shape of the bubble size distribution was obtained using the ultrasonic technique by measurement of the profiles of the ultrasonic velocity and attenuation coefficient versus frequency. The exact size distribution could not be determined, but a good fit between the measured profiles and the model could only be obtained with a distribution that contained a large fraction of small ($< 100\mu$m) bubbles (either in a very broad

Table 3.5: Comparison of the interfacial area as determined with the ultrasonic method and with the Danckwerts-plot technique (assuming ideally mixed gas phase).

430 rpm	k_La **(s^{-1})**	a **(m^2/m^3)**	k_L **(m/s)**	ε **(%)**	d_{32} **(mm)**
Physical (ultrasound)	-	784	-	11.8	0.90
Chemical (Danckwerts-plot)	0.055	433	$1.3{\cdot}10^{-4}$	-	-
550 rpm	k_La **(s^{-1})**	a **(m^2/m^3)**	k_L **(m/s)**	ε **(%)**	d_{32} **(mm)**
Physical (ultrasound)	-	1084	-	13.3	0.74
Chemical (Danckwerts-plot)	0.102	667	$1.5{\cdot}10^{-4}$	-	-

log-normal distribution or in a bimodal distribution). The presence of large fractions of small bubbles was also measured by Machon et al. (1997), who used a microscope/video technique to study bubble size distributions in coalescing and non-coalescing systems.

The bubble size distributions that were obtained, were used in a mass transfer modelling study. The total mass transfer rate from the rising bubbles wit h certain size distribution was determined for the case of chemical absorption of carbon dioxide and for physical desorption of oxygen in buffer solutions. Coalescence and mixing effects were neglected, which is a reasonable assumption in non-coalescing systems. The bubble size was assumed to be constant (non-pure gasses). Furthermore, the effect of the smaller bubbles having a longer residence time in the solution was described by assuming the rise velocity of the bubbles to be proportional to their terminal rise velocity (u_T). The terminal rise velocity of the bubbles was calculated by balancing the buoyancy, gravitational and drag forces (assuming spherical bubbles).

Mass transfer of a gas to or from a single bubble of a certain size class i can be described according to:

$$\frac{dc_{G,i}}{dt} = -\frac{6k_L}{d_{B,i}}(mc_{G,i} - c_L) \tag{3.19}$$

This equation can be solved to obtain:

$$\frac{mc_{G,out,i} - c_L}{mc_{G,0} - c_L} = \exp\left(-\frac{6k_L m}{d_{B,i}}\tau_{B,i}\right) = \exp(-St_i) \tag{3.20}$$

in which $\tau_{B,i}$ is the residence time of a bubble of class i.

The total volume of bubbles in class i is given by:

$$V_i = \Phi_{G,i}\tau_{B,i} = \varepsilon_i \frac{H_L A}{(1-\varepsilon)} \tag{3.21}$$

in which H_L is the clear liquid height and A the cross-sectional area. When the bubbles are assumed to follow a straight line upwards, the expression for the residence time of the bubbles is given by:

$$\tau_{B,i} = \frac{H_L}{(1-\varepsilon)u_{B,i}} = \frac{\varepsilon_i}{\Phi_{G,i}}\frac{H_L A}{(1-\varepsilon)} \tag{3.22}$$

Note that the assumption of the bubble path does not influence the results as only the contact time of the bubble is important. The flow rate of each bubble class is then given by:

$$\Phi_{G,i} = u_{B,i}\varepsilon_i A \tag{3.23}$$

Making use of the constraints $\sum_i \Phi_{G,i} = \Phi_G$ and $u_{B,i} \sim u_{T,i}$ one can derive:

$$\Phi_{G,i} = \Phi_G \frac{u_{T,i}\varepsilon_i}{\sum_i (u_{T,i}\varepsilon_i)} \tag{3.24}$$

and

$$u_{B,i} = \frac{u_{T,i}}{\sum_i (u_{T,i}\varepsilon_i)}\frac{\Phi_G}{A} \tag{3.25}$$

The relative depletion per bubble class can be calculated from:

$$x_i = 1 - \frac{mc_{G,out,i} - c_L}{mc_{G,0} - c_L} = 1 - \exp(-St_i) = 1 - \exp\left(-\frac{6k_L m}{d_{B,i}}\frac{H_L}{(1-\varepsilon)u_{B,i}}\right) \tag{3.26}$$

By making use of the flow rates per bubble class the overall depletion can be calculated:

$$x_{ov} = \frac{1}{\Phi_G} \sum_i x_i \Phi_{G,i} \tag{3.27}$$

which can be back converted to an overall Stanton number:

$$St_{ov} = -\ln(1 - x_{ov}) \tag{3.28}$$

This Stanton number can be compared with the Stanton number obtained with a uniform bubble size at equal Sauter diameter and the ratio is a measure for the ratio of the effective interfacial area compared to the actual interfacial area.

$$\frac{a_{ov}}{a_{geo}} = \frac{St_{ov}}{St_{mono}} = \frac{St_{ov}}{\left(\frac{6k_L m}{d_B} \frac{H_L A}{(1-\varepsilon)\Phi_G}\right)} \tag{3.29}$$

The operating conditions were taken from the continuous experiments as described in Table 3.4. The k_La measured with oxygen (0.136 s^{-1}) was assumed to be the actual value, the interfacial area was measured using the ultrasonic technique (a = 530 m^2/m^3) and the gas hold-up was determined to be 7.0%.

In Figure 3.8 the conversion per bubble class is shown for physical oxygen absorption in the 0.6 M/0.6 M buffer solution ($m = 0.016$) and for chemical absorption of carbon dioxide in the buffer solution ($m = 0.50$). In case of CO_2 absorption bubbles of 440 μm are already completely (99%) depleted from the gas, while in case of oxygen absorption this is only the case for bubbles up to 100 μm in diameter (These results differ slightly at different size distributions). In case of a broad bubble size distribution containing small bubbles, differences in the measured mass transfer rate of oxygen and carbon dioxide can therefore occur.

To study the effect of the ratio of the measured interfacial area and the geometrical interfacial area, two size distributions were investigated; the size distribution that was measured using ultra sound (log-normal, μ = 84 μm, σ =

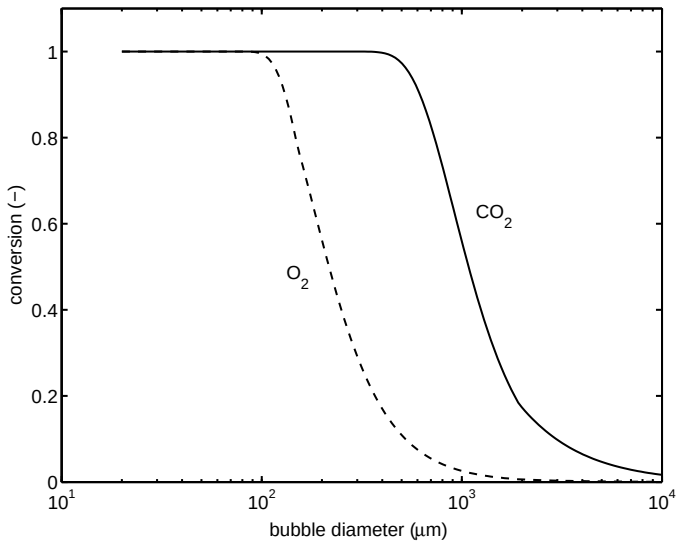

Figure 3.8: Depletion from the absorbed gas of different bubble sizes. (Log-normal distribution ($\mu = 0.36$ mm, $\sigma = 0.25$ mm).

Table 3.6: Ratio of interfacial areas.

μ (μm)	σ (μm)	a_{CO_2}/a_{geo}	a_{O_2}/a_{geo}	a_{O_2}/a_{CO_2}
84	121	0.32	0.75	2.35
358	250	0.54	0.94	1.75

121 μm, with a minimum bubble size of 10 μm) and a good log-normal fit of the distribution obtained by Machon et al. (1997) in a non-coalescing electrolyte system ($\mu = 358$ μm, $\sigma = 250$ μm). The results are shown in Table 3.6. These results only indicate that the measured lower mass transfer coefficient for CO_2 in comparison O_2 is likely to be due to the depletion of small bubbles. The extent of this effect is quite dependent on the size distribution and on the model assumptions.

From the observed phenomena, it can be concluded that the most likely explanation for the obtained lower mass transfer coefficient with carbon dioxide is the high gas phase conversion, which causes almost complete depletion of small bubbles and therefore lowers the effective interfacial area.

3.4 Conclusions

In the present study, design rules for continuous physical mass transfer experiments are derived, to obtain the highest accuracy for the determination of the volumetric mass transfer coefficient. It was shown that concentration measurement in the liquid phase is favourable when $m\tau_G < \tau_L$. In other cases measurement in the gas phase is favourable (assuming the same experimental accuracy). Furthermore, in case of liquid phase concentration measurement desorption is more accurate and in case of gas phase measurement absorption is the preferred direction of mass transfer.

Desorption of oxygen from a carbonate/bicarbonate buffer solution was used to study the effect of the catalyst addition, for the construction of the Danckwerts-plot, on the hydrodynamics of the system. It was confirmed by comparing absorption and desorption rates in water that these two processes are identical, but in a different direction. It was shown that the addition of the catalyst (up to 0.2 M sodium hypochlorite) did not affect the desorption rate of oxygen. The effect of catalyst addition on the hydrodynamics of the system is therefore negligible.

The volumetric mass transfer coefficient of oxygen was, however, much larger (64%) compared to the k_La of carbon dioxide. This is most likely caused by the higher solubility of carbon dioxide compared to oxygen, which causes a higher gas phase conversion. In case of a broad size distribution containing a relatively large fraction of small (<100 μm) bubbles, these small bubbles are at an earlier stage (almost) completely depleted, when they contain carbon dioxide compared to when they contain oxygen. This can cause a lower effective interfacial area with CO_2. Mass transfer experiments with oxygen, with a low gas phase conversion, are therefore preferred, as the measured mass transfer parameters are less affected by the gas phase RTD and the shape of the bubble size distribution.

Acknowledgement

The author wishes to gratefully acknowledge F.T. de Bruijn and E. van Brandenburg for their contribution to the experimental work performed for this chapter. B. Knaken is acknowledged for the construction of the experimental set-up.

Chapter 4

Ultrasonic investigation of hydrodynamics and mass transfer in a gas-liquid(-liquid) stirred vessel

Abstract

The rate of gas-liquid mass transfer is very important in several industrial chemical engineering applications. In many multi-phase reaction systems, however, the mechanism of mass transfer is not well understood. This is for instance the case in Gas-Liquid-Solid (G-L-S) and Gas-Liquid-Liquid (G-L-L) systems. To obtain more knowledge of the mechanism of mass transfer, the mass transfer coefficient, k_L, and the interfacial area, a, should be studied separately.

In this work an ultrasonic measurement technique is used to study the local interfacial area in a standard sized vessel, equipped with a Rushton type impeller. This is done in combination with experimental determination of the volumetric mass transfer coefficient, k_La, using the dynamic oxygen method, to obtain values for k_L. The gas hold-up is determined additionally to obtain values for the Sauter mean bubble diameter at different positions in the vessel. In a coalescing air-water system

the bubble size was non-uniform throughout the vessel and increased from small bubbles at the impeller along with the flow pattern to larger sizes in the bulk of the vessel. In a non-coalescing electrolyte system the vessel was much more uniform and the bubbles were smaller when compared to the air-water system. To obtain overall values of the mass transfer parameters the local values were integrated according to their volume fraction in the reactor. In both coalescing and non-coalescing systems the overall values for the mass transfer parameters were in good agreement with literature correlations.

The addition of small volume-fractions of toluene to an air-water system caused a strong decrease in both the volumetric mass transfer coefficient and in the gas hold-up. The interfacial area increased, however, but it was shown that this was due to the presence of microbubbles in the solution, which do not take part in the mass transfer process. The enhancing effect on gas-liquid mass transfer due to the addition of larger volume-fractions of toluene could be described reasonably well by a homogeneous model of the shuttle mechanism.

4.1 Introduction

Many industrial chemical engineering applications are limited by the gas-liquid mass transfer rate. For this reason, accurate knowledge of mass transfer coefficients is necessary to be able to predict the production rates in these processes. In gas-liquid stirred vessels and bubble columns the volumetric mass transfer coefficient, k_La, which is usually sufficient to predict production rates, is investigated intensively. However, to gain more knowledge about the mechanism of mass transfer, the mass transfer coefficient, k_L, and the gas-liquid interfacial area, a, should be studied separately. This can be established by the use of a chemical method (Danckwerts-plot technique, see Chapter 1), but this has the disadvantage that this method is confined to some specific chemical systems, which require the addition of electrolytes thereby completely changing the nature of these systems in terms of coalescence and break-up of gas bubbles. Another option is to measure simultaneously the volumetric mass transfer coefficient, k_La, by mass transfer experiments and the gas-liquid interfacial

area by using a physical method. Measurement of the interfacial area via physical methods can be performed using photography in combination with determination of the gas hold-up (e.g. Pacek et al. (1994)), using laser scattering (e.g. Calderbank (1958)) or by capillary suction probes (e.g. Barigou and Greaves (1991)). A shared limitation of all these methods is that the interfacial area is determined locally, at a certain, usually fixed, position in the reactor. To obtain a value for the overall interfacial area, values at different positions in the reactor should be integrated according to their volumetric space. When this task is performed, not only an accurate value of the gas-liquid interfacial area is obtained, which can be used together with measurements of $k_L a$ to obtain accurate values of the (average) mass transfer coefficient, but also a profile of interfacial areas inside the vessel is obtained. Such a profile contains information about streamlines and coalescence/break-up processes in for instance stirred vessels or bubble columns, which can be used to gain understanding about the complex hydrodynamics of these reactors and can be useful in validation of models that are based on Computational Fluid Dynamics (CFD).

Similarly to gas-liquid systems, the rate of mass transfer is usually very important in gas-liquid-liquid systems. As an example, Wachsen et al. (1998) have shown that the biphasic hydroformylation of propylene to butyraldehyde, which is an industrially very important reaction, is (at least partially) mass transfer limited. In this system three gaseous components (propylene, CO and H_2) all react in an aqueous phase containing a homogeneous rhodium catalyst, while the products, (n- and iso-butyraldehyde), form an additional third phase. The droplets of this third phase may affect the gas to liquid mass transfer rate.

In systems that not inherently consist of three different phases, gas-liquid mass transfer (and thus the production rate) can be affected or even enhanced by the presence of a dispersed liquid phase with a higher capacity for the component to be transferred. This is the case in some biochemical applications in which an oil phase is deliberately used to enhance the mass transfer rate of oxygen to a water phase containing micro-organisms (Rols et al., 1990).

The mechanism of mass transfer in these systems is not well understood. As early as in 1970 (Yoshida et al., 1970) it was shown that one dispersed phase

(toluene) can enhance mass transfer (after a decrease in the mass transfer rate at low dispersed phase fractions) whereas another dispersed phase (kerosene) decreases mass transfer, while both organic phases have more capacity for oxygen compared to the aqueous, continuous phase. In the study of Yoshida et al. (1970) (and in most other research studies on mass transfer in gas-liquid-liquid systems) the mass transfer rate is reported and determined via the measurement of the lumped volumetric mass transfer coefficient, k_La. This example indicates that, because of the complex influence of the dispersed phase fraction on k_L as well as on a (see Chapter 1), also in gas-liquid-liquid systems k_L and a should be measured individually and preferably simultaneously, to be able to analyze the effects of a dispersed phase on gas-liquid mass transfer, which will lead to a better understanding.

In this chapter experiments will be presented, in which the volumetric mass transfer coefficient (k_La) is measured simultaneously with local values of the interfacial area (a_{local}) and the gas hold-up (ε_{local}). These values can be integrated to overall values ($< a >$) and ($< \varepsilon >$). For coalescing and non-coalescing electrolyte gas-liquid systems these results are compared with similar experiments in literature. In addition, experiments were performed in a gas-water-toluene system in which also, k_La, a_{local}, $< a >$, ε_{local} and $< \varepsilon >$ were determined at different dispersed phase fractions. The droplet size, which may be an important parameter in the mechanism that causes the enhancement of mass transfer, was determined in situ. In this way an attempt is made to increase the insight in influence of a second liquid phase on gas-liquid mass transfer and hydrodynamics.

4.2 Measurement techniques

4.2.1 Gas-liquid interfacial area and bubble size distribution

Ultrasonic spectroscopy is able to determine the local gas-liquid interfacial area and the bubble size distribution, as is explained in Chapter 2. In Figure 4.1 it is shown that the attenuation coefficient increases with an increasing interfacial area. This relationship is linear in the high frequency regime and will approach $a = 4\alpha$ at infinite values of the product of frequency and bubble radius.

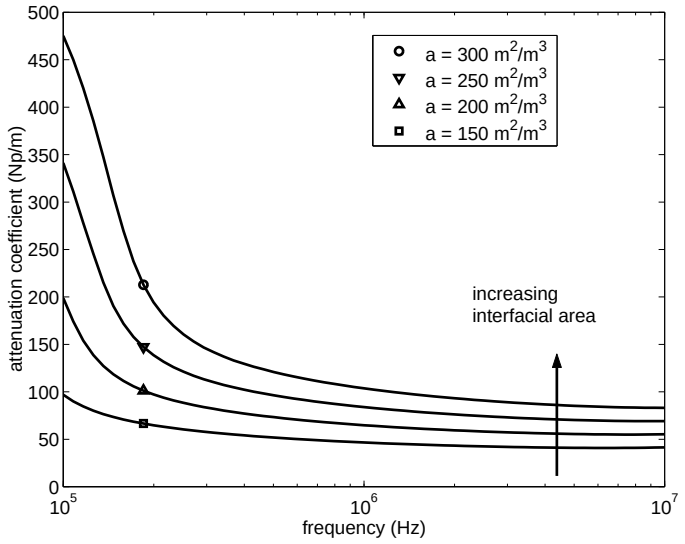

Figure 4.1: Attenuation coefficient as function of the interfacial area. $\varepsilon = 0.08$, $\sigma = 0.1\mu$.

In Figures 4.2a and 4.2b it is shown that in the high frequency regime (> 1 MHz) the ultrasonic velocity and the attenuation coefficient are independent of the bubble size distribution (assuming that the distribution is small enough to exclude very small ($< 100\mu$m) bubbles). This means that at these high frequencies measurement of the interfacial area is possible at a single frequency, without requiring the simultaneous measurement of the gas hold-up. Especially in case of mapping the local interfacial areas over an entire reactor volume, this saves a lot of time performing the experiments.

Figure 4.2 also shows that it is possible to determine the width of the distribution mainly in the low frequency (< 1 MHz) regime. However, as shown in Chapter 2 in that case it is desirable that the local gas hold-up is known, because multiple solutions yielding the same interfacial areas may exist. Furthermore, the attenuation coefficient is not very sensitive to the variance in the log-normal distribution. While the differences of the distribution widths are used in Figures 4.2a and 4.2b (the used distributions are presented in Figure 4.3) are large, the values of the ultrasonic velocity and the attenuation coefficient both differ maximally 10%. With accurate measurements, however, it is possible to determine the width of the distribution in the low frequency regime.

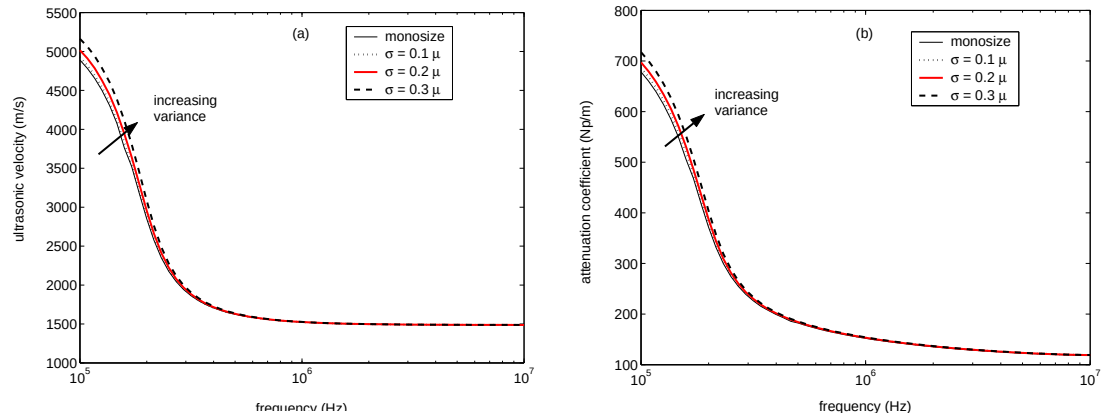

Figure 4.2: Influence of the width of the log-normal distribution on the ultrasonic velocity and attenuation coefficient. $\varepsilon = 10\%$, $d_{32} = 1.4$ mm in all cases.

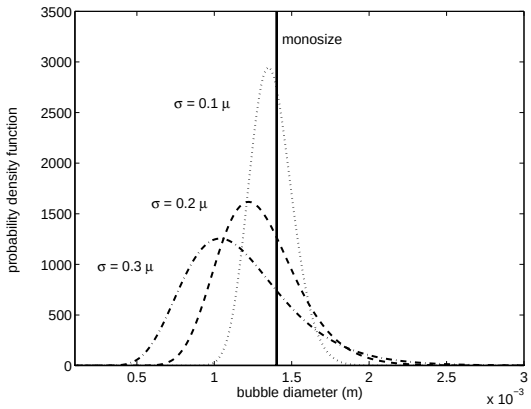

Figure 4.3: Log-normal distributions used in the calculations. d_{32} is 1.4 mm in all cases.

4.2.2 Gas hold-up

Electrical conductivity was used for measurement of local gas hold-up at different positions in the reactor. Details of the method are presented in Chapter 2.

The overall gas hold-up can be determined by measurement of the total liquid height in the reactor with and without gas sparging respectively, according to:

$$\varepsilon = \frac{V_G}{V_T} = \frac{V_T - V_L}{V_T} = 1 - \frac{H_0}{H_T} \tag{4.1}$$

In opaque vessels and in vessels in which height reading is difficult due

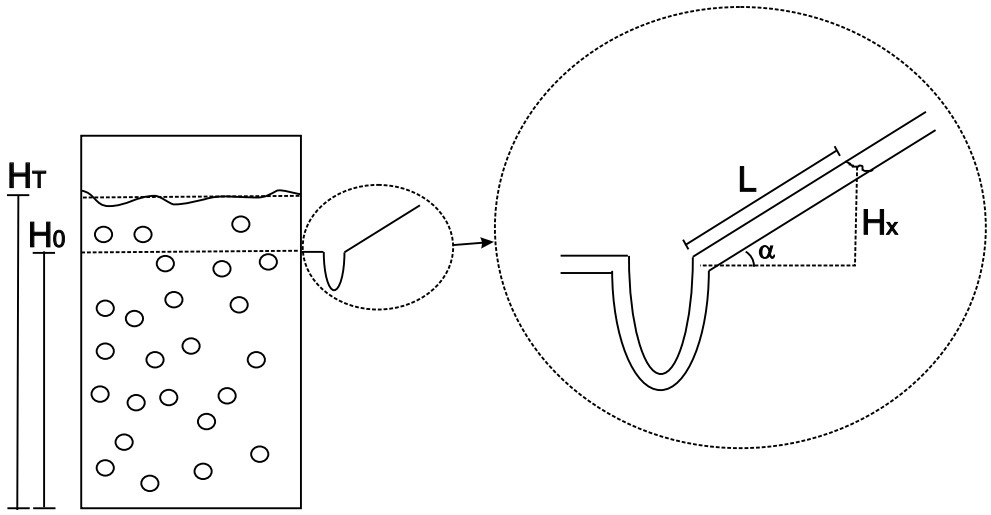

Figure 4.4: Inclined tube method for measurement of the overall gas hold-up.

to a large amount of turbulence induced by a stirrer, a second method for the determination of the overall gas hold-up is necessary. For this reason the overall gas hold-up is measured using the method proposed by Meng et al. (2002), which makes use of an inclined tube outside the vessel at the liquid height without sparging (H_0, see Figure 4.4). These authors obtained accurate results with this method compared to a gamma ray density monitoring system. To stabilize the liquid surface in their inclined tube a known amount of oil was put on top of the surface. This part was not used in this work, because of the risk of contamination of the continuous water phase. The tube is curved at the bottom side to prevent entrance of air bubbles and the measurement tube is put in an angle to improve the accuracy of the measurement.

The gas hold-up is calculated by equating the pressure in the inclined tube to the hydrostatic pressure in the vessel ($\Delta p^{ves} = \Delta p^{it}$). Making use of $\Delta p = \rho g \Delta H$ this results in:

$$\rho_{GL} g \left(H_T - H_0\right) = \rho_L g H_X \tag{4.2}$$

By making use of Equation 4.1, H_T can be written as $H_0/(1-\varepsilon)$. Because ρ_{GL} equals $(1-\varepsilon)\rho_L + \varepsilon\rho_G$, Equation 4.2 results in:

$$H_0 \frac{\varepsilon}{(1-\varepsilon)} \left((1-\varepsilon)\rho_L + \varepsilon\rho_G\right) = \rho_L H_X \tag{4.3}$$

From this equation the gas hold-up can be solved:

$$\varepsilon = \frac{\left(H_0 + H_X\right)\rho_L - \sqrt{\rho_L^2 \left(H_0 - H_X\right)^2 + 4H_0 H_X \rho_L \rho_G}}{2H_0 \left(\rho_L - \rho_G\right)} \tag{4.4}$$

Note that this result is different compared to the erroneous equation in work of Meng et al. (2002). When the gas phase consists of air at room temperature and atmospheric pressure the gas phase density can be neglected and Equation 4.4 simplifies to:

$$\varepsilon = \frac{H_X}{H_0} = \frac{L\sin(\alpha)}{H_0} \tag{4.5}$$

This simplification results in a maximum relative error of 0.05% up to 30% gas hold-up. A possible introduction of error in this method occurs when the gas hold-up in the top part of the vessel (the measurement part) is not equal to the hold-up in the bottom section. The magnitude of the error depends, on the average gas hold-up and the amount of deviation of the top part from the bottom part and is larger at higher average gas hold-ups and at higher deviations in the top section. However, at the maximum gas hold-up applied in the stirred vessel in this work (13%) and in case the gas fraction in the top part is 50% less compared to the average value the relative error is still only 7%, which is quite acceptable in comparison with height reading in a turbulent stirred vessel.

4.2.3 Volumetric mass transfer coefficient

The volumetric mass transfer coefficient is determined using the dynamic oxygen method. In this method the response to a step change in the gas phase oxygen concentration is measured by an oxygen meter in the liquid phase. Furthermore, the probe response time, which has to be known to be able to perform accurate measurement, has to be determined. This is accomplished by rapidly dropping the

oxygen probe in an environment with a different oxygen concentration, while measuring the response of the probe. The probe response time is not important when $\tau_P << 1/(5k_La)$. In this work, however, an oxygen probe with a teflon membrane was used, because of the presence of a dispersed liquid phase (toluene). Due to the membrane, the probe has a higher response time (around 6 seconds) and determination of τ_P is therefore necessary.

Mathematical model

The determination of the volumetric mass transfer coefficient requires the use of appropriate models for the liquid and gas phases. Linek et al. (1987) and earlier van 't Riet (1979) have pointed out that especially for high values of the gas phase residence time it is necessary to take the change in gas phase concentration during the measurement into account. Furthermore, the following assumptions were made:

1. Both the gas phase as well as the liquid phase are well mixed.
2. The probe responds as a first order system and the characteristic probe time is τ_P
3. The counterdiffusion of nitrogen can be neglected. This was verified by Linek et al. (1982)
4. The hydrodynamics in vessel remain unchanged during the interchange of gases with a different composition.
5. The gas flow rate, Φ_G, is constant.

This then results in the following oxygen mass balances:
Gas phase:

$$\frac{dc_G}{dt} = \frac{(c_{G,in} - c_G)}{\tau_G} - k_La(mc_G - c_L)\frac{V_L}{V_G} \tag{4.6}$$

Liquid phase:

$$\frac{dc_L}{dt} = k_La(mc_G - c_L) \tag{4.7}$$

Diffusion in the probe:

$$\frac{dc_P}{dt} = \frac{(c_L - c_P)}{\tau_P} \tag{4.8}$$

At time $t = 0$ the concentrations are: $c_G = c_{G,in}$, $c_L = 0$ and $c_P = 0$.

The solution of this system of three coupled linear differential equations must be compared with the experimental liquid phase concentration to obtain the volumetric mass transfer coefficient. This can be accomplished by moment analysis of both the probe and the liquid phase response according to Dang et al. (1977). Although this method is substantially simpler compared to curve regression methods, wrong absorption curves are not recognized easily (Linek et al., 1987), which can lead to errors in the estimated k_La values. Therefore the experimentally obtained liquid phase concentrations are regressed to the liquid phase concentration as determined by the mathematical model using a Nelder-Mead simplex optimization (Nelder and Mead, 1965). To accelerate the optimization process an analytical solution to the system of differential equations is derived, which is presented in Appendix C.

4.3 Experimental set-up

The experimental set-up consists of a reaction vessel, which is 40 cm in diameter and the operational amount of liquid was 52.6 liter when water was used as the continuous phase and 42.6 liter in the experiments with electrolyte solutions. The reactor was equipped with a 6-bladed Rushton turbine with a diameter of one third of the reactor diameter (13.3 cm) and that was placed at 13.3 cm from the bottom. The turbine was driven by a motor with a variable stirring speed with a maximum of 960 rev/min. Four baffles of 4 cm in diameter ensured adequate mixing inside the vessel. The gas is sparged in the vessel through two 8 mm holes below the impeller. A schematic diagram of the used set-up is presented in Figure 4.5.

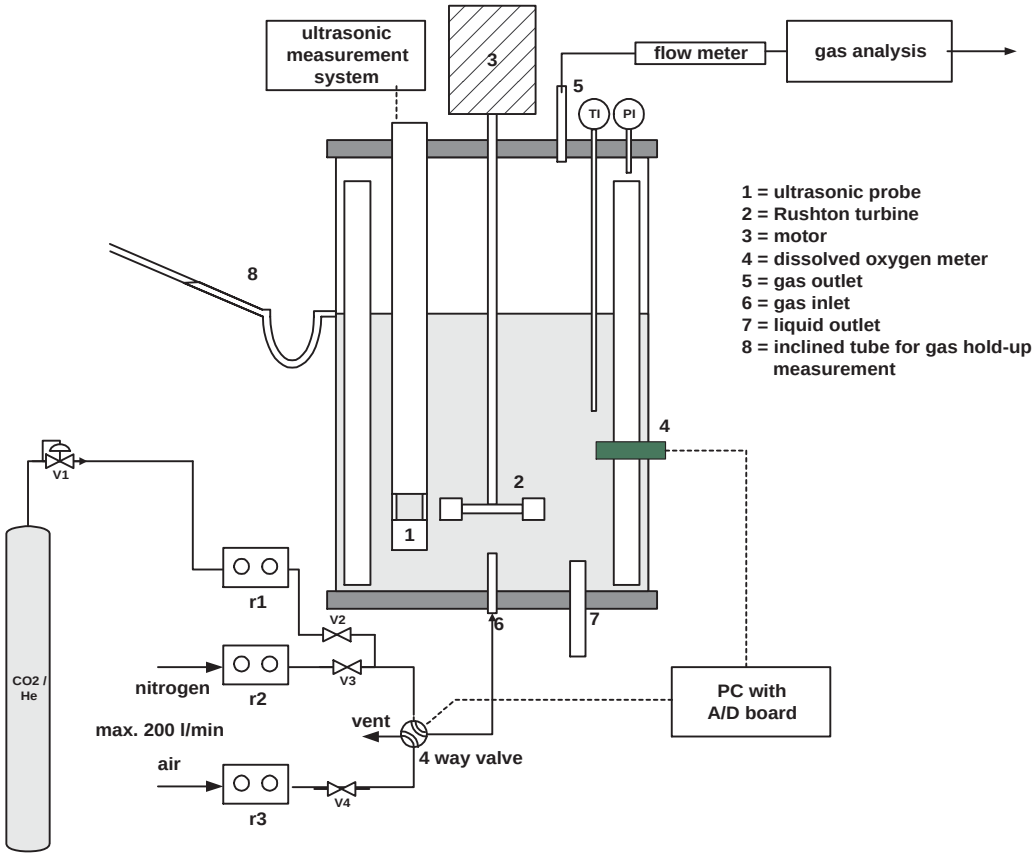

Figure 4.5: Experimental set-up for simultaneous measurement of k_La using the dynamic oxygen method and the interfacial area using ultrasonic spectroscopy.

4.3.1 Probes for measurement of interfacial area, gas hold-up and bubble and droplet size distribution

Measurement of the gas-liquid interfacial area was performed using a stainless steel probe of 5 cm in diameter with a variable distance between the transducers with a maximum of 5 cm. The transducers that transmit the low frequencies are 33 mm in outer diameter and the low frequency transducers were much smaller (12 mm). For this reason, the transducers were covered with a steel jacket to ensure that the shape of the probe was not influenced by the frequency range of the measurement. Furthermore, the probe was designed to cause the least disturbance to the gas-liquid flow pattern as possible. Only three stainless steel rods of 4 mm connected

the transmitting and receiving part of the probe.

The probe for the measurement of the dispersed phase hold-up was constructed of PVC with stainless steel electrodes. The distance between the electrodes was fixed at 5 cm. The stainless steel connection rods were covered with a teflon coating to prevent disturbances by conduction through these rods. Also the inside reactor wall and the connection between the Rushton turbine and the motor were insulated to prevent short-circuiting of electrical current.

4.3.2 Volumetric mass transfer coefficient

For the determination of the volumetric mass transfer coefficient a 4-way valve was used, which was designed for fast (< 100 ms) switching between air and nitrogen. Both the flows were controlled by flowmeters with a maximum of 200 liters per minute. The gas flow that was selected for the measurements in water and water containing different amounts of toluene was 40 l/min. The tubing between the valve and the vessel was 1.5 meter long and had an inner diameter of 10 cm, which means that the time between for the gas to reach the vessel was 0.2 seconds. This time was taken into account in the calculation of the results. The liquid phase oxygen concentration was measured using a Lazar Labs dissolved oxygen meter with a teflon membrane. This membrane has a somewhat higher response time (6.7 seconds), but has the advantage of being resistant to toluene.

4.3.3 Gas phase residence time

For measurement of the gas phase residence time distribution (the method is explained in Appendix D) the nitrogen stream can be diluted with a certain amount of helium. The trigger to switch the valve was sent by the oscilloscope and in this way the starting point, $t = 0$, is always perfectly known.

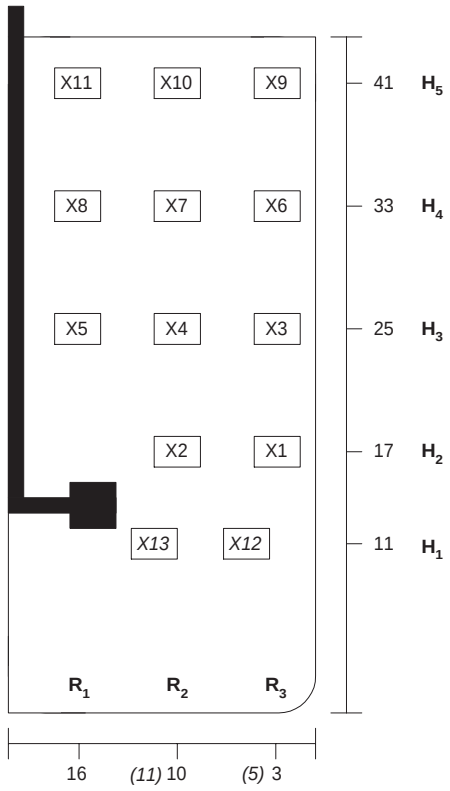

Figure 4.6: Positions in the reactor (dimensions are in centimeters)

4.4 Mapping of local values

To obtain a complete profile of local values, measurements were performed in the mid-plane between two adjacent baffles at 13 well-defined positions in the reactor. The measurement frequency that was used for the ultrasonic technique was 2 MHz. The probe was inserted from the top of the reactor, where the angle and depth of the probe define the positions in the tank (see Figure 4.6). The measurement points were selected to cover a region as large as possible. X12 and X13 have a slightly different horizontal coordinate, because of the curvature of the bottom of the vessel and because there was hindrance of the stirrer. For this reason a (small) part of the bottom region of the vessel could not be reached.

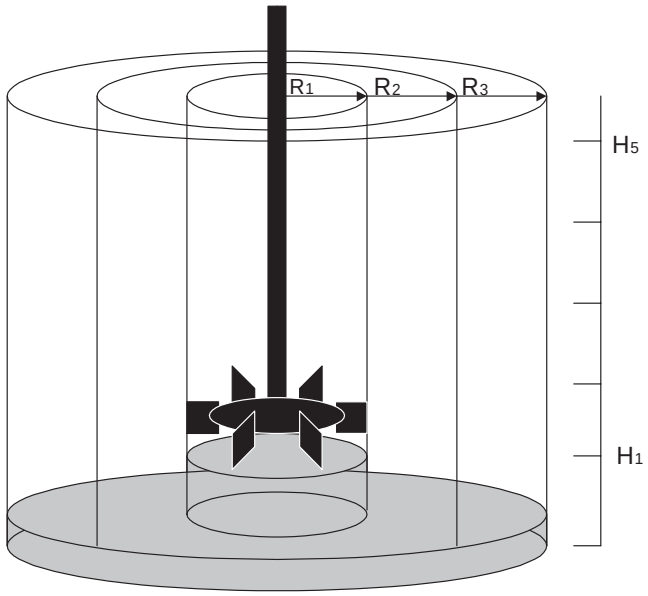

Figure 4.7: Schematic representation of the method to integrate local values to average values in the vessel. (The grey area is not used in the integration).

The overall values of the interfacial area and the gas hold-up can be calculated by integration over the reactor volume they represent, assuming rotational symmetry. Each point in the vessel represents a certain volume V_i, which is defined by its spatial coordinates. The measurements points are defined as the exact mid points of the space between the transducers and the volumes they represent are calculated as $V_i = \pi \Delta r^2 \Delta H$. The volume that could not be reached was omitted from the calculation (see Figure 4.7). This results in loss of information of the bottom of the tank and very close to the impeller. For every measurement point a certain volume fraction can now be calculated, $f_i = V_i / \sum_i V_i$. The integration method did not influence the results for the overall values to a large extent compared to normal averaging. The overall values for the interfacial area, the gas hold-up and the Sauter diameter can be determined:

$$\langle a \rangle = \sum_{i=1}^{13} a_{local,i} f_i \tag{4.9}$$

$$\langle \varepsilon \rangle = \sum_{i=1}^{13} \varepsilon_{local,i} f_i \tag{4.10}$$

$$d_{32} = \frac{6 \langle \varepsilon \rangle}{\langle a \rangle} \tag{4.11}$$

The Sauter diameter can also be calculated using the overall gas hold-up as measured with the inclined tube. Ideally the two methods to determine $< \varepsilon >$ would give the same results.

The inclined tube had a total height of 10 cm, so it could be used up to almost 20% of gas hold-up. The angle of the tube was chosen to be 23 $^\circ$.

4.5 Results and discussion

4.5.1 Validation of gas hold-up methods

To check the validity of both methods for measurement of the overall gas hold-up using the inclined tube and the method for determination of the local gas hold-up using electrical conductivity, a cross-validation of both methods was performed. The experiments were performed in the small bubble column, which was also used in Chapter 2, in which a porous plate gas disperser assured a nice homogeneous flow pattern so that local and overall gas hold-up are comparable. Also standard height reading was possible due to the homogeneous flow and the non-turbulent surface. Tap water was used as the liquid phase to allow the conductivity technique to work optimally. The results of the three methods are presented in Figure 4.8.

As is shown in Figure 4.8 the agreement between the three methods is very good. The maximum relative deviation from the average is 7.6 % and the average relative deviation is 3.6 % and the error seems to be randomly oriented. This result shows that the inclined tube method as well as the conductivity method can be used for gas hold-up measurement in the stirred vessel.

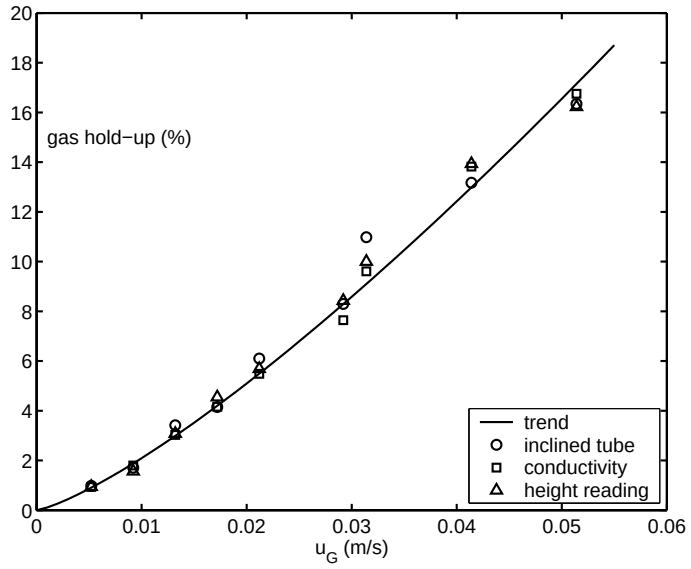

Figure 4.8: Cross-validation of different methods for gas hold-up measurement.

4.5.2 Influence of the ultrasonic technique

Ultrasonic power input

It is very important that the influence of the power input due to the transmission of the ultrasonic waves does not influence the bubble size distribution between the transducers. A high power input can cause breakage of bubbles and can result in unwanted cavitation. In this work, however, the power input was kept very low (< 0.005 W), as a tone burst operation with a 20 Hz signal frequency was used. The applied ultrasonic power input was very small compared to the power generated by the stirrer and can therefore safely be neglected. To validate that the bubbles between the transducers were not affected by the ultrasonic power input the attenuation coefficient, which has an almost linear relationship with the gas-liquid interfacial area, was measured under different applied power inputs and further identical conditions. The results are presented in Figure 4.9 and show that there is hardly an influence of the power input. The maximum deviation from the average is 7%, which is most likely within the experimental error.

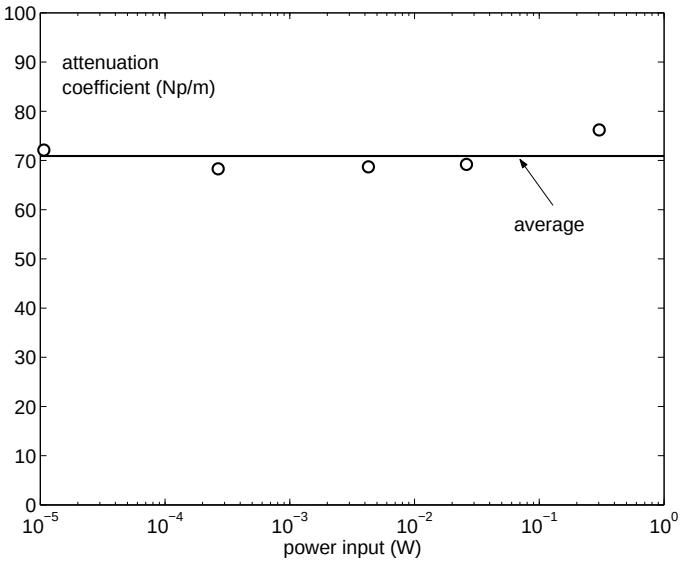

Figure 4.9: Influence of the power input added by the ultrasonic probe on the measured attenuation coefficient. Position: X4, frequency: 300 kHz, Stirring speed: 640 rpm, Superficial gas velocity: 0.58 cm/s.

Ultrasonic probe

The influence of the probe on the measured interfacial area was tested using the model probe, which was also used in Chapter 2, which was completely open, but also less stable when applied to the turbulence in the reactor. The differences in the results with the two probes were always small (relative deviations less than 10 %). The results of the solid probe were better reproducible compared to the open probe, mainly due to the good stability under high turbulence in the vessel. Furthermore, this probe could be put at its correct angle and immersion depth very accurately (within 0.3 $^\circ$ and 0.5 mm, respectively). It is therefore concluded that the probe geometry did not significantly influence the results presented hereafter.

4.6 Results in coalescing systems

4.6.1 Profiles of interfacial area, gas hold-up and Sauter mean diameter

In Figures 4.10 to 4.14 the measured profiles of the local interfacial area, gas hold-up and the calculated Sauter diameter are shown for a system of tap water and air at a superficial velocity of 0.58 cm/s and stirring speeds of 200 - 960 rpm.

From these figures it can be concluded that gas dispersion in vessels containing coalescing media is highly inhomogeneous, which was already observed by a.o. Calderbank (1958). The gas-liquid interfacial area is the highest in the impeller discharge zone (X12, X13) and is much lower (a factor 4 at high stirring speeds) in the upper part of the reactor. Furthermore, the difference between the center and the wall part of the reactor is quite large, mainly in the vertically middle part of the vessel. Large gas hold-ups are found mostly in the center of the reactor approximately 12 cm above the impeller. At the wall the gas hold-up is lower and the

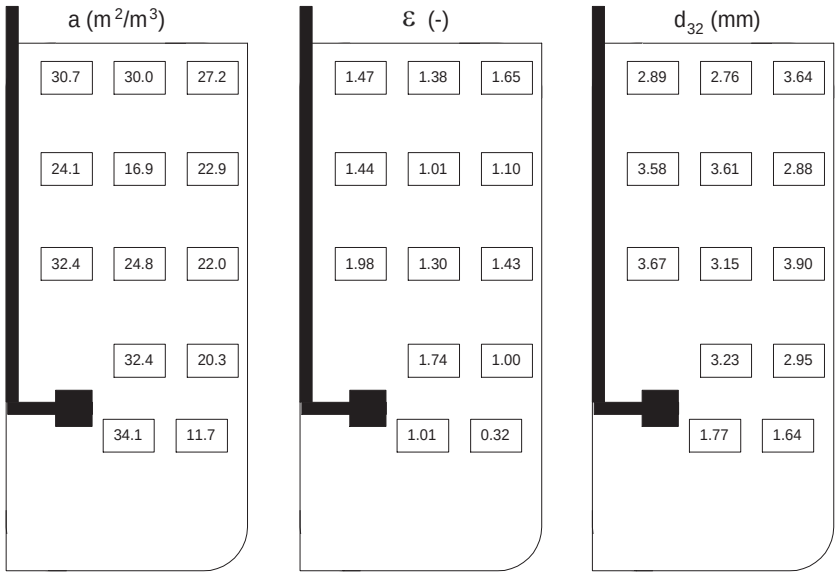

Figure 4.10: Profile of interfacial area, gas hold-up and Sauter mean diameter at a stirring speed of 200 rpm and a superficial gas velocity of 0.58 cm/s.

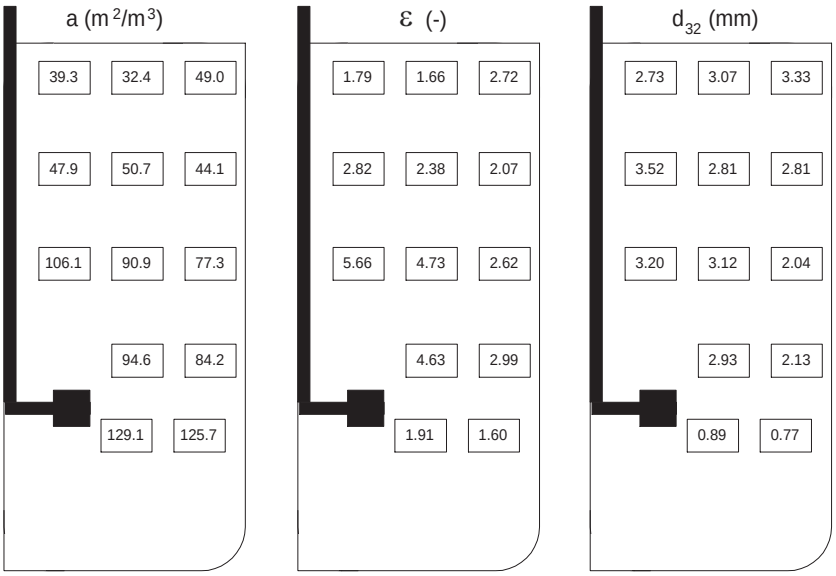

Figure 4.11: Profile of interfacial area, gas hold-up and Sauter mean diameter at a stirring speed of 420 rpm and a superficial gas velocity of 0.58 cm/s.

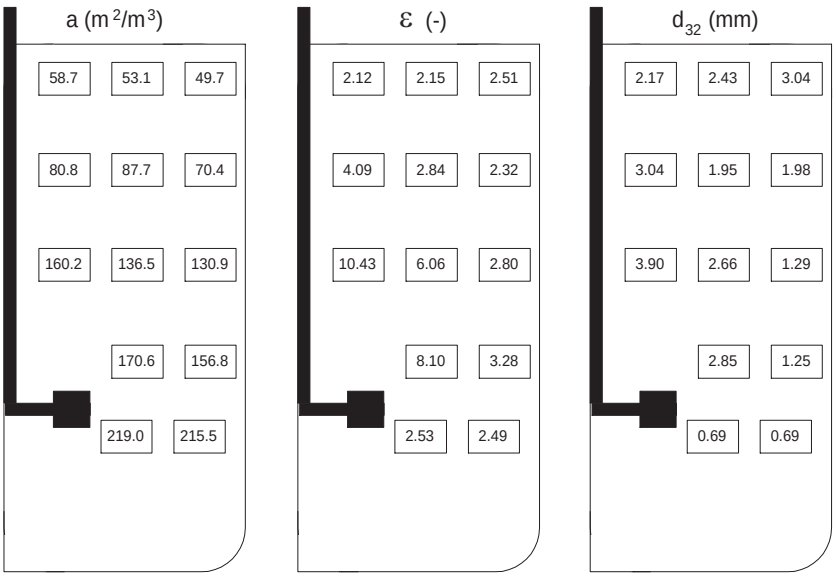

Figure 4.12: Profile of interfacial area, gas hold-up and Sauter mean diameter at a stirring speed of 640 rpm and a superficial gas velocity of 0.58 cm/s.

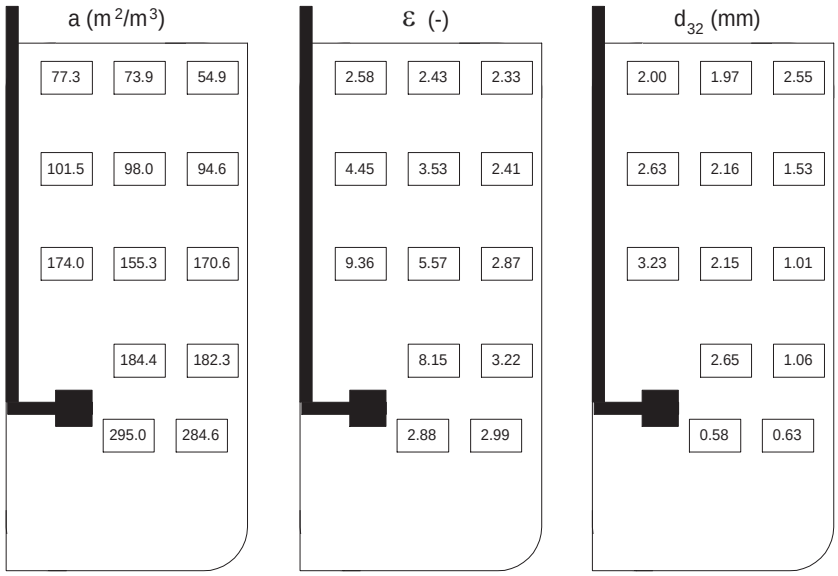

Figure 4.13: Profile of interfacial area, gas hold-up and Sauter mean diameter at a stirring speed of 770 rpm and a superficial gas velocity of 0.58 cm/s.

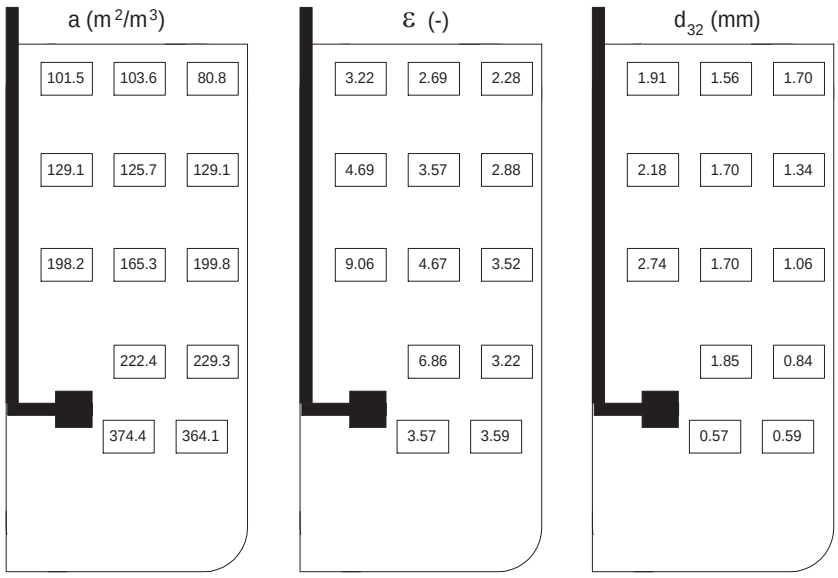

Figure 4.14: Profile of interfacial area, gas hold-up and Sauter mean diameter at a stirring speed of 960 rpm and a superficial gas velocity of 0.58 cm/s.

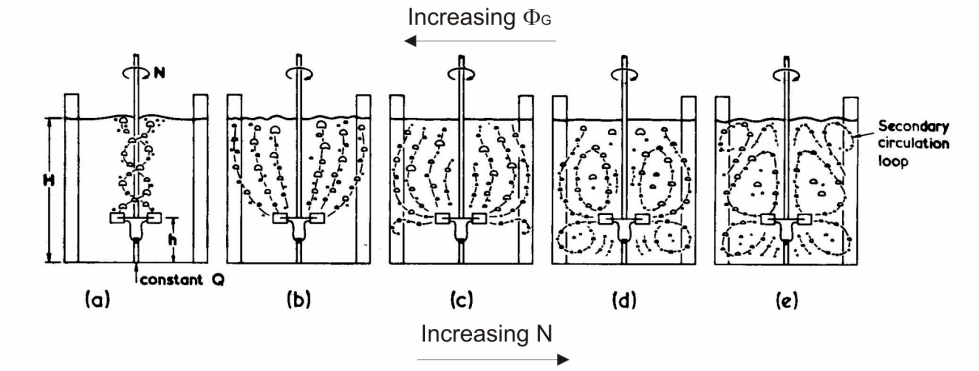

Figure 4.15: The five characteristic stages of gas dispersion defined by Nienow et al. (1977) (a) partial bubble column; (b) full bubble column; (c) onset of dipsersion in the lower part; (d) complete circulation; (e) secondary circulation.

bubbles are smaller, which is probably caused by the typical flow pattern in a Rushton turbine agitated vessel. The energy dissipation is much higher in the impeller zone compared to the rest of the vessel, which causes the formation of small bubbles. Also the velocity of the liquid is very high in the impeller discharge zone, which is the reason that relatively low gas hold-ups are observed in this region. The direction of flow is from the impeller to the wall (see Figure 4.15c-e) and these small bubbles are transported in this direction with a still relatively high speed. The bubbles on positions X1 and X3 are therefore quite small and the gas hold-up is still rather low (while the interfacial area is large !) on these positions. These effects were also observed (to a lesser extent) by Barigou and Greaves (1992), Barigou and Greaves (1996) and Alves et al. (2002).

To compare the present results with other data in literature radially averaged axial profiles were constructed of the gas liquid interfacial area, the gas hold-up and the Sauter mean diameter in the same way as was done by Calderbank (1958) and Barigou and Greaves (1996). The results of the interfacial area are plotted in Figure 4.16 and show a song increase in the impeller plane. Furthermore, a small increase in interfacial area is observed in the plane at 25 cm from the bottom of the tank, which was due to the increased gas hold-up in this plane. The results are in reasonable agreement with the results from Calderbank (1958), who used a light

scattering technique. The main difference between their work and this work is that the peak in interfacial area above the impeller plane is much smaller in our case. As it is clearly shown in 4.16 the interfacial area increases with the stirring speed at all places in the reactor.

The gas hold-up profile, which is shown in Figure 4.17 is quite similar to the work of Calderbank (1958), who made use of a 500 cm^3 glass bulb with a gas burette attached to it. In their study, local sampling was performed by opening and closing a stopcock and the gas hold-up was determined afterwards by measurement of the gas and the liquid volume. Both in this work and in their work the main part of the gas hold-up is situated in the area approximately 2/3 of the clear liquid height from the bottom. The results are somewhat different compared to the work of Barigou and Greaves (1996), who used a contact conductivity probe that measured the time of probe tip touching the gas compared to the time that the probe tip touched the liquid phase. These authors also measured a larger gas hold-up in the region above the impeller compared to impeller plane itself, but the gas hold-up profile in the top region of the tank was quite flat, while in our work and in the work of Calderbank (1958) the hold-up in the upper part was significantly lower compared to the middle part. A reason for this might be the fact that Barigou and Greaves (1996) used a vessel with the impeller at 1/4 of the clear liquid height above the bottom (1/3 in this work), which induces less turbulence in the upper part of the reactor. Because Barigou and Greaves (1996) calculated the interfacial area from measurement of the gas hold-up and the bubble size distribution, these values differed from the interfacial areas in this work in the same way.

The vertical distributions of the Sauter mean diameter as a function of the impeller speed are presented in Figure 4.18. The patterns are very similar for each stirring speed and show a low diameter in the impeller discharge zone and the diameter is increasing to an approximately constant diameter above 25 cm from the bottom. These trends are quite similar compared to the trends obtained by Barigou and Greaves (1992), who made use of a capillary suction probe for measurement of the bubble size distribution. At the lowest impeller speed the bubbles coalesce after they leave the impeller discharge zone at 1.7 mm to reach a value of approximately

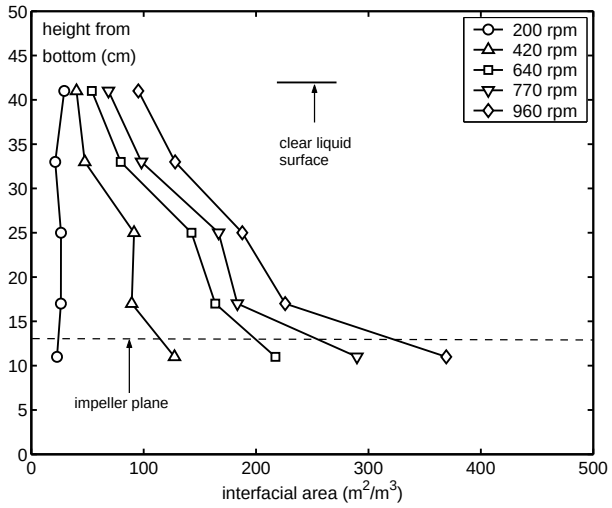

Figure 4.16: Vertical distribution of the gas-liquid interfacial area at different impeller speeds.

3.5 mm. At the highest impeller speed (960 rpm) the bubbles increase from 0.6 mm to reach a maximum value of 1.8 mm (radially averaged). In all profiles a reasonably accurate coalescence pattern is observed from increasing bubble diameters from the impeller discharge zone along with the flow pattern as explained in Figure 4.15d-e. The reason that the bubble diameter is constant above 25 cm from the bottom is therefore more or less a coincidence and due to the radial averaging of small bubbles at the wall with much larger bubbles at the impeller shaft.

4.6.2 Influence of impeller speed

To show the influence of the speed of the impeller on the interfacial area and the gas hold-up at specific regions in the vessel, two different points are selected. X13, which represents the impeller discharge zone and X8, which represents the bulk of the vessel. The effect of the rotational speed on the interfacial area is shown in Figure 4.19a, which makes clear that the interfacial area is a stronger function of the impeller speed near the impeller ($a \sim N^{1.54}$) compared to the bulk ($a \sim N^{1.08}$). Furthermore, the large differences of the absolute values of the interfacial area are clearly shown. In Figure 4.19b the effect of the impeller speed on the gas hold-up at

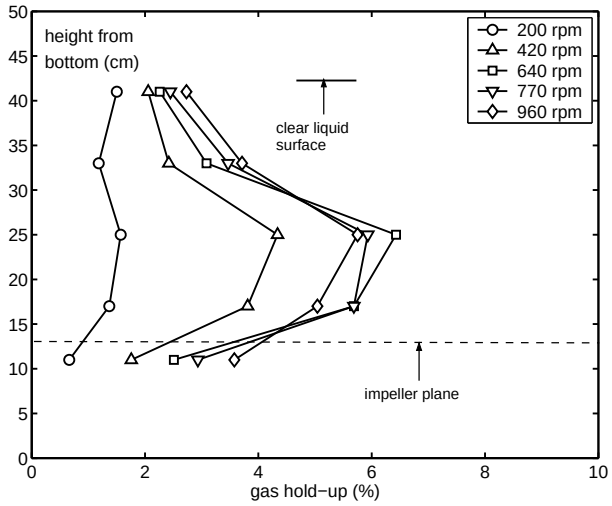

Figure 4.17: Vertical distribution of the gas hold-up at different impeller speeds.

X8 and X13 is presented. The gas hold-up in the center part of the vessel is higher compared to the region close to the impeller. Furthermore, the dependency of the gas hold-up on the stirring speed is similar in the bulk region and in the impeller region (exponent = 0.79), which indicates that the larger exponent in the interfacial area is due to a larger dependency of the bubble size to the impeller speed in the impeller region (-0.75 compared to -0.29).

4.6.3 Influence of superficial gas velocity

The influence of the superficial gas velocity was studied similar to the influence of the impeller speed at two positions, one close to impeller, X2, and one in the top region of the vessel, X10. The results indicate that the interfacial area increases with increasing superficial gas velocity, as can be seen in Figure 4.20. The area is a stronger function of the superficial gas velocity at low stirring speeds, which was also found by Mehta and Sharma (1971). The area is also a stronger function of the superficial gas velocity at positions close to the impeller. The exponents are somewhat lower compared to the work of Calderbank (1958),who predicted $a \sim u_G^{0.5}$, but are in reasonably good agreement with the work of Hughmark (1980), in which the exponent was 1/3. For a better comparison more work on the influence of the

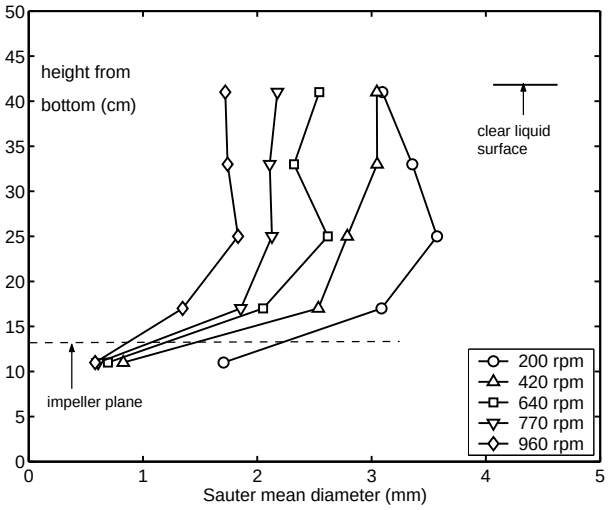

Figure 4.18: Vertical distribution of the Sauter mean diameter at different impeller speeds.

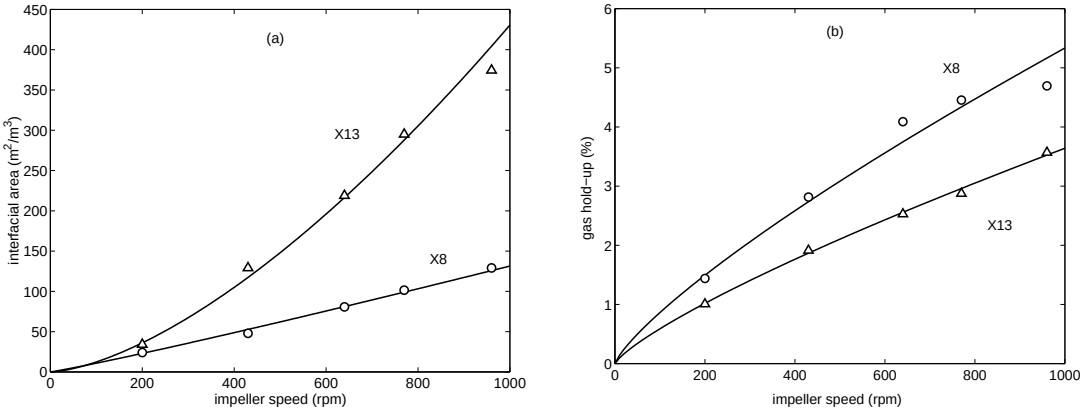

Figure 4.19: Influence of the impeller speed on the interfacial area (a) and on the gas hold-up (b) at two different places in the reactor. Solid lines represent the best fit through the experiments using a power law function. Exponents: a X8: 1.08, a X13: 1.54, ε X8: 0.79, ε X13: 0.79.

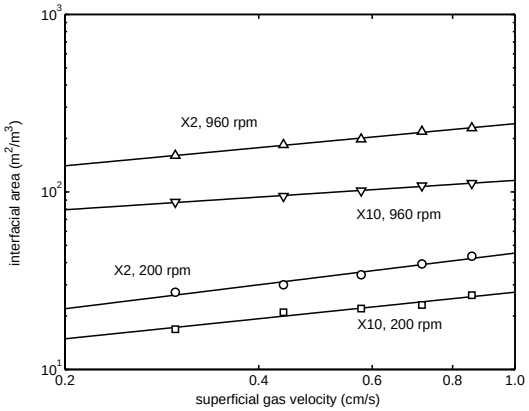

Figure 4.20: Influence of the superficial gas velocity on the interfacial area at two different places in the reactor and at two different impeller speeds. Solid lines represent the best fit through the experiments using a power law function. Exponents: X2 200 rpm: 0.45, X2 960 rpm: 0.34, X10 200 rpm: 0.38, X10 960 rpm: 0.24.

superficial gas velocity should be performed.

4.6.4 Integral values of the mass transfer parameters

The local values of the interfacial area, gas hold-up and Sauter mean diameter can be integrated according to the procedure described in 4.4 and are presented in Table 4.1. The Sauter mean diameter can be calculated in two different ways: on the basis of the integrated gas hold-up, $< \varepsilon >$, or based on the hold-up measurement using the inclined tube, ε_{incl}. This results in two different Sauter mean diameters, $< d_{32} >$ and $d_{32,incl}$, which ideally are equal. The results will be discussed separately in the next paragraphs and a comparison with similar experiments in literature will be performed.

4.6.5 Interfacial area

To validate whether the gas-liquid interfacial areas that were obtained using the ultrasonic technique are in line with similar experiments in literature, a comparison was made with a correlation from the generally accepted work of Calderbank (1958), who made use of a light scattering technique in a 5 liter and 100 liter stirred vessel

Table 4.1: Results of the integral values of the mass transfer parameters.

N (rpm)	$< a >$ (m^2/m^3)	$< \varepsilon >$ (%)	ε_{incl} (%)	$< d_{32} >$ (mm)	$d_{32,incl}$ (mm)
200	24.8	1.25	1.60	3.03	3.88
430	75.7	2.82	3.16	2.23	2.50
640	124.4	3.76	4.49	1.81	2.17
770	153.0	3.86	4.94	1.51	1.94
960	190.8	3.93	5.34	1.24	1.68

with standard dimensions and equipped with a Rushton turbine. These correlations are generally not based on the impeller speed, but on the power input done by the impeller under gassed conditions. The power input by the impeller under ungassed conditions is given by:

$$P = N_P \, \rho N^3 D^5 \tag{4.12}$$

On the introduction of gas in the reactor the power input to reach a certain impeller speed decreases. Calderbank (1958) correlated the ratio of the gassed power input and the ungassed power input, P_g/P, on the basis of the Flow number, $Fl = \Phi_G/(ND^3)$:

$$Fl < 0.035 \rightarrow \frac{P_g}{P} = 1 - 12.6Fl \tag{4.13}$$

$$Fl > 0.035 \rightarrow \frac{P_g}{P} = 0.62 - 1.85Fl \tag{4.14}$$

Calderbank used a maximum stable bubble diameter approach to correlate his experiments on the interfacial area. This maximum stable diameter was derived by balancing the viscous and surface tension forces with the dispersive turbulence forces. Assuming Kolmogoroff's theory of isotropic turbulence this leads to:

$$d = C_1 \left(\frac{\sigma^{0.6}}{\left(\frac{P_g}{V}\right)^{0.4} \rho^{0.2}} \right) \tag{4.15}$$

The gas-liquid interfacial area was measured using a wide variation of power input, surface tension and superficial gas velocity and correlated by this author to be:

$$a = 1.44 \left(\frac{\left(\frac{P_g}{V}\right)^{0.4} \rho^{0.2}}{\sigma^{0.6}} \right) \left(\frac{u_G}{u_T} \right)^{0.5} \tag{4.16}$$

In this equation u_T is the terminal rise velocity which was found to be constant (26.5 cm/s) for bubbles of 2-5 mm in water.
Hughmark (1980) correlated an extensive amount of data on flat blade impellers on the ratio of gassed and ungassed power input to give:

$$\frac{P_g}{P} = 0.10 \left(\frac{\Phi_G}{NV} \right)^{-1/4} \left(\frac{N^2 D^4}{W g V^{2/3}} \right)^{-1/5} \tag{4.17}$$

Both correlations for the gassed power input show, however, a completely different trend with respect to the impeller speed. The equations of Calderbank, (eq. 4.13 and 4.14) show an increasing trend with impeller speed, while the equation of Hughmark (4.17) shows a decreasing trend. For a fair comparison with the work of Calderbank the gassed power input of Calderbank was used, while the correlation of Hughmark is more generally accepted and the trend better represents the gassed power input as measured in this work. The used physical parameters and reactor dimensions are given in Tables 4.2 and 4.3.

The result of the comparison is presented in Figure 4.21 and shows that the interfacial area as measured in this work is in good agreement with the correlation of Calderbank, with an average absolute deviation of 10%. The interfacial area in this work can be well described with an equation of the form: $a \sim N^{1.32}$ (dotted line in Figure 4.21), while the exponent obtained with the correlations of Calderbank was 1.34. In the work of Hughmark (1980) an exponent of 1.23 was obtained, which is also in reasonable agreement with the exponent from this work. From these results

Table 4.2: Reactor dimensions and operating conditions.

parameter	symbol	value	dimension	remarks
tank diameter	T	0.40	m	
impeller diameter	D	0.133	m	
liquid volume	V	0.0526	m^3	in case of electrolyte solution: 0.0465 m^3
impeller blade width	W	0.026	m	
impeller blade length	L_B	0.033	m	
baffle width	B	0.04	m	
impeller height above bottom	H_I	0.133	m	
impeller power number	N_P	5.8	-	
diameter of the sparger	d_s	0.008	m	2 holes below the impeller
gas flow	Φ_G	$7.25 \cdot 10^{-4}$	m^3/s	unless specified otherwise

Table 4.3: Physical properties in water and in a 0.5 M K_2CO_3 / 0.5 M $KHCO_3$ buffer solution at 25 °C.

parameter	symbol	value in water	value in buffer	dimension
density	ρ	997	1084	kg/m^3
surface tension	σ	72	74	10^3 N/m
liquid viscosity	μ_L	0.91	1.11	10^3 Pa s
gas viscosity	μ_G	1.8	1.8	10^5 Pa s
gravitational constant	g	9.81	9.81	m/s^2

it can be concluded that the measurement with the ultrasonic technique at the 13 selected positions gives an accurate representation of the overall gas-liquid interfacial area.

4.6.6 Gas hold-up

A comparison with literature correlations on the overall and local gas hold-up is difficult, because of the large scatter in the reported experimental data. This scatter

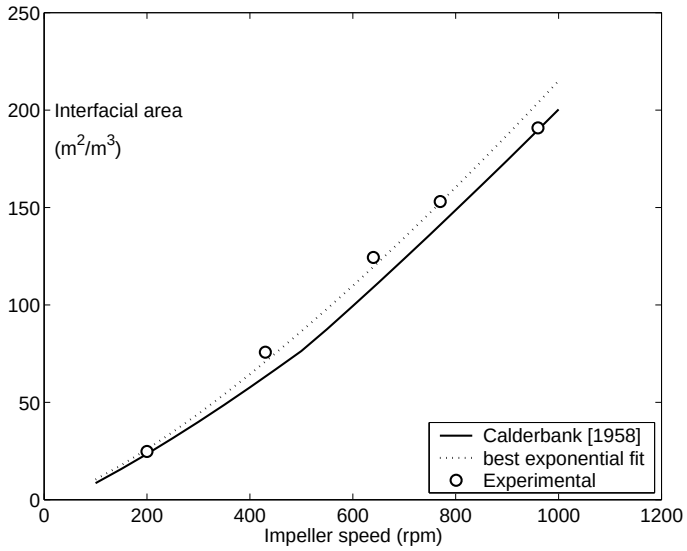

Figure 4.21: Comparison of the measured interfacial area using ultrasonic spectroscopy with the correlation of Calderbank (1958).

can only be partly accounted for by the experimental error. Also the various flow regimes that can occur in a stirred vessel can be very important. Warmoeskerken and Smith (1985) performed an extensive study on the gas loading of disc turbine impellers and have clearly identified different regimes in terms of cavity formation behind the impeller blades:

1. loaded impeller with six vortices or six clinging cavities
2. loaded impeller with stable alternate larger and smaller cavities
3. flooded impeller with 6 clinging or six ragged cavities

According to the criteria of Warmoeskerken and Smith (1985) the experiments in this work at the three highest impeller speeds (640, 770, 940 rpm) are in the regime 1, the experiments at 200 and 430 rpm are in regime 2.
A comparison will be made with the work of Greaves and Barigou (1990), because these authors measured the gas hold-up and correlated the results for the different flow regimes. Their experiments were performed in a stirred vessel of 1 meter in diameter, equipped with a Rushton turbine, at 5 vertical positions, using a contact

conductivity technique. For regime nr.1 these authors found the following correlation for the gas hold-up:

$$\varepsilon = 3.85 N^{0.73} \Phi_G^{0.62} \left(\frac{D}{T}\right)^{1.64} \tag{4.18}$$

For regime nr. 2 Greaves and Barigou (1990) found:

$$\varepsilon = 1.33 N^{0.60} \Phi_G^{0.44} \left(\frac{D}{T}\right)^{1.33} \tag{4.19}$$

Furthermore, a comparison will be made with the work of Calderbank (1958), who used a suction probe with a gas burette attached to it for the measurement of the gas fraction and obtained the following equation:

$$\varepsilon = \left(\frac{u_G \varepsilon}{u_T}\right)^{0.5} + 0.000216 \left(\frac{\left(\frac{P_g}{V}\right)^{0.4} \rho^{0.2}}{\sigma^{0.6}}\right) \left(\frac{u_G}{u_T}\right)^{0.5} \tag{4.20}$$

The results of the measured values of the gas hold-up by integration of the local values and the measured values using the inclined tube in comparison with the above mentioned correlations are presented in Figure 4.22. The obtained results with the inclined tube are in good agreement with the correlation of Greaves and Barigou (1990) for a loaded impeller with clinging cavities. Both the correlation of Calderbank (1958) and the correlation of Greaves and Barigou (1990) for a loaded impeller with alternate cavities are somewhat higher compared to the inclined tube experiments. The suction method of Calderbank might be somewhat inaccurate, because it assumes that gas and liquid are drawn into the probe at the same rate, which is not necessarily true. The deviation is most pronounced at low stirring speed (200 rpm), which should be in regime nr.2 according to the work of Warmoeskerken and Smith (1985). A possible explanation for this is the fact that the stirring speed of 200 rpm is below the critical stirring speed according to the correlations of Westerterp et al. (1963) (367 rpm) and Nienow et al. (1977) (291 rpm). This means that the gas phase is not completely dispersed throughout the reactor, which might account for a lower gas hold-up after integration.

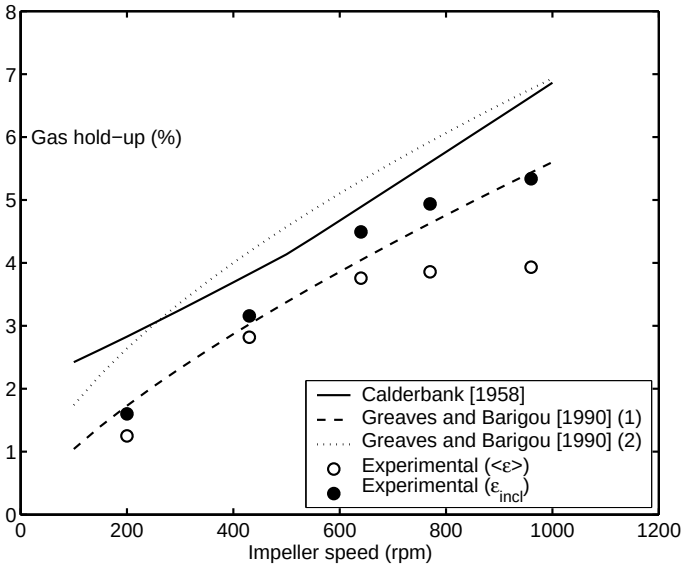

Figure 4.22: Comparison of the measured gas hold-ups using electrical conductivity with the correlations of Calderbank (1958) and Greaves and Barigou (1990).

impeller speed (rpm)	RD (%)
200	22
430	11
640	16
770	22
960	26

Table 4.4: Relative Deviation (RD) between the different gas hold-up methods.

Furthermore, there is a difference between the measured gas hold-up with the inclined tube in comparison with the gas hold-up from the integration of the local values. The average relative deviation between the two methods is 19 % and this is specified per impeller speed in Table 4.4. This means that the 13 selected positions in the vessel are not covering the vessel sufficiently accurate for integration to the overall gas hold-up. This might originate partly from the fact that is was not possible to measure at the bottom of the vessel and closely above the impeller, where high gas hold-ups can be found, mainly at high stirring speeds, when full gas dispersion is achieved. Also the measurements at the wall (X1, X3, X6 and X9), which are very important due to their large volume fraction in the integration, were taken very closely to the vessel wall, where a steep decrease of gas hold-up was found. This can also account for a lower gas hold-up on integration.

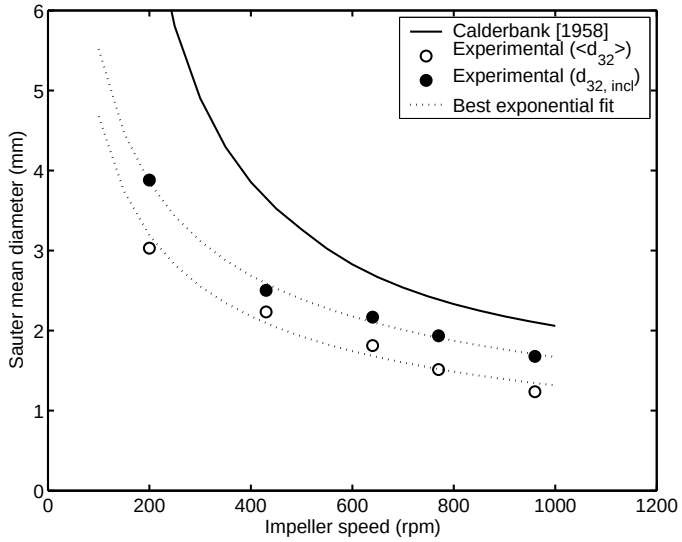

Figure 4.23: Comparison of the calculated Sauter mean diameter with the correlation of Calderbank (1958).

4.6.7 Sauter mean diameter

The Sauter mean diameter of the gas bubbles was compared to the established correlation proposed by Calderbank (1958):

$$d_{32} = 4.15 \left(\frac{\sigma^{0.6}}{\left(\frac{P_g}{V}\right)^{0.4} \rho^{0.2}} \right) \varepsilon^{0.5} + 0.0009 \tag{4.21}$$

The Sauter mean diameter predicted by Calderbank is higher compared to the values measured in this work (Figure 4.23). This was to be expected, because similarly to this work, Calderbank calculated the Sauter mean diameter from measurements of a and ε. While the interfacial area was close to the area in this work, the gas-hold-up was significantly higher, resulting in a higher Sauter mean bubble diameter.

To establish correlations for the Sauter mean diameter Alves et al. (2002) measured bubble sizes at 29 different positions in a stirred vessel using a capillary suction technique. These authors divided the vessel into two regions: the bulk region and the impeller region. The data were combined with data from Martin (1995), Machon et al. (1997) and Bouaifi and Roustan (1998), who all used video/photography

techniques and with data from Barigou and Greaves (1992), who used a capillary suction technique. For the bulk region the Sauter mean diameter was given by:

$$d_{32,bulk} = 0.0076 \left(\frac{P_g}{V} \right)^{-0.14} \tag{4.22}$$

To compare the results obtained in the present study with Equation 4.22 the gassed power input was calculated using the relation of Hughmark (1980) (eq. 4.17) and the bulk region was represented by the positions (X1-X11). The exponent obtained in this work was -0.14, which is in exact agreement with the correlation. As expected the exponent is much lower compared to the exponent as predicted with the theory of isotropic turbulence (Eq. 4.15), which means that the bubble size is strongly influenced by coalescence in the bulk of the vessel. The pre-exponential constant in this work was 0.00685, which is only 10% lower compared to Equation 4.22.

Alves et al. (2002) gave the following expression for the Sauter meter in the impeller discharge zone:

$$d_{32,imp} = 8.5 \left(1 + 32.5 \frac{\Phi_G}{D^2} \right) \left(\frac{P_g}{V_{imp}} \right)^{-0.24} \tag{4.23}$$

The above correlation is not based on the total liquid volume, but on the impeller swept volume, $V_{imp} = 0.25\pi D^2 W$, which gives a better representation of the energy dissipated in the impeller zone. A comparison is made with the Sauter mean diameters in the impeller zone (X12, X13) determined in this work. The obtained exponent in this work was -0.245, which is in good agreement with Equation 4.23 and with the work of Lu et al. (1993) (-0.25). The pre-exponential factor was 17.1, which is somewhat lower (14%) than could be determined from Equation 4.23 (19.9).

From these results it can be concluded that Sauter mean diameters can be measured with a good accuracy using a combination of ultrasonic spectroscopy for measurement of the gas-liquid interfacial area and electrical conductivity for determination of the local gas-hold-up. Overall values are in reasonable agreement with literature and the dependence on power input in different parts of the vessel are confirming literature results.

4.6.8 Mass transfer coefficients

The volumetric mass transfer coefficients are determined according to the method described in Section 4.3.2. The probe time was determined by dropping the measurement probe very fast in a beaker with deoxygenated water and was 6.7 sec, which is somewhat higher than specified by the supplier (5.5 s). In Figure 4.24 two probe response curves are plotted: (1) the response curve of the probe in the beaker with deoxygenated water (squares) and (2) a response curve of the probe in the vessel after switching from nitrogen to air at a superficial gas velocity of 0.58 m/s and and a stirring speed of 640 rpm. The first part of curve 1, which is the most important part for the determination of the probe response time, is fitted by the mathematical model excellently. On the other hand, the curve shows some deviation from the trend of the mathematical model at high values of the normalized concentration, which is probably due to the less defined operation of dropping the probe in the beaker, compared to the steady operation in the vessel. This is supported by the fact that the curve of the probe response concentration in the vessel (2), did not show any large deviations from the mathematical model. This means that the proposed mathematical model is sufficiently accurate to be used for k_La measurements in this system.

In Table 4.5 the volumetric mass transfer coefficients are presented at 430, 640, 770 and 960 rpm. The value at 200 rpm could not be determined due to sticking of air bubbles to the DO-probe, which led to erroneous determinations of the volumetric mass transfer coefficient. The mass transfer coefficients were averaged from a number of experiments (see Table 4.5, which consisted of 50% absorption and 50% desorption experiments. k_La_{abs} was on average 7% higher compared to k_La_{des}, which is comparable with the standard deviations in the measurements. This means that absorption and desorption are mirror image processes, which was also concluded in Chapter 3. Furthermore, the liquid phase mass transfer coefficient, k_L, could be calculated as the ratio of the volumetric mass transfer coefficient and the interfacial area as determined in the previous section. The value of the measured k_La coefficient was always larger than $1/(5\tau_P)$, but never exceeded $1/\tau_P$, which means that accurate measurement of k_La is possible, on the condition that the probe characteristics are

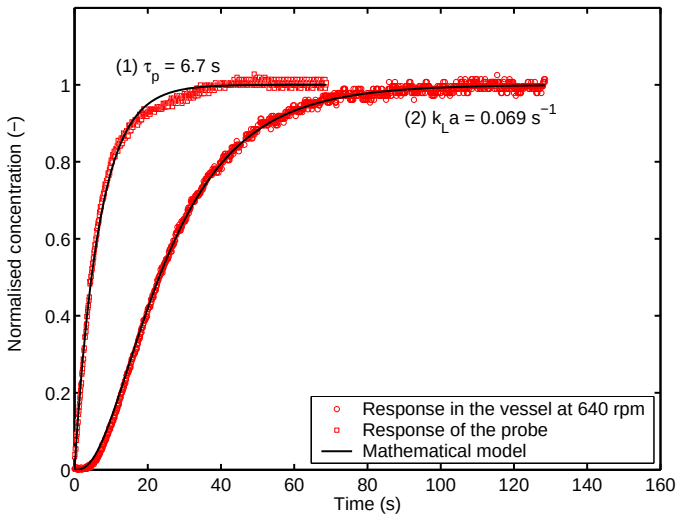

Figure 4.24: Normalized concentration profiles of the dissolved oxygen probe response compared to the mathematical model.

Table 4.5: Mass transfer coefficients at different stirring speeds. u_G: 0.58 m/s.

N (rpm)	nr. of exp. (-)	σ (%)	k_La (s^{-1})	a (m^2/m^3)	k_L (10^4 m/s)
430	4	2.6	0.034	75.7	4.5
640	6	3.6	0.066	124.4	5.3
770	12	4.8	0.086	153.0	5.6
960	4	11.9	0.135	190.8	7.1

taken into account.

As expected the standard deviation (σ) on the measured k_La values increased with increasing stirred speed, due to the higher sensitivity of k_La with the dissolved oxygen concentrations at higher speeds. The spread in these experiments is, however, much less compared to the spread in literature correlations. In Figure 4.25 a comparison is made with the correlation proposed by van 't Riet (1979), who combined number of measurements of k_La by different methods to obtain:

$$k_La = 2.6 \cdot 10^{-2} \left(\frac{P_g}{V}\right)^{0.4} u_G^{0.5} \tag{4.24}$$

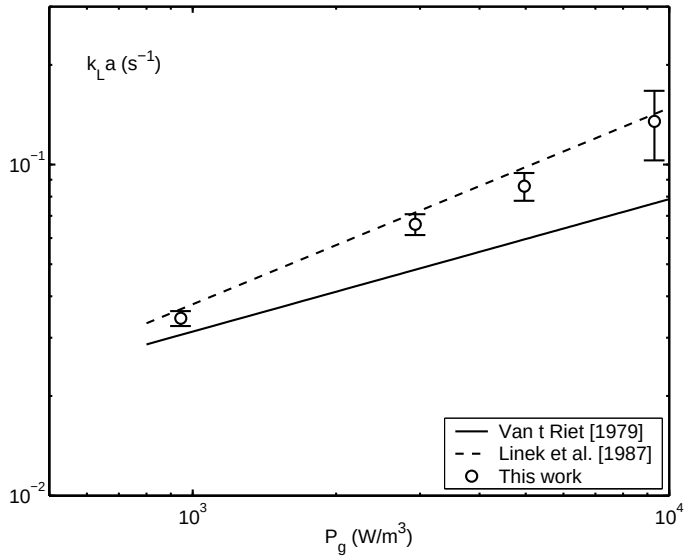

Figure 4.25: Comparison of the measured volumetric mass transfer coefficient using the dynamic oxygen method with literature correlations. Error bars represent the 95% confidence interval (2 σ)

Linek et al. (1987) critically studied different methods of measurement of oxygen mass transfer coefficients and combined their measurements with experiments from correct methods in literature to obtain:

$$k_L a = 4.95 \cdot 10^{-3} \left(\frac{P_g}{V}\right)^{0.593} u_G^{0.4} \tag{4.25}$$

To compare the present data with these correlations, the gassed power input was estimated using Equation 4.17. The results compare good with the equation of Linek et al. (1987) and are higher compared to the work of van 't Riet (1979).

The mass transfer coefficient, k_L, was calculated from the correlations that were obtained for $k_L a$ and a and this resulted in: $k_L \sim (P_g/V)^{0.13}$. When the correlation is based on the individual experiments the obtained exponent is 0.18. This (small) difference is due to the fact that the $k_L a$ was not measured at the lowest stirring speed, which caused a small deviation in the exponent for the interfacial area.

In literature not much work is performed on measurement of the mass transfer coefficient in turbulent stirred vessels. The present results correlate very well with

the results obtained by Linek et al. (1970), who measured k_La and a in sodium sulfite solutions and obtained: $k_L \approx 2 \cdot 10^{-4}(P_g/V)^{0.14}$. Also the correlation of Yoshida and Miura (1963) is in reasonable agreement with the results in this work. These authors combined measurement of k_La using oxygen absorption with photographic measurement of the bubble diameter and height reading for the measurement of gas hold-up. The obtained exponent in their work was 0.2 (assuming $P \sim N^3$).

4.7 Results in non-coalescing systems

4.7.1 Profiles of interfacial area and Sauter mean diameter

In Figure 4.26 the determined profiles of the measured interfacial area and the calculated Sauter diameter are shown for a system of 0.5 M K_2CO_3 / 0.5 M $KHCO_3$ and air at a superficial velocity of 0.58 cm/s and a stirring speed of 430 rpm. The gas hold-up was only measured using the inclined tube technique, because local measurement using electrical conductivity was not possible due to the high overall conductivity of the medium. A constant gas hold-up throughout the vessel was assumed.

In Figure 4.26 it can be seen that the distribution of the interfacial area is much more homogeneous compared to the coalescing air-water system. This is supported by the vertical distribution of the gas-liquid interfacial area as shown in Figure 4.27. The interfacial area is approximately constant with height in the vessel. Only just above the impeller plane (17 cm) a small peak in the area is observed. Furthermore, the bubbles are much smaller compared to an air-water system, which was to be expected, as, according to the work of Craig et al. (1993), the electrolyte concentration was high enough for coalescence of bubbles to be suppressed.

4.7.2 Influence of impeller speed

To show the influence of the speed of the impeller in specific regions in the vessel, two different points are selected; X13, which represents the impeller discharge zone and X7, which represents the bulk of the vessel. The effect of the rotational speed on the

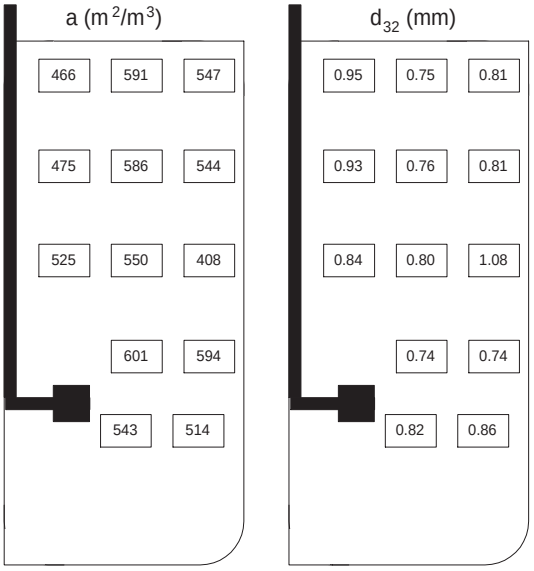

Figure 4.26: Profile of interfacial area and Sauter mean diameter in the buffer solution at a stirring speed of 430 rpm and a superficial gas velocity of 0.58 cm/s.

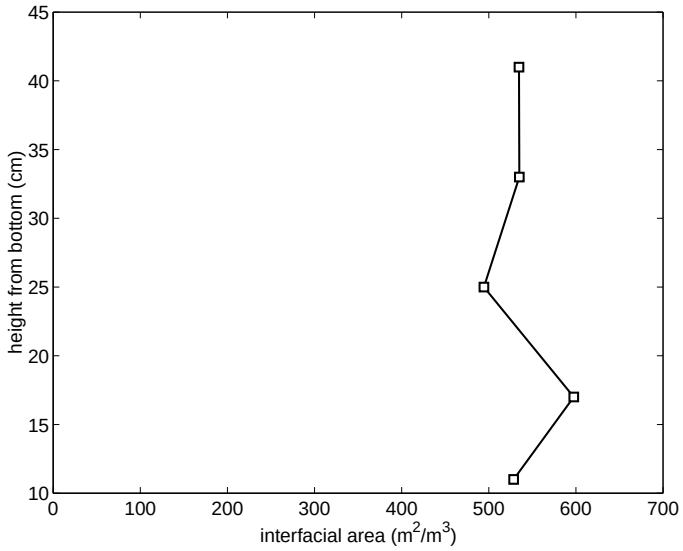

Figure 4.27: Vertical distribution of the gas-liquid interfacial area in the buffer solution at a stirring speed of 430 rpm and a superficial gas velocity of 0.58 cm/s.

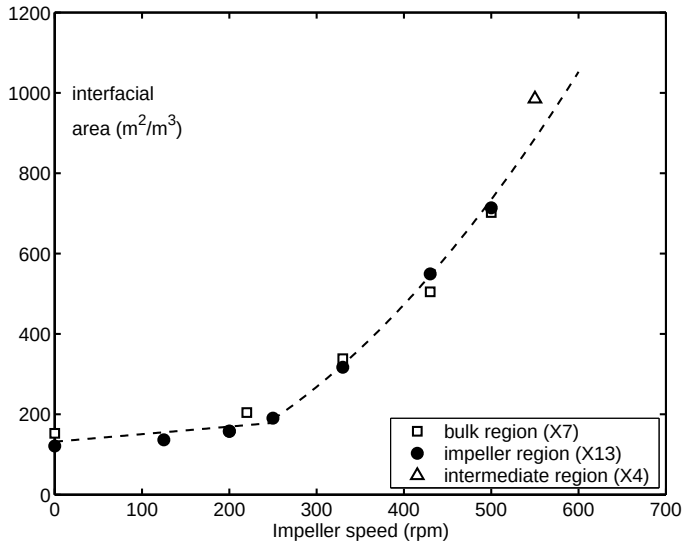

Figure 4.28: Effect of the impeller speed on the interfacial area in a non-coalescing system at different positions in the vessel

interfacial area is shown in Figure 4.28, which shows that the interfacial area is not a strong function of the position in the vessel in non-coalescing systems. Furthermore, the existence of a critical impeller speed is demonstrated clearly in Figure 4.28. A very distinct transition is observed at 250 rpm, below which the interfacial area is almost independent of impeller speed and a region (at higher stirring speeds) where the interfacial area is a strong function of the impeller speed. The critical impeller speed was among others measured by Westerterp et al. (1963) and by Nienow et al. (1977), who found respectively:

$$N_{cr} = \left(\frac{1.22}{D} + \frac{1.25T}{D^2}\right)\left(\frac{\sigma g}{\rho}\right)^{0.25} \tag{4.26}$$

and:

$$N_{cr} = \frac{4\Phi_G^{0.5}T^{0.25}}{D^2} \tag{4.27}$$

From these relations the following critical impeller speeds could be calculated: 367 rpm from Eq. 4.26 and 291 rpm from Eq. 4.27, which are both somewhat higher compared to the observed 250 rpm.

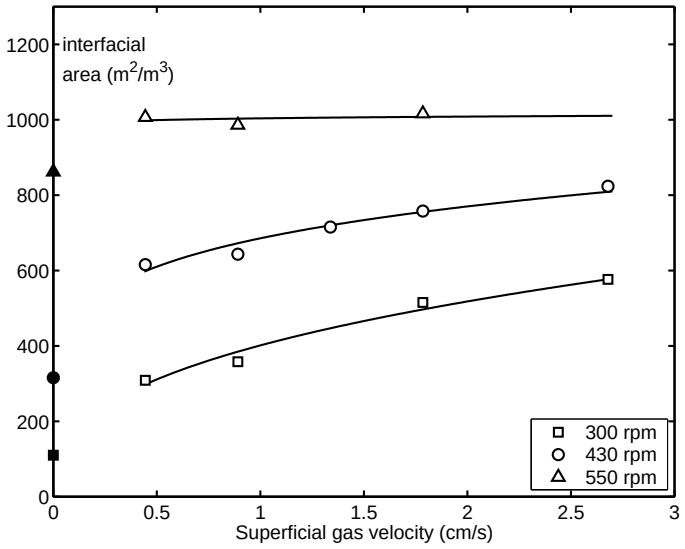

Figure 4.29: Effect of the superficial gas velocity on the interfacial area in a non-coalescing system at different impeller speeds (position X4). Solid points represent the interfacial area when only stirring is applied.

4.7.3 Influence of superficial gas velocity

In Figure 4.29 the interfacial area is plotted as a function of the superficial gas velocity at three different stirring speeds (300, 430 and 550 rpm). The interfacial area is a stronger function of the superficial gas velocity at low stirring speeds. At high stirring speeds the area is almost independent of the gas velocity. The obtained results are in good agreement with a correlation of the form: $a \sim u_G^{\beta}$. The obtained exponents were 0.37, 0.17 and 0.01 with increasing impeller speed. Furthermore, the induction of gas when only stirring is applied ($u_G = 0$, i.e. no feed through the sparger) is very high, mainly at high stirring speeds. The decreasing exponent with increasing impeller speed might be caused by an increased gas induction, although the amount of gas induction at gas sparging conditions is, however, unknown.

4.7.4 Integration to overall values

Due to the homogeneous nature of the non-coalescing systems, mapping of the complete vessels is not necessary. One or two well chosen points in the vessel give a

sufficiently accurate value of the interfacial area. To compare the interfacial area and the Sauter mean diameter with correlations from literature only the data beyond the critical impeller speed were taken into account.

4.7.5 Interfacial area

In literature no established correlations for the interfacial area, measured using a physical technique, in non-coalescing electrolyte systems are available. The comparison will be performed on the basis of the gas hold-up and the Sauter mean diameter, which are more frequently correlated. The interfacial area beyond the critical impeller speed could be described with: $a = 11.2N^{1.97}$ (dashed line in Figure 4.28) .

4.7.6 Gas hold-up

The gas hold-up was determined using the inclined tube method and compared with correlations of Greaves and Barigou (1990) in the different regimes of gas loading as explained in Section 4.6. Similar to the results for gas hold-up in coalescing systems the data are in good agreement with the correlation for a system with six clinging cavities behind the impeller blades (Eq. 4.28) as is shown in Figure 4.30. The equation for 3 large and 3 small cavities (Eq. 4.29) overestimates the data by approximately 300%, although the experiments at the lower impeller are in this regime according to the criteria of Warmoeskerken and Smith (1985) (assuming that these criteria are also valid for air-electrolyte systems). This equation was therefore not plotted in Figure 4.30. Greaves and Barigou (1990) found for the regime with 6 clinging cavities in electrolyte systems (regime 1):

$$\varepsilon = 3.86N^{0.92}\Phi_G^{0.41}\left(\frac{D}{T}\right)^{2.56} \tag{4.28}$$

and for the regime with three alternate cavities (regime 2):

$$\varepsilon = 2.86N^{0.76}\Phi_G^{0.31}\left(\frac{D}{T}\right)^{1.64} \tag{4.29}$$

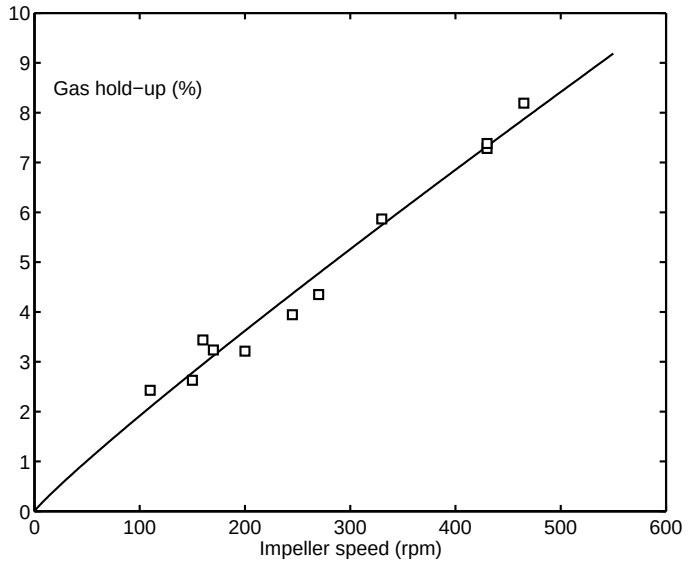

Figure 4.30: Effect of the impeller speed on the gas hold-up in a non-coalescing system. The solid line is Equation 4.28.

In the present study the following relation was obtained: $\varepsilon = 1.29{\cdot}10^{-2} N^{0.87}$. The profile of gas hold-up versus stirring speed does not contain a large change in slope at the critical impeller speed for complete dispersion as was measured in the profile of the interfacial area. This suggests that the obtained discontinuity in this profile was mainly due to a change in bubble diameter.

4.7.7 Sauter mean diameter

The Sauter mean diameter was compared with the well known equation of Calderbank (1958) for the mean diameter in electrolyte systems:

$$d_{32} = 2.25 \left(\frac{\sigma^{0.6}}{\left(\frac{P_g}{V}\right)^{0.4} \rho^{0.2}} \right) \varepsilon^{0.4} \left(\frac{\mu_G}{\mu_L} \right)^{0.25} \tag{4.30}$$

This correlation was determined by measurement of the interfacial area using a laser scattering technique in a closed system with a known gas fraction. The physical properties and process parameters that are used in the comparison are given in Tables 4.2 and 4.3. For fair comparison the gassed power input is estimated

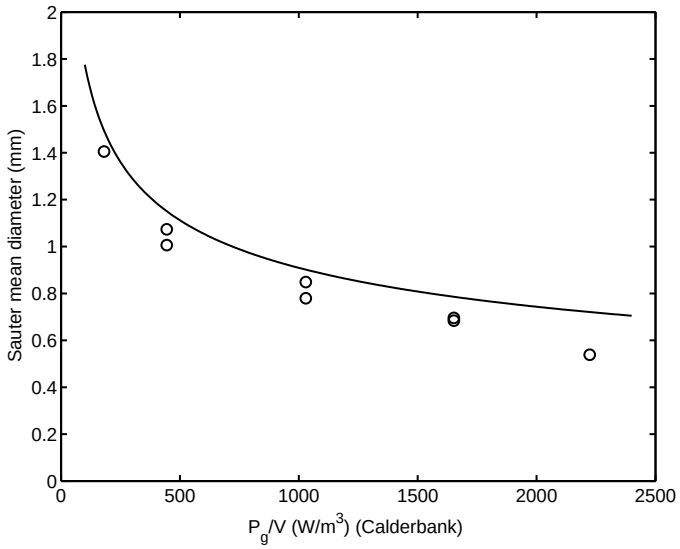

Figure 4.31: Effect of the impeller speed on the Sauter mean bubble diameter in a non-coalescing system. The solid line is Equation 4.30.

by the correlation from Calderbank (1958) (Eq. 4.13 and 4.14). The comparison is presented in Figure 4.31 and shows that the obtained data in this work are in good agreement with the Calderbank correlation. The obtained diameters were 12% (average relative deviation) lower in this work. The data were also in reasonable agreement with the correlation obtained by Alves et al. (2002), who combined their own measurements with data of Martin (1995) and of Parthasarathy and Ahmed (1994):

$$d_{32} = 0.014 \left(\frac{P_g}{V} \right)^{-0.37} \tag{4.31}$$

The present data are in good agreement with this correlation, although the average relative deviation is 27%. The spread in the data used for the correlation was at least a factor 3 at high power inputs. The data obtained in this work can be described (beyond the critical impeller speed) with: $d_{32} = 6.9 \cdot 10^{-3} N^{-1.10}$ and making use of Equation 4.17: $d_{32} = 0.0115 (P_g/V)^{-0.39}$. The exponent is in close agreement with the correlation of Alves et al. (2002) and also with the theoretically suggested -0.40 (Eq. 4.15).

4.8 Results in an air-water-toluene system

In the previous sections measurements were performed in coalescing air-water systems and in non-coalescing air-electrolyte solutions, which were reasonably well investigated in literature. The results were in good agreement with literature correlations and in some parts additional information was obtained. In this section similar techniques will be used to study a system containing air, toluene and water, which is for a large part unexplored.

4.8.1 Gas hold-up

The gas hold-up was measured using the inclined tube technique in water with toluene fractions of 1, 5, 10 and 20 vol-%. The density difference due to the addition of toluene was maximally 2.6%, which is according to Equation 4.3 also the maximum error in the gas hold-up, and was therefore neglected. The applied stirring speed was 640 rpm. The results are presented in Figure 4.32 and show that at low toluene fraction the gas hold-up decreases sharply (more than 30% at 1% toluene). After this initial decrease the gas hold-up increases to approximately the value without toluene present at 20% toluene. This behaviour was also observed by Yoshida et al. (1970), who performed experiments in a 2.57 liter vessel equipped with a 12-vane turbine agitator at two impeller speeds. The gas hold-up was measured in their work by liquid height reading in the vessel. The reason for the initial decrease is not clear. The initial effects were studied separately and the results are reported in Chapter 5.

4.8.2 Interfacial area

The interfacial area was determined using a similar method compared to the previous sections. The attenuation coefficient was measured at 2 MHz, from which the interfacial area was determined. The results are presented in Figure 4.33 and show that the interfacial area in the presence of toluene was higher compared to the value in which no toluene is added to the water phase.

The trend in the interfacial area with increasing toluene volume fraction is

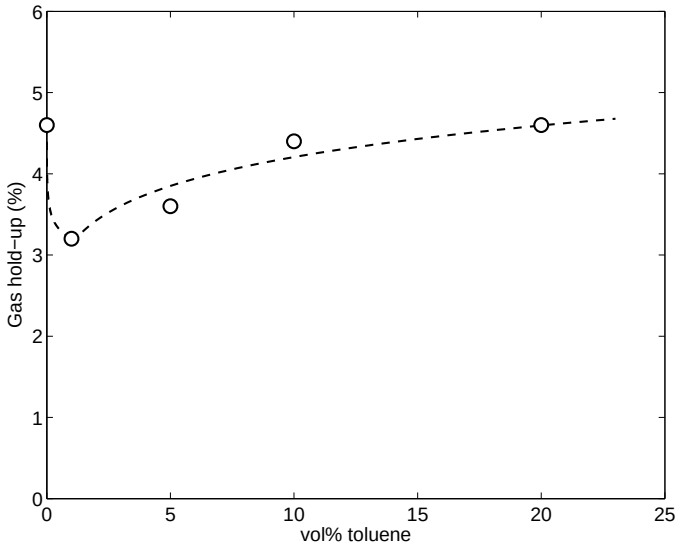

Figure 4.32: Influence of the toluene volume fraction on the gas hold-up at 640 rpm.

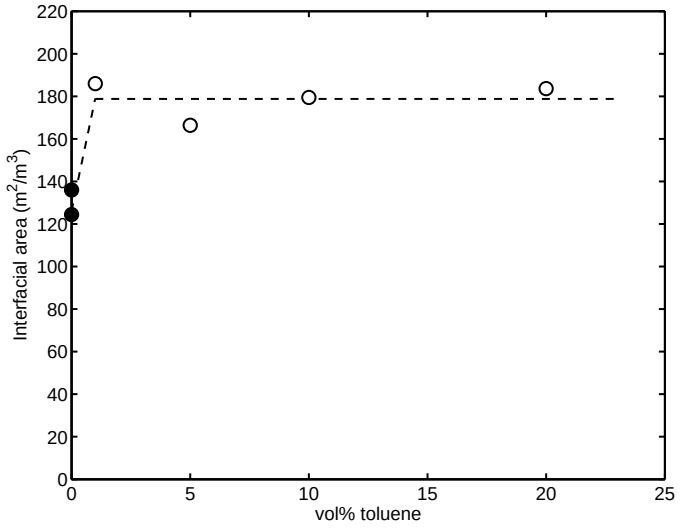

Figure 4.33: Influence of the toluene volume fraction on the gas-liquid interfacial area at 640 rpm (Position X4).

opposite compared to the trend in the gas hold-up. The interfacial area is around 40% higher at 1% toluene compared to pure water, while the gas hold-up is 30% lower. At a volume fraction of 1% toluene several positions in the vessel were measured, and the profile was reasonably homogeneous. This behaviour is unexpected and for this reason further research is performed on the determination of the size distributions in the presence of toluene compared to the distribution in pure water using attenuation and ultrasonic velocity measurements ranging from 300 kHz to 2.5 MHz. The attenuation coefficient profile is shown in Figure 4.34. It was not possible to obtain a good fit through the experiments in water containing 1% toluene using a log-normal or normal distribution. The best fit on the experiments at high frequencies using a log-normal distribution is shown as the dotted line in Figure 4.34. In this case the deviation between the model line and the experiments is very large, mainly at low frequencies. This difference in attenuation coefficient can not be explained by the attenuation caused by the toluene droplets, because this attenuation is mainly in the high frequency regime. In case of water an accurate fit could be obtained using a log-normal distribution in the attenuation coefficient profile as well as in the ultrasonic velocity profile shown in Figure 4.35. A good description of the experiments in water with 1% toluene could only be obtained by making use of a bimodal distribution containing at least a certain amount of small (micro) bubbles (< 200 μm). The bimodal distribution that was used consisted of two log-normal distributions and a scaling parameter (C_1), which determined the height of both distributions:

$$P(x) = \frac{C_1}{S_1 x\sqrt{2\pi}} \exp\left(-\frac{(\ln(x) - M_1)^2}{2S_1^2}\right) + \frac{(1 - C_1)}{S_2 x\sqrt{2\pi}} \exp\left(-\frac{(\ln(x) - M_2)^2}{2S_2^2}\right) \tag{4.32}$$

This distribution has five unknown parameters to be determined in the optimization, C_1, M_1, M_2, S_1 and S_2. The assumption $\sigma = 0.1\mu$ was used for both distributions to reduce the number of fit parameters, which was too high compared to the number of experimental data points. The coefficient, y, from Equation 2.23 that is used in the objective function for minimization of the error of both profiles

was set to 0.5. Due to the large difference in ultrasonic velocity and in attenuation coefficient measurements between low and high frequencies the logarithmic values of the data points were taken into account in the minimization to get a good fit over the complete frequency range. The best fit with this distribution is shown in Figures 4.34 and 4.35 and consisted of two bubble classes of 90 μm and 2.6 mm, respectively. The accuracy of the measurements was lower at 300 and 400 kHz, due to the large attenuation coefficient. This caused large disturbances in the signals and complicated the determination of both the attenuation coefficient and the ultrasonic velocity. Mainly for this reason there is some deviation between model and experiments at low frequencies. Further research on the determination of the exact distribution in these systems containing two bubble classes is therefore necessary. The obtained interfacial areas were 94 m^2/m^3 for the small bubbles and 87 m^2/m^3 for the large bubbles. This means that the total interfacial area as determined using the complete profile is in good agreement with the area that is determined when only the attenuation coefficient at 2 MHz is taken into account.

So far, the increase in interfacial area (Figure 4.33) seems to be due to the presence of micro bubbles in the solution. It remains, however, unclear, whether these micro bubbles participate in the mass transfer process. This will be investigated in the next section.

4.8.3 Volumetric mass transfer coefficient

The volumetric mass transfer coefficients were measured using the dynamic oxygen method for 1, 5, 10 and 20 vol-% toluene in water. The results (Figure 4.36) indicate a somewhat similar trend compared to the measured gas hold-up. At small toluene fractions a sharp decrease is observed followed by an increase at higher volume fractions of toluene. The increase at 20% toluene is stronger than in case of the gas hold-up and was almost a factor 2 compared to 1% toluene in water. The trend is similar as obtained by Yoshida et al. (1970).

A decrease of 21% in k_La at 1% toluene volume fraction is observed, which is in reasonable agreement with the 30% decrease in the gas hold-up. Although an increase in the interfacial area was observed, the decrease in k_La is probably

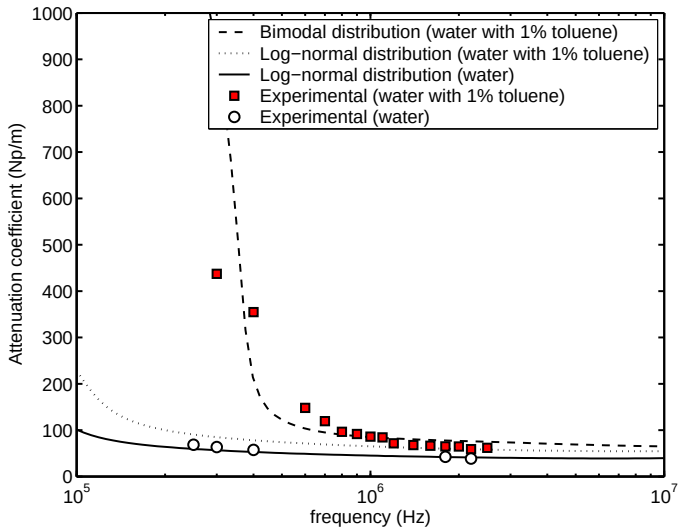

Figure 4.34: Attenuation coefficient profile of air-water and air-water with 1% toluene with best fit model lines.

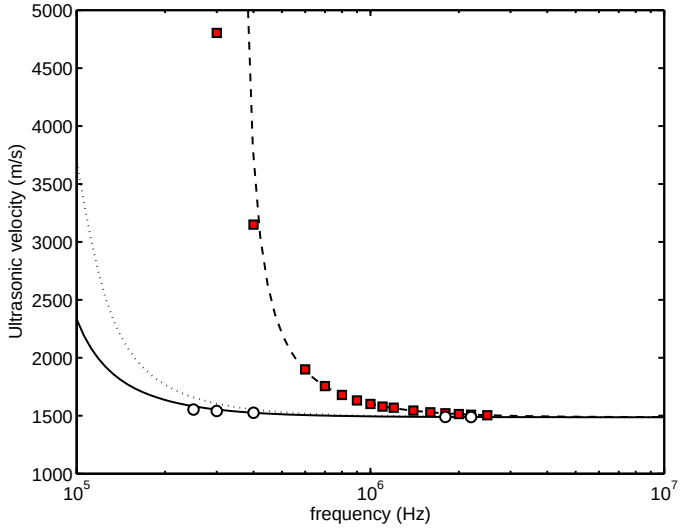

Figure 4.35: Ultrasonic velocity profile of air-water and air-water with 1% toluene with best fit model lines. For legend see Figure 4.34.

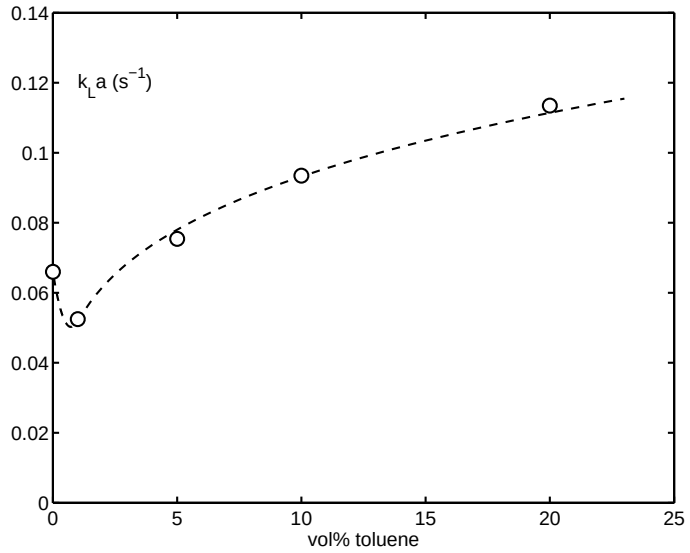

Figure 4.36: Influence of the toluene volume fraction on the volumetric mass transfer coefficient at 640 rpm.

caused by a decrease in the (effective) interfacial area, that was available for mass transfer. The micro bubbles, which were observed, contribute to the measured interfacial area, but do not take part in the mass transfer process. These bubbles might be formed during gas induction from the surface, which was partly supported by measurements of the interfacial area when only stirring was applied (30 m^2/m^3 increase at 1% toluene at position X4). Furthermore, if these small (90 μm) bubbles contain air, they are depleted from oxygen very fast (99% in less than 0.2 s). Their residence time in the solution is probably quite long due to their small rise velocity, while they are only containing nitrogen. This can account for an increase in the interfacial area together with a decrease in k_La. The theoretical possibility that the increase in the interfacial was accompanied by a decrease in the mass transfer coefficient, k_L, is not very likely, as this was also not observed in the measurements using the Danckwerts-plot technique (see Chapter 1). The decrease in k_La and in ε at 1% toluene is in good agreement with the decrease in the interfacial area of the large bubbles (30%), which also supports the above considerations.

Although the exact interfacial area that is available for mass transfer is not known accurately, the assumption that the interfacial area is proportional to the

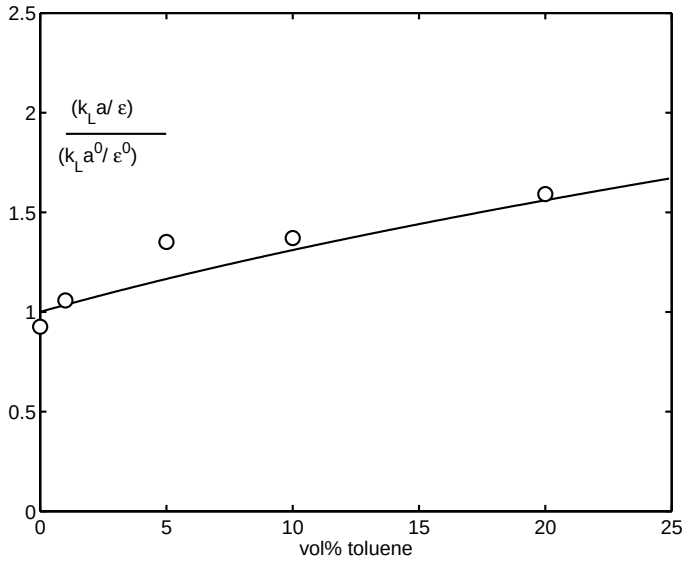

Figure 4.37: Influence of the toluene volume fraction on the volumetric mass transfer coefficient at 640 rpm.

overall gas hold-up can be made. In Figure 4.37 the relative value of the estimated mass transfer coefficient, $(k_L a/\varepsilon)/(k_L a^0/\varepsilon^0)$, is plotted as a function of the toluene volume fraction. The results show a reasonable agreement with a homogenous model of the shuttle mechanism, which is explained in Section 1.4.3. The enhancement factor due to the presence of a dispersed is given by Bruining et al. (1986) and can also be derived from Equation 1.15 in absence of chemical reaction ($Ha = 0$):

$$\mathrm{E_D} = \sqrt{1 + \varepsilon_D(m_R - 1)} \tag{4.33}$$

The value for the relative solubility, m_R, was taken from Yoshida et al. (1970) and was 8.2. The value at 5% toluene is somewhat high (15%) compared to the trend, probably due to a somewhat low value for the gas hold-up.

4.8.4 Droplet diameter

The droplet diameter of toluene was measured at 20% toluene under gassed (G-L-L) and ungassed (L-L) conditions. The attenuation coefficient versus frequency profile

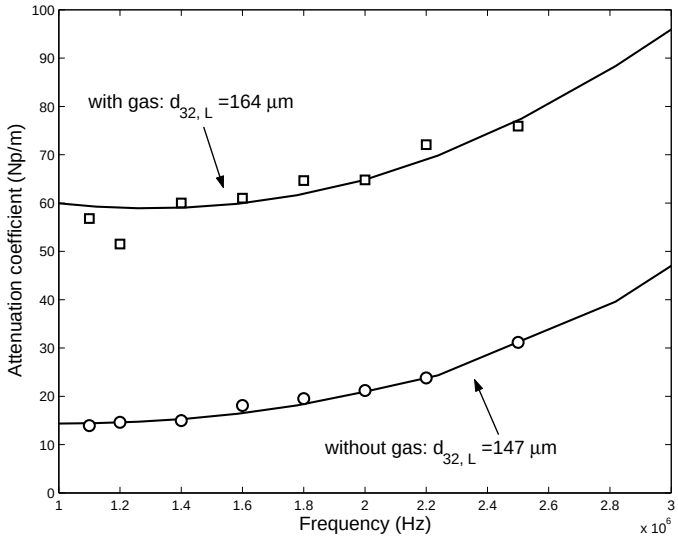

Figure 4.38: Attenuation coefficient profile of 20% toluene under gassed and ungassed conditions.

is shown in Figure 4.38. The effect of the gas phase is present in both experiments. In case of the G-L-L system $a_{gas} = 173$ m^2/m^3 and in case of the L-L system $a_{gas} = 40$ m^2/m^3, due to surface aeration. The Sauter mean droplet diameter could be determined in both cases and was 164 μm in the G-L-L system and 147 μm in the L-L system. To obtain the droplet size distribution a larger frequency range should be measured. The physical properties of toluene to calculate the model lines were taken from Allegra and Hawley (1972).

4.9 Conclusions

In this chapter ultrasonic spectroscopy was used for measurement of the gas-liquid interfacial area in combination with electrical conductivity for measurement of the gas hold-up. These values were used to calculate the Sauter mean diameter at different positions in the vessel.

The profile that was obtained in the coalescing air-water system, was highly inhomogeneous. The interfacial area was very high in the impeller discharge zone and decreased with increasing height in the reactor. Maximum gas hold-up was obtained

at 2/3 of the clear liquid height above the impeller. The bubble diameter increased from small values near the impeller to larger values along with the flow pattern in a stirred vessel. The profile in non-coalescing electrolyte systems was homogeneous. As expected the bubbles were much smaller compared to the coalescing air-water system.

Furthermore, these local values were integrated according to their volumetric space in the reactor to obtain overall values for the mass transfer parameters. The overall gas-liquid interfacial area in the coalescing air-water system could be well described using the established correlation of Calderbank (1958). The correlations from literature for description of the mass transfer parameters that are in best agreement with the obtained results in this work are given in Table 4.6.

The effect of the addition of a small fraction of toluene to a coalescing air-water system is strong. Both the gas hold-up and the volumetric mass transfer coefficient decreased by 20-30%. The gas-liquid interfacial area, however, increased by 40%. It was shown that this was due to the presence of micro bubbles in the solution, which do not take part in the mass transfer process. The enhancing effect due to the addition of larger fractions of toluene could be reasonably well described by a homogeneous model of the shuttle mechanism.

Acknowledgement

The author wishes to acknowledge D.J.W. Jansen for his contribution to the experimental and theoretical part of this chapter. B. Knaken is acknowledged for the construction of the set-up.

Table 4.6: Literature correlations of mass transfer parameters that are in good agreement with this work.

symbol	**correlation**	**reference**
	coalescing	
a	$1.44\left(\frac{\left(\frac{P_g}{V}\right)^{0.4}\rho^{0.2}}{\sigma^{0.6}}\right)\left(\frac{u_G}{u_T}\right)^{0.5}$	Calderbank (1958)
ε [a]	$3.85N^{0.73}\Phi_G^{0.62}\left(\frac{D}{T}\right)^{1.64}$ [b]	Greaves and Barigou (1990)
k_La^c	$4.95\cdot10^{-3}\left(\frac{P_g}{V}\right)^{0.593}u_G^{0.4}$	Linek et al. (1987)
	non-coalescing	
ε	$3.86N^{0.92}\Phi_G^{0.41}\left(\frac{D}{T}\right)^{2.56}$	Greaves and Barigou (1990)
d_{32}	$2.25\left(\frac{\sigma^{0.6}}{\left(\frac{P_g}{V}\right)^{0.4}\rho^{0.2}}\right)\varepsilon^{0.4}\left(\frac{\mu_G}{\mu_L}\right)^{0.25}$	Calderbank (1958)

[a] From the parameters a, ε and d_{32} two relations are given. The third one can be calculated.
[b] The impeller speed can be converted in terms of the power input using Equation 4.17.
[c] The k_L can be calculated from k_La and a.

Chapter 5

The influence of small amounts of additives on gas hold-up, bubble size and interfacial area

Abstract

The gas-liquid interfacial area, which is determined by the gas hold-up and the Sauter mean bubble diameter, determines the production rate in many industrial processes. The effect of additives on this interfacial area is, especially in multi-phase systems (gas-liquid-solid, gas-liquid-liquid), often not understood. The addition of a third phase can cause the gas-liquid system to become completely opaque, which means that conventional techniques to study the interfacial area cannot be used. For this reason ultrasonic spectroscopy was used in this work to study the interfacial area and the bubble size distribution in these systems. The influence of different additives on the interfacial area was studied in a stirred vessel and in a bubble column under coalescing and non-coalescing conditions. It was found that the addition of toluene to a non-coalescing electrolyte system decreased the interfacial area to a large extent by turning it into a coalescing system, due to the interaction between gas bubbles and liquid organic droplets. Furthermore, around the toluene solubility concentration, both the gas hold-up (measured using an electric

conductivity technique) and the interfacial area increased to values similar to those observed in non-coalescing systems. The cause of this remarkable phenomenon lies probably in the presence of a small toluene layer around the gas bubbles, which can be formed beyond the solubility point. This layer is absent below the point of maximum solubility and a large surface tension gradient exists between those two situations, which can be responsible for the sharp change in coalescence behaviour.

5.1 Introduction

In chemical engineering the rate of mass transfer between two different phases often directly determines the production rate of the process (e.g. the gas absorption rate in gas-liquid systems). This mass transfer rate is directly proportional to both the mass transfer coefficient and the specific interfacial area between the different phases respectively. Both parameters depend mainly on the (local) hydrodynamic situation inside the system. For design purposes as well as for improvement of existing production facilities it is very important to have a better insight in the phenomena that affect these parameters. The present study focuses on the pronounced effects of small amounts of additives on the gas-liquid mass transfer rate, with emphasis on the effects on the interfacial area. In industrial applications different kinds of additives are found in aqueous systems: electrolytes, surfactants, polar and non-polar organic components and solid particles (hydrophilic or hydrophobic) in slurry systems. It is known from literature that small amounts of certain additives, typically $< 1\%$, can have substantial effects (up to factors 3) on the interfacial area, which is directly related to the bubble size distribution and the gas hold-up. The average bubble size and the gas hold-up depend mainly on three processes that are occurring in gas-liquid systems: bubble formation, bubble coalescence and bubble break-up. In case of electrolytes and surfactant added systems the influence of these processes on the average bubble size and gas hold-up has been frequently investigated (Calderbank, 1958; Barigou and Greaves, 1992; Alves et al., 2002) and the observed phenomena are relatively well understood. However, for other types of process systems this effect is not understood and thus not predictable.

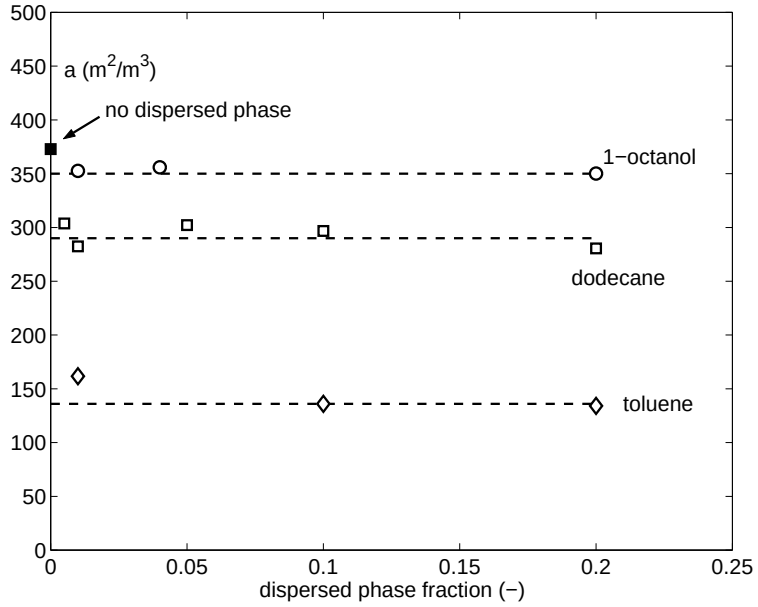

Figure 5.1: Effect of different organic additives on the gas-liquid interfacial area in a 0.5M./0.5M. K_2CO_3/$KHCO_3$ solution measured using the Danckwerts-plot technique.

An example of such an effect on the interfacial area that is still not understood is demonstrated in Figure 5.1. The data of Cents et al. (2001) are presented and contain interfacial areas, as measured using a chemical method (the Danckwerts-plot technique, Danckwerts (1970)). It can be seen that the addition of small amounts of organic phase can have a large influence on the interfacial area in this particular 1 M. electrolyte solution. Especially the large decrease (factor 2.5) upon small additions of toluene is remarkable and cannot be explained. Also the addition of solid particles can influence the mass transfer characteristics already at small volume fractions (see e.g. Ozkan et al. (2000)). At solid contents as low as 0.1 vol-% an increase in the volumetric mass transfer coefficient as high as 3 was observed by Ozkan et al. (2000). However, it was not clear whether the increase must be attributed to the mass transfer coefficient or to the interfacial area. From these two examples it can be concluded that it is very important to have a better understanding of these effects, especially for design purposes of gas-liquid-liquid (G-L-L) systems and gas-liquid-solid (G-L-S) systems.

The scope of this research is to validate the results from previous work

(Cents et al., 2001) using a physical measurement technique and to find the root cause of these effects (in terms of coalescence, break-up and bubble formation). To achieve this, both the gas hold-up as well as average bubble size under different circumstances (for example: coalescing vs. non coalescing systems, with and without bubble break-up) will be measured respectively.

Measurement of the gas-liquid interfacial area in three-phase systems is more difficult than in two- phase systems, because three-phase systems may become opaque at low fractions of the dispersed solid or liquid phase, due to a difference in refractive indices of the various phases. This means that conventional physical measurement techniques for determination of the interfacial area, like photography (combined measurement of bubble size distribution and gas hold-up) and laser scattering are more difficult to operate in these systems and often cannot be used.

For this reason a technique is developed, as explained in Chapter 2, which can measure the bubble size distribution and the gas hold-up independently in opaque media making use of ultrasonic spectroscopy. An additional advantage of this latter technique is the possibility to measure the size distribution and phase hold-up of the dispersed solid or liquid phase together with the gas phase properties. In this way important information can be obtained for better understanding of the mass transfer mechanism in G-L-L or G-L-S three-phase systems.

5.2 Experimental Method

5.2.1 Measurement of size distribution

The experimental technique is based on the difference in ultrasonic wave propagation in a dispersion of particles (solid particles, gas bubbles or liquid droplets) compared to propagation in the continuous liquid. The ultrasonic velocity (c) and attenuation coefficient (α) of a multi-phase system are directly related to the physical properties of the individual phases (e.g. density, compressibility). They are also dependent on the size and volume fraction of the particles and the frequency of the transmitted wave. The theory of ultrasonic propagation in multi-phase systems with an ensemble of particles was first derived by Epstein and Carhart (1953) and Allegra and Hawley

(1972). For more detailed information about the technique the reader is referred to Chapter 2. The ultrasonic velocity and the attenuation coefficient are defined as:

$$c = \frac{d}{t} = \frac{d}{d/c_w(T) + \Delta t} \tag{5.1}$$

$$\alpha = \frac{-\ln\left(I_\varepsilon / I_w\right)}{d} + \alpha_w(T) \tag{5.2}$$

Both quantities are difficult to measure directly, but have to be determined in reference to a single solvent, which was water in the present study (c_w and α_w). Both properties are strongly dependent on temperature and therefore the temperature needs to be known accurately (± 0.05 K). In these equations d is the path length of the measurement, I_w and I_ε are the intensities in the continuous phase and in the dispersion respectively. Δt is the time difference between the signal that has travelled through the dispersion and a reference signal (that has travelled the same distance through the continuous phase).

The experimental set-up (Figure 5.2) consists of an arbitrary waveform generator (AWG), which transmits any desired electric signal to a piezoelectric transducer (T). The transducer converts the electric signal to a pressure wave that is received in a second transducer (R) where the latter is converted back into an electric signal, which is acquired with a digital oscilloscope. Simultaneously, a trigger signal is transmitted to the oscilloscope assuring that in every measurement the starting point, $t = 0$, is known accurately. A tone-burst signal, a limited number of cycles of a certain frequency, is used for determination of the velocity and the attenuation coefficient, which has the advantage of a low power input and the absence of signal disturbances (which may not be the case using continuous signals). The time difference between the signal in the dispersion and the reference signal can be determined using a cross-correlation function, which is also shown in Figure 5.2. In order to determine the size distribution of large bubbles as well as small droplets or particles a frequency range of 100 kHz up to 100 MHz must be covered. For more details of the method and the equipment used the reader is referred to Chapter 2.

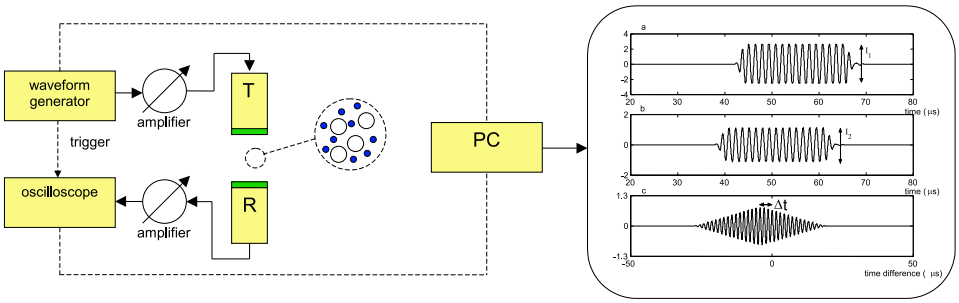

Figure 5.2: Set-up of the ultrasonic measurement system and signal analysis in the PC.

5.2.2 Determination of phase hold-up

From the ultrasound measurements it is, in principle, possible to determine both the size distributions as well as the phase hold-up of the particles, bubbles and droplets. However, in Chapter 2 it is shown that in the case of a gas-liquid system multiple solutions can exist with different types of bubble size distributions and slightly different gas hold-ups. The interfacial area, however, determined via the ultrasonic technique, is not affected by this multiplicity and is determined very accurately. The above mentioned complication implies that for the determination of the exact bubble size distribution the (local) gas hold-up is required. A reliable method to measure the gas hold-up uses the ratio of the electric conductivity in the continuous liquid phase and in the gas-liquid dispersion (G_ε/G_w), which was applied by among others Yianatos et al. (1985). The local gas hold-up (ε) can be determined with:

$$\frac{G_\varepsilon}{G_w} = \frac{1-\varepsilon}{1-0.5\ln(1-\varepsilon)} \tag{5.3}$$

The overall gas hold-up can be measured by comparing the liquid height in the reactor with and without gas phase present, according to:

$$\langle\varepsilon\rangle = 1 - \frac{H_w}{H_\varepsilon} \tag{5.4}$$

The interfacial area (a) of the bubble size distribution can be calculated from the Sauter mean diameter (d_{32}) and the phase hold-up (ε) according to:

$$a = \frac{6\varepsilon}{d_{32}} \tag{5.5}$$

The overall interfacial area $< a >$ in the reactor can be estimated using the overall gas hold-up $< \varepsilon >$ and the Sauter mean $< d_{32} >$ diameter for the complete reactor. Both parameters are not necessarily the same as the locally determined values.

5.2.3 Experimental

The experimental set-up consists of a reactor vessel (15 cm diameter) with a working volume of 3.2 liters, which can be operated in both a bubble column and a stirred vessel mode respectively. The gas is distributed in the reactor through a sintered porous plate (type P1, 90-150 mm) and the gas flow rate is controlled using a mass flow controller. When the reactor is operated as a stirred vessel a Rushton turbine with a variable stirring speed (5 cm in diameter) is placed 6 cm above the porous plate. Four baffles ensure adequate mixing in the reactor. The temperature is measured within 0.1 $^\circ$C using a PT-100. The ultrasonic probe was placed 11 cm above the porous plate in the center of the reactor. The path length between the transducers in the probe can be varied between 1 and 67 mm and can be adjusted to the amount of attenuation of the ultrasonic waves. It is necessary to compare this distance to the size of the measured particles, bubbles or droplets, because the ratio of the distance between the transducers and the particles should be at least 20 to ensure a representative dispersion sample between the transducers. The conductivity probe consisted of 2 stainless steel electrodes and had an exactly equal shape compared to the ultrasonic probe.

After the system under investigation was replaced with another system, the system was cleaned thoroughly. Surface tension measurements were performed in order to check if all impurities were removed.

5.3 Results and Discussion

5.3.1 Ultrasonic velocity and attenuation coefficient profiles

In order to be able to measure the size distribution of the dispersed phase(s) in a two- or three-phase system, the ultrasonic velocity and the attenuation profiles

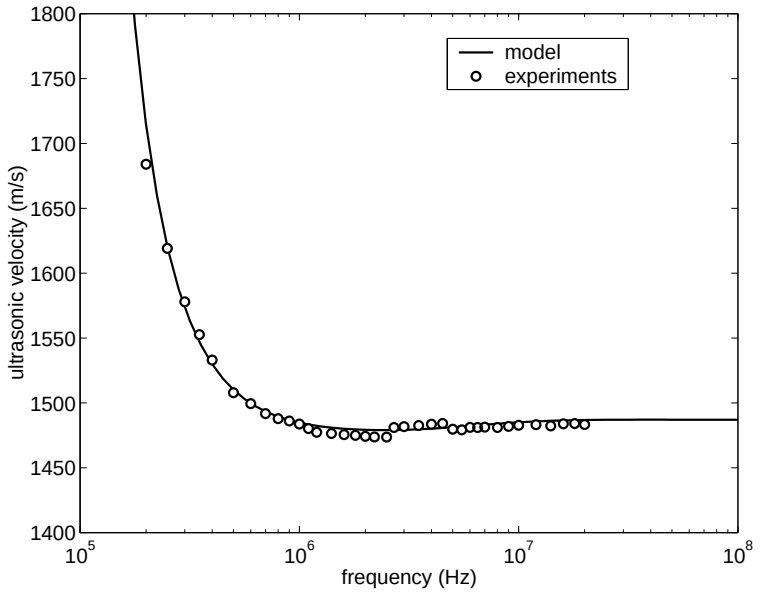

Figure 5.3: Ultrasonic velocity vs. frequency profile of air-water-hexadecane measured in the bubble column. u_G = 2.6 cm/s. The gas hold-up and Sauter diameter of hexadecane and air are determined using the theory of ultrasonic propagation: ε_{AIR} = 6.6%, ε_{HEXA} = 6.3%, $d_{32,AIR}$ = 2.1 mm, $d_{32,HEXA}$ = 0.67 mm.

should contain information in the frequency region where the effect on the ultrasonic parameters is characteristic for the size of the particles. The presence of bubbles in the range of 1-4 mm affects the velocity and the attenuation mainly in the low frequency regime (0.1 - 1 MHz). Particles and droplets usually are much smaller and cause large effects at higher frequencies. In Figures 5.3 and 5.4 the ultrasonic velocity and attenuation coefficient profiles are presented of an aerated dispersion of hexadecane in water. The large increase in the velocity at the lower frequencies is due to the gas bubbles present in this system, whereas the effects at higher frequencies originate from the presence of the droplets. As indicated in Figure 5.4 the attenuation coefficient profile contains influences of both dispersed phases. Examples of velocity and attenuation profiles of G-L, S-L and G-L-S systems can be found in Chapter 2.

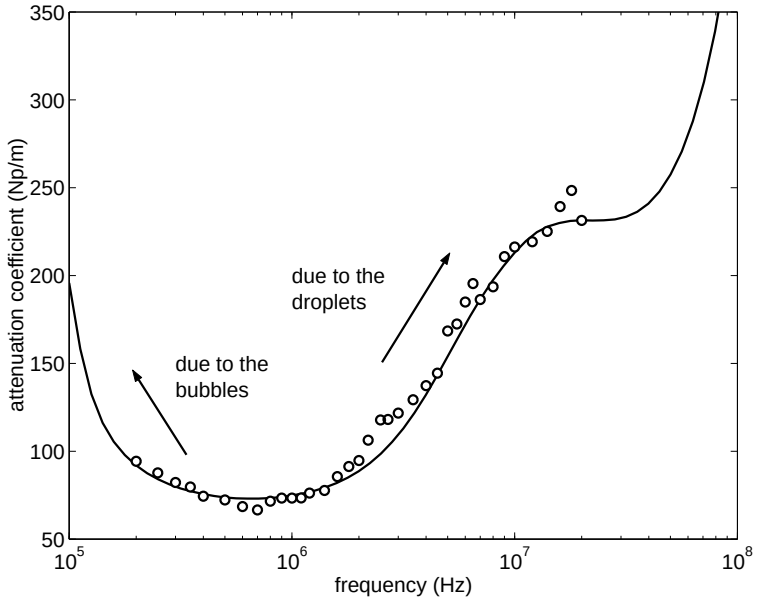

Figure 5.4: Attenuation coefficient vs. frequency profile of air-water-hexadecane measured in the bubble column.

5.3.2 Air-aqueous systems

To study the effects of different additives on the interfacial area measurements are performed in a stirred vessel and in a bubble column. In both cases the gas (air) was distributed through a porous plate, which means a similar initial bubble size can be assumed. In the stirred vessel both coalescence of bubbles as well as break-up are important, due to the high energy dissipation especially in the impeller region. The bubble column is operated in the homogeneous regime, because of the low superficial velocities ($0.2 < u_G < 3$ cm/s) as indicated by Deckwer (1985). In this regime break-up of bubbles is relatively unimportant due to the low energy dissipation and the bubble size is mainly determined by coalescence phenomena just above the gas distributor (chain bubbling). After this initial coalescence region the bubbles are rising with an approximately constant velocity. In this section results are presented of coalescing (air-tap water) and non-coalescing systems (0.5 M. KCl and 0.5 M./0.5 M. K_2CO_3/$KHCO_3$ buffer solutions). Tap water was used to improve the accuracy of the gas hold-up measurement using the electrical conductivity

technique. It was verified that the use of tap water did not significantly influence the determination of the interfacial area, when compared to measurements with deionized water. Although the measured quantities are the interfacial area (using the ultrasonic method) and the gas hold-up (using the conductivity technique), the interfacial area, defined by Equation 5.5, and the Sauter mean diameter, which is a very characteristic parameter, are presented.

The results for the stirred vessel are shown in Figures 5.5 and 5.6. As expected from the work of Craig et al. (1993) the applied electrolyte concentration seems high enough to prevent coalescence of the gas bubbles. In the electrolyte systems the interfacial area is a factor 3-4 higher compared to the coalescing air-water system. In the calculation of the Sauter mean diameter in the electrolyte solutions the overall gas hold-up was applied instead of the local hold-up, because the conductivity technique failed due to the low resistivity in the solution. This did not affect the results to a large extent, owing to the homogeneous nature of the systems. The bubble size distribution was narrow (variance < 0.1 mm) in the electrolyte solutions and the Sauter mean diameter was around 0.8-1.2 mm, which was considerably lower compared to the air-water system (1.5-3 mm). These bubble sizes are in the range of values commonly observed in coalescing and non-coalescing aqueous systems. In the bubble column similar trends are observed, as is shown in Figures 5.7 and 5.8.

5.3.3 Air-electrolyte-toluene system

The influence of toluene on the interfacial area and bubble size distribution was studied in the stirred vessel and in the bubble column under coalescing and non-coalescing conditions using a toluene volume fraction of 2.5% and is visualized in Figs. 5.5-5.8. The addition of toluene to an electrolyte solution in the stirred vessel reduced the interfacial area to values of the same order of magnitude as in the coalescing air-water system. The hydrodynamic conditions in the tank, however, are in the presence of toluene completely different compared to the coalescing system. A very broad size distribution was obtained in this case and the presence of very large (2-3 cm) bubbles rising very fast through the reactor was observed visually.

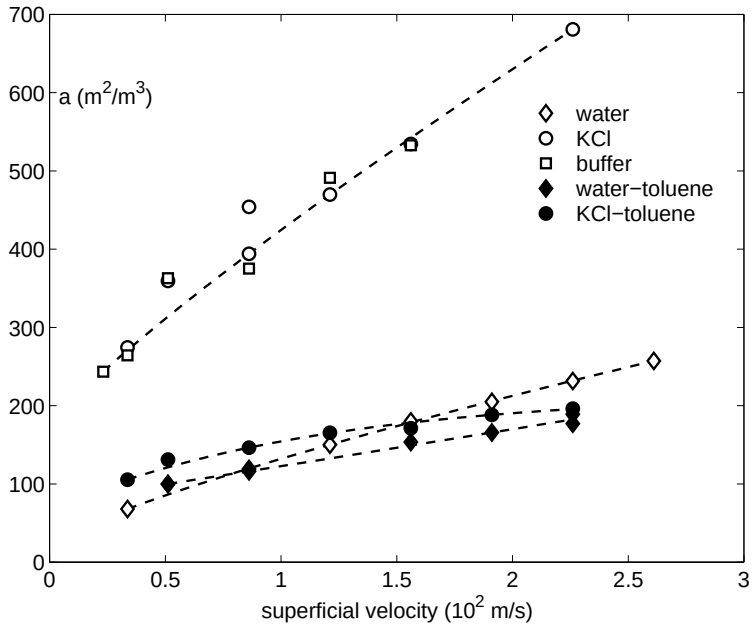

Figure 5.5: Gas-liquid interfacial area of different systems as function of the superficial velocity in the stirred vessel.

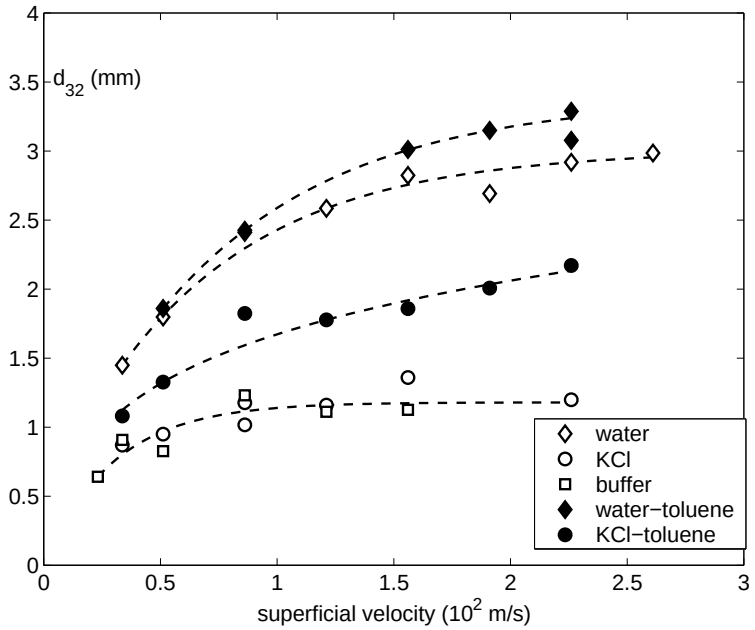

Figure 5.6: Sauter mean diameter of different systems as function of the superficial velocity in the stirred vessel.

Furthermore, a certain fraction of micro bubbles was required to be present in the bubble distribution, to be able to get a reasonably good fit with the scattering model on the experiments. This was also observed in an air-water-toluene system and is described extensively in Section 4.8.2. This indicates that the ultrasound technique can be used to quantify different shapes of distributions, but further study is necessary to determine the exact shape of the distributions.

The interfacial areas measured using this physical measurement technique are in good qualitative agreement with the results obtained in our previous work (in a comparable stirred vessel with the gas distributed from a single orifice) using the Danckwerts-plot technique (Fig. 5.1). Two possible mechanisms for this change are now suggested:

a The additional mass transfer of the organic phase from the liquid to the bubble can cause a change in the coalescence rate, as indicated in the review article by Chaudhari and Hofmann (1994).

b The dissolved or dispersed toluene is present at the bubble surface, either as a monolayer or as a film with a certain thickness, which causes a repression of the electric double layer and thus a reduction of the inhibition of coalescence.

To study the effect of toluene mass transfer, experiments were performed with 2.5 vol-% toluene in the stirred vessel and using a gas stream that was pre-saturated with toluene and water, so no (net) mass transfer occurred between the liquid and the gas phase. Pre-saturation had no effect on the interfacial area, which means that it is unlikely that toluene mass transfer changed the coalescence properties of the dispersion. This result suggests that toluene is present at the surface, but it remains unknown whether interaction of the bubble with the organic droplets or the dissolved toluene is responsible for this effect.

To study this effect, the interfacial area in an initially toluene-free 0.5 M. KCl solution was determined, while the gas stream was saturated with toluene. In this way the toluene is absorbed in the electrolyte solution, but no toluene droplets are formed, as the concentration in the liquid phase can not pass the solubility limit. In these experiments, and in contradiction to the experiments described previously

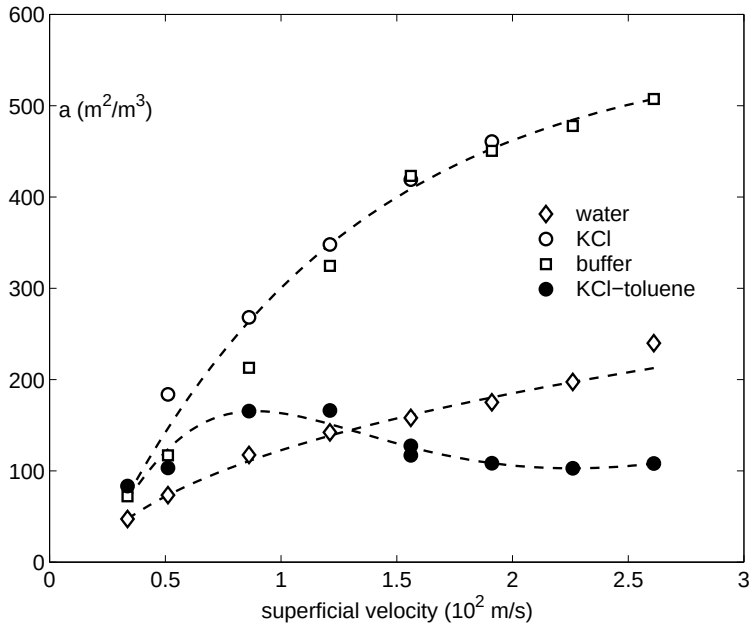

Figure 5.7: Gas-liquid interfacial area of different systems as function of the superficial velocity in the bubble column.

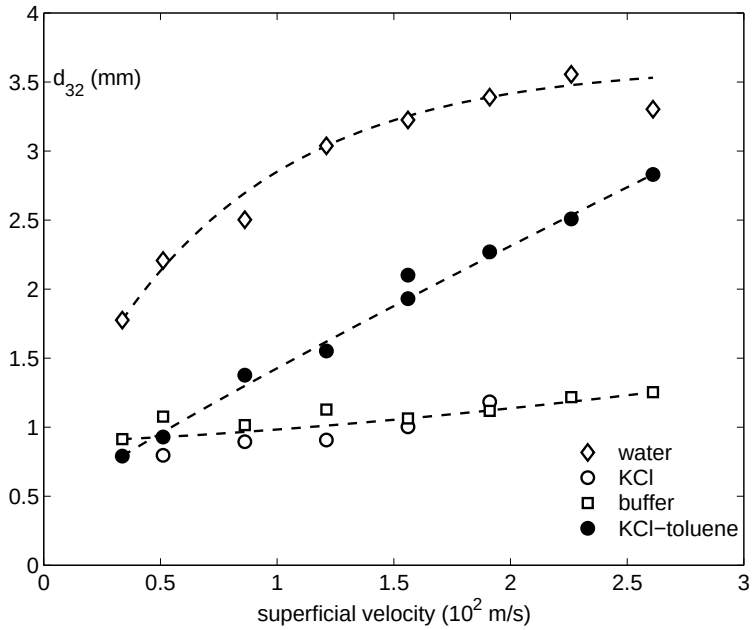

Figure 5.8: Sauter mean diameter of different systems as function of the superficial velocity in the bubble column.

with 2.5% toluene present as droplets, no decrease in interfacial area was observed. This observation strongly supports the hypothesis that the interaction of the gas bubbles with toluene droplets is responsible for the decrease in interfacial area.

This hypothesis was further supported by experiments with 2.5% toluene in an air-KCl-solution in the bubble column mode at homogeneous bubble flow conditions. The use of 2.5% toluene ensured that the continuous phase was completely saturated with toluene, although the toluene was poorly dispersed through the reactor content and the value of the superficial gas velocity determined the amount of toluene dispersion in the reactor. From Figure 5.7 it can be concluded that two different phenomena occurred when the superficial velocity is increased. An initial increase in interfacial area is obtained due to the higher gas content of the bubble column, but above a certain gas velocity (around 1 cm/s) the interfacial area is decreased, which is likely to be caused by the presence of the droplets in the more turbulent reactor. These combined effects resulted in a linear increase in the Sauter mean diameter with the superficial gas velocity (Fig. 5.8).

The most likely form of droplet-bubble interaction to occur is complex formation (Brilman, 1998) in which a droplet and a bubble "coalesce" to form a bubble covered by an organic layer. The spreading of an organic liquid over an aqueous solution is favorable when the final spreading coefficient (at mutually saturated conditions, $S^* = \sigma^*_{W/G} - \sigma^*_{O/G} - \sigma^*_{O/W}$) is positive, which is the case in the air-toluene-electrolyte system (+8 mN/m, see Appendix B).

According to the work of Bartell et al. (1933) a positive spreading coefficient can not exist in a system at equilibrium. In that case a small toluene layer will be formed spontaneously on the gas-liquid interface, and the final spreading coefficient will go to zero. Measurements of the surface tension of water with a small layer of toluene on top (see Figure 5.9) showed that at the point of maximum toluene solubility a sharp decrease of the surface tension occurred and the spreading coefficient decreased to approximately zero. The origin of the molecules, that are required to form the layer around the bubbles is, however, not clear. Toluene droplets might be required to act as small toluene supplies and facilitate the formation of the small organic layers.

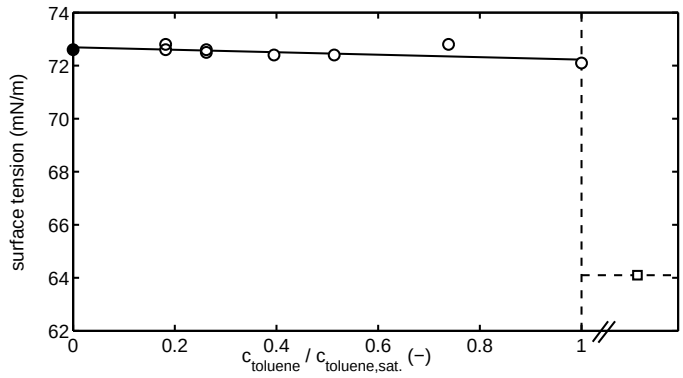

Figure 5.9: Effect of the normalized toluene concentration (c/c_{sat}) on the surface tension. The data point beyond the point of maximum solubility was measured with different organic layer thicknesses (1.2 μm - 3 mm) and the x-coordinate for that point is therefore in arbitrary units.

If toluene is present as a film around the bubble (by one of the two proposed mechanisms), the toluene layer determines the coalescence properties and no coalescence inhibition is expected. This can explain the coalescing nature of the air-electrolyte-toluene system.

5.3.4 Air-water-toluene system

From Figure 5.10 it seems that the addition of toluene (1-6%) to an air-water dispersion does not influence the gas-liquid interfacial area, in contrast to the addition to the electrolyte solution. The bubble size distribution is, however, much wider in the presence of toluene and similar to the experiments with the electrolyte solutions large gas bubbles are observed.

During the stripping of toluene from the aqueous solution a strong increase of both the interfacial area and the gas-hold-up is observed at toluene fractions around the maximum solubility in water (0.53 g/l). Both a and ε were measured on-line and the toluene concentration was determined from the stripping speed of toluene (Fig. 5.11). The observed increase is remarkable, because the coalescing air-water-toluene system ($a = 150$ m^2/m^3, $\varepsilon = 5.7\%$ $d_{32} = 2.3$ mm) is altered in a non-coalescing system ($a = 550$ m^2/m^3, $\varepsilon = 9.9\%$ $d_{32} = 1.1$ mm) around the toluene

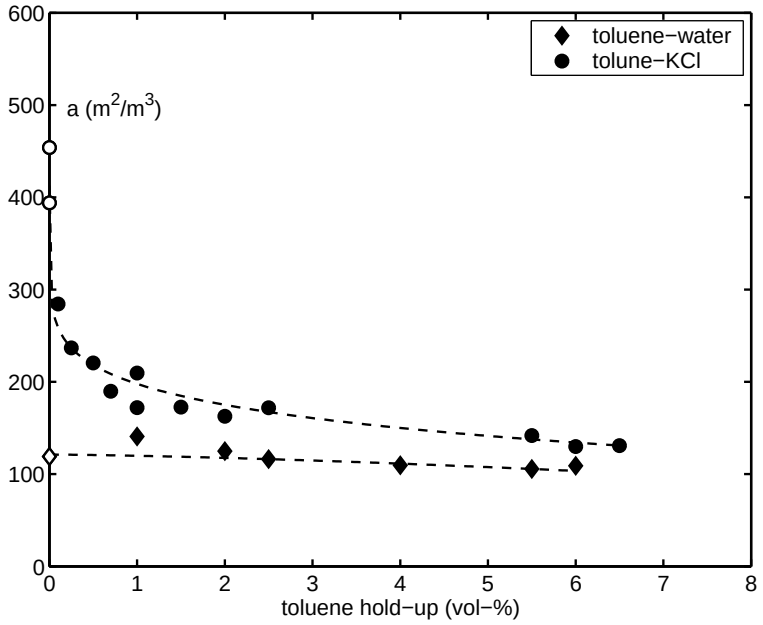

Figure 5.10: Gas-liquid interfacial area of air-water toluene and air-electrolyte-toluene systems as function of the toluene fraction in the stirred vessel. (u_G: 0.86 cm/s).

maximum solubility point. At this point droplets are not present anymore in the solution, which means that the solution is saturated with toluene and the bubble might be covered with a layer of toluene. This remarkable effect was not only observed during stripping, but also (up to the saturation point) during saturating an air-(initially toluene-free) water system with toluene using a gas stream which was pre-saturated with toluene.

The nature of this remarkable phenomenon might be in the large difference in the surface tension when a small toluene layer is present on the gas-liquid interface compared to the surface tension of the saturated solution (64 mN/m and 72 mN/m, respectively, see Figure 5.9). If such a small layer is present beyond the point of maximum solubility and not below the point of maximum solubility a very large value of $d\sigma/dc$ will exist during stripping, which results in high coalescence times, according to different coalescence theories (Marrucci, 1969; Sagert and Quinn, 1978).

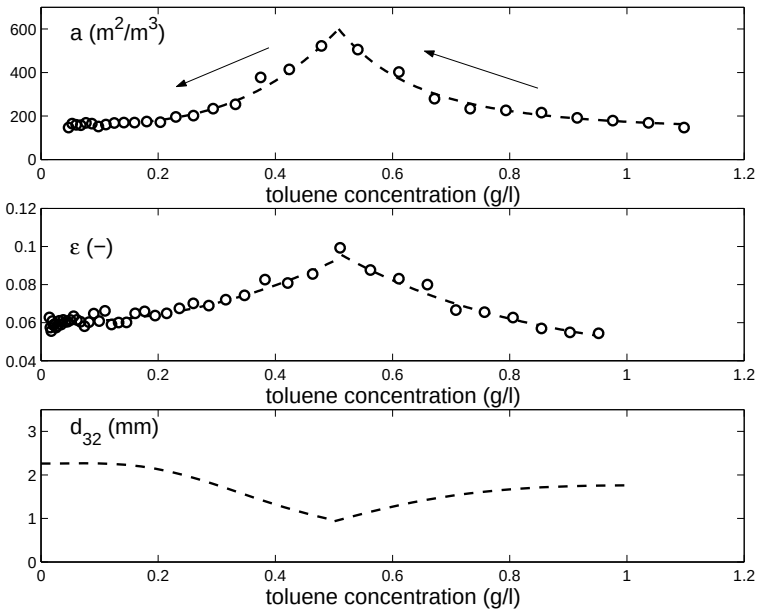

Figure 5.11: Gas-liquid interfacial area, gas hold-up and Sauter mean diameter at low toluene fractions in an air-water system. (u_G: 0.86 cm/s).

5.3.5 Other three-phase systems

The gas-liquid interfacial area in air-water and in air-electrolyte (0.5 M. KCl) systems was also measured in the presence of different organic phases; heptane, hexadecane and 1-octanol. From the results, presented in Table 5.1, it can be concluded that the mechanism accounting for the strong effects on the interfacial area is very sensitive to the type of the organic additive. The large decrease of the interfacial area in air-electrolyte systems is only observed in the presence of toluene. Heptane ($S \approx 0$) and hexadecane ($S < 0$) show no significant effect and the addition of 1-octanol actually increased the area to a large extent. This large increase was also observed in the air-water-octanol system and is probably the result of a smaller initial bubble size; due to a lower air to water surface tension ($\gamma_{A/W(O)} = 30$ mN/m) or due to a more decreased coalescence rate compared to the electrolyte system. The interfacial area in the air-water-heptane system was measured several times and was significantly lower compared to the air-water system and similar to the systems with toluene some large bubbles were observed visually. Spreading of heptane around the

bubbles might have caused this, but further research must be performed to study the spreading behavior of the organic phases (see Appendix B).

Table 5.1: Gas-liquid interfacial areas (m^2/m^3) of water and 0.5 M. KCl solutions with different additives (2.5%) in the stirred vessel. N=550 rpm, u_G=0.86 cm/s.

Additive	Tap water	0.5 M. KCl solution
-	**115**	**394**
Toluene	116	146
Hexadecane	109	378
Heptane	77	375
1-Octanol	670	691

5.4 Conclusions

Ultrasonic spectroscopy was used to study the gas-liquid interfacial area in gas-liquid and gas-liquid-liquid systems, while the gas hold-up was measured separately using an electrical conductivity technique. The ultrasonic spectroscopy technique applied has proven to be a valuable tool in analyzing gas absorption effects in multiphase systems.

The addition of toluene to a non-coalescing air-electrolyte system reduced the interfacial area to a large extent and the formation of large gas bubbles is observed; thus effectively transforming it into a coalescing system. It was found that interaction between gas bubbles and toluene droplets (like bubble-droplet coalescence or the spontaneous formation of a small toluene layer around the gas bubble) causes this effect; effects of dissolved toluene are negligible. Another, possibly related, interesting phenomenon was observed around the solubility concentration of toluene in a coalescing air-water system. The interfacial area at this point increased by a factor 3-4 and the system changed into a non-coalescing system. The cause of this remarkable phenomenon lies probably in the presence of a small toluene layer, which forms beyond the solubility point. This layer is absent below the point of maximum solubility and a large surface tension gradient exists between those two

situations, which can be responsible for the sharp change in coalescence behaviour. In general, it was found that the influence of different additives on the gas-liquid interfacial area is very sensitive to the nature of the added components and further investigation (e.g. on the spreading behavior of these phases) is required to be able to predict on beforehand whether or not certain additives will affect the gas-liquid interfacial area.

Acknowledgement

B. Knaken is acknowledged for the technical support and D.J.W. Jansen is acknowledged for his contribution to the experimental work.

Chapter 6

Mass transfer effects in the biphasic hydroformylation of propylene

Abstract

The hydroformylation of propylene to butyraldehyde is an important industrial process. In this reaction system carbon monoxide, hydrogen and propylene are converted to n-butyraldehyde in an aqueous phase containing a water-soluble rhodium catalyst. This reaction system consists therefore of three different phases; the aqueous catalyst phase, the organic butyraldehyde phase and the gas phase. A modelling study indicated that an optimum value of the production rate is reached at a certain power input. It was shown that mass transfer plays an important role in this reaction system and that accurate knowledge of the mass transfer parameters in the gas-liquid-liquid system is necessary to predict and to optimize the production rate.

Mass transfer experiments of CO, H_2 and propylene in water and in solutions consisting of water with different amounts of n-butyraldehyde were carried out in a stirred autoclave. The results indicated that the addition of small amounts of butyraldehyde caused a relatively small increase increase in k_La, which was probably caused by a larger increase of the gas-liquid interfacial area, a, accompanied by a

decrease in the mass transfer coefficient, k_L. Near the point of maximum solubility of butyraldehyde a strong (factor 3) increase in k_La was observed. The most logical explanation for this is an increase in k_L, because measurement of the interfacial area did not show such an increase. This increase in k_L, i.e. the disappearance of the initial decrease, might be due to the disappearance of the rigid layer of butyraldehyde molecules at the gas-liquid interface by formation and spreading of a butyraldehyde layer around the bubble.

6.1 Introduction

The biphasic hydroformylation of propylene was first reported by Kuntz (1976). Its major advantage over the conventional single phase phase hydroformylation is the higher selectivity (95% compared to 80%) to the desired product, n-butyraldehyde. The reaction scheme is shown in Figure 6.1. The reaction is carried out in the aqueous phase containing a rhodium catalyst with water-soluble ligands. The product butyraldehyde is sparingly soluble and forms a second (dispersed) liquid phase. This catalyst is made water-soluble by the addition of triphenylphosphine-m-trisulfonic acid trisodium salt (TPPTS).

The biphasic hydroformylation of propylene is commercially applied by Ruhrchemie/Rhône-Poulenc (RC/RP, nowadays by Hoechst/Celanese) since 1984. A schematic outline of the process is presented in Figure 6.2 and the relevant process parameters are given in Table 6.1. In this process syngas and propylene are fed to a reactor in which the conversion to butyraldehyde takes place. In the reactor a system of three phases exist; the aqueous phase containing the catalyst, a dispersed phase containing butyraldehyde and a gas phase consisting of the gaseous reactants CO, H_2 and propylene. After the reactor the reaction mixture is transported to a gas-liquid separator in which the unconverted gasses are separated from the liquids and returned to the reactor. The liquid two-phase system is separated by simple decantation and the aqueous catalyst phase is transported back to the reactor. The organic phase is removed from impurities in a stripping column using the syngas stream. The crude butyraldehyde can be further processed to a distillation column

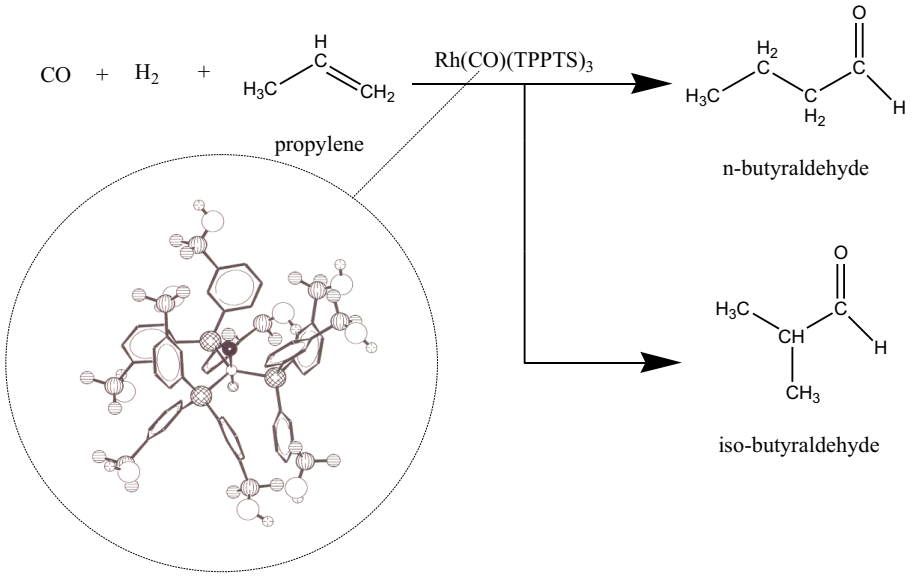

Figure 6.1: Scheme of the reaction the biphasic hydroformylation of propylene using a rhodium catalyst.

in which the n-butyraldehyde is separated from the iso-form. Strengths of this process are the low rhodium losses (less than 10^{-9} gram / kg n-butyraldehyde, Cornils and Kuntz (1995)) and the low energy consumption.

Butyraldehyde is a versatile product and the raw material can be used for numerous other chemicals. A major part of the produced butyraldehyde is converted to butanols and 2-ethylhexanol, and it is also used as the raw material for the production of carboxylic acids and amines.

The influence of mass transfer in this process was investigated by Wachsen

Table 6.1: Estimated relevant process parameters of the RC/RP biphasic hydroformylation of propylene.

parameter	value
Temperature, $^\circ$C	120
Pressure, bar	10-50
Rhodium concentration, ppm	300-1000
n:iso ratio	13-30:1

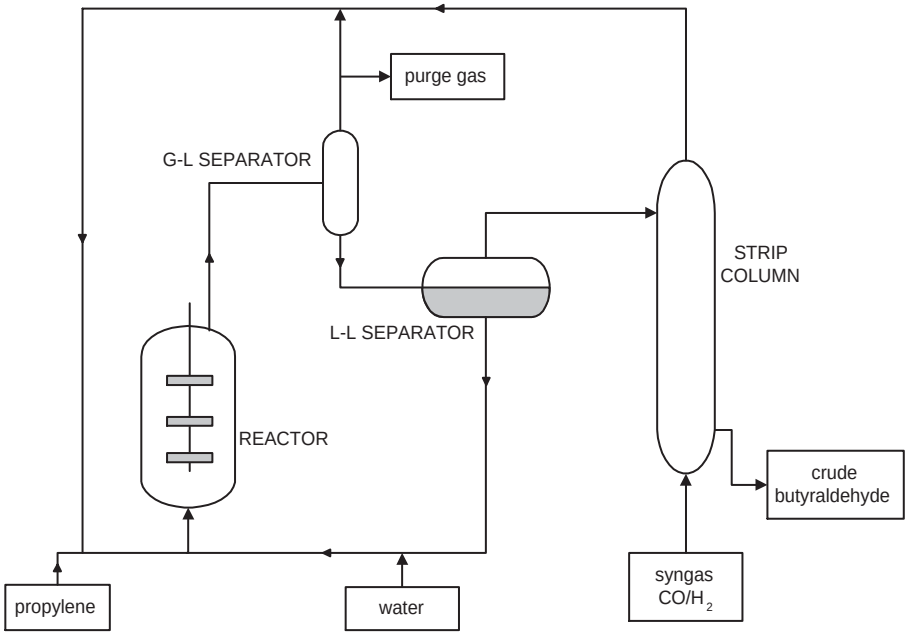

Figure 6.2: Simplified process scheme of the RC/RP biphasic hydroformylation of propylene.

et al. (1998). These authors concluded from their experimental work that the process was (at least partially) mass transfer limited. With the development of improved, more active catalysts (Cornils et al., 1997) mass transfer will be more and more important in this reaction system.

In this chapter the influence of the volume fraction butyraldehyde on the volumetric mass transfer coefficient in the biphasic hydroformylation of propylene is investigated. In the first section a modelling study is performed using the mass transfer parameters determined in Chapter 4 and the reaction kinetics as measured by Yang et al. (2002). In the second part of this chapter mass transfer experiments involving the different gasses found in the hydroformylation reaction (CO, H_2 and propylene) into water with different fractions butyraldehyde are described.

6.2 Modelling of mass transfer and chemical reaction

The model that is used in this section takes both the mass transfer and the chemical reaction into account. The governing equations that determine the flux of the three gasses (A = H_2, B = CO and E = propylene) into the aqueous liquid phase are:

$$\frac{dc_A}{dt} = D\frac{d^2c_A}{dx^2} - R_A \tag{6.1}$$

$$\frac{dc_B}{dt} = D\frac{d^2c_B}{dx^2} - R_B \tag{6.2}$$

$$\frac{dc_E}{dt} = D\frac{d^2c_E}{dx^2} - R_E \tag{6.3}$$

with boundary conditions:

$$\begin{array}{lllll} t = 0, x > 0: & c_A(x,t) = c_{A,bulk} & c_B(x,t) = c_{B,bulk} & c_E(x,t) = c_{E,bulk} \\ t > 0, x = 0: & c_A(x,t) = m_A c_{A,G} & c_B(x,t) = m_B c_{B,G} & c_E(x,t) = m_E c_{E,G} \\ t > 0, x = \infty: & c_A(x,t) = c_{A,bulk} & c_B(x,t) = c_{B,bulk} & c_E(x,t) = c_{E,bulk} \end{array}$$

From these equations the flux of the different gasses into the liquid can be calculated according to:

$$J(t) = D\frac{dc(t)}{dx}\bigg|_{x=0} \tag{6.4}$$

The average flux in time can be determined using the penetration model:

$$\overline{J} = \frac{1}{\tau_p}\int_0^{\tau_p} J(t)dt \tag{6.5}$$

In the reactor model a constant partial pressure of the gaseous reactants was assumed and the overall loss of CO, H_2 and propylene from the liquid phase is neglected. In the steady state the fluxes of all components are then equal to the total reaction rate in the solution:

$$R_X = \overline{J_A}a = \overline{J_B}a = \overline{J_E}a \tag{6.6}$$

The bulk concentrations of the three different reactants can be determined from this equation.

6.2.1 Kinetics

The kinetics of the hydroformylation reaction in the presence of a $RhCl(CO)(TPPTS)_2$/TPPTS complex catalyst were experimentally determined by Yang et al. (2002). These authors varied the propylene concentration, the initial pressure, the H_2/CO ratio, the temperature, the rhodium concentration and the ligand to rhodium ratio in an orthogonal experimental design to obtain the following rate expression:

$$R_X = k_0 \exp\left(\frac{-E_A}{RT}\right) \frac{p_A p_B p_E c_{Rh}}{(1+k_1 p_A)(1+k_2 p_B)^2(1+k_3 p_E)^2(1+k_4 c_{Lig})^3} \tag{6.7}$$

The constants are defined in Table 6.2:

Table 6.2: Kinetic parameters as determined by Yang et al. (2002).

k_0 [a]	E_A	k_1	k_2	k_3 [b]	k_4
$7.545 \cdot 10^{12}$	83.15	1.367	0.5641	0.4995	$1.823 \cdot 10^{-2}$

[a] The units of R_x, E_A, c and partial pressures (p_i) are mol/(m^3 s), kJ/mol, mol/m^3 and bar, respectively

[b] The partial pressure of propylene, p_E, is at 16 °C. Other pressures are at reaction temperature.

The concentration of the three different gasses was calculated from the partial pressure using the Peng-Robinson equation of state with standard mixing rules to combine the kinetic rate expression with the flux calculations.

6.2.2 Mass transfer

The results obtained in Chapter 4 for the standard stirred tank contactor with Rushton type agitator and baffles will be used in this work to determine the mass transfer properties for the absorption of the three hydroformylation gasses in the water-butyraldehyde solution. The addition of butyraldehyde to water is likely to prevent coalescence of gas bubbles in the solution (due to the strong decrease in surface tension, see Appendix B), which means that the obtained results and recommended correlations for the non-coalescing system are most appropriate. The bubble diameter can probably be best described with the equation proposed by Calderbank (1958) for aliphatic alcohol solutions:

$$d_{32} = 1.90 \left(\frac{\sigma^{0.6}}{\left(\frac{P_g}{V}\right)^{0.4} \rho^{0.2}} \right) \varepsilon^{0.65} \left(\frac{\mu_G}{\mu_L} \right)^{0.25} \tag{6.8}$$

The gassed power input could be calculated from the relation given by Hughmark (1980):

$$\frac{P_g}{P} = 0.10 \left(\frac{\Phi_G}{NV} \right)^{-1/4} \left(\frac{N^2 D^4}{W g V^{2/3}} \right)^{-1/5} \tag{6.9}$$

The gas hold-up in non-coalescing systems was given by Greaves and Barigou (1990):

$$\varepsilon = 3.86 N^{0.92} \Phi_G^{0.41} \left(\frac{D}{T} \right)^{2.56} \tag{6.10}$$

The interfacial area is calculated using: $a = 6\varepsilon/d_{32}$. The mass transfer coefficient, k_L, was calculated according to the work of Linek et al. (1970), using a correction for the diffusion coefficient:

$$k_{L,W} = 2 \cdot 10^{-4} \left(\frac{P_g}{V} \right)^{0.14} \left(\frac{D^T}{D_{O_2}^{25}} \right)^{0.67} \tag{6.11}$$

It is well known that the addition of surfactant-like components (like butyraldehyde) reduces surface tension and can form a somewhat stagnant, more rigid,

layer of molecules around the bubble. This hydrodynamic effect causes a decrease in the mass transfer coefficient. Llorens et al. (1988) investigated this and found the following relation:
For $0.4 < \pi < 16$ mN/m:

$$\frac{k_L}{k_{L,W}} = \frac{1}{1.25 + 73\pi} \tag{6.12}$$

For $\pi > 16$ mN/m:

$$\frac{k_L}{k_{L,W}} = 0.41 \tag{6.13}$$

in which π (N/m) is the interfacial pressure, defined as: $\pi = \sigma_W - \sigma$.
This k_L can be used in the calculation of the penetration time according to:

$$\tau_p = \frac{4D}{\pi k_L^2} \tag{6.14}$$

6.2.3 Dispersed phase

The addition of a dispersed phase can increase the rate of mass transfer when the solubility for the component to be transferred is higher in the dispersed phase compared to the continuous phase. In Chapter 1 it was shown that this increase of mass transfer in case of toluene and 1-octanol could be well described using a homogeneous model of the shuttle mechanism. When it is assumed that this is also applicable to the biphasic hydroformylation of propylene with butyraldehyde as the dispersed phase the governing equations are:

$$\left(1 + \varepsilon_D \left(m_{R,A} - 1\right)\right) \frac{dc_A}{dt} = D_A \frac{d^2 c_A}{dx^2} - (1 - \varepsilon_D) R_X \tag{6.15}$$

$$\left(1 + \varepsilon_D \left(m_{R,B} - 1\right)\right) \frac{dc_B}{dt} = D_B \frac{d^2 c_B}{dx^2} - (1 - \varepsilon_D) R_X \tag{6.16}$$

$$(1 + \varepsilon_D (m_{R,E} - 1)) \frac{dc_E}{dt} = D_E \frac{d^2 c_E}{dx^2} - (1 - \varepsilon_D) R_X \tag{6.17}$$

The boundary conditions are similar compared to the system without a dispersed phase. The following assumptions are made:

1. The dispersed phase is equally divided throughout the gas-liquid mass transfer zone.

2. The concentration of all three gasses in the dispersed phase is at any time and place within the mass transfer zone at equilibrium with its concentration in the surrounding continuous phase.

3. The presence of the microphase droplets does not influence the surface renewal frequency of the continuous liquid phase.

Neglecting the liquid-liquid mass transfer is likely to be justified, because of the low water-butyraldehyde interfacial tension. This means that the butyraldehyde droplets are very small, thus creating a high liquid-liquid interfacial area. Assumption 3 seems reasonable as it was found in Chapter 1 that for all dispersed liquid phases, whether or not enhancing mass transfer, the apparent k_L value remained constant.

6.2.4 Numerical

The bulk concentrations of the different gasses can be determined starting with an empty bulk and increasing the bulk concentration using the average flux after every penetration time, until a steady-state situation is reached. In this situation (with and without a dispersed phase) the following relation holds:

$$(1 - \varepsilon_D) R_X = \overline{J_A} a = \overline{J_B} a = \overline{J_E} a \tag{6.18}$$

This is, however, very time consuming and in this case an algorithm is used which calculates an initial guess of the bulk concentrations using the film

model by solving $R_X = k_L a(mc_G - c_{bulk})$ and in case of a dispersed phase present $R_X = k_L a\sqrt{1+\varepsilon_D(m_R-1)}(mc_G - c_{bulk})$ for all three components. After this the bulk concentrations are solved from Equation 6.18 using the full set of equations in an optimization routine.

The set of three partial differential equations is solved using the method of lines. The system is converted to ODE's by central discretization of the diffusion term and solved using a variable order, stiff ODE-solver. The number of place steps was (in the mass transfer zone) 50 and the number of times steps (during the penetration time) was 500. This combination gave good agreement with the analytical solution in a simple first order reaction system and the increase of steps did not influence the results. The penetration depth for physical absorption ($\delta_p = 4D/k_L$) was taken as 1.5 times the penetration depth of the gas with the largest diffusion coefficient (hydrogen), which ascertained that $dc/dx = 0$ at $x = \infty$. The flux was approximated as: $J(t) = D(3c_0 - 4c_1 + c_2)/\Delta x^2$ and the fluxes were integrated in time using the Simpson rule.

6.3 Modelling results

6.3.1 Effect of partial pressure on reaction rate

The effect of partial pressure of the three hydroformylation gasses on the reaction rate (no mass transfer limitations) is shown in Figure 6.3. The reaction rates are calculated for a temperature of 120 °C and partial pressures of 10 bar H_2 and 10 bar CO and 10 bar propylene (at reaction temperature), unless the partial pressure is the parameter under investigation. The reaction rate versus partial pressures of CO and propylene shows a maximum around 2-3 bar. At higher partial pressures a decreasing rate is found with increasing partial pressure.

6.3.2 Effect of catalyst concentration

The effect of negative-order dependencies can have large influence on the production rates when both mass transfer as well as chemical reaction are both partially

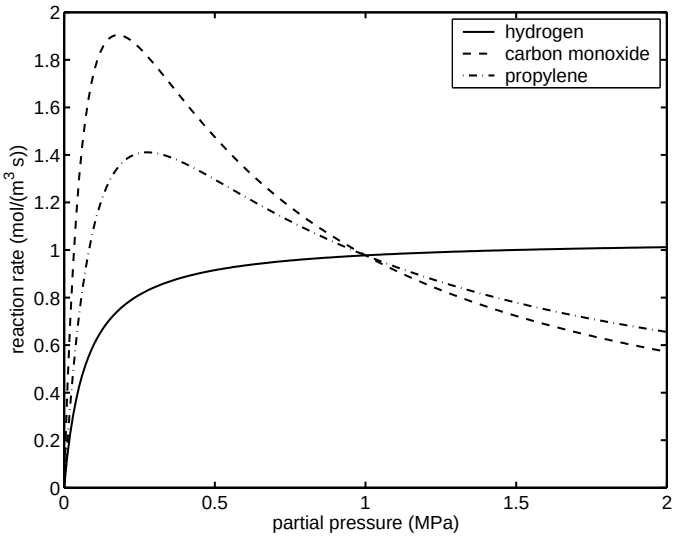

Figure 6.3: Effect of partial pressures of H_2, CO and propylene on the reaction rate.

limiting. An example of this is shown in Figure 6.5. In this figure the reaction rate versus the gassed power input is shown for three catalyst concentrations. The physical properties and operating conditions that were used are given in Table 6.3. At low power input per unit volume the rate increases with increasing power input; it then passes through a maximum and eventually it becomes independent of the power input done by the impeller. This kind of behaviour was also observed by Bhattacharya and Chaudhari (1987), who studied the homogeneous one-phase hydroformylation of 1-hexene.

At low gassed power input mass transfer of CO is limiting (in this example), which means that the bulk concentration of CO remains almost zero. An example of the concentration profiles in the liquid phase at low power input at the end of the penetration time are shown in Figure 6.4. The mass transfer rate is not enhanced by the reaction as no influence of the increased catalyst concentration is found at low values of the power input. The maximum in Figure 6.5 occurs at the conditions in which the bulk concentrations of CO and propylene are at an optimum level (close to 2-3 bar or 20-30% of the saturation concentration). This maximum will occur at lower power inputs for lower catalyst concentrations, as the bulk concentrations will increase at lower power inputs at a lower reaction rate. At high power input the

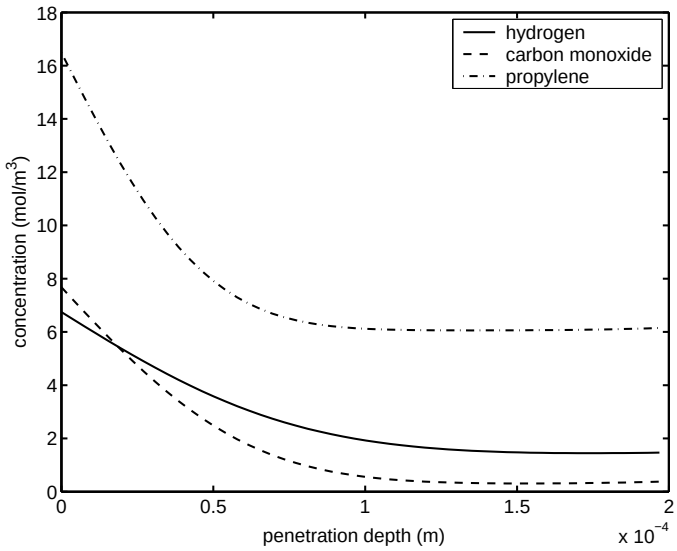

Figure 6.4: Concentration profiles in the liquid phase at $P_g = 50$ W/m^3 and operating conditions given in Table 6.3.

reaction rate is kinetically controlled and all concentrations in the bulk are almost equal to the concentrations at the interface. A large increase in reaction rate is observed from 200 to 600 ppm rhodium. The increase in production rate from 600 to 1000 ppm is much less, mainly due to a larger reaction rate inhibition due to the higher ligand concentration.

6.3.3 Effect of CO partial pressure

The influence of CO partial pressure on the reaction rate is shown in Figure 6.6. At low CO partial pressures (5 bar) and at low power input the production rate suffers from severe CO mass transfer limitations. The bulk concentration of CO is close to zero. The maximum production rate (at an optimum level of CO and propylene bulk concentrations) is reached at at a relatively high power input. This maximum production rate is lower compared to the case with 10 bar CO, because of a less optimal combination of CO and propylene bulk concentrations. At higher CO partial pressures (15 and 20 bar) and low power inputs the reaction is not limited by CO mass transfer, but in this example by hydrogen mass transfer. The optimum

Table 6.3: Physical parameters and operating conditions used in the modelling study of the biphasic hydroformylation of propylene.

parameter	value	unit	parameter	value	unit
T	120	$^\circ$C	c_{Rh}	600	ppm
p_A	10[a]	bar	$c_{Lig} : c_{Rh}$	30:1	-
p_B	10[a]	bar	m_A	0.022[b]	-
p_E	10[a]	bar	m_B	0.025[b]	-
ρ_L	940	kg/m^3	m_E	0.050[b]	-
μ_L	2.4	10^4 Pa s	$m_{R,A}$	6.4[b]	-
μ_G	1.7	10^5 Pa s	$m_{R,B}$	9.6[b]	-
σ[c]	0.027	N/m	$m_{R,E}$	48[b]	-
D_A^{393}[d]	2.59	10^8 m^2/s	V [e]	50	10^3 m^3
D_B^{393}[d]	1.60	10^8 m^2/s	u_G	0.58	10^2 m/s
D_E^{393}[d]	9.51	10^9 m^2/s			

[a] at reaction temperature, unless specified otherwise
[b] estimated from the IUPAC solubility data series (Lorimer, 1979)
[c] surface tension of water saturated with butyraldehyde
[d] estimated using the work of Díaz et al. (1987)
[e] other properties were similar compared to the vessel from Chapter 4 (see Table 4.2)

production rate is reached at lower power inputs, at which the mass transfer rate is still relatively low. A lower optimum production rate is therefore obtained. In this example the optimum CO partial pressure seems to be around 10 bar. Further optimization of the production rate is possible.

6.3.4 Effect of the dispersed phase

The above modelling results show that in this reaction system the production rate is very sensitive to the power input of the impeller. This means that accurate knowledge of the mass transfer parameters is required to predict the correct concentration profiles and to optimize the production rate. It is known that the presence of a dispersed phase can change the concentration profiles and thereby the flux of the gaseous components to the aqueous phase (for instance by the shuttle model).

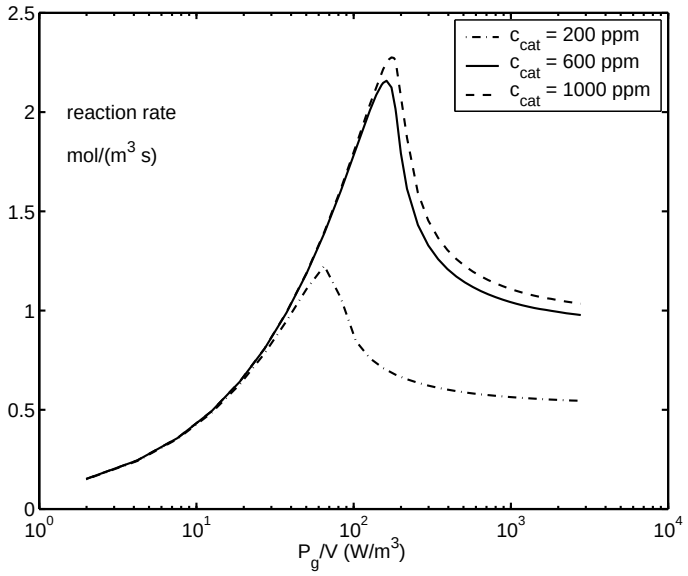

Figure 6.5: Reaction rate versus gassed power input at different rhodium concentrations.

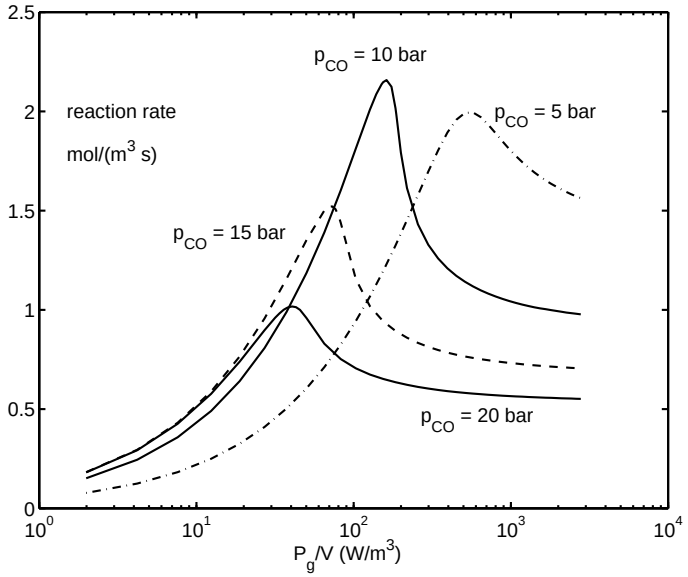

Figure 6.6: Reaction rate versus gassed power input at different CO partial pressures.

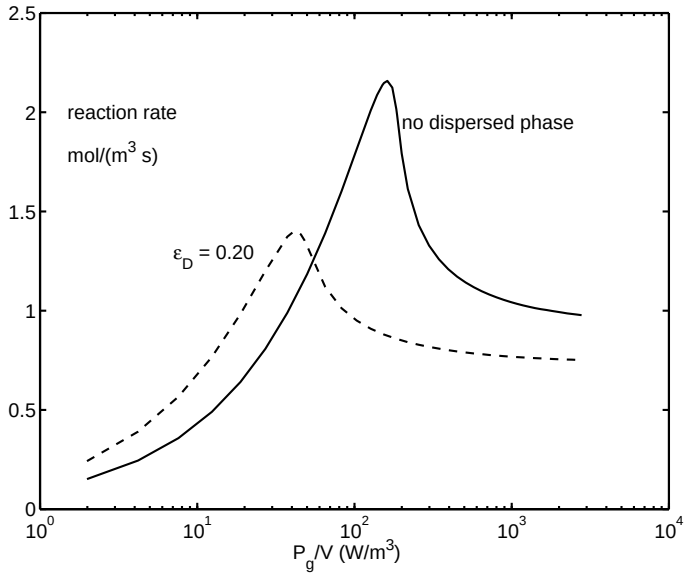

Figure 6.7: The influence of dispersed butyraldehyde on the reaction rate assuming a homogeneous model of the shuttle mechanism.

In Figure 6.7 the effect of 20 vol-% dispersed butyraldehyde on the production rate is shown, assuming a homogeneous model of the shuttle mechanism. At low power input the mass transfer is enhanced by the dispersed butyraldehyde, which has a higher solubility for the gasses compared to the aqueous phase. This higher solubility decreases the concentration of the dissolved gasses in the mass transfer zone near the interphase, which leads to a higher gas-to-liquid flux. Due to the increased mass transfer rate, compared to the case where there is no dispersed phase present, the concentrations in the bulk increase to this optimum level at lower power inputs and the maximum productivity is reached when the flux is still rather low due to the small mass transfer rate. The optimum production rate is lower in this case. When lower partial pressures are applied, the optimum will be at higher power inputs and a higher production rate can be achieved. At high power inputs the concentration in the bulk is almost equal to the concentrations at the interphase for both cases. The production rate is lower in case when the dispersed phase is present, due to a lower continuous phase volume available for the reaction to occur.

In Chapter 1 it was shown that two components increased mass transfer

(toluene and 1-octanol) and two organic liquids did not (n-heptane and n-dodecane). In the next section experimental results of mass transfer (absorption) experiments will be presented for the three hydroformylation gasses in water, water with dissolved butyraldehyde and water-butyraldehyde dispersions. In this way the influence of butyraldehyde on the mass transfer coefficient $k_L a$ will be investigated.

6.4 Experimental

Mass transfer experiments were carried out in a 640 ml capacity autoclave (Büchi) equipped with a gas inducing turbine with a variable speed up to 2200 rpm. The gas was induced in the stirrer shaft by 4 holes in the top of the shaft and retrieved in the solution by 4 holes between two round plates on which the impeller blades were mounted. The total impeller diameter was 4.5 cm and the blade width was 1 cm. The reactor was jacketed and temperature controlled by an oilbath up to 150 $^\circ$C with an accuracy of 0.1 $^\circ$C. A fast pressure transducer (up to 60 bar, 0.01 bar accurate) was used to measure the pressure in the reactor. The temperatures and pressures were recorded by a PC. A schematic diagram of the set-up is shown in Figure 6.8.

In a typical absorption experiment the gas was introduced in a jacketed and stirred storage vessel; hydrogen and carbon monoxide were taken from gas bottles by making use of a pressure reducer, propylene was introduced as a liquid using a pressurized syringe. In the experiments with propylene the storage vessel was heated to 120 $^\circ$C at which all the propylene was in the gas phase. The experiments were performed below the vapour pressure of propylene at the measurement temperature to avoid condensation in the reactor. The gasses were transported to the reactor using a pressure reducer at the desired pressure. The liquid in the vessel was degassed on beforehand by applying vacuum. After the gas is introduced in the reactor and the pressure has stabilized the stirrer is switched on and the pressure versus time curve is recorded by a personal computer. In case of a dispersed phase present in the reactor, stirring was applied before the introduction of the gas to obtain a well dispersed system at the start of the experiment. All experiments were performed at

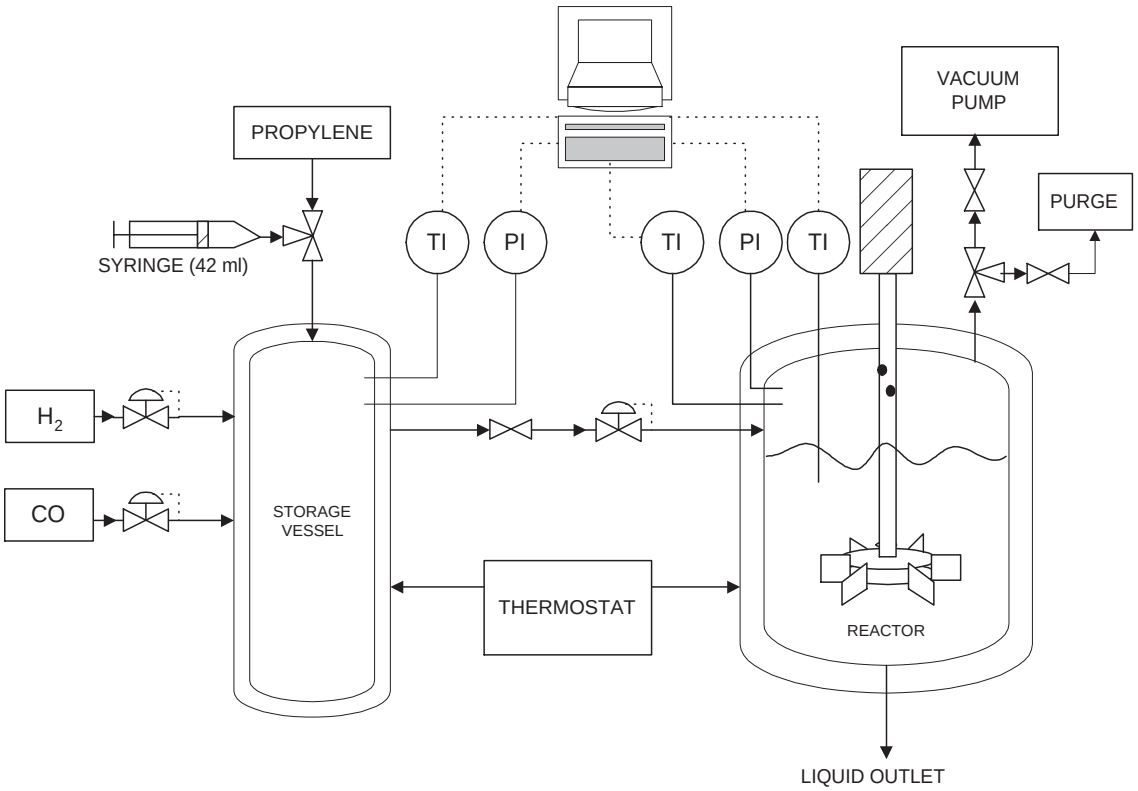

Figure 6.8: Schematic diagram of the set-up.

a temperature between 22 °C and 25 °C, a pressure of 8 bar (in case of propylene around 3 bar) and at a stirring speed of 800 rpm.

6.4.1 Chemicals

The experiments were performed with n-butyraldehyde as the dispersed phase, because this is the main product in the biphasic hydroformylation of propylene. N-butyraldehyde was obtained from Merck with a purity higher than 99%. Deionized water was used as the continuous phase. All gasses were obtained from Hoek Loos. Carbon monoxide had a purity of 99.997%, hydrogen had a purity of 99.999% and propylene was 99.8% pure.

6.4.2 Interpretation of the mass transfer experiments

In a gas-liquid system the k_La is determined from the pressure drop by making use of a mole balance of the absorbed gas:

$$\frac{dn_G}{dt} = -k_La\left(m\frac{n_G(t)}{V_G} - c_L(t)\right)V_L \tag{6.19}$$

with boundary conditions: $t = 0 : n_G = n_{G,0}, t = \infty : n_G = n_{G,eq}$.
The measured pressures are converted to moles by using the Peng-Robinson equation of state. The concentration in the liquid phase can be determined from the number of moles that have been absorbed from the gas phase, according to:
$c_L(t) = (n_{G,0} - n_G(t))/V_L$.
The equation can be integrated to obtain:

$$k_La \cdot t = -\frac{n_{G,eq}}{n_{G,0}}\ln\left(\frac{n_G(t) - n_{G,eq}}{n_{G,0} - n_{G,eq}}\right) = Y \tag{6.20}$$

When the right hand side of Equation 6.20 is plotted versus time, the slope equals k_La. The distribution coefficient, m, can be determined according to:

$$m = \frac{c_{L,eq}}{c_{G,eq}} = \frac{n_{G,0} - n_{G,eq}}{n_{G,eq}}\frac{V_G}{V_L} \tag{6.21}$$

The determination of k_La in G-L-L three-phase systems is not as straightforward as in G-L two-phase systems. The driving force for mass transfer depends on the presence of butyraldehyde in the mass transfer zone. The difference between these two situations is clarified in Figure 6.9. In case the dispersed phase is present in the mass transfer zone the driving force is larger and a smaller k_La will be calculated from the experiments.

Similar to the one-phase system, the determination of the k_La (without dispersed phase in the mass transfer zone, D1) starts with the mole balance of the absorbed gas (Eq. 6.19). The concentration in the continuous liquid phase is now given by:

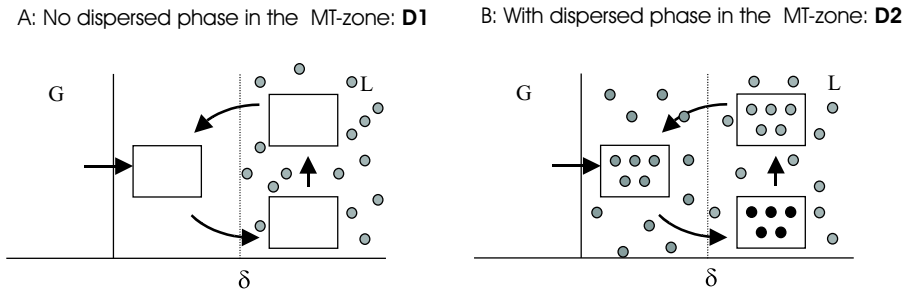

Figure 6.9: Mass transfer in systems with butyraldehyde as the dispersed phase.

$$c_{L,C}(t) = \frac{n_{L,C}(t)}{V_L} = \frac{n_{G,0} - n_G(t) - n_{L,D}(t)}{V_L} \tag{6.22}$$

The number of moles in the dispersed phase can be determined using the definition of the relative solubility:

$$m_R = \frac{c_{L,D}(t)}{c_{L,C}(t)} = \frac{(1-\varepsilon_D)}{\varepsilon_D}\frac{n_{L,D}(t)}{n_{L,C}(t)} \tag{6.23}$$

By combining these two equations, the continuous liquid phase concentration can be described with:

$$c_{L,C}(t) = \frac{n_{G,0} - n_G(t)}{(1+\varepsilon_D(m_R-1))} \tag{6.24}$$

The volumetric mass transfer coefficient in case of a dispersed phase, which is not present in the mass transfer zone, can now be determined with:

$$k_L a_{D1} \cdot t = -\frac{n_{G,eq}}{n_{G,0}} \ln\left(\frac{n_G(t) - n_{G,eq}}{n_{G,0} - n_{G,eq}}\right)(1+\varepsilon_D(m_R-1)) = Y_{D1} \tag{6.25}$$

The solubility in the continuous phase (saturated with butyraldehyde), m_C^*, can be calculated according to:

$$m_C^* = \frac{c_{L,C,eq}}{c_{L,G,eq}} = \frac{1}{(1+\varepsilon_D(m_R-1))}\frac{V_G}{V_L}\frac{n_{G,0} - n_{G,eq}}{n_{G,eq}} \tag{6.26}$$

The solubility ratio, m_R, can be determined from measurements in the presence of a dispersed phase. In this case the following relation holds:

$$m_{ov} = (1 - \varepsilon_D)m_C^* + \varepsilon_D m_D^* \qquad \text{and} \qquad m_R = \frac{m_D^*}{m_C^*} \tag{6.27}$$

in which m_{ov} is the overall solubility ratio as measured as if there was no dispersed phase present.

In case there are dispersed phase droplets present in the mass transfer zone (D2) and the mass transfer is enhanced according to a homogeneous model of the shuttle mechanism the k_La can be determined by making use of the enhancement factor proposed by Bruining et al. (1986). The mass transfer coefficient can be determined from the case without droplets in the mass transfer zone (D1) and is given by:

$$k_L a_{D2} = \frac{k_L a_{D1}}{\sqrt{1 + \varepsilon_D(m_R - 1)}} \tag{6.28}$$

6.5 Results

In Figure 6.10 the results of two typical mass transfer experiments are presented. One experiment is shown with 1.1 vol-% butyraldehyde, which is smaller than the solubility of butyraldehyde in water (10.4 vol-% at 25 °C, Gerhartz et al. (1985)). The other experiment was performed with 25.6 vol-% butyraldehyde and thus consisted of approximately 15% dispersed phase. The decrease in pressure was very fast in both cases. In most cases a measurement time of 15 seconds was possible. After this the changes in pressure were too small and the Y versus time plot contained a lot of scatter. From Figure 6.10 it can be seen that the value of k_La is about three times larger in the presence of the dispersed phase compared to the one-phase system. This phenomenon will be studied more intensively in the next sections.

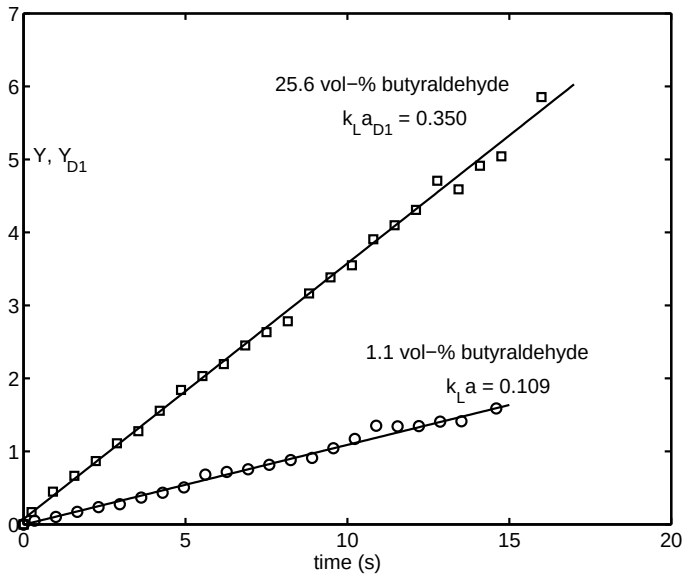

Figure 6.10: Linearity of the Y versus time plot in the measurement of k_La using the batchwise absorption method.

6.5.1 Mass transfer of carbon monoxide

The results of the relationship between k_La and the volume fraction of n-butyraldehyde in case of carbon monoxide absorption are shown in Figure 6.11. On the addition of a small amount of butyraldehyde a small increase of k_La is observed. At low (1-6 vol-%) butyraldehyde fractions the k_La remains relatively constant. At butyraldehyde fractions close to the maximum solubility of butyraldehyde in water (7-10 vol-%) a sharp increase (approximately a factor 3) in k_La is observed. At butyraldehyde fractions beyond the maximum solubility no further enhancement of mass transfer is observed. The value of k_La_{D1} remained practically constant. Enhancement of mass transfer according to a homogeneous model of the shuttle mechanism is therefore unlikely and k_La_{D2} showed a decreasing trend with increasing butyraldehyde volume fraction.

From the plot of the overall solubility, m_{ov}, as shown in Figure 6.12, the solubilities of CO in the aqueous phase and in butyraldehyde can be determined. The solubility of CO in water is not affected by dissolved butyraldehyde. The maximum solubility of butyraldehyde in water can be determined as 9.5 vol-%,

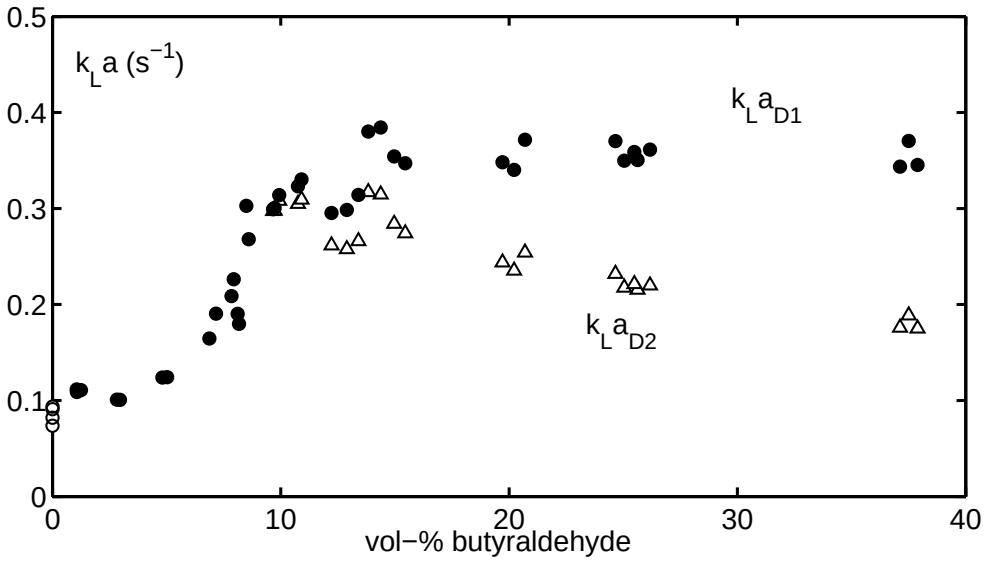

Figure 6.11: Effect of the butyraldehyde volume fraction on k_La of CO in: ○ :water; ● : water/butyraldehyde (k_La, k_La_{D1}); △ : water/butyraldehyde (k_La_{D2})

which is somewhat smaller compared to the literature value of 10.4 vol-%. Beyond the point of maximum solubility of butyraldehyde , $m_{ov,CO}$ increases linearly with dispersed phase fraction. The physical properties that can be derived from these plots for all gasses are given in Table 6.4.

6.5.2 Mass transfer of hydrogen

The effect of the butyraldehyde volume fraction on the mass transfer coefficient is shown in Figure 6.13. The addition of small fractions of butyraldehyde causes an increase in k_La of 80%, which is significantly more when compared to the increase in the experiments with carbon monoxide (30%). Similarly to the results with CO as the gas phase, a sharp increase in the mass transfer coefficient was observed near the maximum solubility point. No enhancement of mass transfer was obtained after this point, but a decrease. The value of the mass transfer coefficient when a homogenous model of the shuttle mechanism is applied (k_La_{D2}) is also shown in Figure 6.13, although the validity of this model in case of a decreasing mass transfer rate is not very realistic. The solubility of H_2 is approximately constant below the

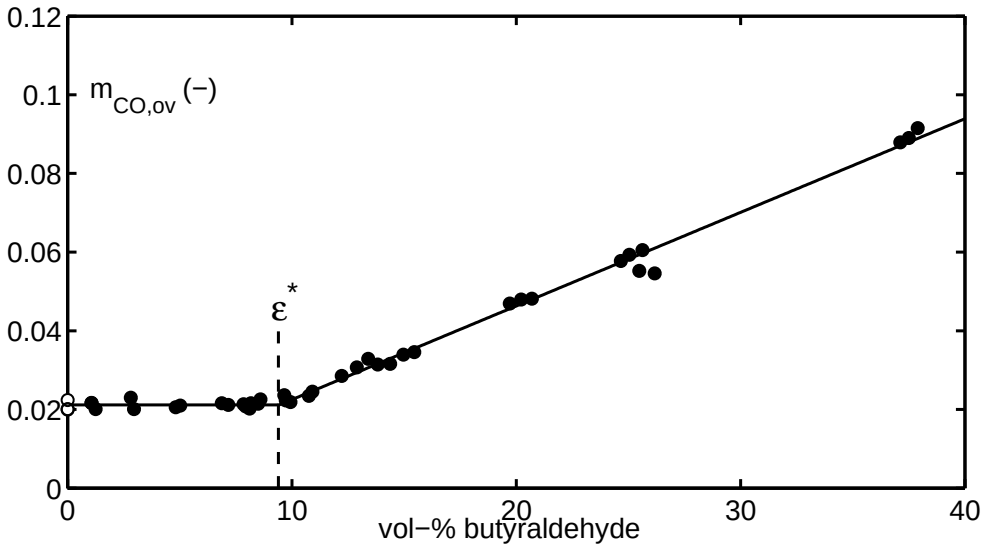

Figure 6.12: Effect of the butyraldehyde volume fraction on the solubility of CO in: ∘ :water; • : water/butyraldehyde

maximum butyraldehyde solubility (Table 6.4). Beyond this point a linear increase in the overall solubility was obtained, similar to Figure 6.12. The value for the relative solubility, m_R was 4.5, which was much lower compared to the value with CO (11.2).

6.5.3 Mass transfer of propylene

Mass transfer experiments with propylene at 8 bar were more difficult compared to experiments with carbon monoxide and hydrogen. The solubility as well as the k_La were dependent on the propylene concentration in the solution. This caused non-linear plots of Y versus time and non reproducible results. Therefore the experiments were performed at a pressure around 3 bar. At these pressures the values of m and k_La were relatively independent of the gas phase propylene pressure.

The mass transfer coefficient, k_La, is plotted versus the volume fraction of butyraldehyde in Figure 6.14. A similar trend compared to the experiments with CO and H_2 was obtained. The value for k_La in the presence of dissolved butyraldehyde was approximately 90% higher compared to pure water. The point of maximum

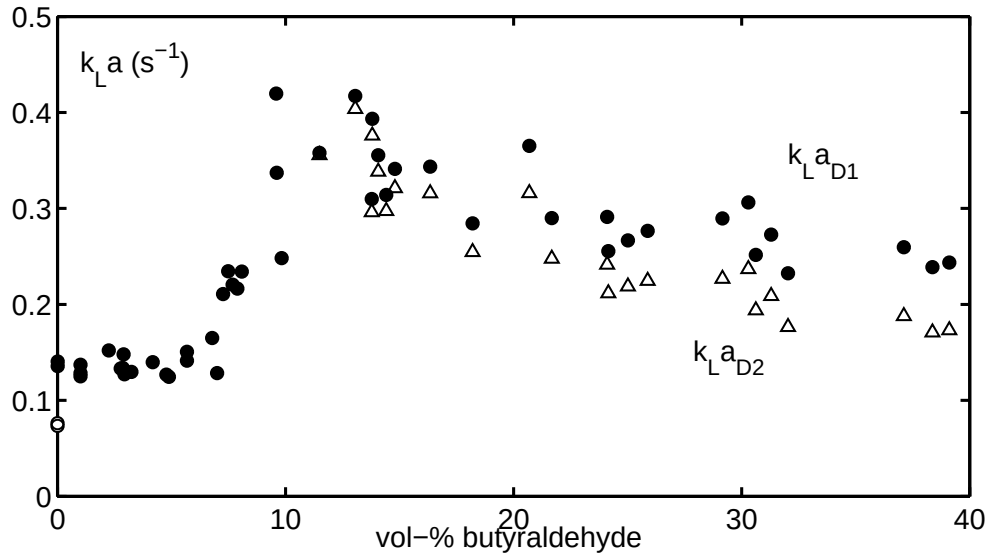

Figure 6.13: Effect of the butyraldehyde volume fraction on k_La of H_2 in: ○ :water; ● : water/butyraldehyde (k_La, k_La_{D1}); △ : water/butyraldehyde (k_La_{D2})

butyraldehyde solubility was reached at 7.7% according the the overall solubility plot. This value is somewhat lower compared to hydrogen and carbon monoxide, which might be due to the dissolved propylene in the solution. After the maximum solubility point again an increase with approximately a factor 3 is observed. At higher dispersed phase fractions the mass transfer rate is somewhat higher (k_La_{D1}), but is not likely that this enhancement is due to the shuttle mechanism, because a strongly decreasing trend in k_La_{D2} is observed. An enhancement due to the shuttle mechanism would result in a higher enhancement due to the high relative solubility in case of propylene.

6.6 Discussion

In the experiments with all three gasses a more or less similar trend was obtained for k_La and in the presence of a dispersed phase, k_La_{D1}, which is shown in Figure 6.15. The increase in mass transfer rate rate from pure water to water with dissolved butyraldehyde (A) varied from 30-90% depending on the gas. This increase in k_La is

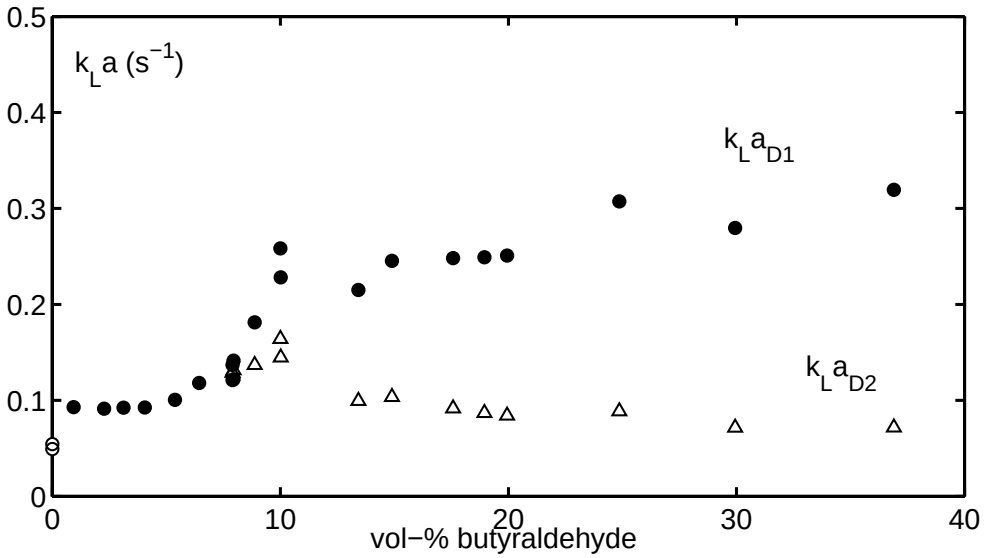

Figure 6.14: Effect of the butyraldehyde volume fraction on k_La of propylene in: ∘ :water; • : water/butyraldehyde (k_La, k_La_{D1}); △ : water/butyraldehyde (k_La_{D2})

small compared to the expected increase in the interfacial area, a, according to the mass transfer correlations from Section 6.2.2 and the correlations obtained for water in Chapter 4. It seems that the expected increase in interfacial area is accompanied with a decrease in the mass transfer coefficient, k_L, as indicated in Equation 6.13 from the work of Llorens et al. (1988). To test this hypothesis two types of additional

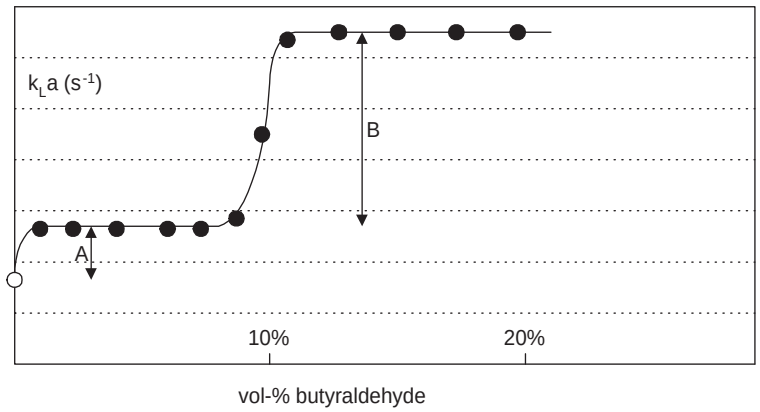

Figure 6.15: General trend in the mass transfer experiments

Table 6.4: Solubilities and mass transfer coefficients of CO, H_2 and propylene in water and butyraldehyde at 22-25 $^\circ$ C.

parameter	CO	H_2	propylene
solubility in water, m_C [-]	0.0208	0.0185	0.143
solubility in the aqueous phase, m_C^* [-]	0.0211	0.0194	0.20
relative solubility, $m_R = m_D/m_C^*$ [-]	11.2	4.5	65.3
max. solubility of butyraldehyde ,ε^* [%]	9.4	11.1	7.7
k_La in water, k_La [s^{-1}]	0.085	0.075	0.052
k_La in the aqueous phase, k_La^* [s^{-1}]	0.112	0.136	0.098
k_La. after the maximum sol., k_La_{D1} [s^{-1}]	0.355	0.38	0.27

experiments were carried out:

1. measurement of k_La in a non coalescing electrolyte system.

2. measurement of the interfacial area using ultrasonic spectroscopy.

In the experiments with the non-coalescent electrolyte solution, 0.6 M KCl was used as the aqueous phase. This concentration was high enough to suppress coalescence according to the results of Craig et al. (1993) and from the results obtained in Chapter 5. The results with the different fractions butyraldehyde are given in Figure 6.16 and show that the value of k_La without butyraldehyde in the solution is much higher compared to the value in water. The addition of butyraldehyde caused a strong decrease in the volumetric mass transfer coefficient to the level of water/butyraldehyde system. This is most likely caused by a decrease in the mass transfer coefficient, k_L, and not by a decrease in the interfacial a. The decrease in the mass transfer coefficient is a factor 2.3, which is very close to the factor 2.4 that was predicted according to Equation 6.13. With the exception of the experiments without butyraldehyde the trend is approximately similar compared to the CO-water-butyraldehyde system.

It was, unfortunately, not possible to measure the gas-liquid interfacial in the autoclave that was used in this chapter. In order to get a qualitative impression of the interfacial area in water/butyraldehyde systems, measurements were per-

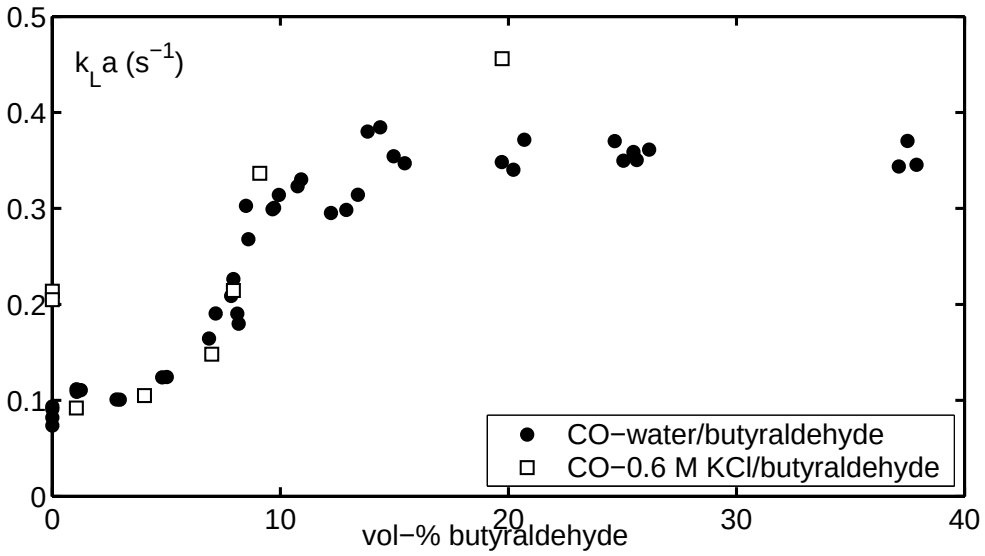

Figure 6.16: Effect of the butyraldehyde volume fraction on k_La and k_La_{D1} of CO in water/butyraldehyde and in 0.6 M KCl/butyraldehyde.

formed in the vessel that was used and described in Chapter 5. Nitrogen was used as the dispersed gas phase. Measurement of the interfacial area by using ultrasonic spectroscopy indicated that the area in water containing butyraldehyde is approximately a factor 4 higher compared to pure water. The results are presented in Figure 6.17. These results indicate that together with the above discussed decrease in k_L by a factor 2.3, it seems that the small increase in k_La (A in Figure 6.15) on addition of butyraldehyde to water is determined by two largely compensating effects: a decrease in k_L together with a increase in the interfacial area a. Beyond the point of maximum solubility a small increase in a is observed, but this increase is not large enough to explain the sharp increase in k_La (B in Figure 6.15) that was obtained in the mass transfer experiments.

The most logical explanation for the sharp increase in k_La at the point of maximum butyraldehyde solubility (B in Figure 6.15) is an increase in the mass transfer coefficient, k_L. The increase is approximately a factor 2.5-3 for all gasses. A further increase of the interfacial area is unlikely, as this increase was also not observed in the interfacial area measurements.

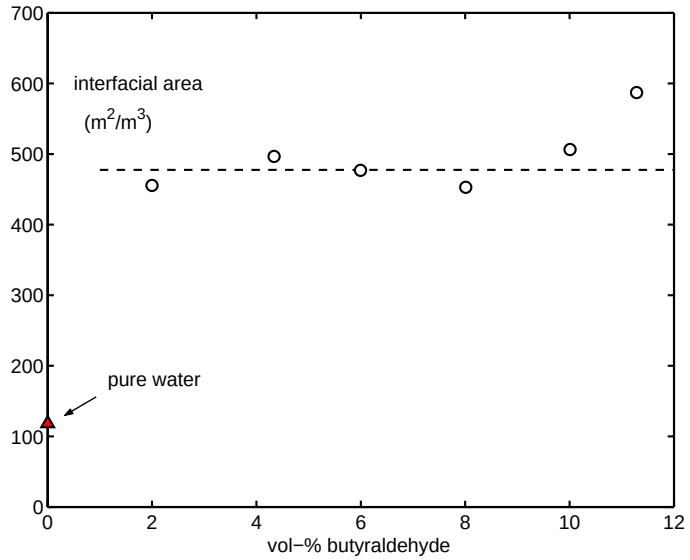

Figure 6.17: Effect of the butyraldehyde volume fraction on the gas-liquid interfacial area measured using ultrasonic spectroscopy.

A possible explanation for the increase in the mass transfer coefficient (step B in Figure 6.15) is that the rigid layer of molecules that is responsible for the original decrease in the mass transfer coefficient has disappeared. This might be due to the formation of a larger butyraldehyde layer around the bubble. This layer is probably more mobile and therefore not able to suppress the turbulence acting on the bubble wall. The final spreading coefficient, which indicates whether it is favourable for an organic layer to spread over a bubble under mutually saturated conditions, is positive (+ 7 mN/m, see Appendix B), which indicates that the spreading of a butyraldehyde layer on a gas bubble is energetically favourable. It was shown in Appendix B that the presence of a small layer of butyraldehyde on the saturated solution decreased the spreading coefficient to approximately zero. Bartell et al. (1933) showed that the formation of such a small layer can occur spontaneously, when the initial spreading coefficient is positive.

For the modelling case these results imply that the decrease in the mass transfer coefficient should not be taken into account, as the reactor operates above the solubility limit (around 10 vol-%). Furthermore, mass transfer is not enhanced

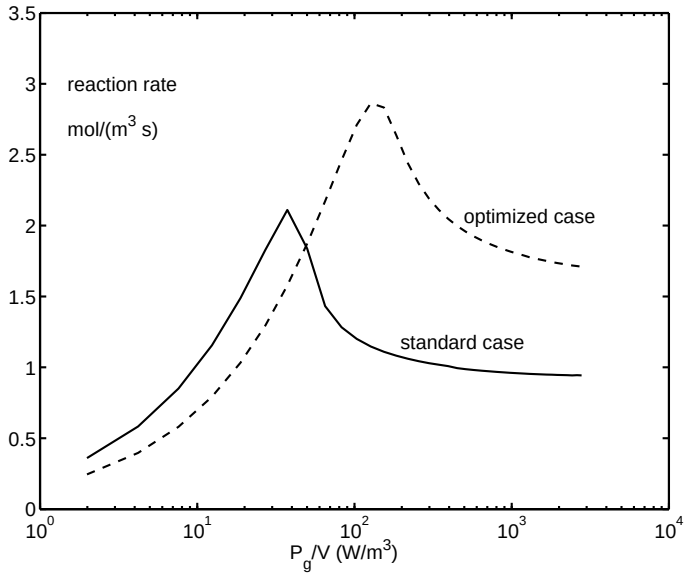

Figure 6.18: Optimized solution compared to the standard case. Optimum is at 140 W/m^3 and with $p_{H_2} = 36.9$ bar, $p_{CO} = 6.8$ bar, $p_{propylene} = 6.3$ bar, $c_{Rh} = 0.92$ mol/m^3 and $c_{Rh} : Cc_{Lig} = 1 : 30$.

at higher dispersed phase fractions. These results can be used in the selection of the optimum process parameters for the biphasic hydroformylation of propylene (and probably in other biphasic hydroformylation reactions). In Figure 6.18 it is shown that high production rate can be obtained at a relatively low power input, which is compared to the standard case. For both cases the reduction of k_L due to the butyraldehyde molecules was not taken into account. In optimizing the production rate the following constraint were used: $p_{tot} < 50$ bar, $T = 120\ ^\circ$C, $c_{Rh} < 1.5$ mol/m^3 and $c_{Rh} : Cc_{Lig} > 1 : 30$. An optimal production rate is achieved at a gassed power input of 140 W/m^3 and was almost 3 mol/(m^3 s).

6.7 Conclusions

In this work a modelling study was performed on the biphasic hydroformylation of propylene to butyraldehyde. Due to the negative order dependencies of the CO and propylene partial pressures in the kinetic rate expression, an unusual effect of

the power input on the production rate was observed. The production rate firstly increased with increasing power input to an optimum value. Beyond this maximum a decrease was observed to a value at which the concentrations in the liquid bulk were equal to the concentrations at the interface.

Furthermore, it was shown that the addition of a dispersed phase (in this case butyraldehyde) could change the concentration profiles in the mass transfer zone, which can cause a shift in the the optimum production rate to lower power inputs. These examples showed that accurate knowledge of the mass transfer properties in gas-liquid-liquid systems is necessary to predict and optimize the production rate in the biphasic hydroformylation of propylene.

Experiments made clear that the addition of small amounts of butyraldehyde caused a relatively small increase in the volumetric mass transfer coefficient, k_La. This small increase was due to a larger increase in the interfacial area, a, accompanied by a decrease in the mass transfer coefficient, k_L. Near the point of maximum solubility of butyraldehyde a strong (factor 3) increase in k_La was observed. The most logical explanation for this is an increase in k_L, since independent measurement of the interfacial area using an ultrasonic technique did not show such an increase. This increase in k_L might be due to the disappearance of the rigid layer of butyraldehyde molecules at the gas-liquid interface by spreading of a butyraldehyde layer around the bubble. This hypothesis was supported by surface tension measurements.

The results obtained in this work lead to an increased insight in the biphasic hydroformylation of propylene and can therefore be used to increase the production rate of this process.

Acknowledgement

The author wishes to thank B.J. Frowijn and S.M. Biewenga for their assistance in the experimental work. B. Knaken is acknowledged for the construction of the experimental set-up and for the technical support.

Nomenclature

a	gas-liquid interfacial area [m^2/m^3]
a_c, a_s, a_T	radius of particle times the wave number of the compressional, shear and thermal waves [-]
A, A_ε	cross-sectional area [m^2]
$\mathbf{A}$	shear wave potential [m^2]
A_n, B_n, C_n	scattering coefficients [-]
b_c, b_T	parameters defined in equations 2.8 and 2.9 [K/m^2]
B	baffle diameter [m]
c	adiabatic speed of sound [m/s]
c_1	speed of sound for spherical compressional wave in elastic isotropic fluid [m/s]
c_A	concentration of component A [mol/m^3]
c_w	speed of sound in water [m/s]
C_p	specific heat [J/(kg K)]
d	bubble diameter [m]
d	measurement path length [m]
d_{32}	Sauter mean diameter [m]
d_s	diameter of sparger holes [m]
D	diameter of the impeller [m]
D_A	diffusion coefficient of component A [m^2/s]
E_A	activation energy [J/mol]

E_D	enhancement factor due to the dispersed phase [-]
E_V	bulk modulus of elasticity [Pa]
f	frequency [s^{-1}]
f_i	fraction of volumetric space in the vessel [-]
$f(0)$, $f(\pi)$	far field scattering amplitudes [m]
F	Faraday constant [96485 C/mol]
g	gravitational constant [m/s^2]
G, G_ε	conductivity [S]
h_i,h_G	parameters in equation 1.7 [m^3/mol]
h_n	spherical Hankel functions of the first kind [-]
H	liquid height [m]
He	Henry's law constant [mol/(Pa m^3)]
H_I	impeller height above the bottom [m]
i	$\sqrt{-1}$ [-]
I_1, I_2	amplitudes in water, multi-phase fluid [V]
j_n	spherical Bessel functions [-]
k_c	forward reaction rate constant of the reaction of CO_2 with water catalysed by hypochlorite [m^3/(mol s)]
k_c, k_T, k_s	propagation constant of the compressional, thermal, and shear wave [m^{-1}]
k_G	gas phase mass transfer coefficient [m/s]
k_{H_2O}, k_{-H_2O}	forward and backward reaction rate constant of the reaction of CO_2 with water [s^{-1}]
k_{OH^-}, k_{-OH^-}	forward and backward reaction rate constant of the reaction of CO_2 with hydroxyl ions [m^3/(mol s)]
k_L	liquid phase mass transfer coefficient [m/s]
k_La	volumetric liquid phase mass transfer coefficient [s^{-1}]
K	complex propagation constant [m^{-1}]
K_1	equilibrium constant [mol/m^3]

K_2	equilibrium constant [m^3/mol]
K_W	equilibrium constant [mol^2/m^6]
ℓ_i^∞	ionic conductivity at infinite dilution [$m^2/(\Omega$ mol)]
L, L_ε	effective pathlength [m]
m	ratio of solubility in the liquid phase and in the gas phase [-]
m_R	ratio of the gas solubility in the dispersed and in the continuous phase [-]
M	parameter in log-normal distribution [-]
n	order of spherical harmonics [-]
N	number density of particles [m^{-3}]
N	impeller speed [rpm or s^{-1}]
p	pressure [Pa]
P	power input [W]
P_g	gassed power input [W]
r	particle radius [m]
r_A	reaction rate of component A [mol/(m^3 s)]
R	resistivity [Ω]
R_A	rate of absorption of component A [mol/(m^3 s)] or [mol/s]
S	parameter in log-normal distribution [-]
S	spreading coefficient [N/m]
T	temperature [K]
T	vessel diameter [m]
t	time [s]
u_G	superficial velocity [m/s]
u_T	terminal rise velocity [m/s]
V	volume [m^3]
V_{imp}	impeller swept volume = $0.25\pi D^2 W$ [m^3]
W	impeller blade width [m]
y	coefficient in Equation 2.23 [m/Np or s/m]

Y, Y_{D1} quantities used in Equations 6.20 and 6.25 [-]

Greek

α attenuation coefficient [Np/m]
α_w attenuation coefficient in water [Np/m]
β thermal expansion coefficient [K^{-1}]
δ_p penetration depth [m]
ϵ dispersed phase fraction [-]
γ ratio of specific heats [-]
$\gamma_{A/B}$ surface tension of component A to component B [N/m]
η viscosity [kg/(m s)]
μ mean particle size [m]
μ shear rigidity [kg/(m s)]
ν kinematic viscosity = μ/ρ [m^2/s]
π interfacial pressure [N/m]
ρ density [kg/m^3]
σ standard deviation in size distribution [m]
σ thermal diffusivity = $\tau/(\rho Cp)$ [m^2/s]
τ residence time [s]
τ thermal conductivity [W/(m K)]
τ_p penetration time [s]
τ_P probe time of the DO probe [s]
ϕ_c, ϕ_T potential of compressional and thermal waves [m^2]
φ_G gas phase space velocity [s^{-1}]
Φ flow rate [m^3/s]
φ space velocity of the gas = Φ_G/V_L [s^{-1}]
χ tortuosity [-]
ω angular frequency [rad/s]

Dimensionless numbers

Fl	Gas flow number = $\Phi_G/(N D^3)$
Ha	Hatta number = $\sqrt{k_{app} D}/k_L$ (first order reaction)
N_P	Power number = $P/(\rho D^5 N^3)$
St	Stanton number = $6 k_L \tau_B / d_B$ (first order reaction)

Subscript and superscript

0	initial value
1	of the continuous phase
2	of the dispersed phase
A	with respect to component A
b	in the bulk liquid
b	bubble
d	droplet
D	with respect to the dispersed phase
ε	dispersion
E	experimental
G	with respect to the gas phase
i	at the interface
im	ideally mixed
ini	initially
L	with respect to the liquid phase
M	model
O	of the organic liquid
W	of water

Appendix A

Modelling study on the Danckwerts-criterion

The criterion that determines whether or not the reaction of CO_2 in a carbonate/bicarbonate solution can be regarded as pseudo-first order is given by Danckwerts and Sharma (1966).

$$m \cdot [CO_2] \cdot \left(\frac{1}{[CO_3^{2-}]} + \frac{2}{[HCO_3^-]} \right) \cdot \left(\sqrt{\left(1 + \frac{D_{CO_2} \cdot k_{1,app}}{k_L^2} \right)} - 1 \right) << 1 \quad \text{(A.1)}$$

The reaction can be regarded as pseudo-first order when the concentrations of all the ions are uniform throughout the mass transfer zone. Although this Danckwerts-criterion is often referred to in literature, its derivation has never been published. Moreover, it was found that although the left hand side of Equation A.1 is much smaller than 1, still large concentration gradients could exist, and thus considerable deviations from the pseudo-first order region may occur. To study the validity of the above criterion the flux of CO_2 from the gas- to the liquid phase was determined numerically by solving the mass balances for all components.

A.1 Reaction system

The following reactions occur in the carbonate/bicarbonate solution:

$$CO_2 + OH^- \underset{k_{12}}{\overset{k_{11}}{\rightleftharpoons}} HCO_3^- \tag{A.2}$$

$$HCO_3^- + OH^- \underset{k_{22}}{\overset{k_{21}}{\rightleftharpoons}} CO_3^{2-} + H_2O \tag{A.3}$$

$$OH^- + H^+ \underset{k_{32}}{\overset{k_{31}}{\rightleftharpoons}} H_2O \tag{A.4}$$

$$CO_2 + H_2O \underset{k_{42}}{\overset{k_{41}}{\rightleftharpoons}} HCO_3^- + H^+ \tag{A.5}$$

The corresponding equilibrium constants are defined as:

$$K_1 = \frac{[H^+][HCO_3^-]}{[CO_2]} \tag{A.6}$$

$$K_2 = \frac{[CO_3^{2-}]}{[HCO_3^-][OH^-]} \tag{A.7}$$

$$K_W = [H^+][OH^-] \tag{A.8}$$

The reaction rate per component is then given by:

$$R_{CO_2} = k_{12}[HCO_3^-] - k_{11}[CO_2][OH^-] + k_{42}[HCO_3^-][H^+] - k_{41}[CO_2] \tag{A.9}$$

$$\begin{aligned} R_{OH^-} =& k_{12}[HCO_3^-] - k_{11}[CO_2][OH^-] + k_{22}[CO_3^{2-}] \\ & - k_{21}[HCO_3^-][OH^-] + k_{32} - k_{31}[OH^-][H^+] \end{aligned} \tag{A.10}$$

$$\begin{aligned} R_{HCO_3^-} =& k_{11}[CO_2][OH^-] - k_{12}[HCO_3^-] + k_{22}[CO_3^{2-}] \\ & - k_{21}[HCO_3^-][OH^-] + k_{41}[CO_2] - k_{42}[HCO_3^-][H^+] \end{aligned} \tag{A.11}$$

$$R_{CO_3^{2-}} = k_{21}[HCO_3^-][OH^-] - k_{22}[CO_3^{2-}] \tag{A.12}$$

$$R_{H^+} = k_{32} - k_{31}[OH^-][H^+] + k_{41}[CO_2] - k_{42}[HCO_3^-][H^+] \tag{A.13}$$

The bulk concentrations of all species are calculated using the equilibrium constraints, the overall carbon balance and the electroneutrality constraint:

$$K_1/K_W[CO_2]_b[OH^-]_b = [HCO_3^-]_b \tag{A.14}$$

$$K_2[OH^-]_b[HCO_3^-]_b = [CO_3^{2-}]_b \tag{A.15}$$

$$[HCO_3^-]_{ini} + [CO_3^{2-}]_{ini} = [CO_2]_b + [HCO_3^-]_b + [CO_3^{2-}]_b \tag{A.16}$$

$$K_W - [H^+]_b[OH^-]_b = 0 \tag{A.17}$$

$$[H^+]_b + [K^+]_b = [OH^-]_b + [HCO_3^-]_b + 2[CO_3^{2-}]_b \tag{A.18}$$

For all components the flux is solved according to the penetration model from the following balance:

$$\frac{dc_A}{dt} = \frac{d^2c_A}{dx^2} + R_A \tag{A.19}$$

The following boundary conditions are used:

$$\begin{aligned} &t = 0, x > 0 : c_A(x,t) = c_{A,bulk} \\ &t > 0, x = 0 : c_{CO_2}(x,t) = c_{CO_2,iL} \\ &t > 0, x = 0 : \frac{dc_{ion}(x,t)}{dx} = 0 \\ &t > 0, x = \infty : c_A(x,t) = c_{A,bulk} \end{aligned} \tag{A.20}$$

This system of partial differential equations are solved using the method of lines. Details of the method are explained in Chapter 6.

A.2 Physical parameters

The solubility and diffusivity of CO_2 in the 0.5 M/0.5 M potassium carbonate/potassium bicarbonate solution are given in section 1.3.2. All physical parameters at 24 $^\circ$C are given in Table A.1.

The ionic diffusion coefficients have been estimated using the Nernst equation (Horvath, 1985).

$$D_i^\infty = \ell_i^\infty \frac{RT}{z_i F^2} \tag{A.21}$$

The ionic conductivities at infinite dilution, ℓ_i^∞, have been fitted to the experimental values of Horvath (1985).

A.3 Chemical parameters

The value of k_{11} in the presence of co-electrolytes is given by Pohorecki and Moniuk (1988):

$$\log \frac{k_{11}}{k_{11}^\infty} = 0.11 \times 10^{-3}[K^+] + 0.17 \times 10^{-3}[CO_3^{2-}] \tag{A.22}$$

The influence of the bicarbonate ion was not given by these authors and was therefore neglected. The reaction rate constant at infinite dilution, k_{11}^∞, is given by:

$$\log k_{11}^\infty = 11.916 - \frac{2383}{T} \tag{A.23}$$

Reaction A.3 is fast as it involves only a proton transfer. The reaction rate constant, k_{21} , was determined to be $6 \cdot 10^6$ m^3/(mol s) (Eigen, 1963). The neutralization rate constant, k_{31}, was also determined by this author and was $1.4 \cdot 10^8$ m^3/(mol s). The reaction rate between CO_2 and water, k_{41}, is very slow (0.024 s^{-1}, Danckwerts and Sharma (1966)). This reaction can, however, be catalyzed by a number of agents. In Chapter 1 sodium hypochlorite was used, for which a reaction rate constant was determined to be 1.8 m^3 mol^{-1} s^{-1}.

The backward reaction rate of reaction A.2, k_{12}, is defined by the value of the equilibrium constant for this reaction ($k_{12} = k_{11}\, K_W/K_1$). K_1 is given as a function of temperature by Edwards et al. (1978):

$$K_1 = \exp\left(-\frac{12092.1}{T} - 36.786\ln(T) + 235.482\right)\rho_W \tag{A.24}$$

Table A.1: Used physical and chemical parameters at 297 K for the absorption of CO_2 in a 0.5 M $KHCO_3$ / 0.5 M K_2CO_3 solution.

parameter	value	parameter	value
k_{11}, $m^3\ mol^{-1}\ s^{-1}$	$1.40 \cdot 10^1$	D_{CO_2}, $m^2\ s^{-1}$	$1.59 \cdot 10^{-9}$
k_{12}, s^{-1}	$3.05 \cdot 10^{-4}$	D_{OH^-}, $m^2\ s^{-1}$	$5.15 \cdot 10^{-9}$
k_{21}, $m^3\ mol^{-1}\ s^{-1}$	$6.00 \cdot 10^6$	$D_{HCO_3^-}$, $m^2\ s^{-1}$	$1.18 \cdot 10^{-9}$
k_{22}, s^{-1}	$1.21 \cdot 10^6$	$D_{CO_3^{2-}}$, $m^2\ s^{-1}$	$9.18 \cdot 10^{-10}$
k_{31}, $m^3\ mol^{-1}\ s^{-1}$	$1.40 \cdot 10^8$	D_{H^+}, $m^2\ s^{-1}$	$9.21 \cdot 10^{-9}$
k_{32}, $mol\ m^{-3}\ s^{-1}$	$1.28 \cdot 10^0$	m_{CO_2}, -	$5.29 \cdot 10^{-1}$
k_{41}, s^{-1}	$0.24 \cdot 10^{-1}$	ρ_W, $kg\ m^{-3}$	$9.97 \cdot 10^3$
k_{42}, $m^3\ mol^{-1}\ s^{-1}$	$5.72 \cdot 10^1$		

where ρ_W is the density of water (kg/m^3).
The value of the solubility product K_W is taken from Tsonopoulos (1976):

$$\log\left(\frac{K_W}{\rho_W^2}\right) = -\frac{5839.5}{T} + 22.4773\log(T) + 61.2062 \tag{A.25}$$

The equilibrium constant (K_2) at infinite dilution that determines the value of the backward reaction of reaction A.3, $k_{22} = k_{21}/K_2$, is given by Hikita et al. (1976):

$$\log(K_2) = -\frac{1568.9}{T} - 2.5866 + 6.737 \cdot 10^{-3}T \tag{A.26}$$

The values of the backward reactions, k_{32} and k_{42} can be calculated from the equilibrium constants and are k_{31}/K_W and k_{41}/K_1, respectively.

A.4 Results

In Figure A.1 typical concentration profiles of the different components are presented. The absorption of CO_2 is enhanced due to the reaction, but this enhancement is less compared to the case when a pseudo-first order reaction is assumed, due to the depletion of hydroxyl ions near the interface. The average flux of CO_2 from

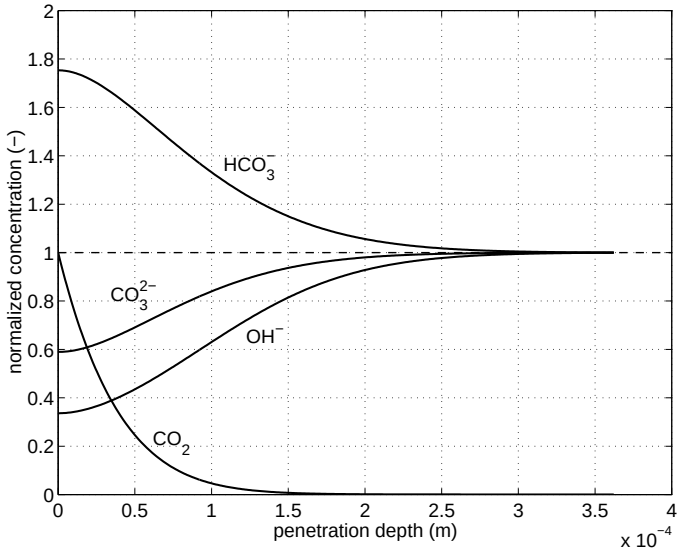

Figure A.1: Concentration profiles in the a 0.5 M $KHCO_3$ / 0.5 M K_2CO_3 buffer solution at the end of the contact time. $p_{CO_2} = 4$ bar, $k_L = 2 \cdot 10^{-5}$ m/s.

the gas phase to the liquid phase is 23% lower, when the concentration profiles of all components are taken into account, compared to case with the assumption of a pseudo-first order reaction.

The significance of the Danckwerts criterion is shown in Figure A.2. The ratio of the actual flux and the flux when a pseudo-first order reaction is assumed is plotted versus the left hand side of Equation A.1 for two different cases: by variation in the mass transfer coefficient k_L and by variation of the CO_2 partial pressure. In the variation of the k_L a constant pressure of 1.0 bar was applied and in the variation of the pressure a constant k_L of $5 \cdot 10^{-5}$ m/s was taken. The results show that the left hand side of the equation should be less than 0.1 in order to sustain an error less than 3% when the assumption of a pseudo-first order reaction is made.

To test the modelling results, CO_2 absorption experiments were carried out in a 0.5 M $KHCO_3$ / 0.5 M K_2CO_3 buffer solution using the stirred autoclave that was also used in Chapter 6. The dimensions of the reactor are given in Section 6.4 and the only modification to this is that the gas inducing stirred is replaced with a flat blade stirred with four blades and a total diameter of 4.5 cm. A stirring speed of 60 rpm was used, which ensured a flat gas-liquid interfacial area, as shown from

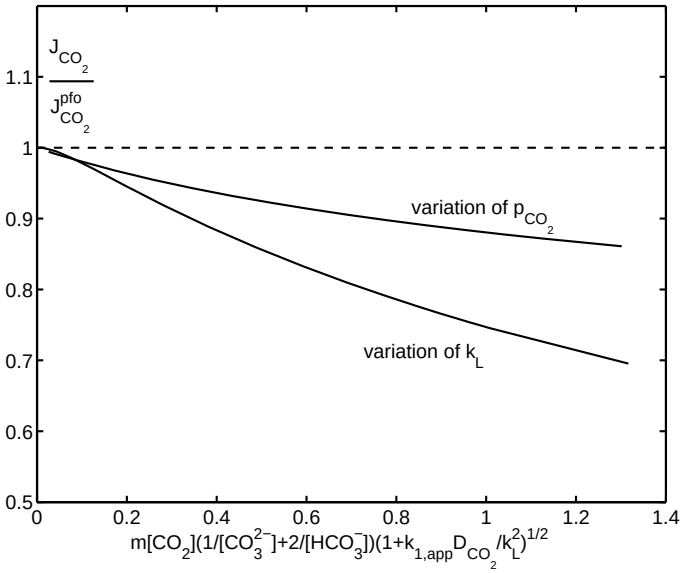

Figure A.2: Ratio of the flux calculated with the full model and the flux calculated with the assumption of a pseudo-first order (pfo) reaction.

experiments with different stirring speeds. The mass transfer coefficient, k_L, was determined according to the method explained in Section 6.4.

In the experiments the pressure the CO_2 partial pressure was varied from 0.7 to 16 bar to change the value of the left hand side in the Danckwerts criterion (eq. A.1). The value of the mass transfer transfer coefficient in the buffer solution was estimated from experiments in pure water using a correction for the diffusion coefficient according to the film model:

$$k_{L,buffer} = k_{L,water} \frac{D_{CO_2,buffer}}{D_{CO_2,water}} \tag{A.27}$$

The value of k_L in pure water was not dependent on the pressure and was found to be $1.95 \cdot 10^{-5}$ m/s. The results are presented in Figure A.3 and show a maximum relative deviation of 10% between the model and the experiments. This means that the model can describe the experiments reasonably well. This error might be due to the effect of ionic strength on the equilibrium constants, which influences the concentration of hydroxyl ions in the solution.

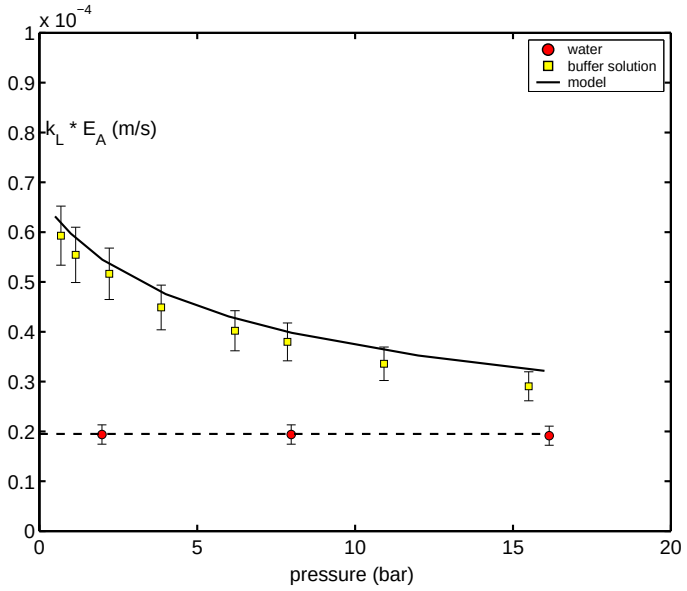

Figure A.3: $k_L \cdot E_A$ versus the pressure of CO_2 in a stirred cell reactor. Error bars represent the 10% error level.

A.5 Conclusions

The results of this study show that the presented equations and psycho-chemical parameters form a consistent set to describe CO_2 absorption in (0.5 M / 0.5 M) carbonate/bicarbonate solutions. The Danckwerts criterion as presented in Equation A.1 should be confined to $m \cdot [CO_2] \cdot \left(\frac{1}{[CO_3^{2-}]} + \frac{2}{[HCO_3^-]}\right) \cdot \left(\sqrt{\left(1 + \frac{D_{CO_2} \cdot k_{1,app}}{k_L^2}\right)} - 1\right) < 0.1$ to reduce the possible error in the flux calculation to less than 3% when a pseudo-first reaction is assumed.

Appendix B

Determination of surface tension to predict spreading behaviour of an organic phase on aqueous solutions

B.1 Introduction

In gas-liquid-liquid systems the interaction between bubbles and dispersed droplets can have a large influence on the mass transfer of the gas to the continuous liquid phase. It is therefore very important to determine whether or not there is direct contact between the gas phase and the dispersed liquid phase (spreading). Direct contact between the gas phase and the dispersed phase can provide for an additional mass transfer path, through which enhancement of mass transfer, compared to standard gas to the continuous liquid phase mass transfer, is possible. Roques et al. (1987) and Brilman (1998) demonstrated from droplet-bubble contact experiments that formation of gas-organic complexes can take place (Figure B.1). The occurrence of spreading of the organic on the aqueous phase is mainly determined by the sign of the spreading coefficient:

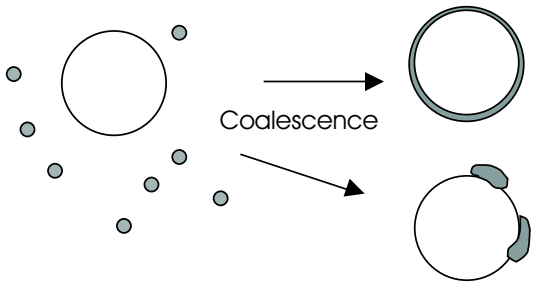

Figure B.1: Bubble-droplet complex formation.

$$S = \sigma_{W/G} - \sigma_{O/G} - \sigma_{O/W} \tag{B.1}$$

In literature often the initial spreading coefficient (S) is used, but in most practical applications the phases are mutually saturated and the final spreading coefficient (S^*) should be used, which can be calculated using Equation B.1 with mutually saturated surface tensions. When the spreading coefficient is positive it is always energetically favourable for the organic phase to spread over the aqueous phase. In case of a negative spreading coefficient, Brilman (1998) derived that the formation a organic-gas complex is favourable if the bubble-to-droplet size ratio satisfies the criterion in B.2

$$\left(\frac{d_b}{d_d}\right)^2 < \frac{\sigma^*_{O/W}}{\sigma^*_{O/W} + \sigma^*_{O/G} - \sigma^*_{W/G}} = \frac{\sigma^*_{O/W}}{-S^*} \tag{B.2}$$

In this appendix surface tension measurements will be presented in order to predict the spreading of different organic liquids on aqueous solutions. Additionally, experiments to study the spreading of organic liquids on a flat surface of an aqueous solution is studied.

B.2 Experimental

The surface- and interfacial tensions were measured using a Krüss K9 Tensiometer. The Wilhelmy plate method was used for the measurement of the surface tensions

and in case of interfacial tension measurement the Du Nöuy ring method was employed. The measurements were performed at 22-24 $^{\circ}$C. These temperature differences caused a maximum error in the surface tension measurements of 0.3 mN/m (for water).

Toluene, 1-octanol, n-heptane, n-dodecane and n-butyraldehyde were used as the organic phase in the visual observation of the spreading behaviour of these liquids on water. All chemicals were analytical grade (> 99% purity). Double-distilled water was used as the aqueous phase. The organic phase was added drop by drop using a 1 μl syringe to the water phase in a 20 cm petri dish. The dish was placed on a overhead projector to be able to see the processes taking place on a larger scale. The organic phases were coloured with Scarlet Red (Fluka) to make a clear distinction between the (colourless) aqueous and organic phases. It was verified that scarlet-red did not influence the surface tension of the organic liquids nor the surface tension of the aqueous phase (in which the Scarlet Red-dye is almost insoluble). The spreading behaviour was captured using a digital camera.

B.3 Results

B.3.1 KCl-solutions

To investigate the influence of electrolytes on the spreading coefficient, KCl was chosen as a model component. The surface tension of 1-3 M KCl solutions is given in Table B.1. From the results in Table B.1 is is made clear that the surface tension of water is increased strongly by the presence of KCl. The increase is approximately 1.7 mN m^{-1} M^{-1}, which is in reasonable agreement with the work of Craig et al. (1993) (1.85) and with the work of Hård and Johansson (1977) (1.62).

B.3.2 1-octanol - water system

The effect of 1-octanol on the surface tension was studied in water as well as in 3 M KCl solutions. The exact octanol concentration during the measurement was determined using GC-analysis. The results are presented in Figures B.2a and b.

Table B.1: Surface tensions at 23 ° C of different solutions of KCl in water.

concentration (M)	surface tension (mN/m)
0	72.6
1	74.1
2	75.3
3	77.9

In both cases a decreasing surface tension was obtained with increasing octanol concentration. Furthermore, a high value for $d\sigma/d\ln(c)$ is obtained, which results in high coalescence times, according to different coalescence theories (Marrucci, 1969; Sagert and Quinn, 1978). The coalescence time is defined as the time necessary for two bubbles to be in contact for coalescence to occur. Drogaris and Weiland (1983) measured coalescence times of approximately 30 s. in water with 100-500 mg/l octanol, which ascertained that coalescence is completely inhibited in these systems.

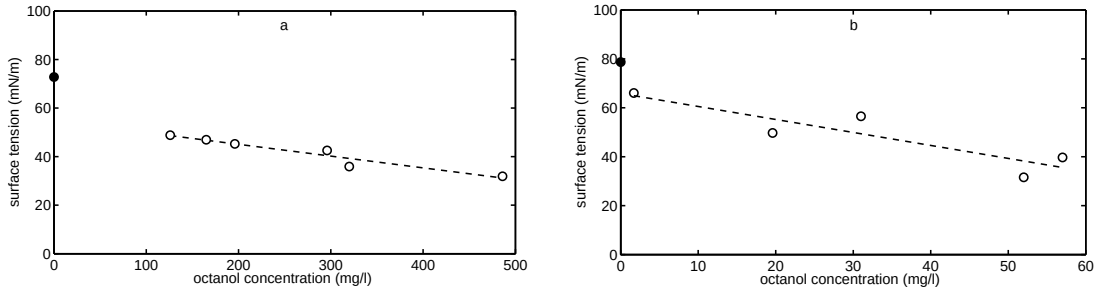

Figure B.2: Effect of octanol concentration on the surface tension. a: water, b: 3 M KCl in water.

B.3.3 Toluene - water system

The effect of the toluene concentration of the surface tension is presented in Figure B.3. Below the point of saturation no significant effect is found on the surface tension (circles), but just after the point of maximum solubility a strong decrease (8 mN/m) in surface tension is observed (open square). This decrease is found

when a small layer of toluene is put on top of the mutually saturated liquid. These measurements do not seem to be completely in line with the experimental values of Bartell et al. (1933), who measured that the surface tension of water saturated with toluene at 25 $^\circ$C was 63.65 mN/m, which is almost equal the value in the present work beyond the maximum solubility. These authors claimed, however, that the decrease in surface tension is caused by the spontaneous formation of an oil film on the water phase, which actually creates a supersaturated water phase and thereby confirms the experimental values as obtained in this work. These authors showed that in case when the surface tension of pure water is larger than sum of the oil-water interfacial tension and the surface tension of the oil phase ($\sigma_W > \sigma^*_{O/W} + \sigma^*_{O/G}$), Antonoff's relation holds:

$$\sigma^*_{W/G} = \sigma^*_{O/W} + \sigma^*_{O/G} \tag{B.3}$$

The spreading coefficient decreased from +9.0 (initially) to +8.3 (at saturation) to +0.3 mN/m (beyond the point of maximum solubility), which actually confirms Antonoff's rule. The +0.3 is probably within the experimental error. The values for the interfacial tension and the surface tension of the oil phase were not influenced significantly by the saturation with water and can therefore be replaced with $\sigma_{O/W}$ and $\sigma_{O/G}$, respectively.

These results indicate that at the point of maximum solubility a very large value of $d\sigma/dc$ exist, which might be responsible for the sudden change in coalescence phenomena in the air-toluene-water system (Section 5.3.4).

Similarly to the toluene-water system, the presence of toluene did not affect the surface tension of the 3 M KCl solution below the point of maximum solubility.

B.3.4 N-butyraldehyde - water system

In Figure B.4 the surface tension is shown versus the relative n-butyraldehyde concentration. A strong decrease is observed at low butyraldehyde fractions and at higher fractions of butyraldehyde a contant level is reached ($\approx$ 38 mN/m). Beyond the point of maximum solubility a strong decrease is observed. The spreading coeffi-

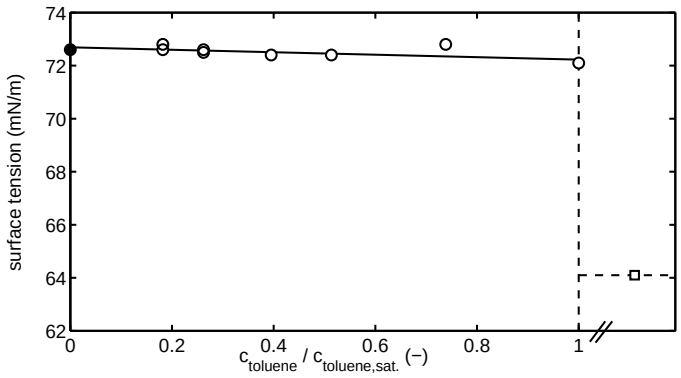

Figure B.3: Effect of the normalized toluene concentration (c/c_{sat}) on the surface tension. The data point beyond the point of maximum solubility was measured with different organic layer thicknesses (1.2 μm - 3 mm) and the x-coordinate for that point is therefore in arbitrary units.

cient decreased from +42.3 (initially) to +7.1 (at saturation) to +0.3 mN/m (beyond the point of maximum solubility). Similar to the results with toluene, Antonoff's relation seems to hold and the spreading coefficient with the presence of a small organic layer is zero and the +0.3 mN/m is due to the experimental error.

B.3.5 Spreading coefficient

From the measurements of the interfacial- and surface tension of the pure components and when the liquids are mutually saturated, the initial and final spreading coefficients, S and S^* respectively, can be determined. The results are presented in Table B.2 and show that for the toluene water system a positive spreading coefficient is obtained. When the water surface contains a small layer of toluene this spreading coefficient will be approximately zero, which can be calculated from the results in Figure B.3. In case of octanol the initial spreading coefficient is much larger than zero, but in case the liquid is saturated with octanol the sign of the spreading coefficient changes and lenses of octanol will form on the surface.

With heptane and dodecane the initial spreading coefficient is approximately equal to the final spreading coefficient. Heptane just spreads over water, while dodecane will form lenses according to these data. Similarly to 1-octanol,

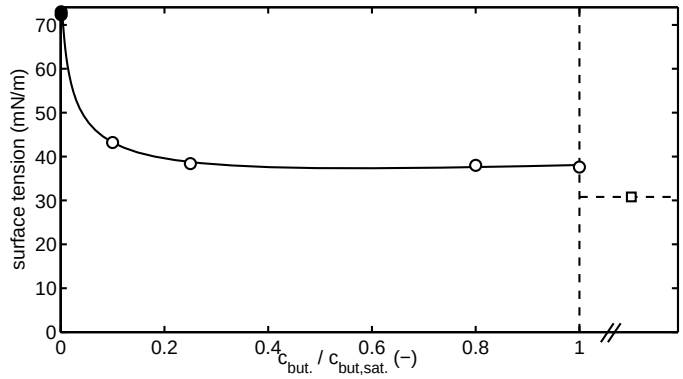

Figure B.4: Effect of the normalized n-butyraldehyde concentration (c/c_{sat}) on the surface tension. The data point beyond the point of maximum solubility was measured with different organic layer thicknesses (0.2 mm - 1 mm) and the x-coordinate for that point is therefore in arbitrary units.

n-butyraldehyde has a very large initial spreading coefficient. The final spreading coefficient remains positive, contrary to 1-octanol.

Using a 3 M KCl solution instead of water did not effect the spreading coefficient to a large extent. The interfacial tension and the surface tension of the aqueous phase were both somewhat higher compared to pure water. The surface tension of the organic phase was not effected significantly by the saturation with a 3 M KCl solution.

B.3.6 Visual observations of the spreading behaviour

With toluene, 1-octanol, n-heptane, n-dodecane and n-butyraldehyde as the organic phase on the aqueous water phase, experiments were performed to confirm the signs of the spreading coefficients as determined with the surface- and interfacial tensions.

In order to describe the phenomena occurring during the spreading experiments, three different events were encountered:

1. fast spreading
2. formation of lenses
3. slow spreading with the formation of a larger lens

Table B.2: Spreading coefficients at 22-24 °C of different systems. All values are in mN/m. For the calculation of the initial spreading coefficient 72.8 and 77.9 were taken as the surface tensions of water and 3 M KCl, respectively.

system	$\sigma^*_{W/G}$	$\sigma^*_{O/G}$	$\sigma^*_{O/W}$	S	S^*
toluene-water	72.1	28.4	35.4	+9.0	+8.3
1-octanol-water	30.7	27.0	8.2	+37.6	−4.5
n-dodecane-water	72.4	25.4	48.7	−1.3	−1.7
n-heptane-water	72.8	20.6	50.2	+2.0	+2.0
n-butyraldehyde-water	37.6	24.1	6.4	+42.3	+7.1
toluene-3 M KCl	77.9	28.7	41.2	+8.0	+8.0
1-octanol-3 M KCl	32.4	27.1	10.8	+40.0	−5.5
n-dodecane-3 M KCl	76.5	25.6	51.2	+1.1	−0.3
n-heptane-3 M KCl	76.1	20.6	53.6	+5.7	+1.9

Table B.3: Experimental spreading behaviour of different organic liquids on water

organic phase	initial	final
1-octanol	1	2
toluene	1	2
n-heptane	3	3
n-dodecane	3	3
n-butyraldehyde	1	3

In the third case the spreading behaviour is not well defined and it is difficult to compare the results with the calculated spreading coefficient from the surface- and interfacial tension measurements. For both the initial spreading behaviour and the final situation of the organic phase the results are categorized according to the three events in Table B.3.

Initial spreading of n-butyraldehyde and 1-octanol on water is very fast, as was expected from their high initial spreading coefficient. A high amount of turbulence is induced, due to the low interfacial tension. After saturation a large amount of small lenses is formed in case of octanol, which confirms the measurements

of the spreading coefficient. In case of butyraldehyde, after saturation, a larger lens is formed. Although the final spreading coefficient is positive, the formation of a small organic layer on the water phase can decrease the spreading coefficient and causes this behaviour (see Section B.3.4).

In case of toluene the results are somewhat similar to n-butyraldehyde. Initial spreading is, however, less fast, which can be explained by the lower value of S. After saturation the formation of a lens is clearly visible and similar to n-butyraldehyde the formation of a small toluene layer on the water phase seems likely (see Section B.3.3), as the fast spreading did not occur after saturation.

With n-heptane and n-dodecane the spreading behaviour is less defined. Spreading is very slow and the formation of large lenses takes place. With small values (positive and negative) of the spreading coefficients the spreading behaviour is more difficult to confirm by performing these kind of experiments.

B.4 Discussion and conclusions

The Wilhelmy plate method was used to perform measurement of the surface tension of pure water, electrolyte solutions (KCl), organic phases (1-octanol, toluene, n-heptane, n-dodecane and n-butyraldehyde) before and after when they were (partly) saturated with another phase. Interfacial tension measurements were performed using the Du Nöuy ring method. In this way the spreading coefficients of the different organic phases could be determined. These spreading coefficients were confirmed by spreading experiments, that were captured using a digital camera.

It was shown that in case of toluene and n-butyraldehyde the final spreading coefficient remains positive, but after supersaturation the spreading coefficient was approximately zero, due to the formation of a small organic layer on top of the water phase. This behaviour was also observed by Bartell et al. (1933), who claimed that at a positive initial spreading coefficient ($S > 0$) the final spreading coefficient is zero ($S^* = 0$). In this work it was shown that this is only true when the final spreading coefficient, before the formation of a small layer is positive. In case of octanol the initial spreading coefficient was positive, while the final spreading coefficient was

negative, which was confirmed by visual observations.

Acknowledgement

The author wishes to to thank Suvan Bokhove, Wim Lengton and Adrie Hovestadt for their contribution in the experimental work.

Appendix C

Analytical solution for the oxygen concentration with time after a step change in the gas phase concentration

In this appendix the solution of the oxygen concentration in the gas phase and in the liquid phase and the probe response as a function of time on a step change in the gas phase concentration is derived from the oxygen mass balances in the gas- and the liquid phase and the probe response characteristics:
Gas phase:

$$\frac{dc_G}{dt} = \frac{(c_{G,in} - c_G)}{\tau_G} - k_L a(mc_G - c_L)\frac{V_L}{V_G} \tag{C.1}$$

Liquid phase:

$$\frac{dc_L}{dt} = k_L a(mc_G - c_L) \tag{C.2}$$

Probe response:

$$\frac{dc_P}{dt} = \frac{(c_L - c_P)}{\tau_P} \tag{C.3}$$

Note that by using these equations it is assumed that both the gas phase as well as the liquid phase are ideally mixed.

At time $t = 0$ the concentrations are:
$c_G = c_{G,in}$, $c_L = 0$ and $c_P = 0$.
For a convenient notation the following transformations are introduced:

$$x = k_L a \tau_G = k_L a \frac{V_G}{\Phi_G} = k_L a \frac{\varepsilon_G}{(1-\varepsilon_G)} \frac{V_L}{\Phi_G} \tag{C.4}$$

$$y = m \frac{V_L}{V_G} = m \frac{(1-\varepsilon_G)}{\varepsilon_G} \tag{C.5}$$

$$D = \sqrt{(1+y)^2 x^2 + (2y-2)x + 1} \tag{C.6}$$

The solution for the liquid phase concentration in case of a step change in the gas phase concentration from $c_G = 0$ to $c_G = c_{G,in}$ (absorption experiment) is:

$$c_L(t) = m c_{G,in} \left(1 + \frac{A}{D} \exp\left(-B \frac{t}{\tau_G} \right) - \frac{B}{D} \exp\left(-A \frac{t}{\tau_G} \right) \right) \tag{C.7}$$

with: $A = {}^1\!/_2(x + 1 + xy - D)$ and $B = {}^1\!/_2(x + 1 + xy + D)$.

The solution for the probe response concentration now becomes:

$$\begin{aligned} c_P(t) = m c_{G,in} & \left(1 + \frac{A}{D\left(1 - B\frac{\tau_P}{\tau_G}\right)} \exp\left(-B \frac{t}{\tau_G} \right) - \frac{B}{D\left(1 - A\frac{\tau_P}{\tau_G}\right)} \exp\left(-A \frac{t}{\tau_G} \right) \right) \\ & + m c_{G,in} \left(-\frac{A}{D\left(1 - B\frac{\tau_P}{\tau_G}\right)} + \frac{B}{D\left(1 - A\frac{\tau_P}{\tau_G}\right)} - 1 \right) \exp\left(-\frac{t}{\tau_P} \right) \end{aligned} \tag{C.8}$$

In case of desorption of oxygen from the liquid phase (switching from air to nitrogen with a step change from $c_G = c_{G,in}$ to $c_G = 0$) the probe response concentration equals:

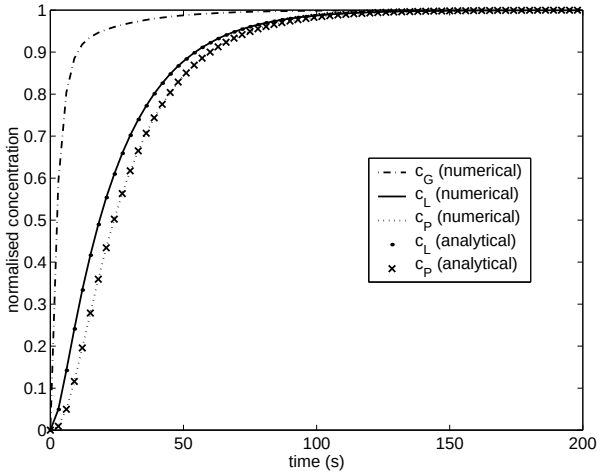

Figure C.1: Comparison of the analytical and numerical solution

The following parameters were used in the calculation:
$k_L a = 0.05$ s^{-1}, $V_L = 40 \cdot 10^{-3}$ m^3, $\Phi_G = 40 \cdot 10^{-3}$ m^3 s^{-1}, $\varepsilon_G = 0.05$ and $\tau_P = 5$ s.

$$c_P(t) = mc_{G,0}\left(-\frac{A}{D\left(1-B\frac{\tau_P}{\tau_G}\right)}\exp\left(-B\frac{t}{\tau_G}\right)+\frac{B}{D\left(1-A\frac{\tau_P}{\tau_G}\right)}\exp\left(-A\frac{t}{\tau_G}\right)\right)$$
$$-mc_{G,0}\left(-\frac{A}{D\left(1-B\frac{\tau_P}{\tau_G}\right)}+\frac{B}{D\left(1-A\frac{\tau_P}{\tau_G}\right)}+1\right)\exp\left(-\frac{t}{\tau_P}\right) \tag{C.9}$$

in which $c_{G,0}$ as the gas phase concentration at $t = 0$ in the reactor. In case of air $c_{G,0} = 0.21 \cdot p/(RT)$.
To check the validity of the analytical solution a comparison with the numerical solution was performed. The results are shown in Figure C.1 and show an excellent agreement between the two solutions. The maximum deviation in the probe response is $3 \cdot 10^{-5}\%$. The analytical solution is used in this work to save time in the fit procedure to determine the volumetric mass transfer coefficient from the experiments.

Appendix D

Measurement of the gas phase residence time distribution

In this appendix the measurement principle of the gas phase RTD measurement using ultrasound is explained. Furthermore, the adaptations to the experimental set-up that was used in Chapter 4 are described. Finally, some results of the gas-phase RTD measurements of the systems as used in this chapter will be presented and discussed.

D.1 Measurement principle

The measurement principle makes use of the dependence of the speed of sound in a material on the bulk modulus (of elasticity) and density of this medium. This dependence is given for a fluid by equation D.1.

$$c = \sqrt{\frac{dp}{d\rho}} = \sqrt{\frac{E_V}{\rho}} \tag{D.1}$$

The average density and bulk modulus of a binary mixture of ideal gases are given by:

$$\rho = (1 - \varepsilon)\rho_1 + \varepsilon\rho_2 \tag{D.2}$$

$$\frac{1}{E_V} = (1-\varepsilon)\frac{1}{E_{V,1}} + \varepsilon\frac{1}{E_{V,2}} \tag{D.3}$$

Both the density and the bulk modulus of the pure components are well tabulated in literature or can be calculated easily. For an ideal gas undergoing an isotropic change (pressure wave), for instance, the bulk modulus of elasticity is defined as:

$$E_V = \frac{dp}{d\rho/\rho} = \gamma p \tag{D.4}$$

In this equation is γ the ratio of the Cp and the Cv. Povey (1997) suggested to calculate the bulk modulus of the pure components from their tabulated density (ρ) and ultrasonic velocity (c) values:

$$E_{V,i} = c_i^2 \rho_i \tag{D.5}$$

When doing so, the composition of the binary mixture can be expressed as function of the measured velocity of sound in the mixture and the known ρ and c of the pure components:

$$\varepsilon = \frac{-B \pm \sqrt{B^2 - 4AC}}{2A} \tag{D.6}$$

where:

$$\begin{aligned} A &= c_1^2\left(1 - \frac{\rho_1}{\rho_2}\right) + c_2^2\left(1 - \frac{\rho_2}{\rho_1}\right) \\ B &= c_2^2\left(\frac{\rho_2}{\rho_1} - 2\right) + c_1^2\left(\frac{\rho_1}{\rho_2}\right) \\ C &= c_2^2\left(1 - \frac{c_1^2}{c_{exp}^2}\right) \end{aligned}$$

In this work, equation D.6 was used to convert the experimentally determined sound velocity (c_{exp}) values to the mixture's composition. Note that, in the above analysis,

the term binary is not restricted to two pure components. The relation also holds when a component, the tracer-gas, is considered next to a mixture of components (e.g. air) of which the relative composition does not change during the measurement. This concentration measurement technique can be used to determine the system's response to a pulse- or a step-function in the inlet concentration of a tracer component.

D.2 Experimental method

Helium was selected as the tracer gas as the velocity of ultrasonic velocity is very high (985 m/s), which means that a low helium fraction can be used in order to get a large change in the velocity and a high accuracy can be obtained. Furthermore, the solubility of helium in water is low ($m \approx 0.01$) and it was verified that mass transfer of helium does not have a large influence on the results. For the determination of the helium concentrations in time, the ultrasonic velocity is determined using method as explained in Sections 2.3.2 and 2.3.3. A schematic representation of the set-up is given in Figure D.1. At the start of the measurement the waveform generator sends a trigger signal to the oscilloscope as well as to a fast-opening valve (V1). In this way the time $t = 0$ is known and is the exact time at which the valve opens and releases the helium. The signals are recorded versus time in the oscilloscope and the determination of the ultrasonic velocity, from which the helium concentrations can be determined, is performed afterwards in a personal computer. Using this method a maximum sampling frequency of 33 Hz can be reached. The ultrasonic transducers are mounted in a measurement cell on top of the vessel described in Section 4.3. The measurement cell itself has a small volume and diameter (and therefore a high Peclet number), which assures that the residence time in the cell does not influence the results. Further details of this measurement technique are given by Cents et al. (2003).

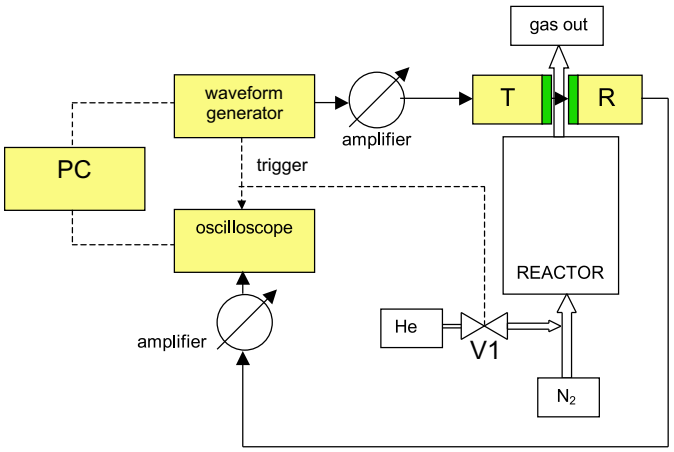

Figure D.1: Schematic representation of the set-up for RTD-measurements.

D.3 Results

The validation of the helium concentration versus ultrasonic velocity and the application of the technique in (close-to-) model reactors (CISTR and PFR) is given in the work of Cents et al. (2003).

D.3.1 Coalescing systems

In Figure D.2 the gas phase RTD-curves of nitrogen and with 9% helium in a vessel as used in Chapter 4 containing water, water with 0.5% and with 5% toluene are shown. The RTD-curves could be well described using a model of N-CISTR's in series. The number of CISTR's was lower when the water contained toluene (1.5-1.6) compared to pure water (2.3). The increase of impeller speed increased the number of CISTR's in pure water to 2.6. This might be due to a diminished level of coalescence in the reactor in combination with a larger volume fraction of bubbles inside the liquid (higher gas hold-up).

Unfortunately these numbers do not necessarily give detailed information about the residence time distribution of the gas phase inside the liquid. The RTD-curve is the combination of the distributions of the gas phase inside the liquid and the gas cap above the liquid. These curves, therefore, give only indications of the residence time distributions of the gas bubbles in the solution.

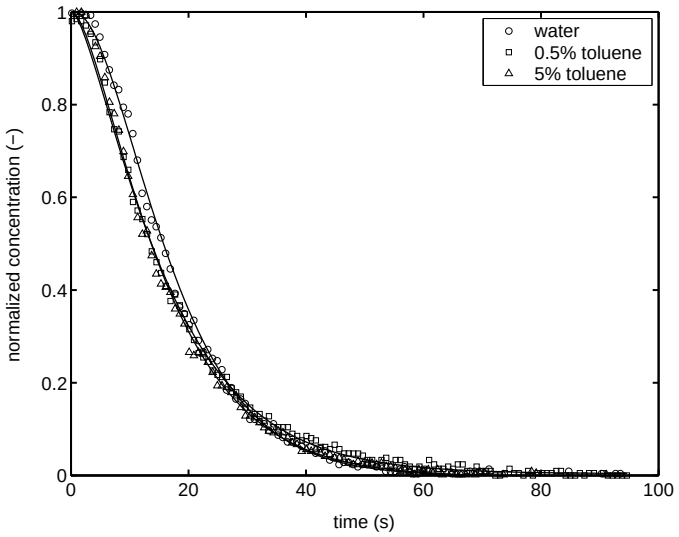

Figure D.2: Gas phase RTD-curves in different coalescing systems. u_G = 0.58 cm/s, V_L = 52.6 liter. V_{tot} = 64.0 liter.

D.3.2 Non-coalescing systems

The RTD-curves of the gas phase in a non-coalescing 0.5 M K_2CO_3 /0.5 M $KHCO_3$ buffer system are shown in Figure D.3. The curves could not be described with a model of a number of CISTR's in series, due to the first parts of the curves which did not show a decrease in concentration. This suggested that a plug flow reactor (PFR) should be present in the model description. For this reason, the model of a PFR of a variable length with 1 CISTR in series was used as the model, which described the experimental curves well, as can be seen from Figure D.3. The length of the PFR increased with increasing stirring speed, and the volume of the PFR agreed reasonably well with the volume of the gas phase in the liquid as calculated from the experimentally determined gas hold-ups. This suggests that the gas phase in contact with the liquid phase should be described as a PFR. Again, this is only an indication, as the RTD is a combination of the gas phase in the liquid and the gas phase present in the head space of the reactor.

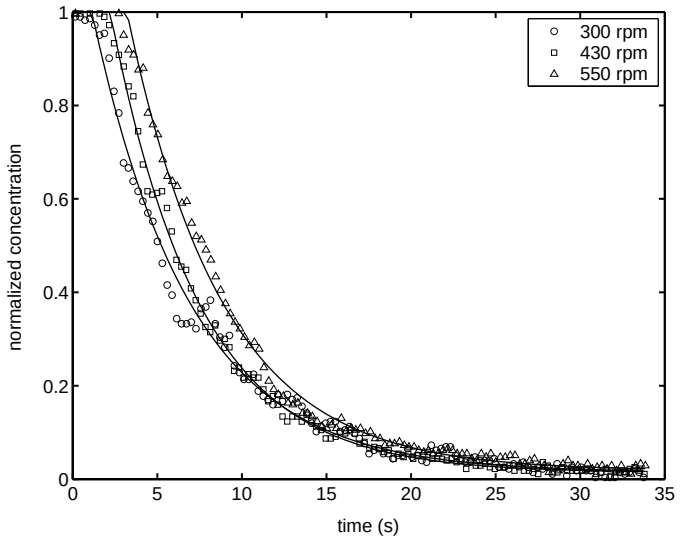

Figure D.3: Gas phase RTD-curves in 0.5 M K_2CO_3 /0.5 M $KHCO_3$ buffer system. u_G = 1.79 cm/s, V_L = 46.5 liter.

D.3.3 Implications for the mass transfer coefficients

The residence time of the gas phase has a direct influence on the determination of the k_La from the mass transfer experiments. When the gas phase is not ideally mixed, the calculated k_La on the basis of an ideally mixed gas phase will be higher compared to the actual k_La. Two examples of this are presented in this appendix:

1. The mass transfer experiments with the dynamic oxygen method as performed in Chapter 4.

2. Mass transfer experiments using the carbonate/bicarbonate buffer system in the vessel that was used in Chapter 4.

In Table D.1 the ratio of the k_La, taking a different gas phase RTD into account, and the k_La as determined assuming an ideally mixed gas phase, is given. The maximum error when the gas phase is described with 2 CISTR's in series, which is probably a good description for the gas phase in these systems, is at the maximum measured k_La (0.14 s^{-1}) approximately 20%, which has to be considered.

In Table D.2 similar results are given for the CO_2 absorption in the carbonate/bicarbonate buffer system. The results are somewhat similar to the oxygen

Table D.1: Ratio of k_La and $k_La^{(im)}$ for different situations in the dynamic oxygen method. u_G = 0.58 cm/s, V_L = 52.6 liter, ε = 0.05 and m=0.0326.

$k_La^{(im)}$	$\frac{k_La^{(2-CISTR)}}{k_La^{(im)}}$	$\frac{k_La^{(PFR)}}{k_La^{(im)}}$
0.05	0.91	0.86
0.10	0.86	0.76
0.15	0.81	0.69

Table D.2: Ratio of k_La and $k_La^{(im)}$ for different situations in absorption of CO_2 in the buffer solution. u_G = 1.79 cm/s, V_L = 46.5 liter and m=0.55.

$k_La^{(im)}$	$\frac{k_La^{(2-CISTR)}}{k_La^{(im)}}$	$\frac{k_La^{(PFR)}}{k_La^{(im)}}$
0.05	0.89	0.79
0.10	0.81	0.67
0.15	0.75	0.58

system, due to the fact that the depletion of the gasses is almost equal. CO_2 is absorbed faster due to the higher distribution coefficient, m, but the depletion is decreased by the higher gas flow rate that is used in this case. The maximum error at a k_La of 0.10 is 33% when the actual gas phase residence time distribution is described as a PFR.

D.4 Conclusions

Gas-phase RTD measurements were performed in a gas-liquid stirred tank using an ultrasonic technique. In coalescing systems (with low gas hold-up) the RTD-curves could be well described using a model with a number of CISTR's in series (≈ 2). In non-coalescing systems, in which the gas hold-up was higher, this was not possible. A good description of the results was possible using a model of a PFR with a certain volume with 1 CISTR in series. The volume of the PFR was in good agreement with the volume of the gas bubbles in the liquid, which could be calculated from the gas hold-up. These results imply that at least for non-coalescing systems the gas phase inside the liquid should be described as a PFR. For coalescing systems this could

also be the case, but the gas hold-up is much smaller, which makes it more difficult to obtain the exact RTD of the gas phase below the liquid surface.

In the calculation of the volumetric mass transfer coefficient it is very important to take the correct gas phase RTD into account. For the systems used in the present study (Chapter 4) errors up to 30% can be made when a CISTR is assumed, while the gas moves in plug flow through the reactor.

Appendix E

Sensitivity analysis on the mass transfer parameters as determined by the Danckwerts-plot technique

E.1 Introduction

The Danckwerts-plot is used in chemical engineering in order to obtain the mass transfer parameters, k_L and a simultaneously. In this appendix the sensitivity of the obtained absolute values for k_L, a and k_La to the gas phase residence time distribution (RTD) and the CO_2 equilibrium bulk concentration will be discussed. The chemical absorption of CO_2 into carbonate/bicarbonate buffer solutions will be taken as the system under consideration.

E.2 Gas phase RTD

The general expression for the gas phase balance in case of stationary gas absorption in a batchwise operated liquid is:

$$0 = \Phi_{G,in} c_{CO_2,in} - \Phi_{G,out} c_{CO_2,out} - k_L a E_{CO_2} \Delta c_L V_L \tag{E.1}$$

in which E_{CO_2} is the enhancement factor for a first order reaction from the Danckwerts surface renewal model

$$E_{CO_2} = \sqrt{1 + \frac{k_{1,app} D_{CO_2}}{k_L^2}} \tag{E.2}$$

Δc_L is the driving force for mass transfer in the liquid phase. Two asymptotic cases of the gas phase residence time distribution will be discussed; CISTR-behaviour and plug-flow (PFR). In case of an ideally mixed gas phase, the concentration at all positions in the vessel is equal to the outlet concentration and the driving force can be represented as:

$$\Delta c_L = m c_{CO_2,out} - c_L \tag{E.3}$$

When the gas phase is passing in plug flow through the vessel the average driving force can be described according to:

$$\Delta c_L = \frac{m c_{CO_2,in} - m c_{CO_2,out}}{\ln\left(\frac{m c_{CO_2,in} - c_L}{m c_{CO_2,out} - c_L}\right)} \tag{E.4}$$

These equations were used to model the effect of the residence time distribution at different apparent first order reaction rates. The conditions are given in Table E.1. In Figure E.1 the obtained Danckwerts-plots are presented for the CISTR and the PFR case. The difference in the slope of both lines is very large. The obtained interfacial area for the plug flow case was 245 m^2/m^3, which is more than a factor two lower compared to the CISTR case (500 m^2/m^3, which was an input parameter). This result shows that the absolute values for the mass transfer parameters, obtained with the Danckwerts-plot technique, using CO_2 as the gas phase to be transferred, are very sensitive to the gas phase residence time distribution. Note that even in the plug flow case a reasonably straight line is obtained (correlation coefficient 97.5%) .

Oyevaar and Westerterp (1989) claimed that for systems that are first order in CO_2 and for a conversion less than 80% the assumption of an ideally mixed gas

Table E.1: Conditions used in the modelling study.

property	value	units
interfacial area (CISTR), a	500	m^2/m^3
mass transfer coefficient (CISTR), k_L	$1.5 \cdot 10^{-4}$	m/s
liquid volume, V_L	$2.5 \cdot 10^{-3}$	m^3
gas flow rate, Φ_G	$1.9 \cdot 10^{-4}$	m^3/s
inlet CO_2 concentration, $c_{CO_2,in}$	0.82	mol/m^3
CO_2 bulk concentration, c_L	0.05	mol/m^3
distribution coefficient, m	0.56	-
diffusion coefficient, D_{CO_2}	$1.5 \cdot 10^{-9}$	m^3/s
apparent first order rate constant, $k_{1,app}$	0-250	s^{-1}

phase led to accurate values of the interfacial area. Care must be taken with this statement as the RTD curves, as shown in Appendix D, in the non-coalescing buffer system clearly show a certain amount of plug flow behaviour. This can influence the measured interfacial area to a large extent, although the maximum conversion in the Danckwerts-plot of Figure E.1 was only 62%. The value for the volumetric mass transfer coefficient, k_La (determined from the intercept of the vertical axis), is always determined quite accurately. In this example the difference was only 2.5%.

E.3 CO_2 equilibrium bulk concentration

When the Danckwerts-plot is used with the liquid phase operated batch-wise, concentration changes of the potassium bicarbonate and potassium carbonate ions in the solution can occur due to reaction of CO_2 with carbonate ions to bicarbonate ions. To prevent this, a low concentration of CO_2 was chosen, which decreases this effect. A disadvantage of a lower CO_2 concentration is the fact that the equilibrium bulk concentration of CO_2 can no longer be neglected. The complete system of reactions occurring in this system is given in Appendix A. The concentration of dissolved carbon dioxide in the liquid phase can be calculated from the equilibrium constants:

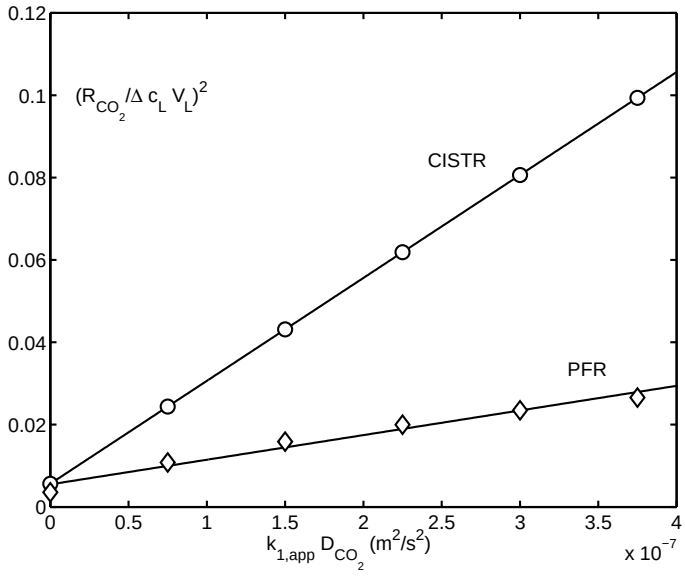

Figure E.1: Danckwerts-plots with different gas phase residence time distributions.

$$[CO_2]_b = \frac{K_2 K_W}{K_1} \frac{[HCO_3^-]^2}{[CO_3^{2-}]} \tag{E.5}$$

The value of the equilibrium constant can be calculated using the relations given in Appendix A. According to Hikita et al. (1976), the value of K_2 should be corrected with an effect of the concentration of potassium ions in the solution, according to:

$$\log K_2 = \log K_2^0 + \frac{1.01[K^+]^{1/2}}{1 + 1.49[K^+]^{1/2}} + 0.061[K^+] \tag{E.6}$$

At 21 $^\circ$C the value of the CO_2 bulk concentration in the buffer solution without taking the ionic effect into account is 0.053 mol/m^3, and with the ionic effect the bulk concentration is 0.179 mol/m^3. As this difference is very large, the influence of the CO_2 bulk concentration on the absolute value mass transfer parameters was studied with the operating conditions from Table E.1. The influence of the CO_2 bulk concentration is quite large. In case the bulk concentration is neglected, the value of

the interfacial area decreased from 500 to 350 m^2/m^3. When the bulk concentration was calculated by taking the ionic effect into account the k_La could not be calculated from the Danckwerts-plot as the intercept was negative.

Because the effects are very strong it was decided to measure the CO_2 equilibrium bulk concentration. In the experimental set-up described in Chapter 1, a small nitrogen stream (2 liter/min) was led through an intensely stirred (2000 rpm) 0.5 M potassium carbonate / 0.5 M potassium bicarbonate buffer solution. Sodium hypochlorite (0.1 M) was added to ascertain that the solution was at equilibrium with the gas stream and the outlet CO_2 concentration was measured using a CO_2 analyzer. Making use of the distribution coefficient of carbon dioxide in the buffer solution the equilibrium CO_2 concentration in the bulk could be calculated and was found to be 0.051 mol/m^3 at 21 °C. To verify that the solution was at equilibrium the experiment was repeated with 1.5% CO_2 present in the nitrogen stream, which reacted in the solution and reached equilibrium. The CO_2 concentration in the bulk of the liquid was, again, determined to be 0.053 mol/m^3. These results indicate that the ionic effect should not be taken into account in a 0.5 M potassium carbonate / 0.5 M potassium bicarbonate buffer solution. These results were supported by the good description of the experimental results that were obtained by the model, without taking the effect of ionic strength on K_2 into account, in the absorption experiments in a buffer solution with a flat surface (Appendix A).

E.4 Conclusions

The residence time distribution of the gas phase is very important in the determination of the mass transfer parameters using a Danckwerts-plot with CO_2 as the transferred component. Furthermore, when low inlet concentrations of carbon dioxide are applied, the CO_2 equilibrium bulk concentration cannot be neglected and is important for the determination of the absolute values of the mass transfer coefficients. The bulk concentration was measured and was 0.052 mol/m^3 at 21 °C in a 0.5 M potassium carbonate / 0.5 M potassium bicarbonate buffer solution. These results imply that in the calculation of the bulk concentration the ionic effect

on the equilibrium constant K_2 should not be taken into account.

Bibliography

Alig, I. and Lellinger, D. Frequency dependence of ultrasonic velocity and attenuation in two-phase composite systems with spherical scatterers. *J. Appl. Phys.*, 72:5556–5570, 1992.

Allegra, J.R. and Hawley, S.A. Attenuation of sound in suspensions and emulsions: Theory and experiments. *J. Acoust. Soc. Am.*, 51:1545–1564, 1972.

Alper, E., Deckwer, W.-D. and Danckwerts, P.V. Comparison of effective interfacial areas with the actual contact area for gas absorption in a stirred cell. *Chem. Engng Sci.*, 35:1263–1268, 1980.

Alves, S.S., Maia, C.I., Vasconcelos, J.M.T. and Serralheiro, A.J. Bubble size in aerated stirred tanks. *Chem. Eng. J.*, 89:109–117, 2002.

Bae, J.H. and Tavlarides, L.L. Laser capillary spectrophotometry for drop-size concentration measurements. *A.I.Ch.E. J.*, 35:1073–1084, 1989.

Barigou, M. and Greaves, M. A capillary suction probe for bubble-size measurement. *Meas. Sci. Technol.*, 2:318–326, 1991.

Barigou, M. and Greaves, M. Bubble-size distributions in a mechanically agitated gas-liquid contactor. *Chem. Engng Sci.*, 47:2009–2025, 1992.

Barigou, M. and Greaves, M. Gas hold-up and interfacial area distributions in a mechanically agitated gas-liquid contactor. *Trans. Instn Chem. Engrs*, 74:397–405, 1996.

Bartell, F.E., Case, L.O. and Brown, H. The surface tension of mercury and of water in contact with saturated vapors. *J. Am. Chem. Soc.*, 55:2769–2776, 1933.

Benadda, B., Prost, M., Ismaily, S., Bressat, R. and Otterbein, M. Validation of the gas-lift capillary bubble column as a simulation device for a reactor by the study of CO_2 absorption in $Na_2CO_3/NaHCO_3$ solutions. *Chem. Eng. Proc.*, 33:55–59, 1994.

Bhattacharya, A. and Chaudhari, R.V. An analysis of mass transfer effects in hydroformylation reactions. *Ind. Eng. Chem. Res.*, 26:1168–1173, 1987.

Bouaifi, M. and Roustan, M. Bubble size and mass transfer coefficients in dual impeller reactors. *Can. J. Chem. Eng.*, 76:390–397, 1998.

Brilman, D.W.F. *Mass transfer and chemical reaction in gas-liquid-liquid systems.* PhD thesis, University of Twente, 1998.

Brilman, D.W.F., Goldschmidt, M.J.V., Versteeg, G.F. and van Swaaij, W.P.M. Heterogeneous mass transfer models for gas absorption in multiphase systems. *Chem. Engng Sci.*, 55(12):2793–2812, 2000.

Bruining, W. J., Joosten, G.E.H., Beenackers, A.A.C.M. and Hofman, H. Enhancement of gas-liquid mass transfer by a dispersed second liquid phase. *Chem. Engng Sci.*, 41:1873–1877, 1986.

Burgess, J.M. and Calderbank, P.H. The measurement of bubble parameters in two-phase dispersions–I: The development of an improved probe technique. *Chem. Engng Sci.*, 30:743–750, 1975.

Calderbank, P.H. Physical rate processes in industrial fermentation. part I: The interfacial area in gas-liquid contacting with mechanical agitation. *Trans. Instn Chem. Engrs*, 36:443–463, 1958.

Calderbank, P.H., Evans, F. and Rennie, J. The mass transfer efficiency of distillation and gas-absorption plate columns. part I: Techniques for measuring gas-liquid

interfacial areas and foam densities in plate columns. *Proceedings of the International Symposium on Distillation (Instn Chem. Engrs)*, pages 51–72, 1960.

Calderbank, P.H. and Pereira, J. The prediction of distillation plate efficiencies from froth properties. *Chem. Engng Sci.*, 32:1427–1433, 1977.

Carberry, J.J. and Varma, A. *Chemical reaction and reactor engineering.* Marcel Dekker, New York, 1987.

Cents, A.H.G., Brilman, D.W.F. and Versteeg, G.F. Gas absorption in an agitated gas-liquid-liquid system. *Chem. Engng Sci.*, 56:1075–1083, 2001.

Cents, A.H.G., Kersten, S.R.A. and Brilman, D.W.F. Gas-phase RTD measurement in gas and gas-solids reactors using ultrasound. *Ind. Eng. Chem. Res.*, 42:5506–5515, 2003.

Chaudhari, R.V. and Hofmann, H. Coalescence of gas bubbles in liquids. *Rev. Chem. Eng.*, 10:131–190, 1994.

Cornils, B. Bulk and fine chemicals via aqueous biphasic catalysis. *Journal of Molecular Catalysis A: Chemical*, 143:1–10, 1999.

Cornils, B., Hermann, W.A. and Eckl, R.W. Review: industrial aspects of aqueous catalysis. *Journal of Molecular Catalysis A: Chemical*, 116:27–33, 1997.

Cornils, B. and Kuntz, E.G. Introducing TPPTS and related ligands for industrial biphasic processes. *J. Organometal. Chem.*, 502:177–186, 1995.

Craig, V.S.J., Ninham, B.W. and Pashley, R.M. The effect of electrolytes on bubble coalescence in water. *J. Phys. Chem.*, 97:10192–10197, 1993.

Danckwerts, P.V. Absorption by simultaneous diffusion and chemical reaction. *Trans. Faraday Soc.*, 46:300–304, 1950.

Danckwerts, P.V. *Gas-liquid reactions.* McGraw-Hill, New York, 1970.

Danckwerts, P.V., Kennedy, A.M. and Roberts, D. Kinetics of CO_2 absorption in alkaline solutions- II absorption in a packed column and tests of surface renewal models. *Chem. Engng Sci.*, 18:63–72, 1963.

Danckwerts, P.V. and Sharma, M.M. Absorption of carbon dioxide into solutions of alkalis and amines. *J.Chem Eng. Rev.*, Ser. No. 2, The Chemical Engineer:CE 244–280, 1966.

Dang, N.P.D., Karrer, D.A. and Dunn, I.J. Oxygen transfer coefficients by dynamic model moment analysis. *Biotech. Bioeng.*, 19:853–865, 1977.

Das, T.R., Bandopadhyay, A., Parthasarathy, R. and Kumar, R. Gas-liquid interfacial area in stirred vessels: the effect of an immiscible dispersed phase. *Chem. Engng Sci.*, 40:209–214, 1985.

Deckwer, W.-D. *Reaktionstechnik in Blasensaülen.* Otto Salle Verlag GmbH & Co., Frankfurt am Main, Verlag Sauerländer AG, Aarau, 1985.

Del Grosso, V.A. and Mader, C.W. Speed of sound in pure water. *J. Acoust. Soc. Am.*, 55:1442–1446, 1972.

Díaz, M., Vega, A. and Coca, J. Correlation for the estimation of gas-liquid diffusivity. *Chem Eng. Comm.*, 52:271–281, 1987.

Drogaris, G. and Weiland, P. Coalescence behaviour of gas bubbles in aqueous solutions of n-alcohols and electrolytes. *Chem. Engng Sci.*, 38:1501–1506, 1983.

Duraiswami, R., Prabhukumar, S. and Chahine, G.L. Bubble counting using an inverse acoustic scattering method. *J. Acoust. Soc. Am.*, 104:2699–2717, 1998.

Eckenfelder, W.W. and Barnhart, E.L. The effect of organic substances on the transfer of oxygen from air bubbles in water. *A.I.Ch.E. J.*, 7:631–634, 1961.

Edwards, T.J., Maurer, G., Newman, J. and Prausnitz, J.M. Vapor-liquid equilibria in multicomponent aqueous solution of volatile weak electrolytes. *A.I.Ch.E. J.*, 24:966–976, 1978.

Eigen, M. Protonenübertagung, säure-base-katalyse und enzymatische hydrolyse. teil I: Elementarvorgänge. *Angewandte Chemie*, 75:489–508, 1963.

Epstein, P.S. and Carhart, R.R. The absorption of sound in suspensions and emulsions.∗ I. water fog in air. *J. Acoust. Soc. Am.*, 25:553–565, 1953.

Falbe, J. *New synthesis with carbon monoxide; Chapter V.: Koch Reactions (H. Bahrmann)*. Berlin: Springer, 1980.

Foldy, L.L. The multiple scattering of waves. *Phys. Rev.*, 67:107–119, 1945.

Gaunaurd, G.C. and Überall, H. Resonance theory of bubbly liquids. *J. Acoust. Soc. Am.*, 69:362–370, 1981.

Gerhartz, W., Yamamoto, Y.S., Campbella, F.T., Pfefferkorn, R. and Rounsaville, J.F. *Ullmann's encyclopedia of industrial chemistry*, volume 4. Weinheim, 1985.

Greaves, M. and Barigou, M. Estimation of gas hold-up and impeller power in a stirred vessel reactor. In *Fluid Mixing III*, Inst. Chem. Engr., Inst. Chem. Eng. Symp. Series no. 108, pages 235–255, 1990.

Hallensleben, J. *Simultaner stoffaustausch von CO_2 und sauerstoff an einzelblasen und in blasenschwärmen*. PhD thesis, Universität Hannover, 1980.

Hård, S. and Johansson, K. Surface tension of concentrated aqueous solution of 1.1 electrolytes by means of Wilhelmy and laser light scattering methods. *J. Coll. Int. Sci.*, 60:467–472, 1977.

Herrmann, N. and McClements, D.J. Ultrasonic propagation in highly concentrated oil-in-water emulsions. *Langmuir*, 15:7937–7939, 1999.

Hikita, H., Asai, S. and Takatsuka, T. Absorption of carbon dioxide into aqueous sodium hydroxide and sodium bicarbonate solutions. *Chem. Eng. J.*, 11:131–141, 1976.

Horvath, A.L. *Handbook of aqueous electrolyte solutions : physical properties, estimation, and correlation methods*. Chichester : Ellis Horwood, 1985.

Hughmark, G.A. Power requirements and interfacial area in gas-liquid turbine agitated systems. *Ind. Eng. Chem. Proc. Des. Dev.*, 19:638–641, 1980.

Joosten, G.E. and Danckwerts, P.V. Solubility and diffusivity of nitrous oxide in equimolecular potassium carbonate-potassium bicarbonate solutions at 25 $^{\circ}$C and 1 atm. *J. Chem. Eng. Data*, 17:452–454, 1972.

Khatchikian, P., Riebel, U. and Kräuter, U. Phase velocity of ultrasound in suspensions of large particles. *Acustica*, 85:800–808, 1999.

Kon, N.S. and Sandall, O.C. Comparison of effective interfacial areas with the actual contact area for gas absorption in an agitated vessel. *Can. J. Chem. Eng.*, 56: 658–689, 1978.

Kuntz, E.G. Rhône Poulenc (patent numbers FR 2.349.562, 2.366.273 and 2.733.516), 1976.

Lide, D.R., editor. *Handbook of Chemistry and Physics*. CRC Press, 75^{th} edition, 1994.

Linek, V. and Beneš, P. A study of the mechanism of gas absorption into oil-water emulsions. *Chem. Engng Sci.*, 31:1037–1046, 1976.

Linek, V., Beneš, P., Vacek, V. and Hovorka, F. Analysis of differences in $k_l a$ values in determined by steady state and dynamic methods in stirred tanks. *Chem. Eng. J.*, 25:77–88, 1982.

Linek, V., Mayrhoferová, J. and Mošnerová, J. The influence of diffusivity on liquid phase mass transfer in solutions of electrolytes. *Chem. Engng Sci.*, 25:1033–1045, 1970.

Linek, V., Vacek, V. and Beneš, P. A critical review and experimental verification of the correct use of the dynamic method for the determination of oxygen transfer in aerated agitated vessels to water, electrolyte solutions and viscous liquids,. *Chem. Eng. J.*, 34:11–34, 1987.

Llorens, J., Mans, C. and Costa, J. Discrimination of the effects of surfactants in gas absorption. *Chem. Engng Sci.*, 43:443–450, 1988.

Lorimer, J.W., editor. *IUPAC Solubility Data series*, volume 5/6 and 43. Pergamon Press, Oxford, England, 1979.

Lu, W-M, Chi, R-C, Chien, W-C and Lin, L-C. Measurement of local bubble diameters and analysis of gas dispersion in an aerated vessel with disk turbine impeller. *J. Chem. Eng. Jap.*, 26:551–557, 1993.

Machon, V., Pacek, A.W. and Nienow, A.W. Bubble sizes in electrolyte and alcohol solutions in a turbulent stirred vessel. *Trans. Instn Chem. Engrs*, 75:339–348, 1997.

Marrucci, G. A theory of coalescence. *Chem. Engng Sci.*, 24:975–985, 1969.

Martin, T. *Gas dispersion with radial and hydrofoil impellers in fluids with different coalescence characteristics*. PhD thesis, University of Birmingham, 1995.

McClements, D.J. Principles of ultrasonic droplet size determination in emulsions. *Langmuir*, 12:3454–3461, 1996.

McClements, D.J. and Fairley, P. Ultrasonic pulse reflectometer. *Ultrasonics*, 29: 58–62, 1991.

Medwin, H. Counting bubbles acoustically: a review. *Ultrasonics*, 14:7–13, 1977.

Mehta, V.D. and Sharma, M.M. Mass transfer in mechanically agitated gas-liquid contactors. *Chem. Engng Sci.*, 26:461–479, 1971.

Meng, A.X., Hill, G.A. and Dalai, A.K. Modified volume expansion method for measuring gas hold-up. *Can. J. Chem. Eng.*, 80:194–199, 2002.

Nelder, J. A. and Mead, R. A simplex method for function minimization. *Computer Journal*, 7:308–313, 1965.

Nienow, A.W., Wisdom, D.J. and Middleton, J.C. Effect of scale and geometry on flooding, recirculation and power in gassed stirred vessels. In *Proc. 2nd Euro. Conference on Mixing, Cambridge UK*, F1, pages 1–16, 1977.

Nishi, R.Y. The scattering and absorption of sound waves by a gas bubble in a viscous liquid. *Acustica*, 33:65–74, 1975.

Oyevaar, M. H. and Westerterp, K. R. The use of the chemical method for the determination of interfacial areas in gasliquid contactors. *Chem. Engng Sci.*, 44: 2691–2701, 1989.

Ozkan, O., Calimli, A., Berber, R. and Oguz, H. Effect of inert solid particles on gas-liquid mass transfer in mechanically agitated reactors. *Chem. Engng Sci.*, 55: 2737–2740, 2000.

Pacek, A.W., Moore, I.P.T., Nienow, A.W. and Calabrese, R.V. Video technique for measuring dynamics of liquid-liquid dispersion during phase inversion. *A.I.Ch.E. J.*, 40:1940–1949, 1994.

Parthasarathy, R. and Ahmed, N. Sauter mean and maximum bubble diameters in aerated stirred vessels. *Trans. Instn Chem. Engrs*, 72:565–572, 1994.

Pohorecki, R. and Moniuk, W. Kinetics of reaction between carbon dioxide and hydroxyl ions in aqueous electrolyte solutions. *Chem. Engng Sci.*, 43:1677–1684, 1988.

Povey, M.J.W. *Ultrasonic Techniques for fluids characterization.* Academic Press: San Diego, 1997.

Richards, G.M., Ratcliff, G.A. and Danckwerts, P.V. Kinetics of CO_2 absorption-III first order reaction in a packed column. *Chem. Engng Sci.*, 19:325–328, 1964.

Riet, K. van 't. Review of measuring methods and results in non-viscous gas-liquid mass transfer in stirred vessels. 18:357–364, 1979.

Rols, J.L., Condoret, J.S., Fonade, C. and Goma, G. Mechanism of enhanced oxygen transfer in fermentation using emulsified oxygen-vectors. *Biotech. Bioeng.*, 35: 427–435, 1990.

Roques, H., Aurelle, Y., Aoudjehane, M. and Siem, M. Etude expérimentelle des phénomènes de coalescence dans les systèmes 'bulles-gouttes'. *Rev. de IFP*, 42: 163–177, 1987.

Sagert, N.H. and Quinn, M.J. The coalescence of gas bubbles in dilute aqueous solutions. *Chem. Engng Sci.*, 33:1087–1095, 1978.

Schaafsma, A.S. and Hay, A.E. Attenuation in suspensions of irregularly shaped sediment particles: A two-parameter equivalent spherical scatterer model. *J. Acoust. Soc. Am.*, 102:1485–1502, 1997.

Schlüter, V. and Deckwer, W.-D. Gas-liquid mass transfer in stirred vessels. *Chem. Engng Sci.*, 47:2357–2362, 1992.

Schumpe, A. and Deckwer, W.-D. Analysis of chemical methods for determination of interfacial areas in gas-liquid dispersions with non-uniform bubble sizes. *Chem. Engng Sci.*, 35:2221, 1980.

Sharma, M.M. and Danckwerts, P.V. Fast reactions of CO_2 in alkaline solutions. (a) Carbonate buffers with arsenite, formaldehyde and hypochlorite als catalysts. *Transactions of the Faraday Society*, 59:386, 1963.

Spelt, P.D., Norato, M.A., Sangani, A.S. and Tavlarides, L.L. Determination of particle size distributions from acoustic wave propagation measurements. *Phys. Fluids*, 11:1065–1080, 1999.

Stravs, A.A., Pittet, A., von Stockar, U. and Reilly, P.J. Measurement of interfacial areas aerobic fermentations by ultrasonic pulse transmission. *Biotech. Bioeng.*, 28:1302–1309, 1986.

Stravs, A.A. and von Stockar, U. Measurement of interfacial areas in gas-liquid dispersions by ultrasonic pulse transmission. *Chem. Engng Sci.*, 40:1169–1175, 1985.

Tsonopoulos, C. Ionization constants of water pollutants. *J. Chem. Eng. Data*, 21: 190–193, 1976.

Versteeg, G.F. and Van Swaaij, W.P.M. Solubility and diffusivity of acid gases (CO_2, N_2O) in aqueous alkanolamine solutions. *J. Chem. Eng. Data*, 32:29–34, 1988.

Wachsen, O., Himmler, K. and Cornils, B. Aqueous biphasic catalysis: Where the reaction takes place. *Catalysis Today*, 42:373–379, 1998.

Warmoeskerken, M.M.C.G. and Smith, J.M. Flooding of disk turbines in gas-liquid dispersions: a new description of the phenomenon. *Chem. Engng Sci.*, 40:2063–2071, 1985.

Waterman, P.C. and Truell, R. Multiple scattering of waves. *J. Math. Phys.*, 2: 512–537, 1961.

Weisenberger, S. and Schumpe, A. Estimation of gas solubilities in salt solutions at temperatures from 273 K to 363 K. *A.I.Ch.E. J.*, 42:298–300, 1996.

Weissberg, H.L. Effective diffusioncoefficient in porous media. *J. Appl. Phys.*, 34: 2636–2639, 1963.

Westerterp, K.R., van Dierendonck, L.L. and de Kraa, J.A. Interfacial areas in gas-liquid contactors. *Chem. Engng Sci.*, 18:157–176, 1963.

Yang, C., Mao, Z-S, Wang, Y. and Chen, J. Kinetics of hydroformylation of propylene using $RhCl(CO)(TPPTS)_2$/TPPTS complex catalyst in aqueous system. *Catalysis Today*, 74:111–119, 2002.

Yianatos, J.B., Laplante, A.R. and Finch, J.A. Estimation of local holdup in the bubbling and froth zones of a gas-liquid column. *Chem. Engng Sci.*, 40:1965–1968, 1985.

Yoshida, F. and Miura, Y. Gas absorption in agitated gas-liquid contactors. *Ind. Eng. Chem. Proc. Des. Dev.*, 2:263–268, 1963.

Yoshida, F., Yamane, T. and Miyamoto, Y. Oxygen absorption into oil-in-water emulsions. *Ind. Eng. Chem. Proc. Des. Dev.*, 9:570–577, 1970.

Dankwoord

Met dit dankwoord komt er een eind aan dit proefschrift en ook aan de leuke tijd die ik heb gehad, waarin dit proefschrift to stand is gekomen. Dit was natuurlijk niet gelukt zonder de hulp van een groot aantal mensen. Die wil ik dan ook graag vanaf deze plek bedanken.

Allereerst gaat mijn dank uit naar mijn assistent promotor en directe begeleider Wim Brilman. Zijn enthousiasme tijdens mijn afstuderen met betrekking tot onderzoek en dan met name tot G-L-L systemen, was voor mij mede een aanleiding om met deze opdracht te beginnen. Tijdens de afgelopen 4 jaar heb ik Wim's wetenschappelijke input, nieuwe ideeën en de discussies over het onderzoek erg gewaardeerd. Ook mijn promotor, Geert Versteeg, wil ik bedanken voor het vertrouwen dat hij in mij heeft gesteld en voor de vrijheid die hij mij heeft gegeven om dit onderzoek zoveel mogelijk naar eigen inzicht in te vullen.

In dit proefschrift zou niet zoveel experimenteel werk beschreven staan zonder de hulp van de technici. Benno, Henk-Jan, Wim, Gerrit en Robert (2x) stonden altijd direct klaar als er iets aan een opstelling moest gebeuren. Speciale dank gaat uit naar Benno, die niet alleen alle opstellingen heeft gebouwd, maar ook alle constructies heeft ontworpen en zich daarvoor heeft verdiept in de wondere wereld van het ultrageluid.

Een vijftal afstudeerders heeft een hele grote bijdrage geleverd aan het verloop van dit onderzoek: Bert, Frans, Paul, Marius en Duco, allemaal hardstikke bedankt ! Ook de verschillende projecten gedaan door Harry, Ellen en Egbert hebben het onderzoek zeker verder geholpen. Verder gaat er een woord van dank uit naar de analyse afdeling, waarin Wim, Adri en met name Suvan erg veel werk hebben

besteed aan het ontrafelen van de grensvlakchemie van G-L-L systemen.

Nicole, Britta en Irene wil ik bedanken voor het verzorgen van de administratieve kant van het onderzoek. De inkoopafdeling (Wim, Nelly, Ineke en Marc) zorgden dat alle denkbare onderdelen richting het CT-gebouw kwamen. Verder wil ik de afdeling voor de inkoop van de chemicalin en gassen (Karin, Roy, Henk en Benny) danken voor hun inzet de afgelopen tijd. Ook de mensen van de CT-bibliotheek waren altijd erg hulpvaardig als er weer artikelen uit een ver verleden voor het onderzoek van nut konden zijn.

Natuurlijk is er de afgelopen 4 jaar niet alleen maar gewerkt, maar was het ook een gezellige tijd. De verschillende uitjes en borrels met de collega's en studenten van OOIP en FAP waren hier een goed voorbeeld van. Verdere ontspanning werd bereikt door de CL-avondjes in de Doedelzak, squashen met Sascha, Bert en Alex en natuurlijk de voetbal. Iedereen wil ik hiervoor hartelijk bedanken. Derx (toch niet in het ondankswoord) en Duux wil ik bedanken, omdat ze het hebben willen optreden als mijn paranimfen en zeker ook voor de gezelligheid van de afgelopen tijd.

Zeer veel dank ben ik ook verschuldigd aan mijn ouders, zus(je) en natuurlijk aan Leonie, die mij constant hebben gesteund.

Toine, 04-12-2003